Accessible biomarkers of inflammatory lung pathophysiology arising from exposure to traffic related particulate matter

---

Thesis submitted by

Liza Selley

For the degree of Doctor of Philosophy of Imperial College London

Supervisors: Dr Toby Athersuch and Professor Tim Gant

Section of Computational Systems Medicine

Department of Surgery and Cancer

Faculty of Medicine

Imperial College London

2017

Abstract

Exposure to traffic-related particulate matter (TRPM) is a major cause of pulmonary inflammation, inducing symptoms that range from mild coughing or sore throat to life-threatening asthma attacks or exacerbations of chronic obstructive pulmonary disorder. At present, the molecular mechanisms that underlie pulmonary responses to TRPM *in vivo* require further characterisation (particularly for those that are stimulated by non-exhaust particulates) but cohort recruitment is hindered by the invasive and uncomfortable nature of sampling via biopsy or bronchial lavage. Extracellular microRNA and metabolite biomarkers offer an attractive alternative measure of responses to TRPM as they are detectable in a number of non-invasively accessible bio-fluids, can be profiled using agnostic, data-driven omics strategies and have been associated with diesel exhaust particle (DEP) exposure in recent studies.

Based on evidence that the mechanistic relevance and exploratory power of omics-derived biomarkers can be enhanced through integration of multiple molecular platforms, this study sought to identify miRNA and metabolite biomarkers of pulmonary inflammatory pathways using a combination of microtranscriptomic and metabolomic profiling techniques. Using diverse rodent models of pulmonary inflammation (pharmaceutical, nanoparticle and cytokine-induced), next generation sequencing and microarray analysis identified miR-34b/449a as stimulus-independent, tissue markers of pulmonary specific inflammatory responses.

Targeted analyses confirmed the translation of miR-34b/449a over-expression signatures into serum during prototypical (lipopolysaccharide-induced) pulmonary inflammatory responses and into the supernatants of TRPM exposed macrophages *in vitro*. Meanwhile, ^{1}H nuclear magnetic resonance spectroscopy identified that the miRNA biomarkers were accompanied by changes in the concentrations of energy metabolism substrates, intermediaries and products in both models. The technique also determined that responses

to TRPM could be differentiated from lipopolysaccharide-induced responses based on additional changes to extracellular amino acid and *myo*-inositol content but that no significant differences were made to the biomarker panel where responses to exhaust and non-exhaust particulate exposures were compared. This absence of discriminatory power supported hypothesis-driven characterisations of TRPM-induced toxicity in macrophages. Both DEP and brake abrasion dust (BAD) disrupted mitochondrial membrane potential, inhibited phagocytosis activity and induced cytokine secretion to the same degree.

Integrative pathway over-representation analysis (ORA) identified a wide range of cellular pathways that were disrupted in common during prototypical and TRPM-induced pulmonary inflammation. Many of these pathways were eluded to by the metabolite-only ORA but others (such as lipid metabolism and hypoxia signalling pathways) were only detected by the integrative technique. An additional few that belong to characterised responses to TRPM (including glutathione synthesis and xenobiotic metabolism) were excluded by the multi-omics analysis indicated that while the integrative approach enhanced the mechanistic and informative potential of the biomarkers overall, single-omics results were also useful in their own right.

Statement of originality

I certify that this thesis, and the research to which it refers, are the product of my own work, conducted during my doctoral studies at Imperial College London. Any ideas or quotations from the work of other people, published or otherwise, or from my own previous work are fully acknowledged in accordance with the standard referencing practices of the discipline.

Collection of data for the characterisation of U937 responses to particle and endotoxin exposure was assisted by Linda Schuster under my supervision. Particle preparation and analysis by ICP-MS was conducted by Dr Ian Mudway and Mr Andy Cakebread (King's College London)who provided me with pre-processed data to analyse. *In vivo* modelling, BALF analysis and RNA extraction for the AZD2230 exposure study were performed by unrecorded personnel at AstraZeneca prior to my project, and sequencing of RNA from these samples (including library preparation) was performed by the Beijing Genomics Institute. Similarly, the *in vivo* modelling, BALF analysis and serum preparation for the GSK project was performed by Dr Graham Paul *et al.* at Glaxo Smith Kline. All other RNA isolations and downstream analyses relating to these sample were performed by me.

Copyright declaration

The copyright of this thesis rests with the author and is made available under a Creative Commons Attribution Non-Commercial No Derivatives licence. Researchers are free to copy, distribute or transmit the thesis on the condition that they attribute it, that they do not use it for commercial purposes and that they do not alter, transform or build upon it. For any reuse or redistribution, researchers must make clear to others the licence terms of this work

Acknowledgements

First and foremost I would like to thank Dr Toby Athersuch and Professor Tim Gant for being such helpful and supportive supervisors. Alongside their time and their advice I have truly appreciated their continued encouragement to take on extracurricular challenges and the confidence that they have given me to go off into the world as an independent researcher. It has been an absolute pleasure to work with such positive and thoughtful people.

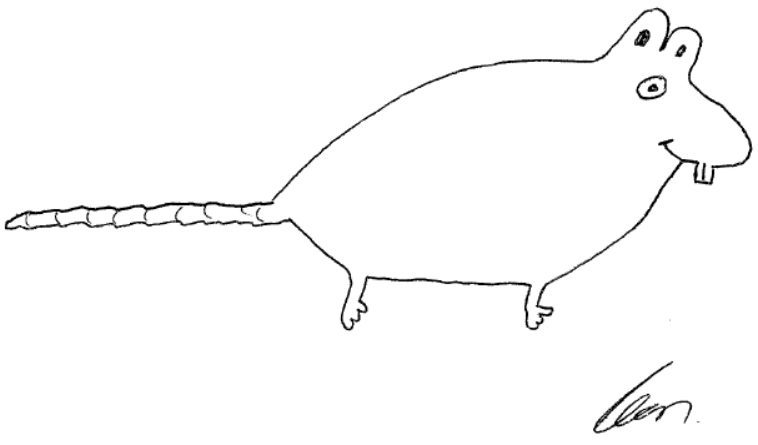
I am also enormously grateful to Dr Ian Mudway, Professor Ben Forbes and Dr Abhinav Kumar for hosting me in their groups at King's College, London for my mini fellowship (and of course, the *In Vitro* Toxicology Society for funding it!). I learnt a huge amount about particulate toxicology and had an extremely enjoyable 12 months, working with Linda, Theresa and Magda as part of the L-Team. I will take many of those experiences on with me as I enter post-doctoral life, particularly Waffle Thursdays and basil-infused gin.

Drs Emma Marczylo and Martin Leonard have also been extremely kind, sharing their expertise in molecular techniques, allowing me to take over their PCR machine for weeks on end and organising illicit particle drops at conferences. I really enjoyed the time I spent at the PHE labs and I would like to thank the entire department for being so very welcoming. Similarly I am very grateful to Dr Tom McKevitt and Graham Paul at GSK and to the team at Astra Zeneca for sharing their samples and data for my rat studies.

PhD life wouldn't have been half as fun without my lovely friends. I really don't know how I would have coped without three dart darts, the promise of entry into Pete's mole bunker or Helena's amazing cooking on a Friday night. Similarly, Professor Andy Smith and the MRC ITTP group have been wonderful, those weeks in Leicester were just so fun, finding out about the stranger sides of toxicology, eating far too much steak and securing a double win for Team Toby in croquet. I am also incredibly grateful to the MRC for funding my project and for the opportunity that they provided to participate in the Max Perutz writing competition.

Mum and Dad, you have been brilliant. Thank you for feeding me, taking away my phone and putting up with the tantrums as I battled through writing…also for actually pointing out the PhD advert in the first place! Nana, I definitely got my sciencey genes from you, you were the first family member to understand the link between lungs and pollution! You also kept me smiling on the rubbish days where my cells didn't want to play or the data looked ridiculous.

Finally Leon….thank you for being the smiling face that helped me leave my frustrations at the front door, for helping me see the bigger picture…and for providing this very important figure; a tribute to the little rats that gave their lives for my science.



Abbreviations

^{1}H	Hydrogen-1
AA	Ascorbic acid
ABC	ATP binding cassette
Acetyl-CoA	Acetyl-coenzyme A
ADCY6	Adenylate cyclase
Ago	Argonaute
ALDOA	Fructose-bisphosphate aldolase A
ALI	Acute lung injury
Akt	Serine/ threonine protein kinase
AMPK	5'-adenosine monophosphate-activated protein kinase
ANOVA	Analysis of variance
AP-1	Activating protein-1
AQP4	Aquaporin
ARE	Adenylate-uridylate -rich element
As	Arsenic
AT1	Alveolar type II epithelial cells
AT2	Alveolar type I epithelial cells
ATP	Adenosine trisphosphate
ATP1B3	Sodium/potassium-transporting ATPase subunit β-3transporter proteins
Ba	Barium
BAD	Brake abrasion dust
BALF	Bronchoalveolar lavage fluid
BCA	Bicinchoninic acid
BCAA	Branched chain amino acid
BEC	Bronchial epithelial cells

BGI	Beijing Genomics Institute
BGN	Biglycan
Ca	Calcium
CAM	Cellular adhesion molecule
CC16	Clara cell secretory protein
Cd	Cadmium
CDK	Cyclin-dependent kinase
cDNA	Complimentary deoxyribonucleic acid
CF	Cystic fibrosis
CFU	Colony forming units
chH_2O	Chelator treated H_2O
ChREBP	Carbohydrate-responsive element binding protein
CM	Culture medium
COPD	Chronic obstructive pulmonary disorder
CPMG	Carr-Purcell-Meiboom-Gill
Cr	Chromium
CSPG4	Chondroitin sulphate proteoglycan 4
C_T	Cycle threshold
Cu	Copper
CYP	Cytochrome P450
DEA	Differential expression analysis
DEmiRNA	Differentially expressed miRNA
DEP	Diesel exhaust particles
DLS	Dynamic light scattering
dNTPs	Deoxyribonucleotides
E2F1	E2F transcription factor
ELF	Epithelial lining fluid

ENO3	Enolase-3
ERG	Environmental Research Group
FDR	False discovery rate
Fe	Iron
FID	Free induction decay
FOXO1	Forkhead box protein O1
FXYD3	FXYD domain containing ion transport regulator 3
GCLC	Glutamate cysteine ligase
GEO	Gene Expression Omnibus
GLUD1	Glutamate dehydrogenase 1
GM-CSF	Granulocyte-macrophage colony-stimulating factor
GNG5	Guanine nucleotide-binding protein subunit γ5
GO	Gene ontology
GSH	Glutathione
GSK	p38 Mitogen activated protein kinases inhibitor (product of GlaxoSmithKline)
GYG1	Glycogenin 1
H_2O_2	Hydrogen peroxide
HCA	Hierarchical clustering analysis
He	Helium
HEXA	β-hexosaminidase
HIF-1	Hypoxia inducible factor 1
HIF-1α	Hypoxia inducible factor 1
ICAM-1	Intracellular cellular adhesion molecule-1
ICP-MS	Inductively coupled plasma mass spectrometry
IKK	Inhibitor of nuclear factor kappa-B kinase
IKK2	Inhibitor of nuclear factor kappa-B kinase subunit beta
IL	Interleukin

IMPaLA	Integrated Molecular Pathway Level Analysis
IRAK	IL-1 receptor associated kinase-1
KHK	Ketohexokinase
LBP	LPS binding proteins
LEZ	Low emission zone
LPS	Lipopolysaccharide
MAPK	Mitogen activated protein kinase
MH	Müeller Hinton
Mn	Manganese
Mo	Molybdenum
miRISC	miRNA inducing silencing complex
miRNA	microRNA
mRNA	Messenger RNA
MTT	3-(4,5-dimethylthiazol-2-yl)-2,5-diphenyltetrazolium bromide
MyD88	Myeloid differentiation primary response gene 88
n.d.	Not-detected
NFκB	Nuclear factor kappa-light-chain-enhancer of activated B cells
NGS	Next generation sequencing
Ni	Nickel
NMR	Nuclear magnetic resonance
Nrf2	Nuclear factor erythroid 2 -related factor 2
Nucleotides	Nt
NUP35	Nucleoporin 35
ORA	Over-representation analysis
pI3 kinase	Phosphoinositide 3-kinase
p38 MAPK	p38 Mitogen activated protein kinases
P body	Processing body

PABP	Poly-A binding proteins
PAH	Polycyclic aromatic hydrocarbon
PBS	Phosphate buffered saline
PC	Principal component
PCA	Principal component analysis
PDI	Polydispersity index
PGE-1	Prostaglandin 2
PLS-DA	Partial least squares- discriminant analysis
PM	Particulate matter
PMA	Phorbol 12- myristate 13-acetate
$PM_{0.1}$	Ultrafine particulate matter (≤ 0.1μm diameter)
PM_{10}	Coarse particulate matter (≤ 10 μm diameter)
$PM_{2.5}$	Fine particulate matter (≤ 2.5 μm diameter)
Poly-A	Poly-adenylated
PQN	Probabilistic quotient normalisation
Pre-miRNA	Precursor miRNA transcript
pri-miRNA	Primary miRNA transcript
PRR	Pattern recognition receptor
Rb	Retinoblastoma protein
RNS	Reactive nitrogen species
ROS	Reactive oxygen species
RT	Room temperature
RTqPCR	Reverse transcription quantitative polymerase chain reaction
S. aureus	Staphylococcus aureus
Sb	Antimony
SCFA	Short chain fatty acid
SDC4	Syndecan-4

SEM	Standard error of the mean
Si	Silica
SLC	Solute carrier
Sn	Tin
Snai1	Snail Family Transcriptional Repressor 1
SREBP	Sterol regulatory element-binding protein
STOCSY	Statistical total correlation spectroscopy
TAK1	Transforming growth factor-B-activated kinase 1
TF	Transcription factor
Ti	Titanium
TiO_2	Titanium dioxide
TIRAP	Toll-interleukin-1-receptor domain containing adaptor inducing interferon-β
TLR	Toll-like receptor
TMREC	Database of transcription factors and miRNA regulatory cascades
TNF-α	Tumour necrosis factor α
Tp53	Tumour protein p53
TRAF6	TNF receptor associated factor 6
TRAM	Toll-interleukin-1-receptor related adaptor molecule
TRPM	Traffic related particulate matter
TSP	Sodium 3-(trimethylsilyl)propionate-2,2,3,3-d4
UNG	Uracil *N*-glycosylase
UTR	Untranslated region
V	Vanadium
VCAM-1	Vascular cellular adhesion molecule-1
VIP	Variable importance plot
W	Tungsten

List of units

pM	picomolar
nM	Nanomolar
µM	Micromolar
mM	Millimolar
Nm	Nanometer
µm	Micrometer
µg	Microgram
Mg	Milligram
Kg	Kilogram
µl	Microlitre
ml	Millilitre
AU	Arbitrary units
kDA	Kilo daltons
CFU	Colony forming units
Nt	Nucleotides

Table of Contents

Abstract ..... **i**

Statement of originality ..... **iii**

Copyright declaration ..... **iii**

Acknowledgements ..... **iv**

Abbreviations ..... **v**

List of units ..... **xi**

Chapter 1. Introduction **1**

1.1 Pulmonary inflammation 1

1.1.1 Structure and function of the respiratory tract 1

1.1.2 Pulmonary defence mechanisms 4

1.1.3 Inflammatory defences of the alveoli 5

1.1.4 Termination or development of the acute pulmonary response 7

1.2 Traffic related particulate matter and pulmonary inflammation 9

1.2.1 Traffic related particulate matter 9

1.2.2: Associations between TRPM exposure and pulmonary inflammation 9

1.2.3: Mechanisms of TRPM-induced pulmonary inflammation 11

1.3: Biomarkers and their application to TRPM-induced toxicity 15

1.3.1 Hypothesis-driven response biomarker discovery 19

1.3.2 Data-driven biomarker discovery 20

1.3.3: Multi-omics approaches to data-driven biomarker discovery 21

1.3.4: Integration of microtranscriptomic and metabolomics datasets 23

1.4 miRNAs 26

1.4.1 Biogenesis of miRNAs 26

1.4.2 Post-translational regulation by miRNAs 27

1.4.3: miRNAs as accessible biomarkers of pulmonary inflammatory responses to TRPM exposure 30

1.4.4: Methods for deriving miRNA biomarkers 33

1.6: Metabolites and the metabolome 36

1.6.1: Metabolic profiling for biomarker identification 37

1.6.2: Metabolic profiling for the detection of TRPM-associated biomarkers 38

1.6.3: Methods employed for metabolic biomarker detection 39

1.6.4: Statistical interrogation of metabolomic datasets 41

1.7 Modelling pulmonary exposures to xenobiotics 43

1.7.1 In vivo models 44

1.7.2 In vitro models 47

1.8: Project aims and hypotheses 51

1.8.1: Project hypotheses 51

1.8.2 Project aims 51

Chapter 2. miRNA markers of pulmonary inflammation in the rat 54

Chapter overview 54

2.1: Introduction 54

2.1.2: Hypotheses and aims 57

2.2: Methods 58

2.2.1: AZD2230-exposed tissue samples: 58

2.2.2: Statistical analysis of BALF metadata: 59

2.2.3: miRNA sequencing data analysis: 59
2.2.4: mRNA sequencing data analysis: 60
2.2.5: Prediction of miRNA-mRNA pairing: 60
2.2.6: Hierarchical clustering analysis 61
2.2.7: Pathway over-representation analysis 61
2.2.8: Identification of pulmonary-enriched DEmiRNAs 61
2.2.9: Analysis of publically available microarray datasets 62
2.3: Identification of miRNA-associated transcription factors: 62
2.3: Results 63
2.3.1: AZD2230 exposure induced an inflammatory response in rat pulmonary tissue 63
2.3.2: AZD2230 exposure modulated miRNA expression in AZ rat lung tissue 66
2.3.3: Validation of DEmiRNA activity using mRNA sequencing data 70
2.3.4: DEmiRNA activity modulates inflammatory mechanisms 74
2.3.5: miR-34b and miR-449a are predominantly expressed by pulmonary tissue: 79
2.3.6: Differential expression of miR-34b and 449a is not specific to AZD2230 induced pulmonary inflammation 83
2.3.7: miR-34b expression was driven independently of transcription factor activity 85
2.4: Summary of results 87
2.5: Discussion 88
2.5: Conclusion 93
Chapter 3: Circulating markers of pulmonary inflammation 94
Chapter overview 94
3.1: Introduction 94

3.1.2: Aims, hypothesis and study design 97

3.2: Methods 100

3.2.1: Rat serum samples 100

3.2.2: RNA extraction 100

3.2.3: RNA purification: 100

3.2.4: Total RNA and total miRNA quantifications 101

3.2.5: cDNA synthesis 101

3.2.6: RTqPCR 101

3.2.7: Functional annotation of predicted miR-34b/449a gene targets 102

3.2.8: ^{1}H NMR spectroscopy 102

3.2.9: Processing of ^{1}H NMR spectroscopic data 103

3.2.10: Multivariate statistical analysis of ^{1}H NMR spectroscopic data 103

3.2.11: Integrated pathway analysis of miRNA quantification and ^{1}H NMR spectroscopic data 104

3.2.12: Univariate statistical analysis of RTqPCR and ^{1}H NMR spectroscopic data 104

3.3: Results 106

3.3.1 miRNAs are detectable within the serum of rats 106

3.3.2 Serum concentrations of miR-34b and 449a are enhanced by pulmonary exposure to LPS 109

3.3.3 LPS-induced increases in miR-34 and 449 expression are inhibited by p38 MAPK inhibition 111

3.3.4: ^{1}H NMR spectroscopy characterised the serum metabolomes of rats following exposure to LPS in the presence or absence of a p38 MAPK inhibitor 113

3.3.5: Pulmonary exposure to LPS induces changes in the serum metabolome 119

3.3.6: LPS induced changes in the serum metabolome are p38 MAPK dependent 122

3.3.7 Intratracheal LPS exposure alters metabolic relationships within the serum of rats 124

3.3.5: miR-34b and 449a activity may regulate transport and metabolism of glutamine and acetate 133

3.4: Summary of results 138

3.5: Discussion 139

3.5: Conclusion 144

Chapter 4: Extracellular markers of pulmonary inflammation induced by traffic-related particulates 146

Overview 146

4.1: Introduction 146

4.1.1: Hypothesis and aims 149

4.2: Materials and methods 150

4.2.1: Nanoparticles 150

4.2.2: Particle size measurement using dynamic light scattering (DLS) 150

4.2.3: Measurement of particulate oxidative potential 150

4.2.4: U937 culture and differentiation 151

4.2.5: Particle exposure 151

4.2.6: Quantification of intra and extracellular metals by inductively coupled plasma mass spectroscopy (ICP-MS): 151

4.2.7: 3-[4,5-dimethylthiazol-2-yl]-2,5 diphenyl tetrazolium bromide (MTT) assay: 152

4.2.8: Cytokine enzyme linked immunosorbent assays (ELISAs): 152

4.2.9: Maintenance of bacterial stocks: 152

4.2.10: Quantification of bacterial phagocytosis behaviour 153

4.2.12: Bicinchoninic acid (BCA) protein quantification assay 153

4.2.13: Univariate statistical analysis of toxicological data 154

4.2.14: RNA extractions: 154

4.2.14.1: RNA extraction from U937 lysates: 154

4.2.14.2: RNA extraction from U937 supernatants 155

4.2.14.3: RNA quantification 155

4.2.15: cDNA synthesis: 155

4.2.16: RTqPCR data acquisition and analysis: 155

4.2.17: ^{1}H NMR spectroscopy 155

4.2.17.1: Processing of ^{1}H NMR spectroscopic data: 155

4.2.17.2: Feature identification from ^{1}H NMR spectroscopic data 156

4.2.18: Over-representation analysis of metabolite and transcriptomic datasets: 156

4.3: Results 157

4.3.1: Physicochemical characteristics of BAD and SRM-2975 particles 157

4.3.2: U937 macrophages ingest BAD and SRM-2975 particles 161

4.3.3: BAD and SRM-2975 are not cytotoxic to U937 macrophages but cause mitochondrial dysfunction 163

4.3.4: BAD and NIST induce inflammatory responses in U937 168

4.3.5: BAD and SRM-2975 inhibit phagocytic function in U937 171

4.3.6: TRPM-induced up-regulation of miR-449a is detectable within U937 supernatants 175

4.3.7: U937 metabolic profiles are altered in response to pro-inflammatory stimuli 181

4.3.8: Inflammatory stimuli induce alterations in common metabolic pathways in U937 macrophages 184

4.3.9: miR-34b/449a activity may influence inflammatory responses to particle exposure in U937 cells 186

4.4: Results summary 190

4.5: Discussion 191

4.6: Conclusion 198

Chapter 5: General discussion, conclusions and possible future directions 199

5.1: Summary of findings 199

5.1.1: Inflammation -associated miR-34b/449a over-expression signatures translate from pulmonary tissue to serum and from macrophages to supernatants 199

5.1.2: Metabolite markers of pulmonary inflammatory responses distinguished between endotoxin and TRPM-induced responses 203

5.1.3: Multi-omics approaches enhanced the mechanistic value of pulmonary inflammatory biomarkers 205

5.2: Advantages and limitations of study designs 207

5.2.1: Use of an *in vitro* exposure system for TRPM studies 207

5.2.2: Choice of methods for data integration 209

5.2.3: Choice of serum as an extracellular matrix for biomarker detection 211

5.2.4: Absence of a continuous control between studies 212

5.3: Impacts of findings 213

5.3.1: Applications for research 213

5.3.2: Applications for policy makers 215

5.4: Considerations for future work 216

5.4.1: *In vivo* validation of TRPM-associated biomarkers 216

5.4.2: Validation of pathway identifications for biomarkers 218

5.4.3: Untargeted lipidomics analysis 219

5.5: Conclusion 220

References 222

List of figures

Chapter 1

Figure 1. 1: Schematic representation of the human respiratory tract. 2

Figure 1. 2: Structural organisation of the gas-exchange region of the lower airways. 3

Figure 1. 3: Known mechanisms of TRPM induced inflammation. 13

Figure 1. 4: The nature and interplay of relationships between biomarkers 18

Figure 1. 5: Omics profiles are influenced by regulators of transcription, translation and protein-protein interactions. 25

Figure 1. 6: Biogenesis of miRNAs. 28

Figure 1. 7: Mechanisms of post-transcriptional regulation by miRNAs. 31

Figure 1. 8: Schematic explanation of the workflow followed in this study. 53

Chapter 2

Figure 2. 1: Absolute inflammatory cell counts measured in BALF samples of rats treated with 0, 1 or 3mg/kg AZD2230. 65

Figure 2. 2: HCA of pulmonary tissue samples (miRNA) 69

Figure 2. 3: HCA of pulmonary tissue samples (mRNA). 73

Figure 2. 4: Regulatory interactions between DEmiRNAs and mRNA targets. 77

Figure 2. 5: Numbers of tissues that express lower concentrations of DEmiRNAs than lung tissue in healthy male rats. 80

Figure 2. 6: Differences in expression levels of miR-34b-5p and miR-449a-3p between lung and other tissues in healthy male rats. 81

Figure 2. 7: Expression levels of miR-449a-3p and miR-34b-5p in the pulmonary tissue of mice exposed to nanoTiO2 or IL-13 84

Figure 2. 8: Expression of transcription factors that target miR-34 86

Chapter 3

Figure 3. 1: LPS signalling pathways 99

Figure 3. 2: Spectra displaying the quantities of total RNA and miRNA detectable in a representative sample of rat serum. 108

Figure 3. 3: Fold increases in miR-34b and 449a concentrations in the serum of rats following LPS exposure..... 110

Figure 3. 4: Fold increases in miR-34b and 449a concentrations in the serum of rats following LPS and p38/MAPK inhibitor exposure ……..110

Figure 3. 5: Representative ^{1}H NMR spectrum generated from rat serum. 115

Figure 3. 6: PCA analysis of serum samples from LPS and GSK treated rats.. 116

Figure 3. 7: Inter-sample variability in serum glucose, alanine and taurine concentrations 117

Figure 3. 8: PCA scores plot displaying intrinsic metabolic variation within rat serum samples 118

Figure 3. 9: PLS-DA analysis of the rat serum metabolome. 120

Figure 3. 10: Concentrations of feature metabolites measured within the serum of rats treated with LPS or a vehicle control.. 121

Figure 3. 11: Concentrations of feature metabolites measured within the serum of rats treated with LPS, LPS and GSK or vehicle control 123

Figure 3. 12: Heat map visualisation of moderate to very strong metabolite-metabolite correlations in LPS and vehicle exposure serum samples..... 125

Figure 3. 13: Log fold differences in concentration between glutamine and strongly correlated metabolites in LPS and vehicle exposure samples. 127

Figure 3. 14: Comparison of serum concentrations of metabolites that display correlating concentrations to glutamine in rats following exposure to LPS or vehicle control 128

Figure 3. 15: Log fold differences in concentration between acetate and strongly correlated metabolites in LPS and vehicle exposure samples..... 131

Figure 3. 16: Comparison of serum concentrations of metabolites that display correlating concentrations to acetate in rats following exposure to LPS or vehicle control. 132
Figure 3. 17: Gene ontology classifications for the predicted mRNA targets of miR-34a/449b. 136

Chapter 4

Figure 4. 1: The oxidative potential of SRM-2975 and BAD..... 162
Figure 4. 2: Light micrographs of U937s 164
Figure 4. 3: Viability of U937s following particle exposure 166
Figure 4. 4: The influence of particle exposure on metrics of cellular health 167
Figure 4. 5: Particle-induced cytokine secretion 169
Figure 4. 6: The influence of metals on cytokine secretion 170
Figure 4. 7: The influence of particles on phagocytosis behaviour 173
Figure 4. 8: Influence of particle exposure on bacterial growth 174
Figure 4. 9: RNA content of supernatant samples 177
Figure 4. 10: Fold increases in miR- 449a concentrations in cellular lysates and supernatants of U937s following 24h exposures to LPS, BAD or SRM-2975 180
Figure 4.11: Typical ^{1}H NMR spectra generated from the supernatants of U937 macrophages cultured in RPMI 1640 medium. 182
Figure 4.12: Quantities of feature metabolites detected within the supernatant of U937 macrophages following 24 h incubations with media control, 1 µg/ml LPS or 4- 14 µg/ml BAD or SRM-2975 185

Chapter 5

Figure 5. 1: Key observations made during the search for mechanistically relevant, accessible biomarkers of pulmonary inflammation. 202

List of tables

Chapter 1

Table 1. 1: Comparative summary of the beneficial and limiting features of techniques used for miRNA biomarker detection 35

Chapter 2

Table 2. 1: Experimental characteristics of publically available datasets used for comparison with the AZD2230 model of inflammation. 62
Table 2. 2: miRNAs that displayed differential expression in the pulmonary tissue of rats following intratracheal exposure to 1 or 3mg/kg AZD2230. 68
Table 2. 3: Percentages of predicted DEmiRNA targets that were biologically validated in the AZD2230 exposure model using next generation mRNA sequencing data. 72
Table 2. 4: Over-represented pathways within the list of correlating mRNAs. 76
Table 2. 5: List of DEmiRNA-targeted inflammatory mRNAs with metabolic functions 78
Table 2. 6: Log2 fold change differences in DEmiRNA expression between pulmonary and other tissue types within the healthy rat 82

Chapter 3

Table 3. 1: Concentrations of total RNA and total miRNA within representative samples of rat serum. 107
Table 3. 2: Integrated pathway over-representation analysis for LPS associated metabolites and predicted miR-34b/449 gene targets. 137

Chapter 4

Table 4. 1: Hydrodynamic diameter of BAD and SRM-2975 as determined by DLS..... 159

Table 4. 2: Metal and metalloid content of BAD and SRM-2975 as determined by ICP-MS 160

Table 4. 3 : Metal and metalloid content of U937 lysates following 24 h exposure to 4-25 µg/ml BAD or SRM-2975..... 165

Table 4. 4: Average concentrations of total RNA and total miRNA detected in the lysates of U937s by nanodrop spectroscopy and bioanalyzer small RNA assays. 178

Table 4. 5: Concentrations of total RNA and total miRNA detected in the supernatants of U937s by nanodrop spectroscopy and bioanalyzer small RNA assays. 179

Table 4. 6: Metabolic pathways enriched in the media samples of U937s following particle or endotoxin exposure..... 188

Table 4. 7: Cellular pathways that were enriched for exposure-associated feature metabolites and predicted mRNA targets of miR-449a. 189

Chapter 1. Introduction

1.1 Pulmonary inflammation

1.1.1 Structure and function of the respiratory tract

The respiratory tract functions to allow the continuous exchange of O_2 and CO_2 from the body, facilitating cellular function and removing toxic waste. As such it possesses a gas-exchange region composed of respiratory bronchioles and alveoli and a conducting region that carries air from the nose and mouth (the primary respiratory openings), through the pharynx, larynx and trachea to the lungs and passes through the bronchi and larger bronchioles towards the alveoli. Much of the conducting system (the nose, mouth, pharynx and larynx) is referred to as the upper airways while the remainder (the trachea, bronchi and bronchioles) plus the gas-exchange region make up the lower airways (**Figure 1.1**) (1).

The tubular structures of the respiratory tract are lined by an uninterrupted epithelium containing a mosaic of cell types that originate from the basement membrane. These cells (including basal cells, epithelial cells, goblet cells and clara cells) differ in morphology and distribution according to their function and are coated with a protein and lipid rich epithelial lining fluid (ELF) (2).

Branching from the respiratory bronchioles, the alveoli are suspended in an intricate lacework of connective tissue fibres that extend between the pleura and the alveolar wall (3) and are structured to allow maximal diffusion of gases into and out from the bloodstream (**Figure 1.2**). In addition to their large surface area (~75m^2 in humans) and rich blood supply, 90-95% of their surface area is contributed to by squamous, non-ciliated alveolar type I epithelial cells (AT1). Unlike the ciliated, columnar cells of the conducting region, AT1 possess few organelles and spread broadly over the basement membrane via thin extensions, producing a barrier of only 2-8 μm between the alveoli and the capillary endothelium (4)(5).

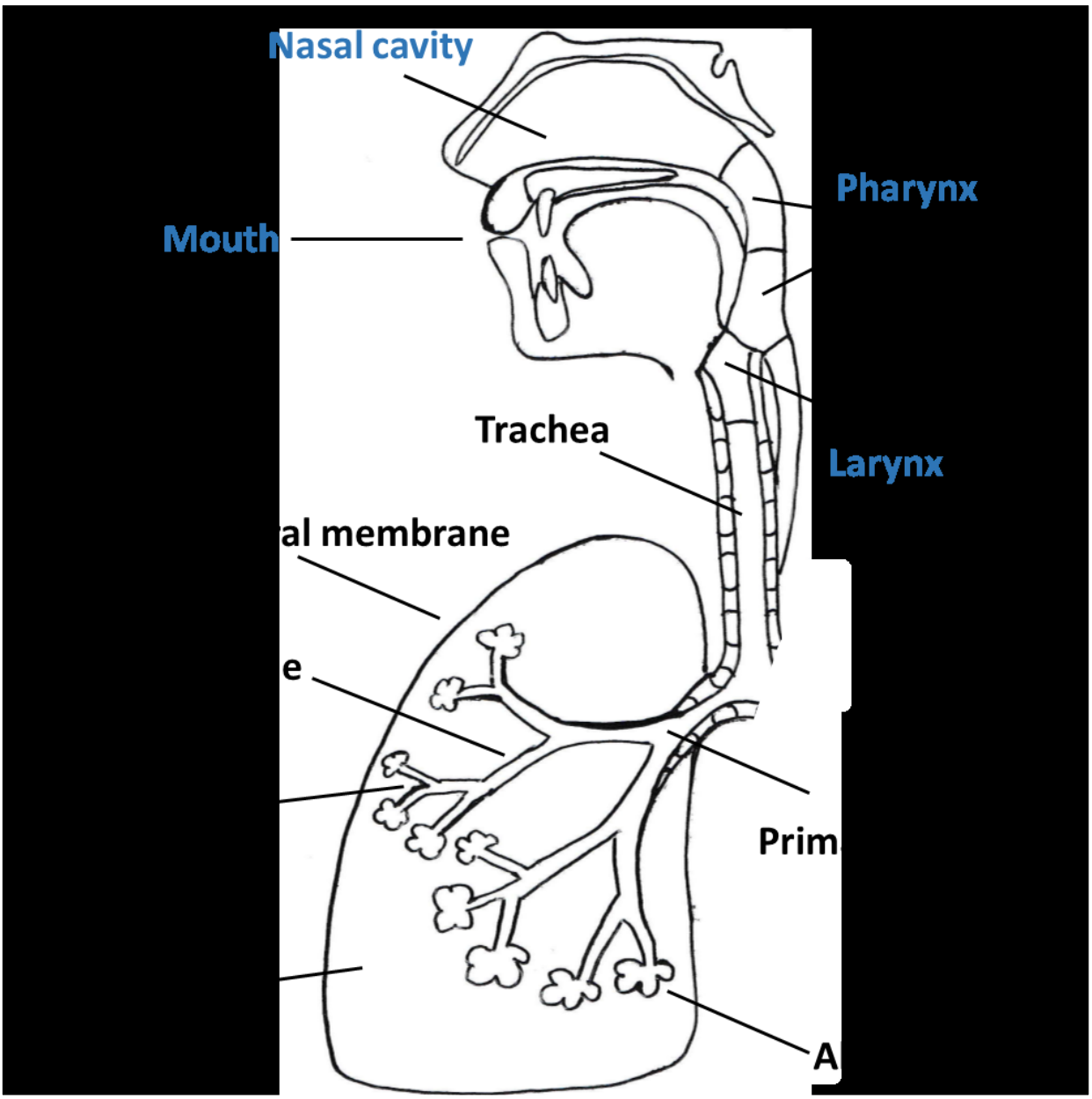


Figure 1. 1: Schematic representation of the human respiratory tract. Features of the upper airways are labelled in **blue**; features of the lower airways are labelled in **black**.

The remaining 5-10% of the alveolar surface is contributed to by cuboidal type II epithelial cells (AT2) which synthesise and secrete surfactant-associated proteins and phospholipids into the alveolar ELF. This protects AT1 from desiccation and prevents the lungs from collapsing at the end of expiration by reducing surface tension in the alveoli (2).

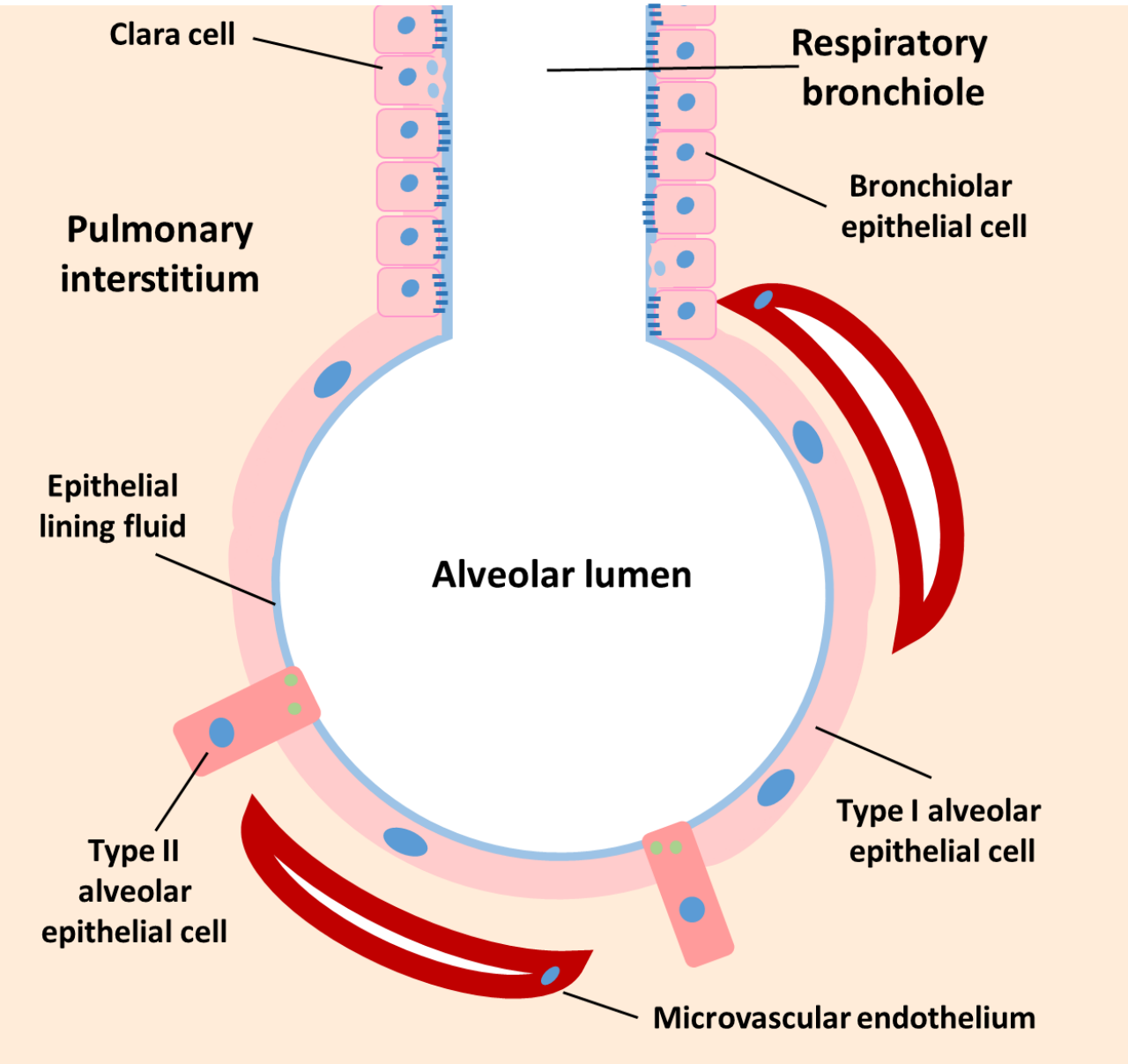


Figure 1. 2: Structural organisation of the gas-exchange region of the lower airways. Branching from the terminal bronchioles, the respiratory bronchioles are lined with ciliated columnar epithelial cells interspersed with secretory Clara cells. Within the alveoli, gas exchange is facilitated by the presence of squamous, non-ciliated AT1 which produce only a thin barrier between the alveolar lumen and the microvascular endothelium. Cuboidal AT2 punctuate the alveolar epithelium where they secrete surfactant into the epithelial lining fluid in order to protect the AT1 from desiccation.

1.1.2 Pulmonary defence mechanisms

Whilst optimising the lungs for gas exchange, the large surface area and thin walls of the alveoli mean that they are highly vulnerable to injury by the pathogens, bio-aerosols, nanoparticles, pollutants and toxic gases that populate inspired air (6). During inhalation, a pressure gradient is generated along the airways, giving rise to convection currents that transport these materials through the airways until diffusional, inertial and gravitational mechanisms cause them to diverge from the airflow streamline and deposit within the ELF (4).

As the primary site of exposure to inhaled agents, the respiratory tract has developed an array of defence mechanisms that neutralise and remove foreign material in order to protect the vital process of gas exchange (6). Most inhaled particles are trapped, neutralised and removed by mechanical and humoral defences in the conducting airways (7), preventing them from reaching the alveoli. Such mechanisms begin in the nose and upper airway with humidification of inspired air and the production of airflow turbulence which encourage smaller hydroscopic particles to clump together and deposit in the periciliary layer of low viscosity mucus that coats the mucosal cells of the epithelium (8,9).

Once trapped, mucosal immunoglobulins, antioxidants, bactericidal enzymes and components of the complement system interact with the particles, degrading pathogenic membranes, reducing oxidative molecules and opsonising non-biological material. Beating cilia move insoluble particles towards the pharyngolaryngeal region to be swallowed or expelled by coughing while liposoluble and hydrosoluble particles are removed through absorption across the epithelium (9).

While these mechanisms prevent the majority of particles from reaching the respiratory airways, gases and smaller particles are able to penetrate the smaller conducting airways and sediment within the alveolar ELF (4). Antioxidant molecules such as glutathione (GSH) and ascorbic acid (AA) can reduce much of the oxidative gases in the ELF, rendering them

less harmful (7) but the lack of a mucociliary layer in this region means that an acute inflammatory response is required to remove deposited particles (5).

1.1.3 Inflammatory defences of the alveoli

Acute inflammation is a non-specific but rapid response to insult by foreign matter which can compartmentalise, destroy and remove injurious agents and promote recovery of damaged tissues (10). In the alveoli this response is initiated by the simultaneous activation of macrophages and epithelial cells, which express a large variety of surface molecules (termed pattern recognition receptors (PRR)) that enable them to recognise a wide range of xenobiotic ligands (including proteins, saccharides, nucleic acids, lipids and opsonisation products) (11).

Upon recognition of these ligands, the receptors initiate numerous signalling cascades that stimulate secretion of antimicrobial products including proteolytic enzymes, reactive oxygen species (ROS) and reactive nitrogen species (RNS) (12) and induce macrophages to remove the foreign material through phagocytic uptake. Here, particles are engulfed within cytoplasmic vacuoles and either fused with lysosomes for subsequent enzymatic degradation, or transported to the lymphatic system (13).

As very few macrophages reside within the alveoli under homeostatic conditions (approximately one macrophage per three alveoli) (14) auxiliary phagocytes must be recruited to sites of contamination in order to remove foreign material rapidly enough to prevent injury or infection from developing. In acute inflammation this support is provided predominantly by neutrophils (rather than monocytes) so activated macrophages and epithelial cells secrete an array of neutrophil-stimulating cytokines, chemokines and lipids that encourage circulating neutrophils to migrate across the pulmonary microvascular endothelium into the alveolar lumen (15).

In healthy adults, circulating neutrophils exist in a resting state, expressing an array of cytokine and chemokine receptors (including those for granulocyte-macrophage colony-stimulating factor (GM-CSF), tumour necrosis factor α (TNF-α) and interleukin (IL)-1β (16) but retaining their arsenal of proteases intracellularly and displaying minimal ROS synthesis. Upon ligand binding in the pulmonary microvasculature, intracellular granules containing pre-synthesised PRRs mobilise to the neutrophilic cell membrane, priming them to phagocytose foreign material and to secrete proteases and ROS within seconds of activation (17).

Mitogen activated protein kinase (MAPK), phosphoinositide 3-kinase (PI3K) and nuclear factor kappa-light-chain-enhancer of activated B cells (NFκB) dependent pathways encourage the neutrophils to migrate towards the microvascular endothelium (16) which is also primed by cytokine exposure; expressing additional cellular adhesion molecules (CAMs) (including P and E selectins, intercellular CAM-1 (ICAM-1) and vascular CAM-1 (VCAM-1)) and additional chemoattractants.

Primed neutrophils tether loosely to the endothelium via interactions between the endothelial selectins and their own. This allows the neutrophils to roll across the endothelium, inducing conformational changes in their surface integrins which, in the presence of endothelial chemoattractant proteins, enable them to bind strongly with ICAM-1 and VCAM-1 on the endothelial surface (17,18). Once bound, neutrophils migrate through the microvascular endothelial layer and alveolar epithelium, towards the source of inflammation, following the chemotactic gradient of epithelial and macrophage derived chemoattractants. Recognition of xenobiotic ligands at the site of exposure activates the neutrophils, encouraging them to secrete their antimicrobial proteases and ROS and aid phagocytosis of foreign material (17).

Initiation of the acute inflammatory response completes a further 24-48 hours later with the recruitment of circulating monocytes. Upon recognition of neutrophilic and endothelial chemokines, monocytes are primed to traverse the alveolar wall in the same manner as neutrophils; through selectin and CAM mediated interactions with the capillary endothelium.

One inside the alveolar lumen, these monocytes differentiate into macrophages, developing a pro-inflammatory M1 phenotype that enables them to assist the phagocytic response (19).

1.1.4 Termination or development of the acute pulmonary response

In health, acute pulmonary inflammation is a self-limiting process that subsides to basal state within days of an inflammatory stimulus being detected, rapidly returning the tissue to homeostasis. However, in instances of excessive or continuous inflammatory stimulation, the response can become unrestrained, developing into injurious chronic inflammation and damaging the pulmonary parenchyma (20).

Acute inflammation does not terminate simply through an absence of the stimulus and downstream signalling responses but via an active, co-ordinated process called resolution which inhibits and counteracts the mechanisms of inflammatory initiation. Resolution removes neutrophils and debris from the alveoli (efferocytosis) and inhibits efflux of further neutrophils, enabling efficient gas-exchange to continue (21).

Inflammatory resolution is primed during the initial stages of neutrophil efflux; interactions with the microvascular endothelium and with prostaglandin-2 (PGE-2) stimulate the neutrophils to express annexin A1 and produce an array of pro-resolving lipid metabolites (including lipoxins and resolvins) (22). These products replace the pro-inflammatory cytokines, leukotrienes and prostaglandins that were produced during propagation of the inflammatory response and encourage the neutrophils to undergo apoptosis (the first hallmark of resolution) (21).

During apoptosis, neutrophils attenuate further neutrophillic influx (the second hallmark of resolution) by sequestering tissue-derived chemokines in their non-functional surface receptors. They also release α-defensin peptides which work in tandem with the pro-resolving lipid metabolites, promoting M1 macrophages to acquire an anti-inflammatory, pro-resolving M2 phenotype and commence the process of efferocytosis (21).

Ingestion of neutrophils initiates a positive feedback mechanism within the macrophages; encouraging up-regulation of pro-resolving and anti-inflammatory mediator secretion, synthesis of chemokine-targeting proteases and further efferocytosis of neutrophils. Once the macrophages reach their engulfment threshold they become ‘satiated’, lose their ability to respond to xenobiotic ligand recognition and migrate to the lymphoid organs, returning the alveolar cellular content to basal levels (23).

Where these mechanisms of resolution are impaired or outbalanced by the magnitude of pro-inflammatory stimulation, neutrophils and macrophages accumulate in the alveoli where they continue to secrete pro-inflammatory mediators, ROS and proteases. This activity transitions the response into chronic inflammation and leads to degradation of the proteinaceous structures of the parenchyma, driving a reduction in gas-exchange capability and development of fibrotic tissue (24). Together these factors propel the lungs towards pathophysiology, leading to the development or exacerbation of inflammatory diseases such as emphysema, chronic obstructive pulmonary disease (COPD), bronchiolitis, asthma, acute lung injury (ALI) or cystic fibrosis (CF).

1.2 Traffic related particulate matter and pulmonary inflammation

1.2.1 Traffic related particulate matter

As well as noxious gases, road transport activity expels heterogeneous mixtures of particulate matter (PM). Commonly divided into coarse (PM_{10}), fine ($PM_{2.5}$) and ultrafine ($PM_{0.1}$) fractions (> 10 μm, < 2.5 μm or < 0.1 μm in diameter respectively), these materials can also be distinguished by source.

Approximately half of traffic related PM (TRPM) is expelled in the exhaust (25), through incomplete combustion of fuels and through volatilisation of lubricant oils during the combustion process. These particles are primarily carbonaceous, consisting of an elemental carbon core upon which organic compounds (including polycyclic aromatic hydrocarbons (PAHs) and nitro-PAHs), sulphates, nitrates, metals and bacterial endotoxins adsorb at trace levels (26,27).

The remaining particles originate from friction-induced wear of mechanical components such as the clutch or brakes, abrasion of the tyres, road surface and road furniture and re-suspension of dust from the road-surface (non-exhaust related PM)(28). These particles vary considerably in terms of composition with brake abrasion dust (BAD) being characterised by high concentrations of Fe, Cu, Zn, Zr, Sn and Sb (29,30) while tyre wear is found in association with road surface materials and contains large quantities of rubber hydrocarbons, carbon black and Si with only trace levels of other metals (29).

1.2.2: Associations between TRPM exposure and pulmonary inflammation

Considerable fractions of exhaust and non-exhaust PM fall within the inhalable and respirable size ranges (defined as ≤ 10 and 4 μm respectively) (31). As examples, 86 and 30% of BAD and road surface abrasion particles (respectively) contribute to total PM_{10} and are inhalable beyond the larynx while a further 63 and 15% (respectively) are classified as $PM_{2.5}$ and can reach the unciliated airways (32,33). In contrast, fresh diesel exhaust particles

(DEP) are smaller than non-exhaust particles, with 92% possessing an aerodynamic diameter ≤ 1μm (34). These properties enable TRPM to deposit in a widespread manner along the respiratory tract with coarse particles impacting in the upper airways and fine and ultrafine particles sedimenting between the trachea and alveoli (35). Human activities (such as commuting and living amongst a rich road infrastructure) mean that exposure is ubiquitous for much of the population with TRPM contributing 25% of ambient $PM_{2.5}$ and PM_{10} levels globally (36) and concentrating in heavily populated regions (37) and commuter routes (38).

Epidemiological studies consistently report that exposure to TRPM associates with the increased onset and prevalence of pulmonary inflammatory pathophysiologies in human populations. Such studies include analyses of hospital data which correlate ambient concentrations of PM_{10} and $PM_{2.5}$ (of which TRPM is a major component) with admissions for asthma (39) acute bronchitis and pneumonia (40) and associate ambient $PM_{0.1}$ exposure with increased relative risk of admission for total respiratory diseases (41).

These findings are supported by analyses of symptom diaries and medical records which report greater prevalence and onset of chronic phlegm production, cough, asthma and COPD in adults and children who are exposed to high levels of urban PM_{10} (42,43) or live in close proximity to major roadways (44,45). Furthermore, acute chamber exposures to fine and ultrafine ambient PM or DEP enhanced neutrophil and monocyte concentrations in the bronchoalveolar lavage fluid (BALF) and sputum of healthy volunteers (46,47) validating observations that TRPM exposure induces pulmonary inflammatory responses *in vivo*.

Concern surrounding TRPM- induced inflammation is enhanced by the breadth of sub-populations that possess biological or behavioural traits that make them more susceptible to pro-inflammatory stimulation by particles. Behaviourally these traits centre around exposure dosage and include the large number of individuals who commute long hours, live areas of high traffic density, work in transport, or spend a lot of time outside (38,48).

Biological susceptibility factors are varied and include age (children have immature lungs and immune systems while alveolar macrophage clearance is significantly reduced in the elderly) and polymorphisms in genes that encode antioxidants and components of inflammatory or detoxification pathways (48,49). They also encompass pre-existing, chronic inflammatory pathophysiologies which are exacerbated by episodes of TRPM exposure, causing physiological deterioration, increased airway inflammation and mortality.

1.2.3: Mechanisms of TRPM-induced pulmonary inflammation

Although the molecular pathways by which TRPM induces and mediates pulmonary inflammation are not fully characterised, it is widely hypothesised that they are induced in response to oxidative stress (50,51) (**Figure 1.3**). This injurious state develops when concentrations of ROS (such as superoxide anions, hydrogen peroxide and hydroxyl radicals) outweigh concentrations of protective anti-oxidant enzymes and proteins, preventing them from being inactivated and excreted from biological environments (52,53).

Usually electrons orbit the nucleus of their atom in pairs but in the case of ROS, unpaired electrons exist within the atomic nuclei and encourage the molecules to react indiscriminately with their neighbours to gain one of their electrons (oxidation and reduction). This becomes injurious where the neighbouring molecule is a lipid, protein or nucleic acid as the molecular structure of the target (including binding and active sites) can become impaired and lose or alter its function (53). Such damage occurs via three primary mechanisms; direct mutation of DNA structures, modification of caspases and enzymes required for DNA repair and peroxidation of lipids with downstream activation of the arachidonic acid pathway, resulting in the production of DNA damaging lipid metabolites (54).

The oxidative potential of TRPM has been demonstrated directly in acellular systems with hydroxyl radicals being produced by urban dust and diesel exhaust particles (55,56) and the antioxidants, glutathione and ascorbic acid being depleted from synthetic ELFs by carbon black (57). These activities are widely attributed to the synergistic actions of transition metal

ions and PAHs (58) which permit the particles to generate ROS through redox cycling with neighbouring molecules, resulting in a depletion of antioxidant pools (59).

Many of the metals that are found in high abundance on TRPM exist stably in more than one valence state, allowing them to catalyse electron transfer and generate ROS directly (59,60). Iron, for example, catalyses the Fenton reaction in its ferrous state, oxidising H_2O_2 to hydroxyl radicals and hydroxide ions while vanadium, chromium and cobalt produce ROS via the Haber-Weiss reaction. Such reactions can occur on the surface of particles, producing either surface bound ROS or within the ELF via the action of dissolved metal ions (61).

In contrast to metals, PAHs are chemically inert in their environmental form and require metabolic activation to display redox activity. Once metabolised to quinones by cytochrome P450 enzymes and epoxide hydrolases however, they are capable of redox cycling with hydroquinone and semiquinone structures and inducing endogenous ROS production by disrupting the mitochondrial electron transport chain (60).

The progression from oxidative stress to inflammation is induced by activation of redox-sensitive MAPKs and transcription factors (TFs) such as NFκB and AP-1. Following exposure to ambient PM or DEP, these key regulators of pro-inflammatory mediator expression have been demonstrated to be induced in a redox-dependent manner in airway macrophages and epithelial cells .

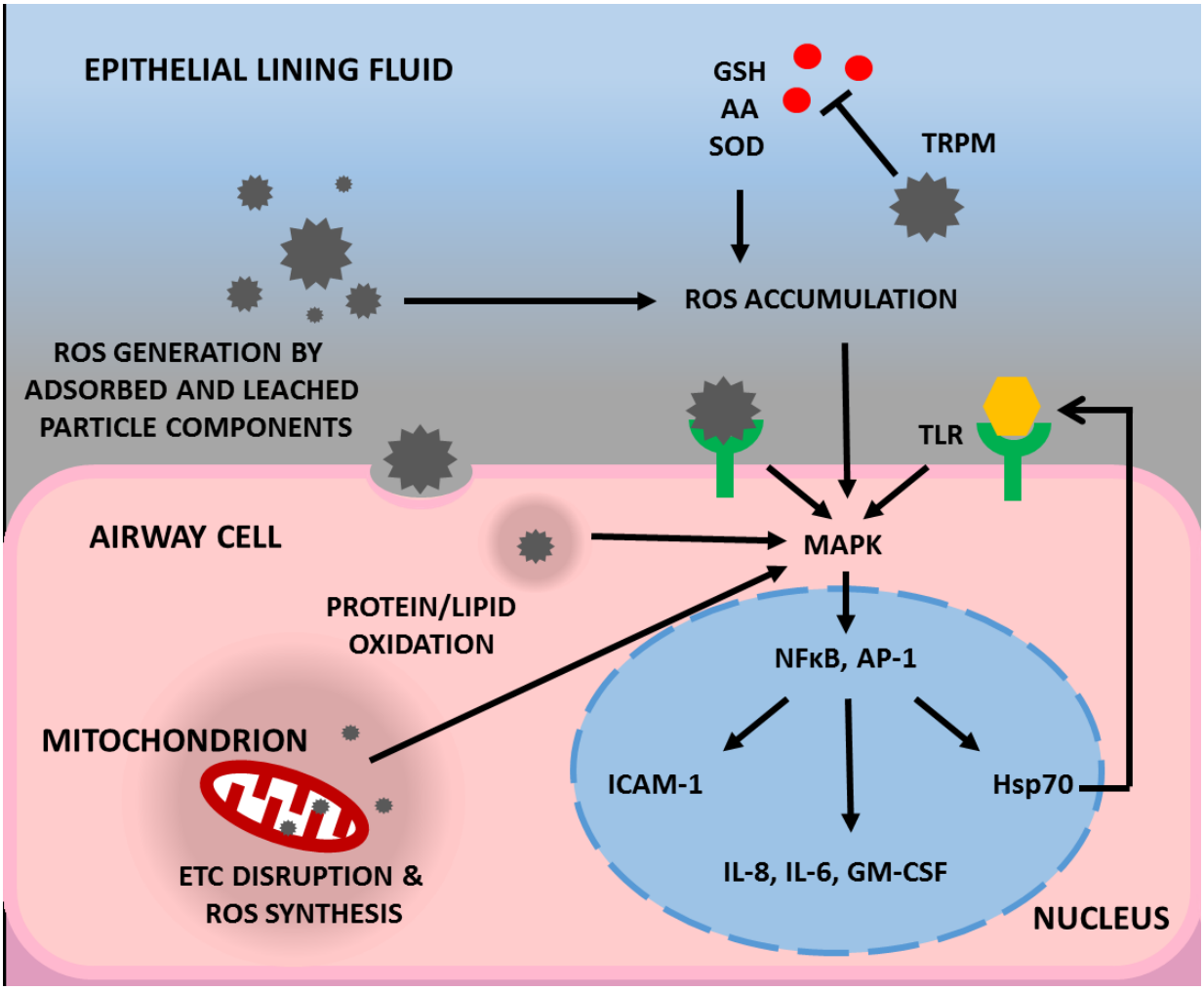


Figure 1. 3: Known mechanisms of TRPM induced inflammation: Following inhalation, TRPM deposits within the ELF where it is capable of inhibiting antioxidant enzymes and generating ROS through redox cycling and metal catalysed electron transfer reactions. As well as promoting extracellular ROS accumulation, many TRPM components are ligands for TLRs, stimulating cytokine, CAM and heat shock protein expression via MAPK dependent activation of NFκB and activating protein 1 (AP-1). Such activity is amplified at the level of MAPK stimulation by the oxidation products of interactions between internalised particles and cellular macromolecules and by ROS that is produced by ultrafine particles entering the mitochondria and disrupting electron transport chain activity. Similarly, heat shock proteins contribute a positive feedback mechanism, stimulating TLR activity in parallel to the TRPM.

Using these systems, increases in TF activity were attributed to the activation of stress related MAPKs which phosphorylated cytosolic subunits of NFκB and AP-1, activating them to translocate into the nucleus (62), enhance expression of cytokines, chemokines and ICAM-1 and promote cyclooxygenase-2 mediated secretion of PGE-2 (62–66). These findings have been supported by proteomic evidence that DEP induces a hierarchical oxidative stress response; stimulating transcriptional activation of phase II antioxidant enzymes at low concentrations, inducing pro-inflammatory NFκB mediated cascades at intermediate concentrations and causing mitochondrial damage and pro-apoptotic signalling at high concentrations (67).

Further to the redox-induced response, induction of NFκB and AP-1 signalling pathways is heightened by the activity of TLRs. Exposure to $PM_{2.5-10}$ has been shown to enhance expression of TLR-4 in bronchial epithelial cells (BEC) (68) and to interact directly with TLR-4 and TLR-2 in cultures of airway epithelial cells and macrophages (69). Such activity may occur in a composition dependent manner with metal rich particles displaying affinity for TLR-2 and endotoxin-bound particles interacting with TLR4 (70). TLR signalling may also be enhanced by interactions with heat shock proteins such as Hsp70 which are over-expressed after exposure to $PM_{2.5-10}$, DEP and tyre wear particles (68,71,72) and have an affinity for TLR binding.

1.3: Biomarkers and their application to TRPM-induced toxicity

Biomarkers are indicators of molecular, biochemical, cellular or physiological changes that are measurable in biological samples following or during a response to an environmental exposure, therapeutic intervention or a pathophysiological event (73). In toxicology, biomarkers are used to quantify exposure to xenobiotic agents, characterise the mechanisms that underlie adverse responses to specific exposures and to predict likely responses to novel exposures or products (74). Importantly for the field of particulate toxicology, they may also be used as indicators for tissue damage that cannot be measured directly (75). In contrast to the field of medicine (which relies heavily on the use of prognostic and diagnostic markers), toxicological markers are categorised as representative of exposure, response or susceptibility according to the information that they provide (**Figure 1.4**). Internal exposure biomarkers include exogenous substances and their metabolites (e.g. PAHs and quinones) that can be detected within a biofluid or tissue (76). These markers can be especially advantageous for epidemiological studies because their concentrations are influenced by interpersonal variation in absorption, distribution and excretion of exogenous agents. Thus they can often provide a more robust indication of internal and target site exposure than estimations made using traditional biomonitoring methods (including personal and fixed site monitors). Instead, these traditional approaches measure exposure externally without providing evidence of which tissues are influenced by the exposure, the proportion of the substance/ metabolite that interacts with them or the duration of interactions with specific metabolites of the substance (74).

Susceptibility markers include inherent or acquired features (primarily genetic polymorphisms) that facilitate responses to specific environmental challenges (76). Such markers generally influence the rates by which xenobiotics are metabolised following exposure, affecting the balance between phase I (bio-activation) and phase II (conjugation) metabolic activity by altering the expression or kinetics of metabolic enzymes and their receptors (77). As examples, individuals with enhanced cytochrome P450 (CYP) activity (a

phase I metabolic enzyme) may produce higher concentrations of toxic metabolites following xenobiotic exposure while individuals with decreased phase II enzyme expression will detoxify and excrete harmful metabolites at a lower rate.

Response biomarkers represent the adverse or adaptive biochemical changes that occur within cells, tissues and biofluids following xenobiotic exposure (76). They include induction or repression of gene expression, alterations in circulating metabolite profiles, production of antibodies for specific xenobiotics and the appearance of DNA adducts. Clara cell secretory protein (CC16) is a prominent example of a response biomarker used in respiratory toxicology. Synthesised primarily by Clara cells of the tracheobronchial tree, concentrations of this anti-inflammatory protein are altered in BALF and serum following exposure to inflammatory agents (78,79). Such changes occur as a result of compromised epithelial integrity (80), meaning that movement of CC16 into the serum can be used as a marker of pulmonary epithelial damage.

Compared with exposure or susceptibility biomarkers, response markers are most informative during characterisation of toxicity mechanisms. In contrast to exposure biomarkers, response biomarkers are generally facilitators, regulators or products of biochemical pathways and thus provide indications of which pathways are induced or inhibited downstream of exposure. Furthermore, changes in the concentration or expression of response biomarkers demonstrate that the pathways alterations have already occurred, rather than have the potential to occur as susceptibility markers might suggest.

As such, our understanding of the mechanisms that mediate TRPM-induced pulmonary inflammation could be progressed through identification of response biomarkers that represent the molecular interactions and pathways that are involved in the process. Unlike existing exhaust exposure markers (such as urinary amino-PAHs (81,82) and phenanthrene (83)) and susceptibility markers (including polymorphisms on chromosome 17, chromosome 11 and the CYP1A1 gene (84,85)) they could provide evidence of which molecular and cellular functions are influenced by TRPM exposure.

While response biomarkers may be sought from tissues, cells or biofluids (73), detection using non-invasively accessible samples is an attractive proposition. Traditionally, studies of pulmonary inflammation have used tissue biopsies but this option can be painful and is ethically challenging, leading to a scarcity in samples obtained from healthy subjects that are not confounded by underlying pulmonary diseases or cancers. Similarly, collection of BALF samples for the detection of inflammatory cell infiltrates is highly invasive and thus, does not appeal widely to study participants.

In contrast, samples such as blood, urine or breath condensates can be obtained quickly and painlessly, encouraging greater study participation in healthy populations and in patients with existing pulmonary complications for whom invasive, non-critical procedures are inadvisable (86). As a result, detection of response biomarkers that exist within these accessible samples because of TRPM exposure would enable the adverse outcomes of TRPM exposure to be detected, characterised and monitored in large human cohorts. This would enhance the representability of study cohorts to the population as a whole and provide physiologically relevant models for mechanistic characterisations.

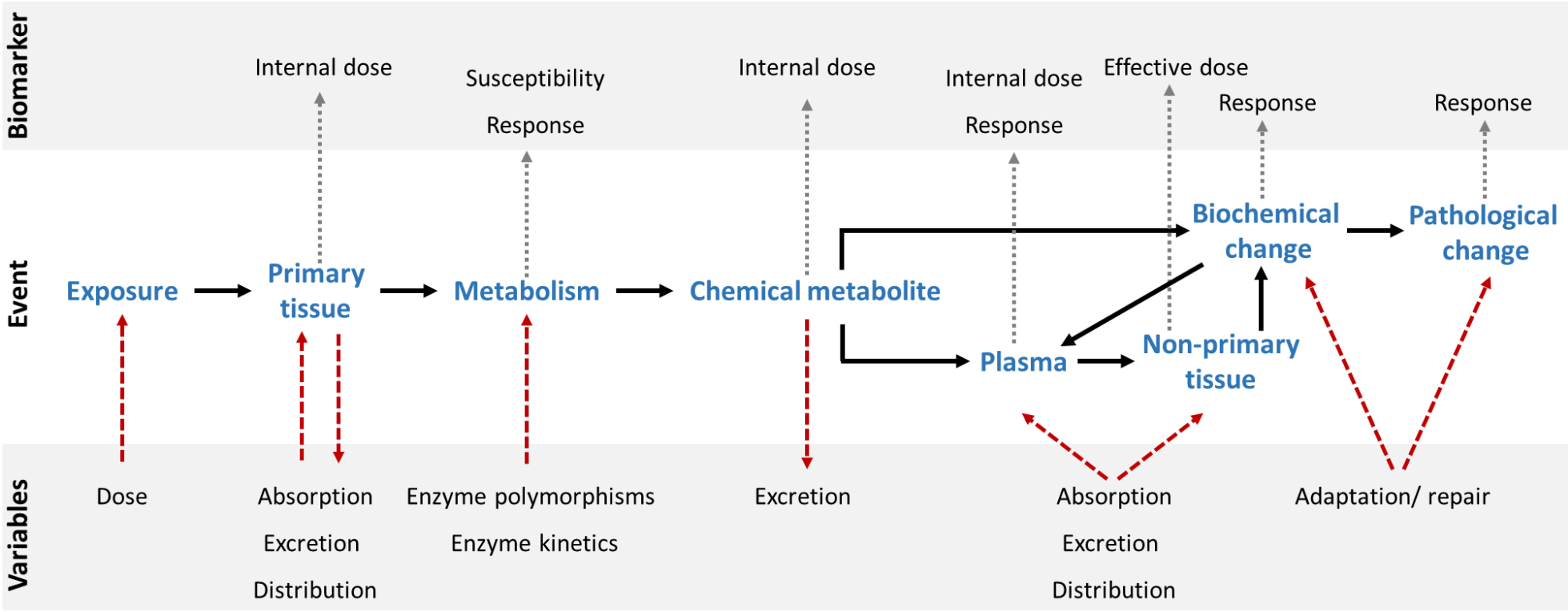


Figure 1. 4: The nature and interplay of relationships between biomarkers following the response to an environmental exposure. Concentrations of xenobiotics within the primary site of exposure provide simple markers of internal dose providing the pharmacokinetic properties of the xenobiotic are measurable or understood. The rate at which the xenobiotic is metabolised (if at all) and the products that these reactions produce provide markers for cellular responses that are induced by the exposure, information regarding individual susceptibility to the toxicity and measures of exposure that incorporate the pharmokinetic properties of the molecule. Biomarkers that illuminate interactions between primary and secondary response sites may be detected within the blood, along with xenobiotic metabolites that are excreted from the primary tissue. Further excretion via the urine or reabsorption of metabolites into non-primary tissues make these biomarkers transient in nature but also facilitates measurement of effective doses in target tissues. The outcomes of interactions between the xenobiotic, its metabolites and host cells may be detected through biochemical changes at primary and non-primary sites. Such changes provide mechanistically relevant biomarkers for the pathways involved in adaptation to exposure or cellular repair and may be used to explain the appearance of pathological changes (Adapted from Timbrell *et al.* (74)).

1.3.1 Hypothesis-driven response biomarker discovery

It has been suggested that markers of responses to chemical exposures (such as the pulmonary response to TRPM exposure) should link backwards to the source of exposure and forwards to the downstream effects of the exposure (87), thus belonging to the 'response' category whilst correlating strongly with measurements of exposure. In relation to exhaust PM exposure, multiple groups have identified markers that meet these criteria, associating TRPM exposure with traditional parameters of toxicity. As examples, ambient DEP and carbon black concentrations have been shown to correlate with decreased CC16 concentrations in BALF (88,89) and with enhanced levels of circulating ICAM-1 (a marker of vascular endothelial dysfunction) (90). Biomarkers for pulmonary responses to non-exhaust particles are yet to be sought specifically but exposure to total truck emissions has been correlated with concentrations of the urinary oxidative stress marker 8-hydroxy-2'-deoxyguanosine and circulating IL-6 with a plausible contribution from metallic non-exhaust PM (81).

These studies have been of considerable value epidemiologically; confirming that the inflammatory and oxidative endpoints that have been observed *in vitro* following TRPM exposure also develop in human lungs under real world exposure conditions. They are however, limited in terms of expanding our understanding of the molecular mechanisms that initiate and propagate TRPM-induced responses because they are hypothesis driven in nature; quantifying cellular processes that are already established as TRPM-associated.

1.3.2 Data-driven biomarker discovery

Recent advances in high throughput technologies and multivariate statistical analysis are helping toxicologists to augment hypothesis-driven approaches to biomarker discovery (75). 'Omics' is a linguistic umbrella term that encompasses a number of high throughput approaches that can quantitatively and qualitatively characterise the expression profiles of different molecular species within bio-samples, measuring 100s-1000s of variables simultaneously (91).

The range of molecular species that can be examined in this manner has increased rapidly over the past decade and includes genomic sequences, expressed genes, proteins, lipids, metabolites, epigenetic features and microRNAs (miRNAs) (91), most of which are easily detectable in accessible bio-fluids. In contrast to the hypothesis-driven approach to biomarker discovery, the initial analyses are agnostic in nature and statistical comparisons of changes in the expression patterns of these molecules after experimental exposures tend to highlight panels of molecules that contribute to cellular responses to the stimulus (92). Collectively, these molecules possess strong biomarker potential which can be harnessed for mechanistic exploration using computational pathway based approaches to identify which cellular processes and molecular interactions they represent. These approaches (including enrichment and over-representation analyses (ORA)) search databases of manually curated pathway annotations for statistically significant overlaps between the panel of biomarker molecules and the molecular content of hundreds of previously characterised pathways. The hypothesis-free manner of these searches means that novel relationships can be discovered between phenotypes and pathways, furthering knowledge of how that phenotype develops (93).

The potential that omics-based biomarker discovery has to further our understanding of pulmonary responses to TRPM exposure has been demonstrated indisputably by Xiao *et al.* (2003). Using proteomic screens, the group showed that DEP exposure stimulated an 8-fold increase in new protein expression in RAW 264.7 macrophages that was reflective of a

hierarchical response to oxidative stress. After low exposure doses (≤ 10 μg/ml) the macrophages up-regulated synthesis of antioxidant enzymes, after mid-exposure doses (10-50 μg/ml) they produced pro-inflammatory signalling proteins and after cytotoxic exposures (≥ 50 μg/ml) they synthesised additional regulators of mitochondrial function and apoptosis (94). While many of these proteomic changes validated hypothesis-driven knowledge of how macrophages respond to exhaust particle exposure, others (including the induction of receptor-induced apoptosis) were previously uncharacterised (94). These newly identified changes provided novel biomarkers for pathways that are triggered by DEP-induced oxidative stress, progressing our understanding of the response.

Transcriptomic and metabolomic screens have also associated DEP exposure with cellular processes that occur downstream or in tandem with inflammation, thus providing more information than can be achieved through quantification of cytokines or cellular infiltration alone. Microarrays have indicated that bacterial phagocytosis (a process consistently found to be impaired by DEP exposure (95,96) and regulated by cytokines (97)) may be influenced by alterations in expression of genes that reflect cytoskeletal rearrangements (98) while metabolomic screens have detected changes in rates of energy metabolism (99,100) that may be caused by immune cell infiltration and activity (101).

1.3.3: Multi-omics approaches to data-driven biomarker discovery

Biological entities have a complex content; alterations in the expression of individual molecular species, their regulation and their activity is highly dependent on that of the other molecular species. For example, gene expression is dependent on the presence and transcription of intact genetic sequences and influences rates of protein synthesis, having downstream effects on protein-protein interactions and metabolic reactions (91) (**Figure 1.5**). As such, the mechanistic value of omics-derived biomarkers can be enhanced by integrating multiple types of dataset e.g. metabolomic and transcriptomic or proteomic and miRNomic profiles (102).

In the context of TRPM exposure, this concept is supported by transcriptomic validation of Xiao *et al.*'s hierarchical proteomic response to DEP exposure (detailed above). Koike *et al.* (2002) demonstrated that exposure to DEP at 10 μg/ml induced expression of genes that encode pro-inflammatory mediators but not antioxidant enzymes (103) and Jardim *et al.* (2009) indicated that such changes could be induced by miRNA regulation of canonical signalling pathways (104).

Multi-omics analysis is often achieved using a split study design, whereby multiple samples are harvested from a single experimental set up and split by volume or by fraction for data acquisition using separate platforms. The resulting data can be integrated to three levels; *conceptual* where biomarkers are sought from the datasets separately and the conclusions matched, *statistical* where associations such as correlations are sought between features of both datasets and *model based* where parameters of one biomarker can be predicted by known parameters of another (102). These systems approaches encompass the interconnecting nature of molecular networks and can provide the added benefit of validating conclusions drawn from single omics analyses (102).

When designing analytical workflows for experiments that aim to integrate data from multiple molecular platforms, it is important to consider the nature of relationships that exist between the different molecular species. Proteomic data (for example) can be linked directly to the transcriptome, providing a strong rationale to seek correlations between the two datasets but expression of an enzyme-encoding gene and activity of that enzyme as part of a biochemical pathway are separated by multiple regulatory steps (**Figure 1.5**) with variable time-courses. As such, strong correlations are not always seen between transcriptomic and metabolomic data meaning that conceptual integration via ORA can be a more informative and reliable option (102), particularly where mechanistic links are sought between different species of biomarkers. Indeed, Cavill *et al.* (2011) found that pathway level integration of transcriptomic and metabolomic data improved the detection rate of mechanistically relevant

pathways by 76% when applied to the context of chemotherapeutic-induced responses (105).

1.3.4: Integration of microtranscriptomic and metabolomics datasets

Recently, pathway-based approaches have been used to integrate microtranscriptomic (referring to the complement of miRNAs within a sample) and metabolomic datasets (to be presented in detail shortly). By including differentially expressed miRNAs and disease-associated metabolites in a combined ORA, miR-642 and 142 were identified as drivers of disrupted phospholipid homeostasis in varicose vein development (106). Similarly, alterations in energy metabolism pathways have been associated with miR-122 activity during a study that used cellular models to verify predicted links between changes to the microtranscriptome and metabolome following gastric bypass surgery *in vivo* (107).

Metabolomic and microtranscriptomic profiles may contribute mechanistically relevant insights independently, but this integrative approach enables an additional depth of mechanistic detail to be harvested from the data. By identifying pathways that are significantly altered at both molecular levels, it demonstrates how dysregulation of post-transcriptional regulatory networks can contribute to changes in metabolic reactions under experimental or pathophysiological conditions.

Only a few studies have explicitly explored the possibility that miRNA networks contribute to regulation of metabolic processes during toxicological responses (108,109). However, targeted studies indicate that a range of miRNAs regulate xenobiotic bioactivation and distribution by targeting transcripts for CYP450 enzymes and ATP-binding cassette (ABC) transporters (110). Given that bioactivation of PAHs by CYP450 enzymes is strongly implicated in TRPM toxicity (60) and that exhaust PM is thought to regulate xenobiotic transporter expression through activation of aryl hydrocarbon receptor cascades (111) it is likely that these interactions between the microtranscriptome and metabolome can be detected in relation to TRPM-exposed samples.

By performing pathway-based integrations of global and agnostic miRNA and metabolite profile data, it should be possible to extend associations between the microtranscriptome and metabolome to cellular processes that occur downstream of TRPM bioactivation. Integrated Molecular Pathway-Level Analysis (IMPaLA) is a publically available web-tool that performs a combined pathway ORA using differentially expressed genes and feature metabolites (105). By identifying pathways that are significantly over-represented at both molecular levels, this tool highlights which metabolic pathways are contributed to by changes in the transcriptome. If the transcriptomic input consisted of predicted targets of TRPM-associated miRNA biomarkers, analysis using IMPaLA could produce hypotheses for how TRPM-induced changes in the metabolome are regulated at the post-transcriptional level. This would enhance the mechanistic value of both the miRNA and metabolite biomarkers that contribute to the pathways and accelerate characterisations of cellular responses to TRPM exposure.

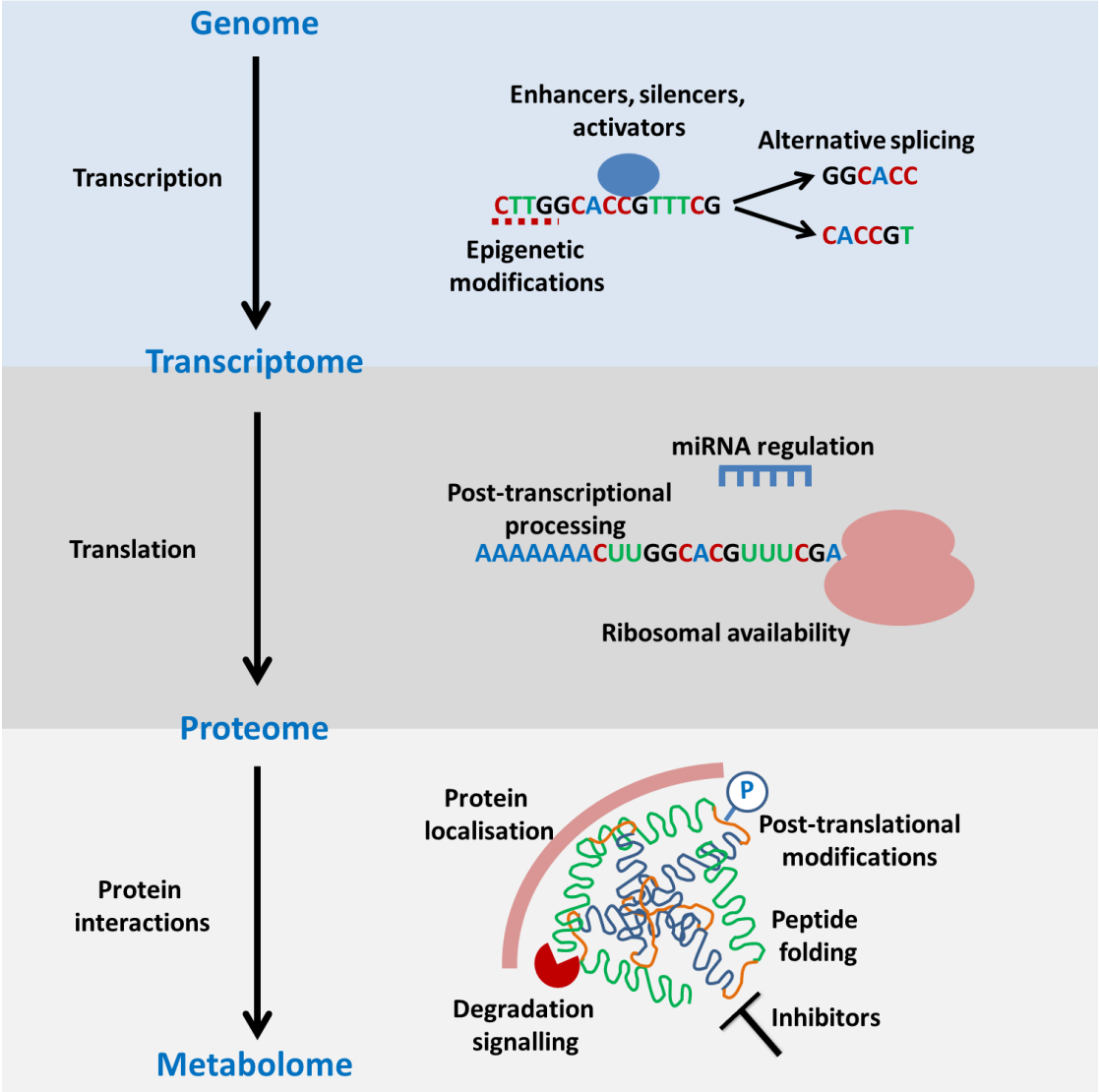


Figure 1. 5: Omics profiles are influenced by regulators of transcription, translation and protein-protein interactions. Complexity of the transcriptome is contributed to by factors including alternative splicing of mRNA transcripts (112), the presence of activator or silencing proteins and enhancer sequences (113), epitranscriptomic modifications and posttranscriptional RNA editing (114). In addition to these factors, protein abundances may be influenced by miRNA activity, integrity of pre-mRNA processing and the availability of ribosomes and transfer RNA (115). The metabolome represents the output of protein activity and is thus influenced by regulators of the transcriptome and proteome along with integrity of peptide folding, post-translational protein modifications (e.g. activating phosphorylation), correct cellular localisation or substrates and enzymes, and the presence or absence of protein degradation signals or inhibitors (116)).

1.4 miRNAs

miRNA have strong potential for use as non-invasive and mechanistically relevant biomarkers due to their major contribution as regulators of the eukaryotic genome, their relative stability and their rich presence in accessible biofluids. Discovered in 1993, miRNAs are endogenous single stranded non-coding RNA molecules of approximately 19-24 nucleotides (nt) that function to regulate gene expression at the post-transcriptional level (117). To date ~ 28650 miRNAs have been discovered in human samples (118) and due to their ability to regulate hundreds of different genes each, are estimated to control the expression of more than 60% of human protein encoding genes and contribute to the activity of almost every genetic pathway (117). As such, miRNA biomarkers have the potential to provide a considerable amount of information regarding the pathways that are dysregulated in response to an environmental exposure.

1.4.1 Biogenesis of miRNAs

miRNAs are encoded by stem loop structures which disseminate throughout the genome, residing individually or as polycistronic clusters within the introns or exons of protein-coding genes (intragenic) or between transcriptional units (intergenic). In response to transcription factor activity, miRNA genes are transcribed into primary transcripts (pri-miRNAs) by RNA polymerases II and III (for intra and intergenic miRNAs respectively). These molecules can be several kilobases long and, like mRNA transcripts, possess 5' caps and 3' polyadenylated tails. As the pri-miRNAs are transcribed, Drosha (a ribonuclease III like endonuclease) cleaves them into shorter (~65 nt) precursor miRNA transcripts (pre-miRNAs) that fold into hairpin loop structures and display a 2nt 3' overhang that signals for them to be transported from the nucleus into the cytoplasm by exportin 5 nuclear export factors (117,119,120).

Within the cytoplasm pre-miRNAs interact with Dicer (a second ribonuclease III like endonuclease) that cleaves the loop, creating double stranded duplexes of 19-24 nts which complex with ribonucleoproteins including argonaute (Ago) proteins to form a miRNA

inducing silencing complex (miRISC)) (117,119,120). This complex is activated through selection of guide and passenger strands within the duplex; the strand with least thermodynamic stability at its 5' terminus (the guide strand) is incorporated into the complex while the remaining strand (the passenger strand) degrades or unwinds from the duplex (121) (**Figure 1.6**).

1.4.2 Post-translational regulation by miRNAs

The miRISC is directed to target mRNAs via the 'seed' sequence of the incorporated miRNA. This 6-8 nt sequence is located at the 5' end of the molecule and binds via Watson-Crick complementarity to 'seed match' sequences within the mRNA transcript (often within the 3' untranslated region). These miRISC-mRNA interactions are well documented to repress synthesis of the target peptide, causing site-specific cleavage or enhanced degradation of the mRNA transcript, inhibition of translation or proteolytic degradation of newly translated peptides **(Figure 1.7**).

The mechanism of repression that follows miRNA-mRNA binding depends partially on the degree of complementarity that exists between the miRNA seed and mRNA seed match sequences but is also influenced by the selection of Ago proteins that are present in the miRISC (122). In cases of perfect or near perfect matching, the miRISC is able to degrade the target mRNA via endonucleolytic cleavage but only where a catalytically competent Ago is present. This mechanism, referred to as RNA interference, is common in plants but mammals possess only one Ago protein that is capable of cleaving mRNA (Ago2) and their miRNA-mRNA duplexes are often interrupted by mismatches or gaps (122). In contrast, all four mammalian Ago proteins (Ago1-4) are capable of performing non-cleavage based mechanisms of repression and commonly do so where mismatched pairing occurs.

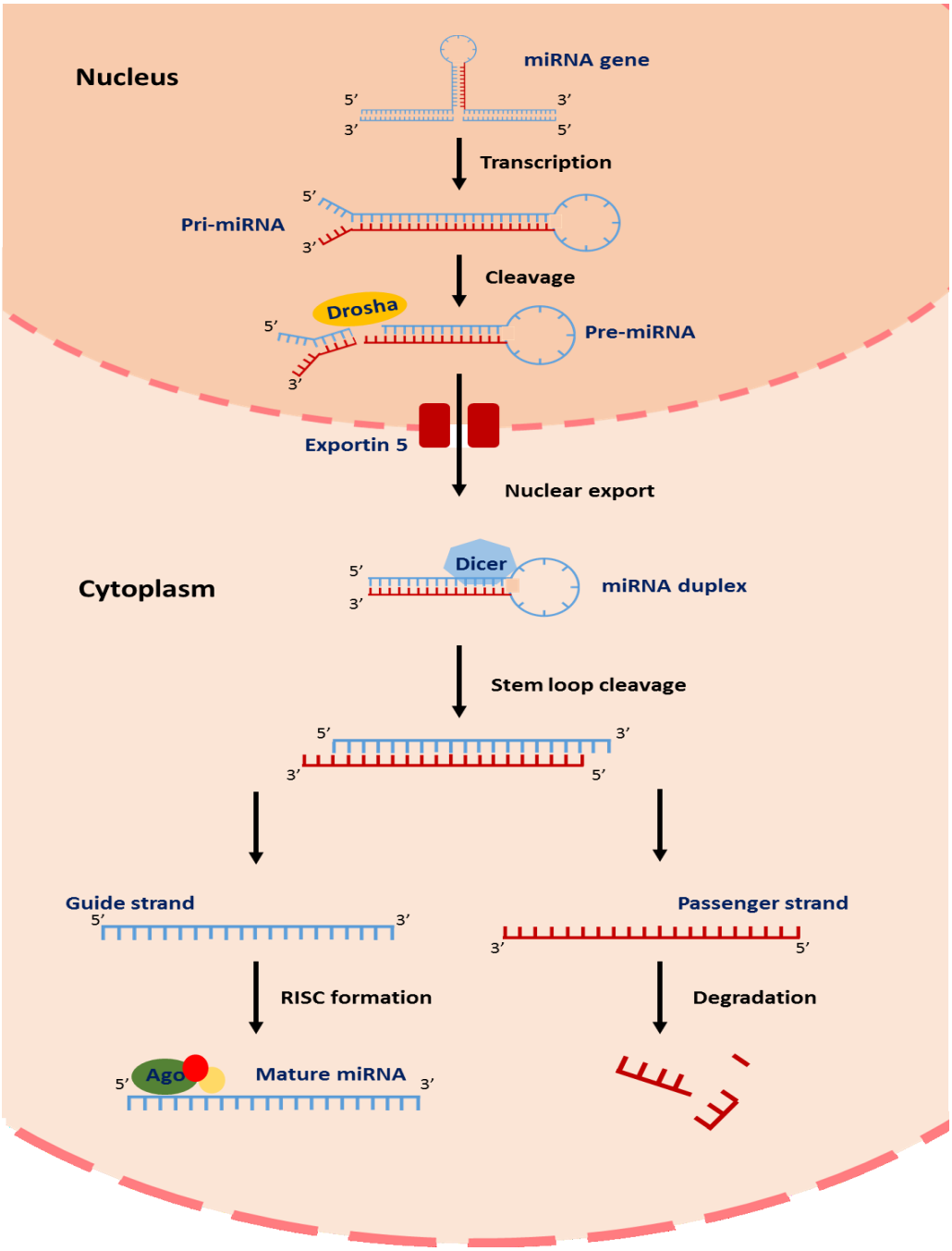


Figure 1. 6: Biogenesis of miRNAs. Following transcription by RNA polymerase II or III, pri-miRNA transcripts are cleaved into shorter pre-miRNA molecules by Drosha endonucleases. Pre-miRNAs are bound by exportin 5 nuclear transport factors which transfer them across the nuclear membrane and into the cytoplasm. Within the cytoplasm, the hairpin loop structure is cleaved from the pre-miRNAs by Dicer endonucleases and the resulting miRNA duplex separates into single stranded guide and passenger strands. While the passenger strand is degraded, the guide strand complexes with RBP to produce a mature miRNA molecule.

Eukaryotic translation has 3 major phases; ribosomal initiation (during which an 80S ribosomal complex forms at the mRNA start codon), elongation (where new peptides are synthesised) and termination (where complete peptides are released from the ribosome) (123,124). A number of studies have indicated that miRISCs interfere with stability of the ribosomal initiation complex (14,125,126) and that they do so through interactions with GW182 family proteins (127) which bind Ago proteins subsequent to miRISC formation (128).

miRISC-bound GW182 proteins interact with cytoplasmic poly-adenylated binding proteins (PABP) that localise with the poly-adenylated (poly-A) tails of transcribed mRNAs. This interaction inhibits circularisation of the mRNAs (a pre-requisite for efficient translation) by reducing the affinity of PABPs for the poly-A tail, preventing the PABPs from complexing with 5' cap-bound initiation factors and accelerating deadenylation of the poly-A tail by recruiting deadenylase complexes to the transcript (129). This deadenylation causes initiation factors to dissociate from the mRNAs, preventing them from entering into translation and encourages them to aggregate within cytoplasmic processing bodies (P bodies). There they are sequestered reversibly or further deadenylated, decapped by 5' decapping factors and degraded via the 5' to 3' exonucleolytic mRNA decay pathway (130).

The majority of evidence that the miRISC represses translation via these mechanisms originates from polysome sucrose density gradient experiments that show that miRNA-repressed mRNAs shift to the lighter portion of the density gradient in response to poor ribosomal loading (14,125,126). Some of these studies, however, have produced contrasting results, showing no difference between the distribution patterns of repressed and non-repressed transcripts and suggesting that post-initiation mechanisms such as nascent polypeptide degradation, premature termination or impaired elongation may also contribute to miRNA-induced translational repression (123,131,132).

Despite the number of studies that support the down-regulatory nature of miRNA activity, evidence has emerged to suggest that they are also capable of stimulating target translation

under specific cellular conditions (**Figure 1.7 E)** and that a single mRNA may be differentially regulated by multiple miRNAs (119). miR-373 for example, induces expression of E-cadherin in prostate carcinoma cells (133) while miR-206 upregulates krüppel-like factor 1 expression in confluent renal epithelial cells (134).

Mechanistically, it is thought that ribonucleoproteins within the miRISC (including Ago2) act in *trans* (binding of a separate regulatory factor to a sequence near to the target gene) to promote expression of target mRNAs. While not fully characterised, this may be through direct interactions with the transcript such as the formation of closed loop structures (135) or via inhibition of repressive protein interactions (136). Additionally, miRNAs may compete with mRNA decay pathways and other expression inhibitors (119). As examples, miR-466 up-regulates IL-10 expression by binding to adenylate-uridylate-rich elements (ARE) on the IL-10 promoter and inhibiting interactions with tristetrapolin (a mediator of the ARE mediated decay pathway) (137).

1.4.3: miRNAs as accessible biomarkers of pulmonary inflammatory responses to TRPM exposure

In 2008, Chim *et al.* showed that placental miRNAs exist within the maternal plasma, making the pioneering discovery that tissue-derived miRNAs are detectable in distal human biofluids (138). This observation was rapidly validated by Lawrie *et al.* (2008) who detected lymphoma tumour miRNAs within the serum of patients (139) and by Chen *et al.* (2008) who suggested that serum miRNAs be used as biomarkers for pathological states having determined that they resist nuclease activity and display reproducible and consistent expression patterns between individuals (140).

Since their discovery in plasma and serum, extracellular miRNAs have been detected in all tested human biofluids including saliva, urine, bronchial lavage and pleural fluid (141)

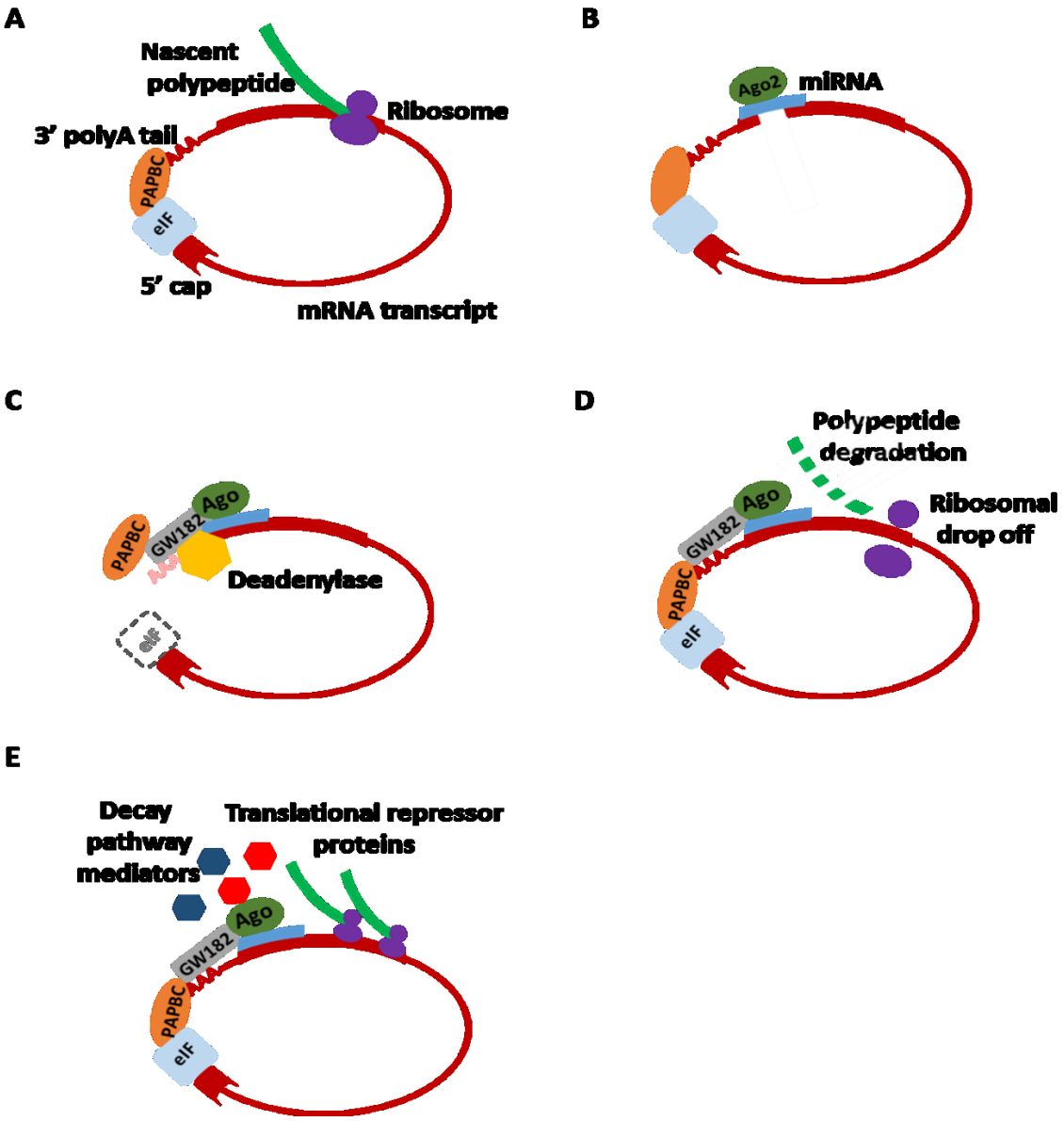


Figure 1. 7: Mechanisms of post-transcriptional regulation by miRNAs. In the absence of complimentary miRNAs, mRNA transcripts are bound by eukaryotic initiation factors (eIF) at the 5' cap and by PABP, enabling their circularisation and translation by ribosomes (A). Perfect pairing between a miRNA and its target facilitates endonucleolytic cleavage of the mRNA by miRNA-bound Ago2 proteins (B) while imperfect pairing of miRNA to the transcript results in GW182 mediated deadenylation of the 3' poly-(A) tail, dissociation of PABP and potential degradation of the 5' cap and transcript (C). miRNAs may also encourage dissociation of ribosomal subunits from the transcript of mediate degradation of nascent polypeptides (D). Under specific cellular conditions, miRNAs enhance translation, potentially by inhibiting interactions between mRNA transcripts and translational suppressors (E).

making them a sensible molecular species to investigate in relation to accessible biomarkers. Packaged within microvesicles or complexed with Ago proteins they are protected from degradation by nucleases and are exchanged between cells via exosome-mediated transport to facilitate intracellular/ inter-organ communications (142). Suggestions for their use as biomarkers were supported by further discoveries that the relative composition of total miRNAs varies between biofluids (141) and that it alters under a range of pathophysiological conditions (143). Furthermore, evidence that extracellular miRNAs alter the proteome of target cells (144,145) and can be synthesised specifically for export (146,147) indicates that their presence in biofluids holds great mechanistic value.

The possibility that mechanistically-relevant, extracellular miRNAs could be secreted by pulmonary tissues during inflammatory responses to TRPM exposure is supported by evidence that NFκB – mediated responses to DEP are accompanied by significant microtranscriptomic alterations (~200) in BECs (104). This response includes up-regulation of miR-21 and its downstream pI3/AKT signalling pathway (148) and of miR-375; a suppressor of aryl hydrocarbon receptor expression (required for transcriptional control of PAH metabolism) (149). Indicating that these responses may relate to additional exhaust particle species, mir-21 has also been shown to be up-regulated in the lungs of mice following exposure to carbon black particles, along with miR-135b and 146b (150).

Supporting translation of these microtranscriptomic changes into biofluids, Rodosthenous *et al.* (2016) found that dysregulation of the extracellular serum microtranscriptome associated significantly with 6 and 12 month moving averages for ambient $PM_{2.5}$ exposure in elderly individuals and that many of the implicated miRNAs contributed to regulation of oxidative stress and inflammatory pathways (151). Similarly Bollati *et al.* (2016) detected 5.6 and 14-fold increases in the expression of microvesicular miR-128 and 302 in the plasma of steel plant workers following 3 days of occupational exposure to metallic particles (152), indicating that this component of TRPM could be a key contributor to microtranscriptomic changes.

While useful as indicators that *in vivo* response to TRPM exposure can be detected using the extracellular microtranscriptome, the value of the biomarkers identified in the above-mentioned studies is limited by the fact that the miRNA signatures are not always organ specific. miR-302 for example, is secreted into the serum by adipose tissue (153) while miR-128 is used as a prognostic marker of hepatocellular carcinoma (154). As $PM_{2.5}$ exposure has been shown to cause oxidative stress in adipose tissue (155) and the liver following translocation from the lungs (156), it is possible that changes in the serum concentrations of these miRNAs may be contributed to by extra-pulmonary mechanisms. Supporting this observation, monocytes, granulocytes and leukocytes have all been shown to alter their patterns of miRNA expression following inhalation of metallic or carbonaceous particles (157–159). As such, it would be useful to identify those that show greatest specificity to the lung because this would help anchor any markers of pathophysiological mechanisms to the tissue from which they were produced.

1.4.4: Methods for deriving miRNA biomarkers

Detection of miRNA biomarkers generally requires the comparison of expression profiles between two or more experimental groups (known as differential expression analysis (DEA)) to identify miRNAs that associate strongly with the experimental condition of interest. Changes in expression across the groups are usually articulated as a fold change that is assessed statistically for significance, and observes the need to account for multiple testing (160). Input for DEA of miRNAs is generally produced via one of two methods; microarray hybridisation or next generation sequencing (NGS), both of which have advantages and limitations relative to one another and with regards to the application of biomarker detection (**Table 1.1**).

Microarrays were amongst the first transcriptomic profiling methods that were optimised for use with miRNAs and are still used extensively because of their cost-effectiveness (161). Microarray chips capture fluorescently labelled miRNAs using complimentary oligonucleotide

probes. The concentrations of these captured miRNAs are quantified relative to endogenous controls using their fluorescence intensity as a proxy for sequence abundance. Whilst able to measure thousands of miRNAs simultaneously and at a lower cost than real time quantitative polymerase chain reactions (RTqPCR) based methods, microarrays are limited in terms of biomarker detection by their inability to distinguish between closely related sequences (such as family members), their restriction to pre-selected miRNA targets and saturation of the probes for highly abundant species (160,161).

NGS avoids these limitations, allowing miRNAs (including novel species) to be quantified in an untargeted manner and differentiated to the degree of single-nucleotide variations. NGS requires miRNAs to be reverse transcribed and fragmented to produce a cDNA library that is amplified and purified before being attached to an oligonucleotide-coated solid phase via 5' adaptors. Each library fragment undergoes amplification to produce distinct clonal clusters before being flooded with deoxynucleotides (dNTPs) in cycles (e.g. guanosine, cytosine, thymine then adenine). The sequences of each cluster can be established using a variety of techniques that detect the complimentary pairing of the dNTPs to the cDNA. As examples, Illumina NGS platforms measure the wavelength and intensity of fluorophore-conjugated dNTPs at the end of each cycle (162) while semi-conductor sequencing methods measure localised changes in charge that are produced by the release of H^+ as nucleotides are incorporated to the growing DNA strand (163). Using bioinformatic tools to align the output against reference genomes for the organism of interest, it is possible to identify and quantify millions of miRNAs in a simultaneous and timely manner (reviewed by Liu *et al*, 2011 (164)).

Differential expression of miRNAs and their applications as biomarkers are generally validated using RTqPCR. Of the techniques available, RTqPCR is the most accurate, has the widest dynamic range and is most cost-effective for the measurement of few transcripts. Additionally, it is the only technique that can produce absolute expression values (160). Due to the small size and lack of a universal sequence (such as a poly-A tail), miRNAs must be quantified slightly differently to mRNAs; Taqman reagents employ a stem-loop primer that

binds complimentarily with the 3' end of the miRNA while the SYBR method includes polyadenylation of the 3' terminus to aid ligation of a sequence-specific reverse primer (160).

Table 1. 1: Comparative summary of the beneficial and limiting features of techniques used for miRNA biomarker detection

Feature	Microarray	NGS
Cost	Relatively low per sample (compared with NGS)	High but improving with technological advancements and the use of library barcoding
Number of parallel quantifications	Thousands (Can be performed in a targeted manner)	Millions (Untargeted)
Discriminatory power	Imperfect specificity for closely related sequences, capture probes susceptible to cross-hybridisation	Differentiates between sequences that differ by one nucleotide (e.g. miRNA family members)
Quantification range	Limited at the upper range by capture probe saturation	Sensitivity enables quantification of low copy number miRNAs
Exploratory potential	Limited to known sequences	Capable of identifying novel miRNAs
Data processing	Normalisation to endogenous controls	Less well-developed normalisation procedures

1.6: Metabolites and the metabolome

Metabolites are the complement of small molecules (≤ 1.5 kDa) that are formed as intermediaries or products of enzymatic reactions (165). The term ‘metabolic pathway’ refers to a series of these reactions which serves to alter the structure and ultimately the function (or ability to function) of a parent compound. Such pathways may be anabolic, incorporating molecules such as amino acids or fatty acids into larger structures like glycoproteins or phospholipids, or catabolic where the parent compound is separated (e.g. via oxidation) into smaller molecules that are generally destined for excretion (165).

Historically, metabolites have been classified as endogenous (arising internally as products of major biosynthetic, energetic and catabolic pathways and regulated by host enzymes and transporters) or xenobiotic (arising from external or chemical sources but able to be metabolised by endogenous enzymes) and have been studied as distinct entities during pathway analysis. Realistically however, endogenous and xenobiotic metabolites represent the extremes of a continuous spectrum of metabolites that is composed of multiple intermediate categories and requires integrative approaches of study (166).

Sym-endogenous compounds for example, include dietary-derived amino acids, lipids, vitamins and co-factors that are essential to endogenous function but are not encoded for by the host genome. Contrastingly, *sym*-xenobiotic molecules such as hippurate are not essential for endogenous function; produced by exogenous genomic sources such as the pulmonary or gut microbiota, they impact on the rates of essential reactions by interacting with, and competing for endogenous metabolic resources. *Trans*-xenobiotic compounds present an intermediate between *sym*-xenobiotic and xenobiotic metabolite classes. Despite originating from external or chemical sources, they can be converted into endogenous metabolites by specific host tissues (166). A prime example is ethanol which is converted to acetaldehyde by hepatic alcohol dehydrogenases and then to acetate by acetaldehyde dehydrogenase; a substrate for multiple biosynthetic and energetic pathways (167).

The ‘metabolome’ refers to the full complement of metabolites (from endogenous to xenobiotic) that exists within an organism, biofluid, tissue or cell at any given time (168). Within these biological systems, the metabolome is highly complex and covers a wide chemical space (169). Not only is it the product of multiple enzymatic systems with variable substrate affinities and reaction rates (170) but it is strongly influenced by environmental exposures such as diet or stress (169). Such exposures contribute to the highly dynamic nature of the metabolome, altering the activity of biosynthetic, degradation, biotransformation and excretion pathways and contributing to the value of the metabolome as a source of mechanistically relevant response biomarkers.

1.6.1: Metabolic profiling for biomarker identification

The terms ‘metabolomics’ and ‘metabonomics’ describe a top-down systems approach and its dynamism to characterising the metabolome (171). Focused on characterising experimentally or environmentally -induced changes to metabolic profiles, such analyses can be targeted to investigate specific adverse response pathways or molecular species (172,173) . Alternatively (and in the case of most *de novo* biomarker identification studies) they can be global in nature, employed to document the metabolic profiles of biological samples and to investigate the effects that stimulus exposures have on the metabolome (174,175).

Metabolic profiling offers a complementary approach to other omics platforms. Although changes in the transcriptome and proteome are useful for elucidation of molecular response mechanisms, there are cases where mRNA and protein biomarkers are difficult to relate to toxicological end points (175). *In vivo* exposure to ethanol, for example, induces widespread alterations in gene regulation but not all of the changes contribute to the drunkenness phenotype (171,176).

In contrast, metabolites (as the products, intermediaries and substrates of biological pathway activities) represent the result of all interconnecting upstream molecular changes (171) making them mechanistically relevant to toxicity phenotypes independent of which molecular profiles were altered by the exposure (175). As an example, mitochondrial toxicity may be eluded to by changes in the abundance of respiratory enzymes, but is better represented by changes in the concentrations of the enzyme products (177,178) as these provide evidence that changes to the reaction rates have occurred rather than have the potential to occur.

This feature, along with the fact that metabolomic profiling methods are comprehensively optimised for use with accessible biofluids (179–181) suggests that metabolic profiling would be an appropriate method to employ during the search for mechanistically relevant biomarkers of pulmonary responses to TRPM exposure.

1.6.2: Metabolic profiling for the detection of TRPM-associated biomarkers

Supporting this suggestion, metabolomics approaches have proved a successful aid for detecting novel biomarkers of pulmonary responses to exhaust PM and for developing hypotheses for which cellular pathways they represent. Leading this work, Oeder *et al.* (2015) performed a conceptual-level integration of metabolomic, proteomic and transcriptomic profiles which identified associations between shipping exhaust particles and reductions in glycolysis, glycine metabolism and pyrimidine metabolism in airway epithelial cells. Interestingly, the study also found that metallic heavy fuel oil PM augmented a greater number of inflammatory and oxidative stress pathways than non-metallic DEP which induced a broader biological response at all omics levels (100). Together, these findings indicate that metallic non-exhaust particles may also yield mechanistically relevant biomarkers at the metabolomic level; a notion that is supported by evidence that metallic particles augment the upstream transcriptome and proteome in pulmonary cells (182,183) and that ambient $PM_{2.5}$ enhances expression of metal binding genes in alveolar macrophages (184).

Through measurement of the human BALF metabolome, Surowiec *et al.* (2016) demonstrated that TRPM-induced changes to the metabolome are translatable to accessible biofluids. The group showed that exposure to biodiesel reduced concentrations of ATP synthesis intermediaries in BALF and enhanced concentrations of lipid catabolism products from cell membranes of the peripheral airways (185). Subsequently Brower *et al.* (2016) found that markers of decreased ATP synthesis were detectable in the circulation following exhaust PM exposure in mice and that they were accompanied by increases in serum concentrations of pro-inflammatory lipid products and anti-oxidant molecules (186).

Support for including metabolic profiling methods in microtranscriptomic searches for TRPM response biomarkers arises from evidence that ambient particles (including highly metallic species) can interact directly with superoxide dismutase and glutathione peroxidase enzymes and inhibit their activity downstream of exposure (187). These enzymes are central contributors during anti-oxidant responses to ambient PM exposure (187) but loss of their activity would not be detected during microtranscriptomic analysis of TRPM responses because the toxicity mechanism is exerted downstream of translation. Downstream changes to the metabolome however, have the potential to encompass such mechanisms and could provide evidence of their activity following exposure to different species of TRPM.

1.6.3: Methods employed for metabolic biomarker detection

As well as > 29,000 endogenous metabolites, the human metabolome is expected to contain approximately 40,000 products of xenobiotic, dietary and microbial metabolism (188). While quantification of the entire metabolome is difficult, or perhaps impossible, in biological systems (189), the use of ^{1}H nuclear magnetic resonance (NMR) spectroscopy and/ or mass spectrometry (MS) coupled with gas or liquid chromatography generally provides sufficient coverage to identify alterations in pathway activities (190). Focusing on accessible biofluids, more than 24,500 compounds have been detected in human blood samples while 4,000 have been measured in the urine using these techniques (191).

Metabolic profiles are produced in the form of spectra; collections of peaks that relate to the intensities and chemical structures or masses (for ^{1}H NMR or MS respectively) of the metabolites that exist within a sample. In MS, these signals are produced by ionising chromatographically separated molecules at an ion source to produce a gaseous phase. Ions within this phase are separated based on their mass to charge ratio (which is characteristic and distinctive to each molecule) within a mass analyser and focused towards a detector which recognises the different ions and calculates their relative abundances, creating peak signals (192). In contrast, ^{1}H NMR signals are generated by the motion of protons flipping between two energy states following excitement by a high frequency pulse when a sample is placed within a magnetic field (193). Fourier transform of the signal creates a chemical shift (a measure that is influenced by the electronic and chemical environments within molecular groups) that is displayed against signal intensity upon spectra, again producing characteristic peak patterns for different metabolites (193).

MS methods benefit from exquisite detection sensitivity (within the pM-μM range) (194), making them especially useful for the detection and structural corroboration of metabolites that naturally occur at low concentrations in biofluids (such as those produced during 2-Amino-1-methyl-6-phenylimidazo[4,5-b]pyridine metabolism (195)). Such sensitivity permits detection of ≥ 1000 small molecules within a single sample (194) which, with methods optimised for urine and serum/plasma samples (196,197), offers strong potential to identify exposure or organ- specific biomarkers in accessible biofluids (198).

In contrast, ^{1}H NMR is less sensitive, permitting annotation of ~50 different metabolites per sample (181,199,200) and limiting biomarker searches to fewer molecules (especially as some smaller peaks can be masked by larger ones in the aliphatic region of the spectrum (194)). This can lead to the repetitive identification of ‘usual suspect’ markers by different metabolomics studies (201) and the requirement to seek biomarker panels rather than lone markers to enhance discriminative power. The collagen metabolite 4-hydroxyproline, for example, has been associated with both primary biliary cholangitis (autoimmune destruction

of the small bile ducts) and silica dust induced-fibrosis in ^{1}H NMR spectroscopy based analyses but many of the other metabolites that distinguished the control profiles from the experimental profiles differed between the two conditions, producing distinct metabolic signatures overall (202,203).

Despite being less sensitive than MS, ^{1}H NMR spectroscopy is a non-destructive technique that benefits from higher technical reproducibility, excellent quantitative accuracy and a wide coverage of metabolite classes (including amino acids, sugars and aromatic groups), meaning that it is employed more regularly during studies of molecular toxicology (175). Furthermore, differentiating metabolites can be identified easily and quickly in ^{1}H NMR spectra given the availability of peak fitting tools and databases of assigned spectra. Such databases are less complete for MS data resulting in the publication of masses and retention times as identifiers for biomarkers rather than metabolite names (204). This excludes the biological context of the biomarkers, drastically reducing their mechanistic value and making those derived from ^{1}H NMR spectra more suitable for contexts that require considerable mechanistic characterisation, particularly where pathway analyses are desired.

1.6.4: Statistical interrogation of metabolomic datasets

The methods used to interpret metabolomics datasets are mainly adapted from those used in transcriptomic studies (205). These approaches aim to assess group-wise differences using values called integrals. Integrals are quantitative measures that are calculated for each metabolite using the areas under their respective spectral peaks. They are proportional to the number of H that contribute to the resonances and therefore provide information regarding the abundance of the metabolites in a sample relative to a reference peak (often glucose).

Group-wise differences in individual metabolite abundances can be explored using univariate or multivariate approaches. Univariate statistics such as analysis of variance

(ANOVA) or t-tests can reduce large numbers of measured analytes to only those that show strong, statistically significant associations with the experimental conditions. However, they are generally the second choice for metabolomic studies given that they treat each metabolite individually, excluding inter-molecular relationships and can overlook small but biologically relevant differences (205).

Multivariate approaches are capable of capturing changes in the concentrations and ratios of related metabolites. This type of analysis usually begins with the use of unsupervised pattern recognition approaches such as Principal Component Analysis (PCA). These tools seek to reduce the dimensionality of spectral data whilst expressing as much of its intrinsic variance as possible using a smaller number of factors called principal components (PC) (206). This facilitates visualisation of metabolic patterns that would be difficult to recognise otherwise (207), allowing trends, groupings and outliers to be identified and attributed to contributory metabolites (206).

Supervised pattern recognition techniques such as Partial-Least Squares Discriminant Analysis (PLS-DA) can follow PCA (but are not limited to this application). In contrast to the unsupervised method, PLS-DA relates the data matrix to sample classifiers using a linear regression model. This allows the detection of more subtle differences between groups and determination of which metabolic changes are the most discriminatory between groups (205). Often univariate methods are used to confirm inter-group differences in the abundance of these metabolites, placing confidence in their use as biomarkers for the response in question.

1.7 Modelling pulmonary exposures to xenobiotics

In terms of physiological relevance, human cohorts provide the most appropriate samples from which biomarkers of pulmonary responses to xenobiotic exposures can be sought (208). Cohort studies can be observational by design, employing participants who are already exposed to pollutants (either occupationally or via their geographical location) or interventional, exposing participants to pollutants within exposure chambers or taking them to highly polluted locations (as examples) (209).

Intervention studies (especially those performed in exposure chambers) are particularly useful for identifying biomarkers for responses to specific components of TRPM. Many ambient particulates can induce pulmonary-derived changes in biochemical signatures (including miRNAs and metabolites (210–212), therefore masking the emergence of biomarkers that relate to the particle of interest during co-exposures. By exposing participants to controlled doses of single pollutants (or characterised mixtures), this type of confounding can be minimised and pollutant-specific biomarkers and mechanisms of toxicity be identified.

Given that TRPM is consistently found to elicit pro-inflammatory responses in pulmonary tissue, ethical concerns restrict the dosages to which human participants can be exposed to during intervention studies. As a result, *in vivo* human biomarkers are generally sought from models of mild pulmonary responses from which only the largest biochemical deviations can be identified. While this has not prevented identification of miRNAs and metabolites that associate with exhaust PM exposure during human chamber studies (185,213), subtle but mechanistically relevant changes may have been ignored or discounted from characterisations of the toxicity, along with the effects of repeated exposures.

In contrast, observational studies are free from ethical constraints on exposure dosage, enabling biomarkers to be sought for responses to environmentally relevant exposure doses and patterns. Occupationally exposed cohorts are particularly valuable because they can experience higher and more consistent exposures than the general population and provide a

greater magnitude of response from which biomarkers can be distinguished clearly from noise (214).

Unlike interventional studies, analysis of data produced by observational methods is strongly limited by the influence of confounding exposures. Advanced statistical models exist to correct for the effects that non-target exposures have on biological responses (215) but these rely on accurate self-reporting of co-exposures (such as cigarette smoke), measurements taken from static monitoring stations and assumptions that all the important covariates have been accounted for.

In addition to ethical constraints and the confounding that can mask biomarker identification in human cohorts, poor participation rates, long time-courses and the high expense that associates with TRPM exposure studies encourage toxicologists to seek putative response biomarkers in simpler non-human models that are designed to reflect key characteristics or behaviours of the true human exposure. Once established and characterised in these controlled and cost-efficient systems, the markers can be validated under authentic human exposure conditions using targeted methods.

1.7.1 In vivo models

In the absence of samples from an appropriate human cohort, animal models offer accessible systems from which *in vivo* responses to particle exposure can be investigated. Ideally, the test species should absorb, distribute and metabolise the particle of interest in a representative manner to humans but choice is also limited by practicality and economics. As such, rodents (with their small sizes, short gestation periods and low maintenance costs) are a popular model for studies of toxicological mechanisms.

For rodents, particle exposures can be performed by inhalation in exposure chambers (whole body, head or nose-only) or by intratracheal instillation (direct insertion of particle suspensions into the lower airways). As well as being less distressing for the animal, inhalation methods

are often selected because they provide the most natural route of exposure, allowing particles to pass through the upper airways and deposit uniformly within the lungs (as opposed to centrally following direct bolus delivery) (216–218).

It must be noted however that the anatomy of rodent airways differs considerably from that of humans (219), reducing the degree to which toxicological responses can be translated between the species. As examples, rodents are obligate nose breathers while humans inhale oronasally and have wider airways, allowing for greater deposition of coarse particles in the respiratory airways (219). Similarly, rodents have much faster mucocilliary clearance rates for PM than humans, with 15% of particles remaining in human lungs for 24 hours after exposure compared to full clearance of rat lungs by 8 hours (220).

Inhalation exposures remove the potential for biological interference by vehicle solvents (216,221) but they also permit deposition of particles on the fur and cage furniture. As well as confounding lung-specific responses by permitting ingestion of particles during grooming or upper airway clearance (222), this drastically reduces the reliability and reproducibility of dosing between animals. While dosimetric modelling can assist estimations of how many particles will be deposited in different airway regions during inhalation time-courses, the final exposure concentrations are not as controlled or consistent as can be achieved with direct instillations of particle samples (219). As such, instillation methods are regularly selected for characterisations of toxicological responses in the lung, particularly where dose-response data is desired.

Independent of the technique used, *in vivo* exposure doses can be calculated to be comparable to those experienced by humans during real world exposures. Depending on the experimental target (e.g. epithelium, interstitium), doses are normalised to parameters like body weight, epithelial surface area, interstitial weight or macrophage counts with the aim of inducing responses that best resemble those experienced by humans in specific scenarios. Despite this consistency, it is necessary to consider that differences in the molecular and cellular composition of human and rodent lungs may influence the degree to which rodent-

derived biomarkers and pathway characterisations can be extrapolated to human populations. Molecules that are differentially expressed during pulmonary inflammation in rats or mice may not be influenced in humans under equivalent conditions.

In the context of inflammatory responses, evolutionary divergence of the immune system may be one such factor. While the genomes of humans and rodents diverged up to 95 million years ago (223), pathogens continue to evolve rapidly (alongside the introduction of novel nanomaterials and pollutants), exerting strong pressure on immune responses to co-evolve and further diverge from one another (224). This is observable at the cellular level through differences in the number and size of alveolar macrophages in human and rat lungs (225,226) and at the molecular level through differences in induced antioxidant concentrations (227) and TLR4 activity (224).

Although TLR4 expression itself is highly conserved across species (228), exposure of mouse and human macrophages to LPS (an archetypal TLR agonist) differentially regulated 70% of orthologous gene pairs, revealing considerable species-specific differences in TLR4-induced responses. In addition to differences in downstream cytokine, chemokine, growth factor and matrix metalloproteinase expression, mouse TLR4 was regulated by stronger and more rapid negative feedback mechanisms, indicating the existence of interspecies differences in sensitivity to inflammatory stimuli (224). Considering the strength of association that has been made between TRPM exposure and TLR4 activity (229,230), this suggests that caution must be taken when attempting to translate biomarkers of TRPM-induced pathways between these species.

Of particular importance to the interpretation of metabolomics data is evidence of inter-species differences in the availability of enzymes and substrates for metabolic pathways that associate with pulmonary inflammation. Pulmonary collagen synthesis for example, is induced in mice following exposure to DEP or silica dust (203,231) and in hamsters following zirconium nanoparticle exposures (232). Such activity is demonstrated by increased concentrations of proline and 4-hydroxyproline (essential collagen substrates) in excised

pulmonary tissue (203) or by heightened incorporation of [^{14}C] labelled proline into collagen fibers (232). Despite the fact that increased collagen production has also been observed in human models of silicosis (233), expression of arginase I (the enzyme required to synthesise proline from ornithine in rats) is non-detectable in human pulmonary fibroblasts (234), indicating that distinct differences could exist between pathways of inflammation-induced collagen metabolism in humans and rodents.

Similarly, Koufaris and Gooderham (2013) suggest that interspecies (or even inter-strain) differences in the regulation, function and repertoire of miRNAs may influence the toxicity that exogenous exposures exert upon different organisms (235). Although miRNA: mRNA interactions are highly conserved between mammalian species (235)(to the extent that mammalian orthologs are frequently used to improve the accuracy of miRNA target prediction algorithms in human studies (236)) evolutionary divergence can occur due to mutations in the mature miRNA or target mRNA sequence or alterations in miRNA editing or biogenesis(235).

Furthermore, evolution of animal miRNAs is a highly dynamic and ongoing process (237) with new miRNAs continually being acquired as species and even intra-species strains evolve (238,239). Given that one miRNA can target hundreds of different mRNA transcripts (117) (including enzymatic facilitators of metabolism) such changes in miRNA repertoire may contribute greatly to inter-species differences in cellular responses to toxicity. Together these factors may influence the degree to which common miRNA biomarkers can be detected between species following equivalent exposures or, where mutations in mRNA sequences are involved, the mechanistic information that they provide.

1.7.2 In vitro models

With less concern regarding cross-species extrapolation and the simplicity with which their parameters can be manipulated, *in vitro* systems are commonly employed to study

mechanisms of toxicity (240). Pharmaceutical industries, for example, have shown a strong upward trend in the use of *in vitro* tests between the 1980s and 2013, including those used to study responses in the respiratory tract (241). While a key aim of *in vitro* modelling is often to accurately reflect *in vivo* exposures and responses, *in vitro* toxicologists generally use one cell type (or a small combination) to model specific features of pulmonary tissue. Rather than attempting to replicate the composition of the entire respiratory tract (which is made up of 40 different cell types) this permits characterisation and comparison of toxicological mechanisms in each of the specialised structures of the airways (242)).

Providing examples of this, A549 adenocarcinoma cells are regularly used to model the alveolar epithelium because they secrete cytokines, metabolise xenobiotics and produce surfactants in a similar manner to *in vivo* AT2 cells. Similarly Calu-3 cells are used to study bronchial epithelial functions due to their ability to secrete mucins and form tight intercellular junctions (243,244). Given their key role in the induction of inflammatory cascades and neutrophil recruitment, macrophage or monocyte-derived macrophage models (including U937 or THP-1) are commonly employed to study responses to particles that possess pro-inflammatory potential.

Cell cultures may be established using primary cells (grown from chemically or enzymatically disaggregated biopsy samples) or from sub-cultured and transformed cell lines (245). Compared with cell lines, primary cells hold the advantage of a more differentiated phenotype that displays greater similarity to the tissue of origin and provides biomarkers that extrapolate more successfully to *in vivo* exposure scenarios (246). Generally however, they dedifferentiate rapidly meaning that an adequate supply of biopsy tissue is required to maintain experimentation on primary cultures (247,248). As well as being low-throughput and time-consuming, this introduces a high degree of inter-donor variability that can confound interpretation of responses to semi-characterised or novel exposures (247). This factor must be weighed against an advantageous increase in representability for the outbred

human population, meaning that primary cells are regularly used to validate responses that have been observed in cell lines initially.

Immortalised cell lines provide a more continuous option than primary cells. Originating from tumour biopsies or undergoing artificial immortalisation through treatment with chemical carcinogens, viral oncogenes or irradiation, these cells possess genetic mutations that allow them to evade senescence (245). Most lines grow rapidly, facilitating their use in high-throughput toxicological screening, but also encouraging clonal expansion of phenotypic changes that differentiate the populations from their parent cells. As such, toxicological responses and biomarkers that are identified in cell lines often require validation in primary cells or *in vivo* models. Furthermore, validations in other systems reduce the confounding impact that mutations that are intrinsic to cell lines (such as over-expression of oxidative stress-related nuclear erythroid factor 2 p45-related factor 2 (Nrf-2) by A549s (249)) may have on data interpretation.

In vitro models can be developed using mono-culture (cultivation of a single cell type) or co-culture (cultivation of two or more complimentary cell types) techniques. Although co-cultures can display greater physiological similarity to *in vivo* tissue and permit the study of inter-cellular interactions, mono-cultures are the classical system used to characterise pulmonary responses to particle deposition *in vitro* (247). As well as being easier and cheaper to develop than co-cultures (which require intensive optimisation of growth conditions), their simplicity facilitates understanding of how individual cell types respond to adverse exposures, especially those that are not broadly characterised (e.g. non-exhaust particles).

Given their association with intercellular communications (250), this feature may be particularly advantageous during exploration of the roles that extracellular miRNA markers play in the development of inflammatory phenotypes. Indeed, monocultures of A549 epithelial cells have been used to confirm that up-regulation of miR-128 expression (but not

miR-302 expression) by metal-rich PM *in vivo* is contributed to by airway epithelial cells (251).

Several methods have been developed for the exposure of cells to PM *in vitro*. Of these, incorporation of particles into the media of submerged cell cultures is the most simple, cost-effective and reproducible (240,247,252), making it a common choice for determining mechanisms of toxicity. The system has however, been criticised for its poor reflection of particle deposition *in vivo* as submerged particles are subject to agglomeration or diffusion of water-soluble components (247). Furthermore, particles can interact with components of culture medium to form protein and lipid rich coronas (coatings of biomolecules that adsorb onto the surface of particles) (252) that are capable of influencing common toxicity metrics (including cytotoxicity, pro-inflammatory potential and oxidative potential) in a medium-specific manner (253).

As a result, air liquid interface (ALI) models have been developed, facilitating aerosol deposition of particles directly onto the apical surface of cells that are supplied with medium from the basal surface. This method has been shown to enhance *in vivo* characteristics of airway cells (encouraging A549 to secrete surfactant (254) and tracheal epithelial cells to become ciliated (255)) indicating that ALI is the superior model. However, it must be considered that both LPS and metallic particles have been shown to induce comparable inflammatory cascades in submerged and ALI cultures of A549 and THP-1 cells, (252). This suggests that submerged cultures could be equally as suitable for the characterisation of inflammatory responses and discovery of inflammation-related biomarkers, (including those induced by highly metallic particles like non-exhaust PM).

1.8: Project aims and hypotheses

1.8.1: Project hypotheses

Given the potential that miRNAs and metabolites possess for use as mechanistically relevant biomarkers of toxicological response pathways and the fact that evidence is emerging for their association with TRPM exposure, the following work sought to address the hypothesis that **mechanistically relevant miRNA and metabolite biomarkers are detectable during pulmonary responses to TRPM exposure**. Furthermore, given that these molecular species are found abundantly within human biofluids (including those that associate with exhaust PM), the project sought to test a second hypothesis- **that these biomarkers are detectable in extracellular samples.** Such biomarkers could facilitate a significant advance in our ability to study pulmonary responses to TRPM in human cohorts, particularly cohorts of 'healthy' individuals.

1.8.2 Project aims

Specifically, the project followed the workflow presented in **Figure 1.8**. Aiming to **identify miRNA biomarkers for pulmonary-specific inflammatory responses,** global microtranscriptomic profiling approaches were used to identify miRNAs that were produced by the pulmonary tissue itself during inflammatory events (**Chapter 2**). These miRNAs (identified using rodent models of exposure to diverse pro-inflammatory stimuli) directed targeted analysis of rat serum from an intratracheal lipopolysaccharide (LPS) exposure model (**Chapter 3**).

This analysis aimed **to determine whether miRNA signatures of pulmonary inflammatory events could be detected within an accessible biofluid** and was paired with untargeted ^{1}H NMR metabolic profiling approaches **to ascertain whether inflammatory pulmonary responses also induce changes to the metabolome that can be detected extracellularly**. Such changes could be used to broaden the panel of pulmonary-specific biomarkers of inflammation and to enhance their mechanistic relevance through the performance of multi-omics pathway analyses. As such, the final aim of the LPS

rat serum study (**Chapter 3**) was **to identify whether the inflammatory miRNAs could have influenced any of the metabolic pathways that associated with the response**.

A U937 human macrophage model was employed as a biologically controllable system **to assess whether any of the accessible miRNA and metabolite markers of pulmonary inflammation are relevant to the context of TRPM exposure** and **whether pathway-level interplay exists between their expression** (**Chapter 4**). Toxicological responses to exhaust (DEP) and non-exhaust particles (BAD) were characterised using traditional, hypothesis-driven toxicological approaches to provide phenotypic anchors for the results of targeted miRNA quantifications and untargeted ^{1}H NMR-based metabolic profiles. Comparing DEP and BAD-associated markers with each other and with those that associated with LPS exposure, the study aimed **to determine whether biomarkers for particle-specific pulmonary responses can be detected extracellularly**. Together these mechanistically relevant tools aim to progress our understanding of uncharacterised *in vivo* responses to non-exhaust PM exposure.

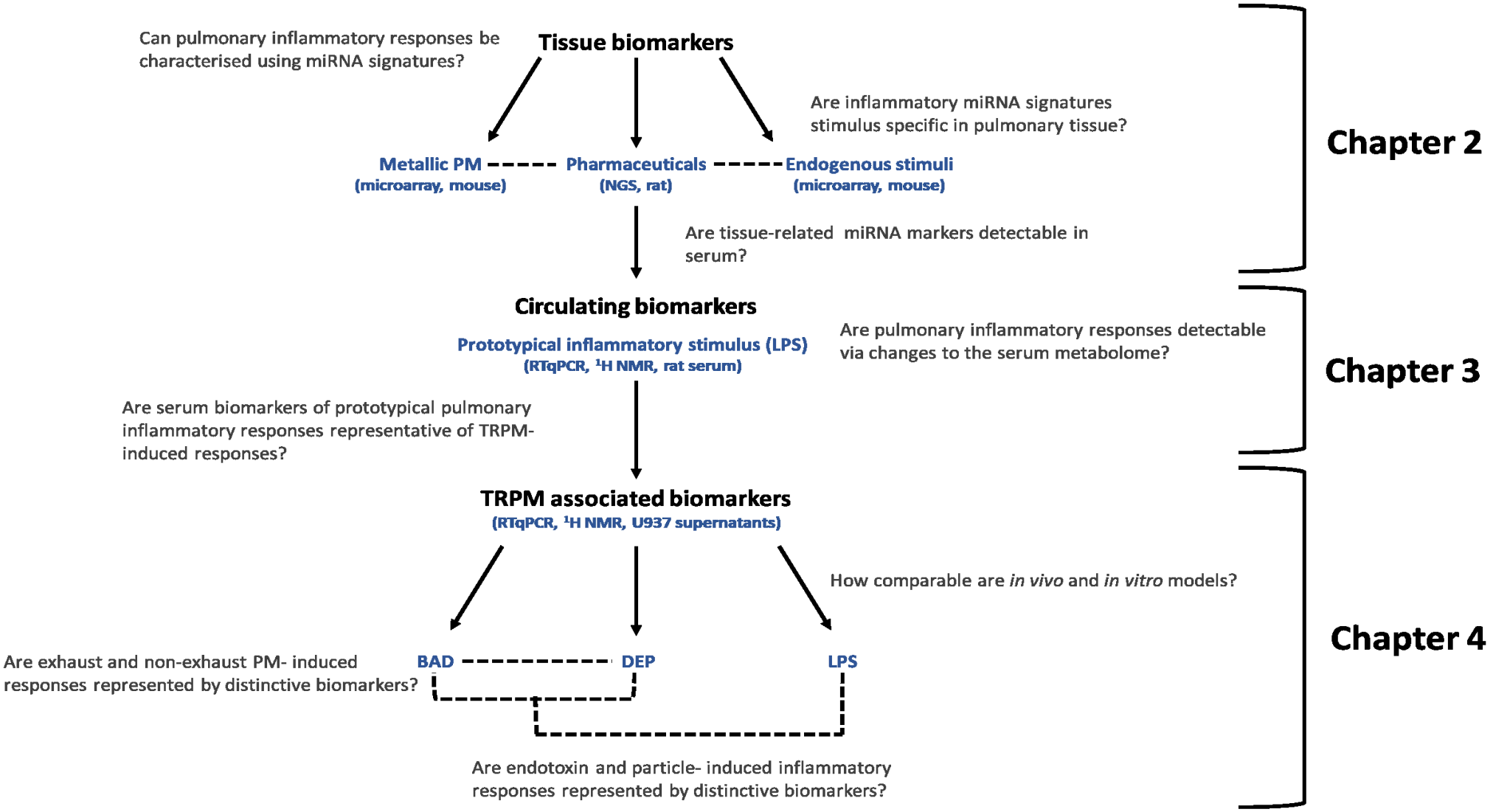


Figure 1. 8: Schematic explanation of the workflow followed in this study. This diagram displays the models used in the study, the relationships between the models and the questions that they aimed to answer.

Chapter 2. miRNA markers of pulmonary inflammation in the rat

Chapter overview

The work detailed in this chapter aimed to identify pulmonary-specific miRNA markers of inflammation that are expressed within the lung tissue itself. The work centres on an integrated analysis of miRNA and mRNA next generation sequencing (NGS) data that was obtained from the pulmonary tissue of rats following exposure to a pro-inflammatory inhaled pharmaceutical.

2.1: Introduction

Differential expression analysis (DEA) is a widely employed tool in the field of biomarker discovery that seeks to identify genes that are over or under expressed as a result of experimental or pathophysiological conditions (256). Using a gene by gene approach, the method performs a series of univariate comparisons that simplify the multivariate output of transcriptomic profiling data by identifying the genes that show the greatest and most statistically significant changes in expression (257).

DEA can be performed using data acquired by microarray or NGS and is applicable to the study of both mRNA and small RNA transcriptomes. For several decades microarrays were the most popular method of RNA profiling but NGS data has since emerged as the input of choice for DEA (256). This change was driven initially by the global nature of NGS which, unlike the microarray, does not rely on *a priori* knowledge of genomic features (258) . Rather than relying on probe hybridisations, NGS expression data is produced by converting RNA molecules to cDNA and sequencing it in a high throughput manner (259) (as detailed in **Chapter 1**). This permits thorough coverage of large genomes- something that has only recently become accessible with microarray technology (260).

Despite the increasing popularity of whole-genome microarrays (which are cheaper to run per sample than NGS), NGS remains a sensible choice when studying miRNA expression patterns. The global nature of the technique facilitates identification of novel transcripts; an important opportunity given that characterisation of the microtranscriptome continues to expand. Furthermore, it distinguishes between highly homologous sequences (such as miRNA family members) with a resolution of one nucleotide, circumventing the cross-hybridisation issues that encumber microarrays (258).

In the context of miRNA biomarker discovery, DEA has been used to identify single miRNAs or panels of miRNAs that separate cases from controls under numerous pathophysiological and toxicological conditions. These include but are not limited to non-alcoholic fatty liver disease, pancreatic cancer, myocardial infarction and drug induced kidney and liver injury (261–264). Alone, these markers provide great clinical value in terms of diagnosing and making prognoses for their respective pathophysiologies or toxicities. This value can be increased by combining DEA with downstream target prediction studies and pathway analyses in order to uncover mechanisms through which the conditions developed.

Algorithms such as miRanda, TargetScan and PITA have been developed to aid miRNA target prediction (265). These algorithms search mRNA 3'UTR sequences for complementarity with the 5' seed sequence of a chosen miRNA and assesses the likelihood of successful binding occurring between these sites based on factors such as evolutionary conservation, repetition of binding sites and site accessibility (265). While this bioinformatics approach is fast and inexpensive, the complex and heterogeneous nature of miRNA-mRNA interactions means that it produces large numbers of false positive and low efficiency predictions that require lengthy and expensive biological validation.

Researchers have begun to address this limitation by integrating miRNA expression data with complementary mRNA expression data, enabling correlations to be made between the expression of miRNA markers and their predicted targets within a single sample. Based on evidence that miRNAs can degrade target mRNAs or enhance their expression through

feed-forward regulation of transcription factors (266), this approach assumes that strongly correlating miRNA-predicted target pairs interacted within the biological context of the experiment and that uncorrelated predicted targets were falsely selected. As a result, ‘noise’ mRNAs are excluded from downstream pathway analyses, enabling the regulatory functions of differentially expressed miRNAs (DEmiRNAs) to be explored without being confounded.

This integrative approach has proved successful in determining that the phenotypes of Alzheimer’s disease and non-obstructive azoospermia (a complete lack of sperm in the seminal fluid) are contributed to by dysregulation of miRNA panels (154,267) and that up-regulation of miR-200c is responsible for dysregulation of IL-8 expression in ulcerative colitis (268). Furthermore, integration of miRNA and mRNA microarray datasets has provided detailed insights into the mechanistic development of several pulmonary pathophysiologies, showing that the miR-23a cluster promotes epithelial to mesenchymal transition in idiopathic pulmonary fibrosis and that the targets of DEmiRNAs include wnt and focal adhesion pathway members in COPD (269).

2.1.2: Hypotheses and aims

Using methods similar to those described in the integrative studies above, the following work tested twin hypotheses; **1) inflammatory responses within the lung are accompanied by characteristic and mechanistically relevant alterations in the miRNA transcriptome** and **2) some differentially expressed, inflammation-associated miRNAs will be released specifically by pulmonary tissue and thus have potential for use as biomarkers of inflammatory responses within the lung**.

The primary aims of the study were to **identify miRNAs that are differentially expressed within pulmonary tissue during a typical *in vivo* inflammatory response** and to **explore the regulatory functions of those miRNAs during the inflammatory response** using complimentary mRNA sequencing data, miRNA target prediction algorithms and pathway enrichment approaches**.** These aims were achieved by sequencing the mRNA and miRNA transcriptomes of pulmonary tissue taken from rats treated with AZD2230 (an inhaled proprietary pharmaceutical compound).

Intended to inhibit inflammatory cascades during exacerbations of COPD, AZD2230 was designed to be retained within the lungs and to inhibit pro-inflammatory NFκB signalling by binding to IKK2 (an agonistic regulatory subunit of NFκB). Despite NFκB being a key mediator of inflammatory signalling within the lung , the rats used in the current model experienced airway infiltration by immune cells in a manner that is typical of the initiation phase of pulmonary inflammation. As such they were considered an appropriate platform from which miRNA markers of pulmonary inflammatory responses could be sought.

As inflammation can be the outcome of exposure to various airborne agents, a secondary aim of the study was **to determine whether any miRNA markers of AZD2230 -induced pulmonary inflammation also associate with pulmonary responses to different types of inflammatory stimuli in additional models..** In order to meet this aim, two rodent miRNA microarray datasets produced from pulmonary tissue were selected from the Gene Expression Omnibus (GEO) for analysis; one a model of nanoTiO_2 exposure and the other

an example of allergic inflammation induced by IL-13 overexpression and doxycycline exposure. Using these data, the expression of ASD2230-induced inflammatory markers was compared between inflammatory and control phenotypes for both models to determine whether their differential expression also associated with responses that were induced by different types of stimuli.

With organ specificity being a desirable property of biomarkers, and particularly those that will be sought in accessible fluids, data from GEO was also used with the aim of **assessing the pulmonary specificity of AZD2230-associated miRNAs**. By comparing the expression of AZD2230 associated miRNAs between the lungs and 18 other tissue types in healthy rats, it was possible to determine which miRNA markers were most likely to be expressed predominantly by the lungs (and therefore have the greatest potential utility in the current context). This final aim served to meet the over-arching aim of the project; **identifying markers of inflammation in accessible bio-fluids that originated from injury within the lungs**.

2.2: Methods

2.2.1: AZD2230-exposed tissue samples: AstraZeneca (UK) (unrecorded personnel) supplied pulmonary tissue harvested from 11 Sprague Dawley rats 24 hours after completion of a 7-day course of intratracheal treatment with 1mg/kg or 3mg/kg AZD2230 in saline or

with only the saline vehicle (for control purposes), administered once daily. These doses were established based on the maximum tolerated dose (determined within AstraZeneca, based on terminal sampling) plus an intermediate dose to provide a dose-response. Cell count values produced from the bronchoalveolar lavage fluid (BALF) of each animal were also provided by the team at AstraZeneca. These data were established using standard staining and flow cytometry methods.

2.2.2: Statistical analysis of BALF metadata: Differences in the cellular content of BALF from each treatment group were identified and examined for significance using one-way ANOVA tests with Bonferroni correction to account for multiple testing. Differences in cell count that produced corrected p values ≤ 0.05 were considered significant. Analysis was performed using GraphPad Prism version 5 (Graphpad Software, USA).

2.2.3: miRNA sequencing data analysis: miRNAs from the AZ samples were prepared and sequenced by Beijing Genomics Institute (BGI). Samples were prepared using the Small RNA v1.5 Sample Preparation Kit (Illumina) in accordance with the manufacturer's instructions and data was acquired by a Hiseq2000 sequencing system (Illumina). The data was imported into CLC Genomics Workbench 7.4.0 where the sequences were adaptor trimmed. Reads were imported into sRNA Workbench and aligned against the *Rattus norvegicus* miRNA reference data available in miRBase release 21 to produce read count values for each known miRNA within the samples. Sequences with >1 mismatched base or expression counts lower than 10 were excluded from the analysis to avoid inclusion of falsely assigned molecules. miRNA precursors were also excluded in order to limit the quantitative analysis to mature molecules that had the potential to interact with mRNA targets at the time of sampling.Expression of mature miRNAs was compared between treatment groups using the *differential expression* module of sRNA Workbench (based on the edgeR package for R). This software normalised the read counts using a trimmed means of M-values approach and calculated fold changes in the expression of known miRNA species between treatment groups in a pair-wise manner. Differential expression between

treatment groups was considered significant where the log fold change was ≥ 2.0 and p values ≤0.05 with a false discovery rate (FDR) ≤ 20% were produced.

2.2.4: mRNA sequencing data analysis: BGI sequenced the mRNA content of the tissue samples using the TruSeq RNA Sample Preparation v2 Kit (Illumina) and Hiseq 2000 sequencing platform (as instructed by the manufacturer). Adaptor trimmed sequence data was imported into CLC Genomics Workbench 7.4.0. Using an RNA-Seq Analysis tool, reads were mapped against genomic, mRNA and transcript reference sequences for *Rattus norvegicus* obtained from the Ensembl database (Release 76). To avoid inclusion of falsely assigned sequences, reads with >2 mismatches or counts of < 100 were excluded from further analysis.

2.2.5: Prediction of miRNA-mRNA pairing: Banks of predicted gene targets were identified for the differentially expressed miRNAs (DEmiRNAs) to limit analysis of the mRNA data to genes that were likely to be regulated by the DEmiRNAs. The *Predicted Targets* module of miRWalk 2.0 was employed for this purpose. The software used the algorithms of four target prediction databases (TargetScan, miRanda, miRDB and miRWalk itself) that searched for 7mer or 8mer complementarity between all known *Rattus norvegicus* gene sequences and each DEmiRNA (individually). To reduce the number of false positive matches, genes that showed complimentary pairing to the DEmiRNAs in ≥3 of the databases were included in the predicted target bank.

Graphpad Prism (Graphpad Software, San Diego) was employed to calculate Pearson's correlations between the read count values of DEmiRNAs and their respective lists of expected targets. Correlations were considered significant and strong where a p value of ≤ 0.05 and a correlation coefficient of ≤ -0.50 (for negative correlations) or ≥ 0.5 (for positive correlations) were produced. These mRNAs will be referred to as 'correlating mRNAs'.

For some analyses, use of correlating mRNAs was restricted to genes that contribute to the mammalian inflammatory response. A list of inflammatory response genes was compiled

from correlating genes that also existed within the *Immport* or *Immunome* Database lists of InnateDB (referred to as inflammatory correlating mRNAs). Contribution of inflammatory genes to metabolic pathways was explored by further restricting the list of inflammatory correlating mRNAs to those that belonged to KEGG pathway *rno01100*.

2.2.6: Hierarchical clustering analysis: Variation and similarities between the expression profiles (both miRNA and mRNA) of tissue samples were visualised by unsupervised hierarchical clustering analysis (HCA) using a Euclidean similarity metric. HCA was performed using Qlucore Omics Explorer V3.0.

2.2.7: Pathway over-representation analysis: Inflammatory pathways that could have been influenced by DEmiRNA activity were identified using the *pathway over-representation* module of IMPaLA. The list of inflammatory correlating mRNAs was computationally compared with 3073 previously defined gene sets (corresponding to cellular pathways) from 11 public databases (270) to identify pathways that significantly overlapped with the correlating mRNA set. The analysis was performed against a background gene set composed of all of the mRNA species that were measured in the tissue samples and had read count values ≥ 100. Pathways were considered to be significantly over-represented in the correlating mRNA dataset if they contained ≥4 correlated mRNAs and if their overlap was assigned a p value ≥ 0.05.

2.2.8: Identification of pulmonary-enriched DEmiRNAs: Pulmonary-enriched DEmiRNAs were identified using the GSE52754 dataset which was obtained by Minami *et al* (2013) and is available from the National Centre for Biotechnology Information Gene Expression Omnibus database (271). The dataset comprised quantile normalised gene expression values for miRNAs expressed in individual tissues of healthy, 9-week-old male Sprague-Dawley rats and was acquired using a customised 8x 15k Agilent Rat miRNA microarray containing probes from miRBase 15.0 and 16.0. Log2 fold changes in DEmiRNA expression were obtained between lung tissue and 18 other tissue types using GEO2R (a web tool that runs BIOquery and limma packages for differential expression analysis in R). DEmiRNAs

were considered to be enriched in pulmonary tissue if their fold change was significant ($p \leq 0.05$) and indicated greater expression in the lung than for 90% of the tested tissues.

2.2.9: Analysis of publically available microarray datasets: miRNA microarray datasets produced during studies of pulmonary inflammation were identified in Gene Expression Omnibus using the search terms 'miRNA AND lung AND inflammation'. Datasets were selected for comparison with the AZD2230 dataset where studies were performed *in vivo* and were accompanied by experimental evidence of an inflammatory phenotype (**Table 2.1**). Differential expression analysis was performed for each quantile normalised dataset using the GEO2 tool to identify miRNAs that were differentially expressed between control samples and samples with an inflammatory phenotype ($p \leq 0.05$).

2.3: Identification of miRNA-associated transcription factors: Transcription factors that may have influenced the expression of inflammatory miRNAs were identified using the TMREC database. Algorithms within the database sought to match the input miRNA against 74,248 curated cascades of miRNA- transcription factor interactions (sourced using TransmiR, TRANSFAC, miRecords and TARBase databases) (272).

Table 2. 1: Experimental characteristics of publically available datasets used for comparison with the AZD2230 model of inflammation.

Dataset	Inflammatory stimulant	Tissue	Species	Data acquisition	Reference
GSE37085	Constitutive IL-13 over-expression induced by exposing	Pulmonary	*Mus musculus* (C57BL/6)	Affymetrix miRNA array	Ooi *et al.* 2012 (273) PMID: 22611474

	CC10-rtTA-IL-13 transgenic mice to 2 mg/ml doxycycline (in H_2O) for 7 days.	(harvested 7 days post-exposure)			
GSE19487	40 mg nanoTiO_2 / m^3 for 1 hour / day for 11 consecutive days	Pulmonary (harvested 5 days post-exposure)	*Mus musculus* (C57BL/6)	Agilent-019119 Mouse miRNA Microarray 1.0 G4472A	Halappanavar *et al.* 2010 (274) PMID: 21259345

2.3: Results

2.3.1: AZD2230 exposure induced an inflammatory response in rat pulmonary tissue

Elevated quantities of inflammatory cells within the BALF are representative of an inflammatory response within the accompanying lung parenchyma (275). The cellular content of BALF collected from the AZD2230-exposed and control rats was therefore used as a marker of inflammation within their pulmonary tissue. This information was compared between dosage groups to establish whether AZD2230 had stimulated a pro-inflammatory response within the lungs (**Figure 2.1**).

In comparison with vehicle samples, the total inflammatory cell content of BALF increased significantly after 7 days of AZD2230 exposure in a dose dependent manner. Specifically, 1mg/kg treatment stimulated significant increases in BALF platelet content (455%) compared with controls. Numbers of neutrophils, macrophages, lymphocytes and eosinophils were also heightened within the BALF (3152, 130, 144 and 244% respectively) but not strongly enough to reach statistical significance. With 3mg/kg treatment, neutrophils, lymphocytes, eosinophils and platelets were significantly more abundant in the BALF compared with control samples (4136, 339, 329 and 507% respectively). Macrophage counts remained heightened when compared with controls (136%) but did not increase when compared to the BALF of animals treated with 1mg/kg AZD2230. These results indicated that AZD2230 treatment induced infiltration of the small airways by inflammatory cells, reflecting a dose-dependent pro-inflammatory pulmonary response.

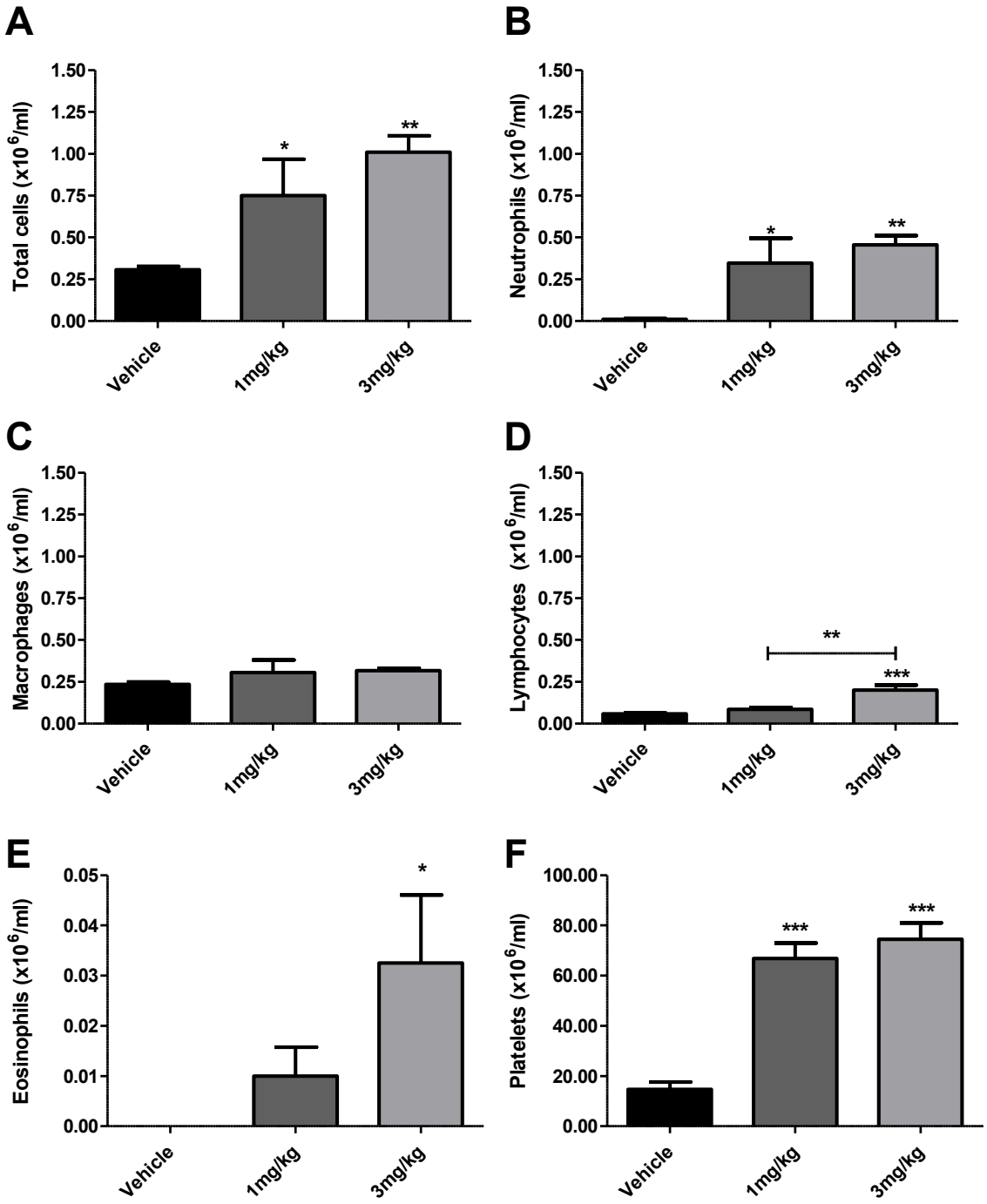


Figure 2. 1: Absolute counts of total inflammatory cells and platelets (A), neutrophils (B), macrophages (C), lymphocytes (D), eosinophils (E) and platelets (F) measured in BALF samples of rats treated with 0, 1 or 3mg/kg AZD2230 once daily for 7 days. Significant differences in the cellular content of BALF from each treatment group were identified using one-way ANOVA tests with Bonferroni correction. Differences in cell count with p values <0.05 were considered significant and are labelled '*'. '**' and '***' represent significant differences with p values of <0.01 and <0.001 respectively. Error bars show the standard error of the mean. n=3-4

2.3.2: AZD2230 exposure modulated miRNA expression in AZ rat lung tissue

Next generation sequencing was employed to collect the miRNA expression profiles of non-exposed, control pulmonary tissue and pulmonary tissue exhibiting an AZD2230-dependent inflammatory phenotype. Sequencing generated an average of 1.8 $x10^7$ reads per sample of which 95% ± 2.4% could be mapped to the genome. On average, 72.2% ± 2.5% of these reads aligned with the sequences of known mature miRNAs with an average of 549 ± 20 mature miRNA species being detected per sample.

Differential expression analysis was employed to explore the cause of variation between the miRNA transcriptomes of different treatment groups. It was used to identify miRNAs that showed significantly different expression levels when compared between control samples and samples exposed to 1mg/kg or 3mg/kg AZD2230. For a miRNA to be considered differentially expressed between two groups its log2 fold change in expression after exposure must have been ≥2.0 with a p value of ≤ 0.05 and FDR ≤ 20%.

miRNAs that fit these criteria are displayed in **Table 2.2**. Following exposure to 1mg/kg AZD2230, 3 miRNAs exhibited differential expression when compared with controls. Of these, 1 was up-regulated with treatment and 2 were down-regulated. Following exposure to 3mg/kg AZD2230, 22 miRNAs exhibited differential expression with enhanced differential expression being evident for the 3 that were significantly altered following exposure to 1mg/kg AZD2230. Of these miRNAs, 7 were down-regulated and 15 were up-regulated. These results suggest that AZD2230 exposure alters miRNA expression in a dose-dependent manner.

HCA was performed using the normalised read count data for DEmiRNAs to confirm whether their expression patterns proved characteristic for the different treatment groups. The resulting dendrogram (**Figure 2.2**) clustered 3mg/kg AZD2230 treated samples from the 1mg/kg AZD2230 and vehicle treated samples at the first branch (with the exception of one sample) then split the vehicles from the 1mg/kg AZD2230 treated samples at the second branch. This confirmed that the greatest difference in DEmiRNA expression profiles existed

between vehicle and 3mg/kg AZD2230 treated groups and that the second largest difference existed between vehicle and 1mg/kg AZD2230 treated samples. The result indicates that altered expression of these miRNAs associates with and represents AZD2230 induced inflammation.

Table 2. 2: miRNAs that displayed differential expression in the pulmonary tissue of rats following a 7 day course of intratracheal exposure to 1 or 3mg/kg AZD2230. Read count values were obtained via next generation sequencing and compared with those obtained from the pulmonary tissue of vehicle- exposed rats using sRNA Workbench. Differentially expressed miRNAs met the following criteria: log2 fold change ≥ 2 or ≤ -2, p≤ 0.05 and FDR ≤ 20%.

Treatments compared	miRNA	Log2 fold change	P Value
Vehicle vs 1mg/kg AZD2230	rno-miR-449a-3p	+5.59	<0.001
	rno-miR-204-5p	+2.38	0.023
	rno-miR-1298	-2.1	<0.001
Vehicle vs 3mg/kg AZD2230	rno-miR-204-5p	+6.69	<0.001
	rno-miR-449a-3p	+6.64	<0.001
	rno-miR-329-5p	+3.71	0.006
	rno-miR-212-3p	-3.69	<0.001
	rno-miR-1298	-3.55	<0.001
	rno-miR-449c-5p	+3.24	<0.001
	rno-miR-133b-3p	+3.12	<0.001
	rno-miR-365-5p	+3.04	<0.001
	rno-miR-483-3p	+3.03	0.044
	rno-miR-448-3p	-2.99	<0.001
	rno-miR-1912-3p	-2.91	<0.001
	rno-miR-212-5p	+2.83	<0.001
	rno-miR-155-5p	+2.79	<0.001
	rno-miR-429	+2.72	<0.001
	rno-miR-3583-5p	-2.56	0.013
	rno-miR-21-3p	+2.56	<0.001
	rno-miR-301b-3p	+2.53	0.002
	rno-miR-6215	+2.41	0.002
	rno-miR-493-5p	-2.39	0.037
	rno-miR-130b-3p	+2.22	<0.001
	rno-miR-15b-5p	+2.13	<0.001
	rno-miR-34b-5p	-2.09	<0.001

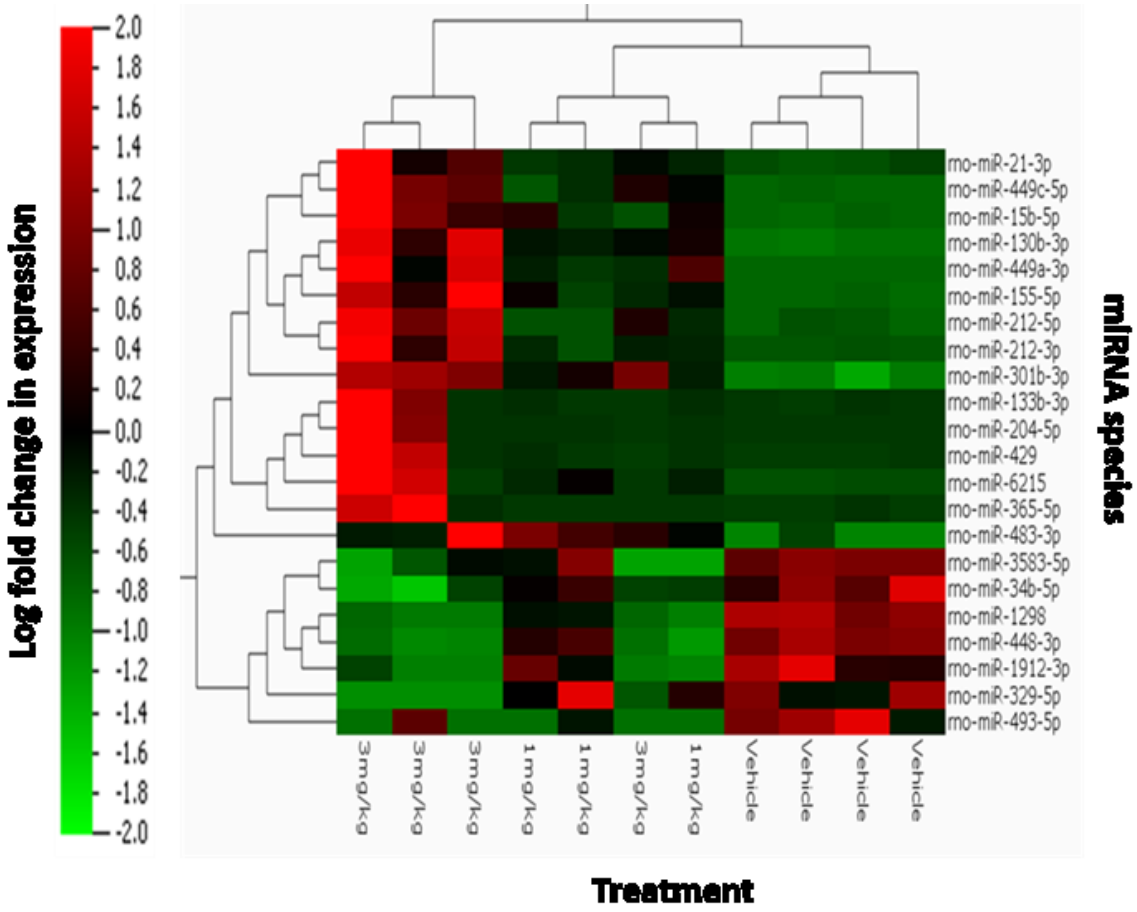


Figure 2. 2: HCA of pulmonary tissue samples following a 7 day course of exposure to AZD2230 (1 or 3mg/kg, administered once daily) or a saline vehicle in the rat. HCA was performed using the expression values of miRNAs that were differentially expressed between vehicle and exposed samples (log2 fold changes in expression of ≤-2 or ≥ 2 and p value <0.05 as measured by the EdgeR package of sRNA Workbench using read count values obtained by next generation sequencing). Analysis was performed on Qlucore Omics Explorer and used a Euclidean similarity metric.

2.3.3: Identification of potential DEmiRNA activity using mRNA sequencing data

The conventional use of bioinformatics based algorithms for miRNA target prediction is limited by a high false positive rate. Therefore, the contributions that DEmiRNAs made to AZD2230-induced pulmonary inflammation were explored by integrating computational target prediction algorithms with mRNA next generation sequencing data. This analysis sought to identify genes that showed evidence of being regulated by the DEmiRNAs in response to AZD2230 exposure.

Next generation sequencing identified 8829 mRNA species in the AZD2230 samples that had expression levels ≥ 100 counts. Of these, 1,065 were identified as putative targets of the DEmiRNAs using the miRNA target prediction module of miRWalk. 465 predicted target mRNAs displayed expression patterns that significantly and strongly correlated with the expression patterns of ≥ 1 of 15 of the DEmiRNAs in response to AZD2230 exposure (p value ≤ 0.05, Pearson's r ≤ - 0.5 for negative correlations or ≥ 0.5 for positive correlations) with 706 unique mRNA-miRNA interactions being identified. This approach was far more stringent than the use of target prediction algorithms alone with only 5-51% of the miRWalk predictions being supported by the AZD2230 exposure model (**Table 2.3**).

Although the down-regulatory role of miRNA activity has been explored in greater detail, interactions between miRNAs and mRNAs have also been shown to enhance gene expression (112). In this study, 52% of mRNA-miRNA pairings displayed negatively correlating expression patterns which are indicative of the miRNAs having inhibitory influences on expression of their target genes. The remaining 48% of miRNAs displayed positively correlating expression patterns with their mRNA targets, suggesting that they may have an inducible role (if found to interact directly). As a result of AZD2230-induced differential expression of the DEmiRNAs, these regulatory relationships resulted in decreased counts of 326 correlating mRNAs (63% due to decreased expression of inducible DEmiRNA activity and 37% due to increased expression of inhibitory DEmiRNAs) and

increased counts of 347 correlating mRNAs (37% due to increased expression of inducible genes and 67% due to decreased expression of inhibitory DEmiRNAs).

As miRNAs commonly function by degrading target mRNAs, it was hypothesised that DEmiRNA-targeted mRNAs would be differentially expressed between AZD2230 and vehicle exposed samples. This was confirmed by performing unsupervised HCA on the read count data of mRNA genes that correlated with ≥1 DEmiRNA.

The analysis indicated that a large difference in gene expression existed between vehicle and AZD2230- exposed samples which were separated by the first branch of the dendrogram. Except for one 3mg/kg sample, samples exposed to 1mg/kg and 3mg/kg AZD2230 were differentially clustered at the second branch of the dendrogram (**Figure 2.3**). This confirmed that expression of DEmiRNA- regulated mRNAs was altered in a dose-dependent manner following AZD2230 exposure, indicating that AZD2230 may have enhanced the biological activity of the DEmiRNAs. The direction of gene regulation was consistent across the dose range with 243 mRNA genes (52% of total miRNA-targeted genes) being down-regulated and 222 genes (48% of total miRNA-targeted genes) being up-regulated following exposure to either 1mg/kg or 3mg/kg AZD2230.

Table 2. 3: Percentages of predicted DEmiRNA targets that display correlated expression patterns with their computationally associated DEmiRNAs in the AZD2230 exposure model using next generation mRNA sequencing data.

miRNA	Number of computationally predicted targets	Number of correlated targets	% of predicted targets that correlate with DEmiRNA expression
miR-130b-3p	218.00	40.00	18.35
miR-133b-3p	237.00	13.00	5.49
miR-15b-5p	438.00	43.00	9.82
miR-204-5p	408.00	21.00	5.15
miR-212	165.00	85.00	51.52
miR-21-3p	165.00	24.00	14.55
miR-301b-3p	221.00	72.00	32.58
miR-329-5p	248.00	18.00	7.26
miR-34b-5p	350.00	102.00	29.14
miR-365-5p	157.00	11.00	7.01
miR-429	367.00	28.00	7.63
miR-448-3p	242.00	65.00	26.86
miR-449	367.00	39.00	10.63
miR-483-3p	244.00	57.00	23.36
miR-493-5p	219.00	54.00	24.66

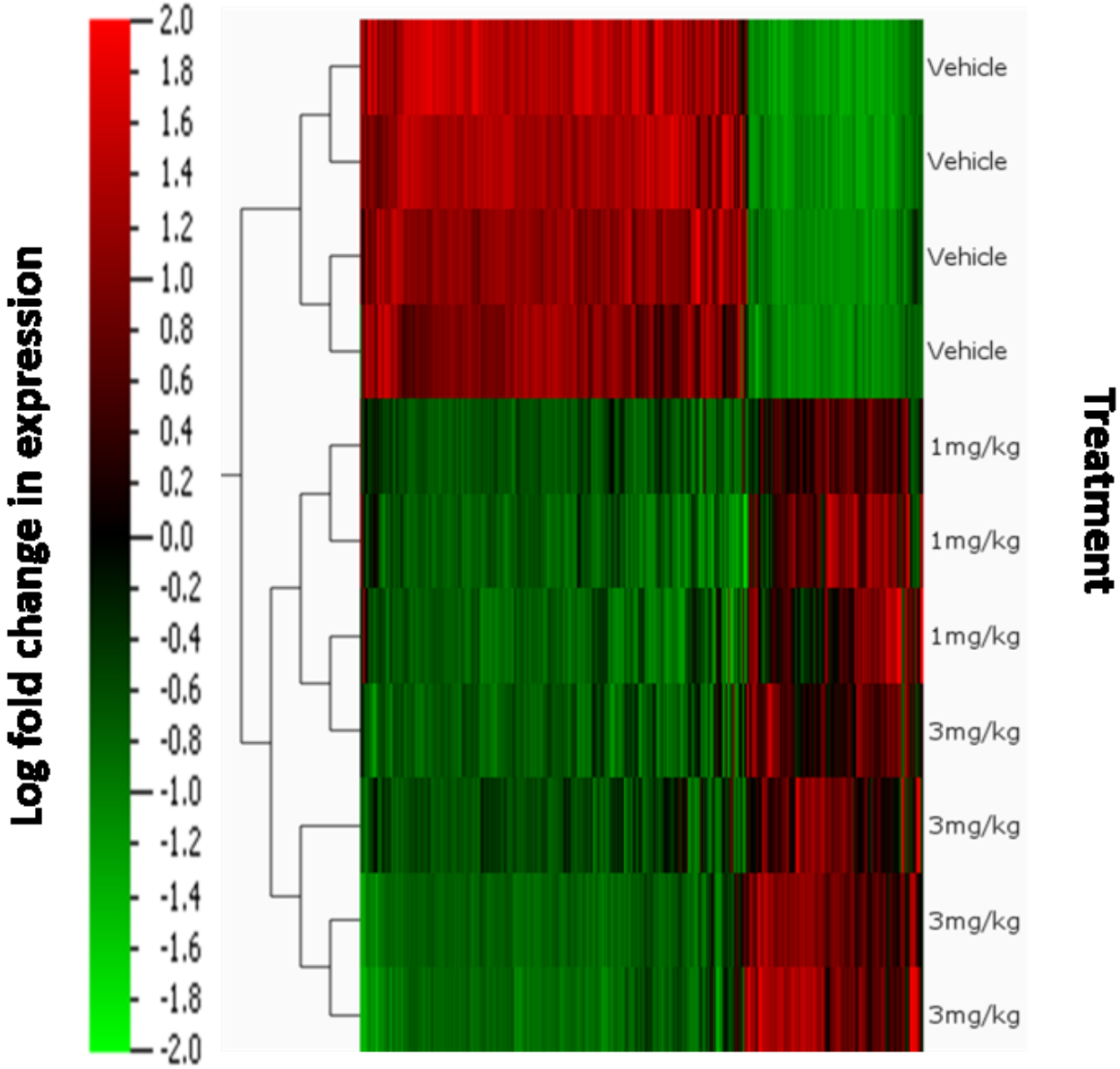


Figure 2. 3: HCA of pulmonary tissue samples following exposure to AZD2230 (1 or 3mg/kg) or a saline vehicle in the rat. HCA was performed using the expression values of mRNAs with expression patterns that correlated strongly and significantly with the expression of ≥ 1 DEmiRNA ($p < 0.05$ and a correlation coefficient of ≤ -0.50 for negative correlations or ≥ 0.5 for positive correlations as determined by Pearson's correlation analysis). Analysis was performed on Qlucore Omics Explorer and used a Euclidean similarity metric.

2.3.4: DEmiRNA activity modulates inflammatory mechanisms

Pathway over-representation analysis was performed upon the set of DEmiRNA-regulated mRNA genes to identify mechanisms by which the differential miRNA activity could have contributed to the pulmonary response to AZD2230 exposure. The analysis also served to determine whether non-inflammatory mechanisms were co-induced by the exposure as these could confound identification of inflammation-specific markers.

Biological pathways relating to lipid metabolism were most over-represented in the gene set (11 pathways identified) followed by cytokine modulated responses (9 pathways identified), cytokine neuronal signalling, small molecule transport, tumour suppression (3 pathways identified per category), endocytosis (2 pathways), apoptosis, calcium signalling, cell cycle progression, airway hyper-responsiveness and hypoxia signalling (1 pathway identified per category). Two pathways that included validated miRNA targets were also identified as over-represented in the gene set (**Table 2.4**).

Literature resources indicated that the majority of over-represented pathways play roles in the mammalian inflammatory response but that some, such as calcium and neuronal signalling, are not inflammation-specific (276–278). To focus on inflammation-specific responses to AZD2230 exposure, genes that did not contribute to a known inflammatory response were discounted from further analysis. This was achieved by selectively focusing on genes that are included in the *Immport* or *Immunome* Database lists of InnateDB (a manually curated list of experimentally validated inflammatory genes) and served the purpose of filtering out differential miRNA activity that regulated cellular functions additional to inflammation.

Visualisation of the inflammatory mRNA-DEmiRNA network showed that 148 of the DEmiRNA-regulated genes had an inflammatory-specific function (32% of the total correlating mRNAs). While miR-34b-5p, miR-301b-3p and miR-212 had the greatest number of interactions with inflammatory mRNAs (35, 29 and 25 targets respectively), all 15 DEmiRNAs regulated expression of ≥1 inflammatory gene following AZD2230 exposure.

Evidence of co-operative regulation was also evident between the DEmiRNAs with 30% of the inflammatory mRNAs being targeted by multiple DEmiRNAs

(18% by 2 DEmiRNAs, 9% by 3 DEmiRNAs and 3% by 4 DEmiRNAs) (**Figure 2.4**). Together these data suggest that the DEmiRNAs influenced the inflammatory component of the pulmonary response to AZD2230 exposure and that they worked co-operatively as a network.

Table 2. 4: Over-represented pathways within the list of correlating mRNAs. Pathways were identified using IMPaLA and selected as contributors to the pulmonary response to AZD2230 exposure in rats where ≥ 4 correlating mRNAs were included in the pathway and when the overlap was assigned a p value ≤ 0.05. Analysis was performed against a background gene set composed of all of the mRNA species that were measured in the tissue samples and displayed read count values ≥ 100.

Pathway category	IMPaLA pathway identifier	p value
Airway responsiveness	Beta-agonist/beta-blocker Pathway	≤ 0.01
Apoptosis	Apoptosis modulation and signalling	≤ 0.01
Calcium signalling	Calcium signalling pathway	≤ 0.05
Cell cycle progression	Aurora A/B signalling	≤ 0.05
Cytokine modulated response	Beta2 integrin cell surface interactions	≤ 0.05
	Gap junction	≤ 0.05
	AP-1 transcription factor network	≤ 0.05
	Syndecan-4-mediated signalling events	≤ 0.05
	Arginine and proline metabolism	≤ 0.05
	Cytokine-cytokine receptor interaction	≤ 0.05
	TNF signalling pathway	≤ 0.05
	ALK1 signalling events	≤ 0.05
	Type II interferon signalling	≤ 0.05
Endocytosis	Nef-mediates down modulation of cell surface receptors	≤ 0.05
	Endocytosis	≤ 0.05
Hypoxia signalling	HIF-1-alpha transcription factor network	≤ 0.05
Lipid signalling	Glycosphingolipid biosynthesis	≤ 0.01
	D-*myo*-inositol-5-phosphate metabolism	≤ 0.01
	Synthesis of PIPs at the golgi membrane	≤ 0.01
	Cholesterol biosynthesis	≤ 0.01
	Activation of gene expression by SREBP	≤ 0.01
	Recycling pathway of L1	≤ 0.01
	L1CAM interactions	≤ 0.05
	Triacylglyceride synthesis	≤ 0.05
	Sphingolipid metabolism	≤ 0.05
	Glycerolipid metabolism	≤ 0.05
	Regulation of cholesterol biosynthesis by SREBP	≤ 0.05
Neuronal signalling	Synaptic vesicle pathway	≤ 0.01
	GABAergic synapse	≤ 0.01
	Serotonergic synapse	≤ 0.05
Small molecule transport	Transport of small molecules	≤ 0.05
	Membrane trafficking	≤ 0.05
Tumour suppression	Validated transcriptional targets of TAp63 isoforms	≤ 0.01
	Direct p53 effectors	≤ 0.05
	BARD1 signalling events	≤ 0.05
Validated miRNA targets	miR-targeted genes in squamous cell	≤ 0.01
	miR-targeted genes in muscle cell	≤ 0.01

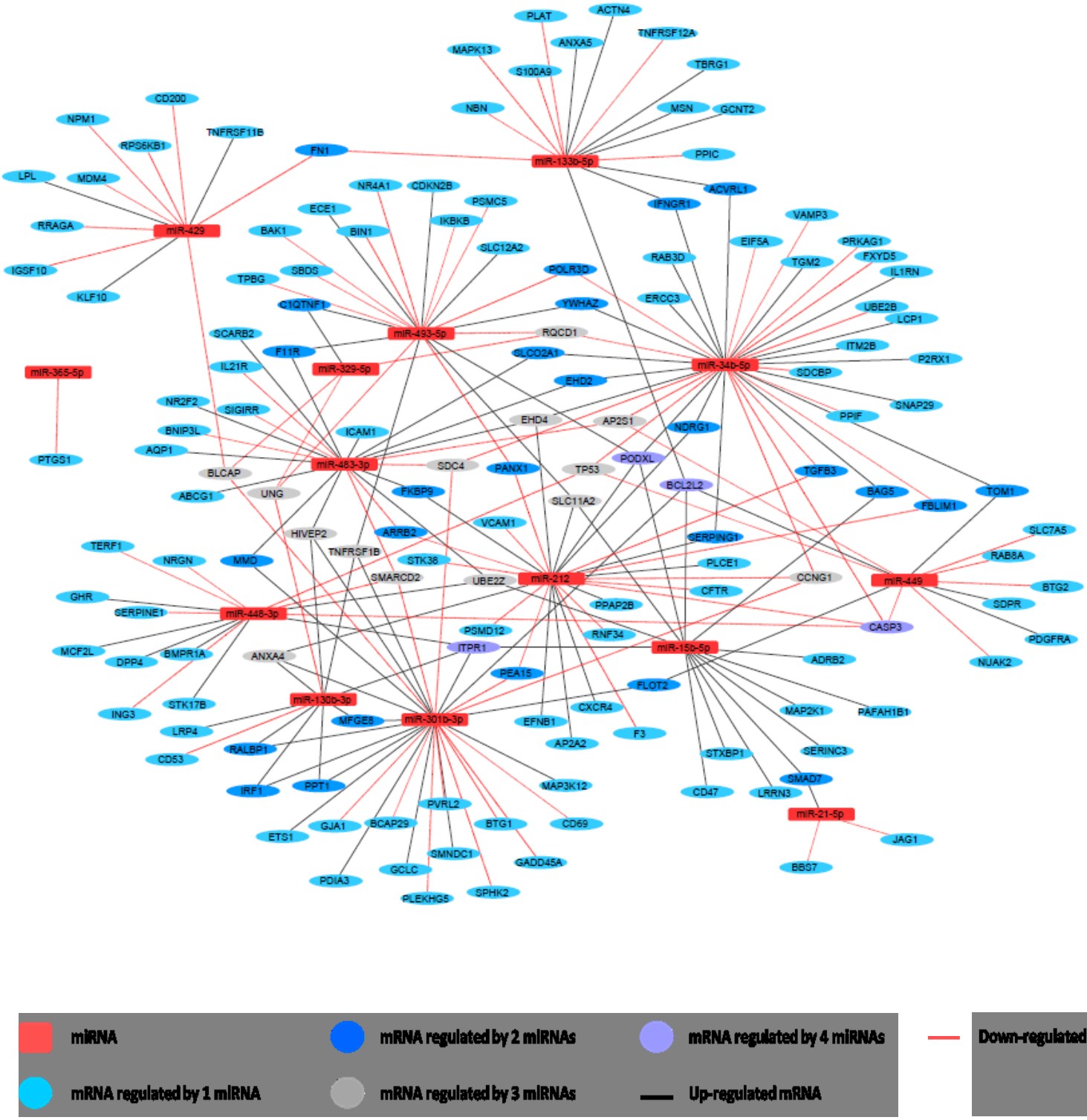


Figure 2. 4: Regulatory interactions between DEmiRNAs and their inflammatory mRNA targets. mRNA genes included in this network are members of the Immport or Immunome Database lists of InnateDB and have correlated expression values with ≥1 DEmiRNA in the pulmonary tissue of rats following intratracheal exposure to 1 or 3mg/kg AZD2230 ($p < 0.05$ and a correlation coefficient of ≤ -0.50 for negative correlations or ≥ 0.5 for positive correlations as determined by Pearson's correlation analysis). Directionality of regulation was determined using read count data for individual genes.

Further interrogation of the inflammatory gene network sought to address the over-arching aim of identifying both miRNA and metabolite markers of pulmonary inflammation by identifying whether any of the DEmiRNA targets encoded proteins with metabolic activity. Of the 148 mRNA genes that belonged to the inflammatory network, 9 were identified as metabolic genes due to the inclusion of their protein products within KEGG pathway *rno:01100* (Metabolic Pathways for *Rattus norvegicus*).

Exploration of the functions of these genes determined that 7 of the metabolic inflammatory genes encoded protein mediators of lipid metabolism with only the genes encoding subunits of RNA polymerase III and glutamate-cysteine ligase belonging to other metabolic pathways (**Table 2.5**).

Table 2. 5: List of DEmiRNA-targeted inflammatory mRNAs with metabolic functions

mRNA	Protein	KEGG Orthology	DEmiRNA regulators
POLR3D	RNA polymerase III subunit D	Nucleotide metabolism	miR-212, 34b
PLCE1	Phospholipase C epsilon 1	Inositol phosphate metabolism	miR-212
GCLC	Glutamate-cysteine ligase catalytic subunit	Glutathione metabolism Cysteine and methionine metabolism	miR-301b
GCNT2	Glucosaminyl (*N*-acetyl) transferase 2, I-branching enzyme (I blood group	Glycosphingolipid biosynthesis	miR-133b
PAFAH1B1	Platelet activating factor acetohydrolase 1B subunit	Ether lipid metabolism	miR-15b
PPAP2B	Lipid phosphohydrolase 3	Glycerolipid metabolism	miR-212
PPT1	Palmymitoyl-protein thioesterase 1	Fatty acid metabolism	miR-130b, 301b
PTGS1	Prostaglandin-endoperoxide synthase	Arachidonic acid metabolism	miR-365
SPHK2	Sphingosine kinase 2	Sphingolipid metabolism	miR-301b

2.3.5: miR-34b and miR-449a are predominantly expressed by pulmonary tissue:

The major aim of the AZD2230 exposure study was to identify miRNAs that associated with inflammation in the lung specifically. As such it was necessary to identify whether any of the AZD2230-associated DEmiRNAs are expressed more predominantly by lung tissue than other tissues. This was achieved using the GSE52754 dataset (acquired by Minami *et al.* 2014 (271)) which enabled comparison of DEmiRNA expression between the lungs of healthy rats and 18 other tissue types.

Differential expression analysis identified that expression of miR-34b-5p and miR-449a-3p was significantly greater in lung tissue than in 95 and 90% of analysed tissues respectively. This indicated that these miRNAs are predominantly expressed by pulmonary tissue in the rat. Indeed, only the testes and bone marrow expressed greater or statistically similar quantities of either miRNA when compared with lung tissue (**Figure 2.5-6, Table 2.6**).

miR-429 and 130b expression levels were significantly greater in the lung than for 63 and 68% of analysed tissues (respectively) suggesting that these miRNAs were largely expressed by lung tissue but not specifically so. Pulmonary expression of the remaining DEmiRNAs was either statistically similar to or less than the expression levels of more than 50% of the analysed tissues with miR-212 and 329 being expressed at higher levels by all other tissues (**Figures 2.5-6, Table 2.6**). As such, only miR-34b and miR-449a were carried forward as potential markers of pulmonary inflammation.

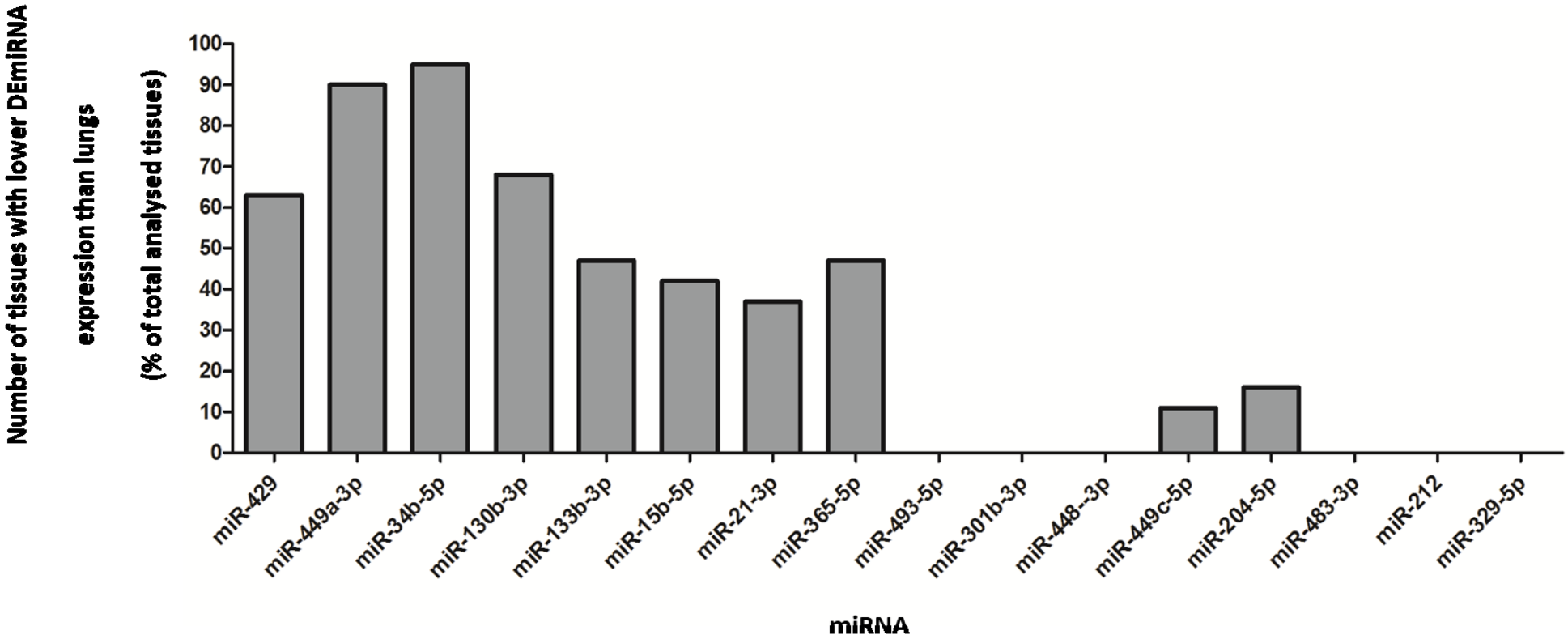


Figure 2. 5: Numbers of tissues that express lower concentrations of DEmiRNAs than lung tissue in healthy male rats. Values were obtained from the GSE52754 dataset (n=3) and are expressed as a percentage of the total number of tissues analysed.

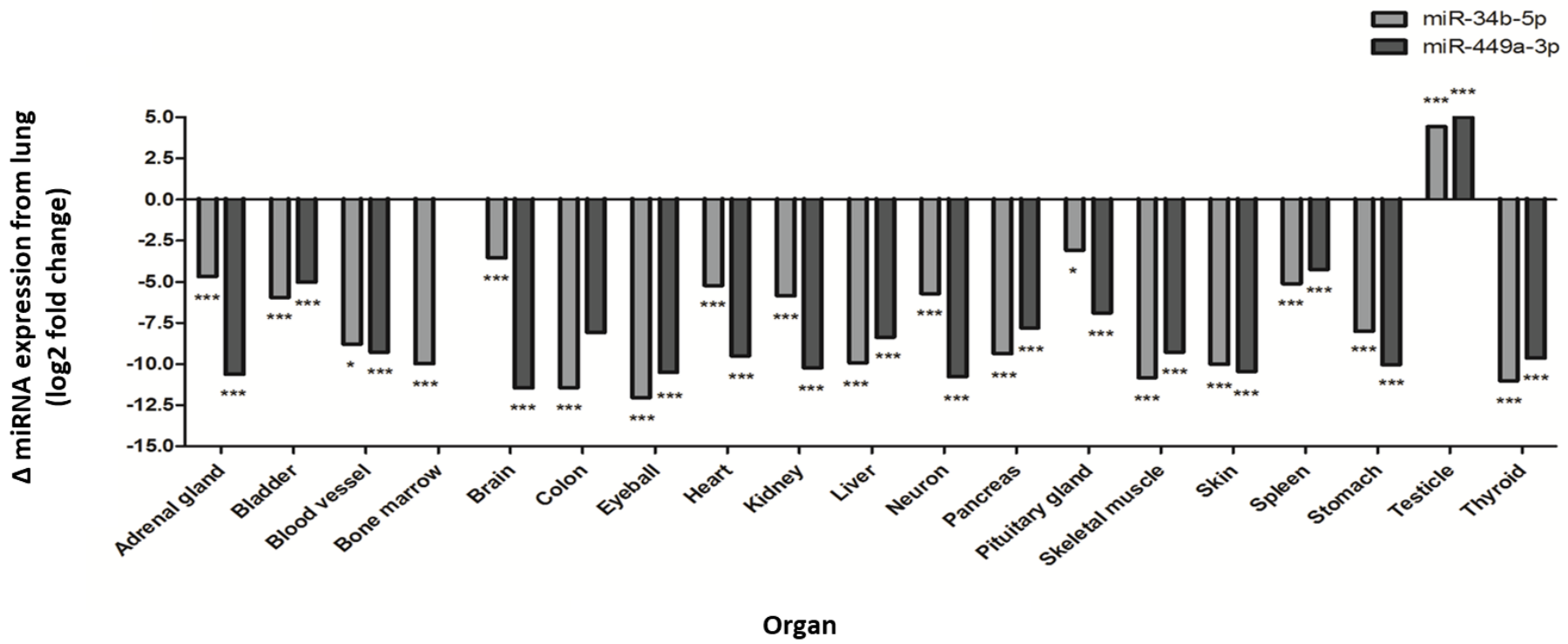


Figure 2. 6: Differences in expression levels of miR-34b-5p and miR-449a-3p between lung and other tissues in healthy male rats. Values were obtained from the GSE52754 dataset (n=3) and represent log2 fold changes in the expression of DEmiRNAs that were significantly enriched in pulmonary tissue ($p \leq 0.05$ and log2 fold change ≤ 0.00 in $\geq 90\%$ of assessed tissue types). * $p \leq 0.05$, *** $p \leq 0.001$.

Table 2. 6: Differences in DEmiRNA expression between pulmonary and other tissue types within the healthy rat. Values were obtained using the GEO2 differential expression module of GEO using data available in the GSE52754 dataset. Differences in miRNA expression were considered significant where assigned p values ≤ 0.05. Red highlighting indicates that a miRNA is expressed at significantly greater levels in the lungs than in the compared tissue while green highlighting indicates that the compared tissue contained greater levels of a miRNA than lung tissue. No highlighting is representative of statistically similar levels of miRNA expression between the lungs and the compared tissue.

	miR-34b	miR-449a	miR-130b	miR-429	miR-133b	miR-365	miR-15b	miR-21	miR-204	miR-449c	miR-493	miR-301b	miR-448	miR-483	miR-212	miR-329
Adrenal gland	-4.66	-10.61	-4.04	-12.70	-3.81	0.02	-1.25	0.02	1.53	0.12	0.12	0.12	0.12	6.12	6.48	11.90
Bladder	-5.97	-5.04	-5.65	0.11	4.65	1.82	-0.40	1.60	2.28	-2.74	0.37	0.37	0.37	2.65	0.37	8.71
Blood Vessel	-8.78	-9.27	-6.58	-11.37	4.12	2.48	-0.04	0.66	2.90	1.46	1.46	1.46	1.46	3.26	1.46	6.69
Bone marrow	-9.98	0.01	4.36	-10.68	-3.30	-0.13	-0.55	-0.31	-6.64	2.15	2.15	3.94	2.15	7.75	6.12	2.15
Brain	-3.54	-11.45	-7.84	-11.43	-2.14	-2.61	-3.01	-3.08	3.64	-3.21	-0.05	-0.05	2.76	0.72	8.76	12.51
Colon	-11.42	-8.09	2.83	2.75	-0.20	-1.67	0.33	1.65	1.81	0.70	0.70	2.70	0.70	4.79	7.47	0.70
Eyeball	-12.04	-10.51	-3.09	-1.50	3.53	-0.65	-1.31	-1.25	8.68	-1.80	0.87	0.87	0.87	2.79	0.87	9.91
Heart	-5.22	-9.50	-5.91	-11.02	9.29	-0.44	-0.08	-0.20	0.30	-1.51	1.94	1.94	1.94	4.57	1.76	1.94
Kidney	-5.85	-10.23	-3.63	1.38	-2.54	-0.57	-0.41	0.72	2.50	-2.24	1.21	1.21	1.21	-0.82	2.17	4.20
Liver	-9.92	-8.36	-4.77	-3.98	-8.05	1.42	-0.09	2.32	-3.19	-0.37	3.08	3.08	3.08	4.10	7.19	3.08
Neuron	-5.73	-10.76	-5.36	-12.30	0.00	0.11	-0.45	-0.56	5.49	-2.53	0.63	0.63	0.63	2.20	1.17	11.27
Pancreas	-9.36	-7.81	-4.22	-1.54	-7.50	-1.89	-4.30	-3.15	-5.45	0.18	12.03	3.63	3.63	6.60	10.39	3.63
Pituitary Gland	-3.09	-6.89	1.30	0.56	-2.09	-3.02	-1.14	-3.19	4.95	-0.26	3.83	5.44	-0.26	1.61	9.69	12.78
Skeletal Muscle	-10.82	-9.27	-5.67	-10.81	10.31	1.10	-0.81	-0.81	2.22	-1.03	2.13	2.13	2.13	4.56	4.94	11.43
Skin	-10.01	-10.44	-2.96	-0.10	6.21	0.05	0.10	0.40	2.95	-2.45	1.00	1.00	1.00	-2.91	6.39	9.44
Spleen	-5.12	-4.25	3.15	-12.14	-2.32	-1.72	2.47	1.87	3.92	-2.63	0.82	4.33	0.82	1.36	6.01	4.79
Stomach	-8.01	-10.03	2.01	3.14	-2.79	-0.78	0.08	0.92	-0.46	-2.04	1.41	1.41	1.41	1.63	6.58	1.41
Testicle	4.43	4.99	-6.13	-11.27	-1.41	-2.53	2.02	-0.04	4.94	-1.50	1.66	1.66	1.66	3.29	2.23	1.66
Thyroid	-11.02	-9.62	-1.14	1.55	2.12	-0.50	-0.30	-1.38	5.72	1.11	1.11	1.11	1.11	6.77	1.11	7.10

2.3.6: Differential expression of miR-34b and 449a is not specific to AZD2230 induced pulmonary inflammation

For use as markers of pulmonary inflammation, differential expression of miR-449a and 34b in inflamed lungs must be validated in additional and different models of pulmonary inflammation. Therefore, the applicability of these miRNAs as markers of general pulmonary inflammation was investigated through differential expression analysis of publicly available miRNA microarray datasets. The datasets selected for analysis provided examples of particulate-induced pulmonary inflammation (nanoTiO_2 exposure, GSE19487) and allergic airway inflammation (constitutive IL-13 expression, GSE37085).

Targeted mining of the lists of miRNAs that were differentially expressed between the pulmonary tissues of mice exposed to filtered air (control) and mice exposed to 40 mg/m^3 nanoTiO_2 identified that the particulate exposure induced log2 1.49 and log2 0.42-fold increases in miR-449a and miR-34b expression ($p \leq 0.001$) (**Figure 2.7A**). log2 0.79 and log2 0.41 fold increases in miR-449a and 34b expression were also identified in the pulmonary tissue of mice with constitutive IL-13 expression when compared to wild-type mice with basal IL-13 expression levels (**Figure 2.7B)**. These patterns of differential expression were equivalent to those induced by AZD2230 for miR-449a **but not** for miR-34b which was down-regulated in the AZD2230 model (see **Table 2.2**). These data suggest that over-expression of miR-449 during inflammation occurs independently of the stimulus type but that miR-34b expression may be regulated by different or additional processes following AZD2230 exposure.

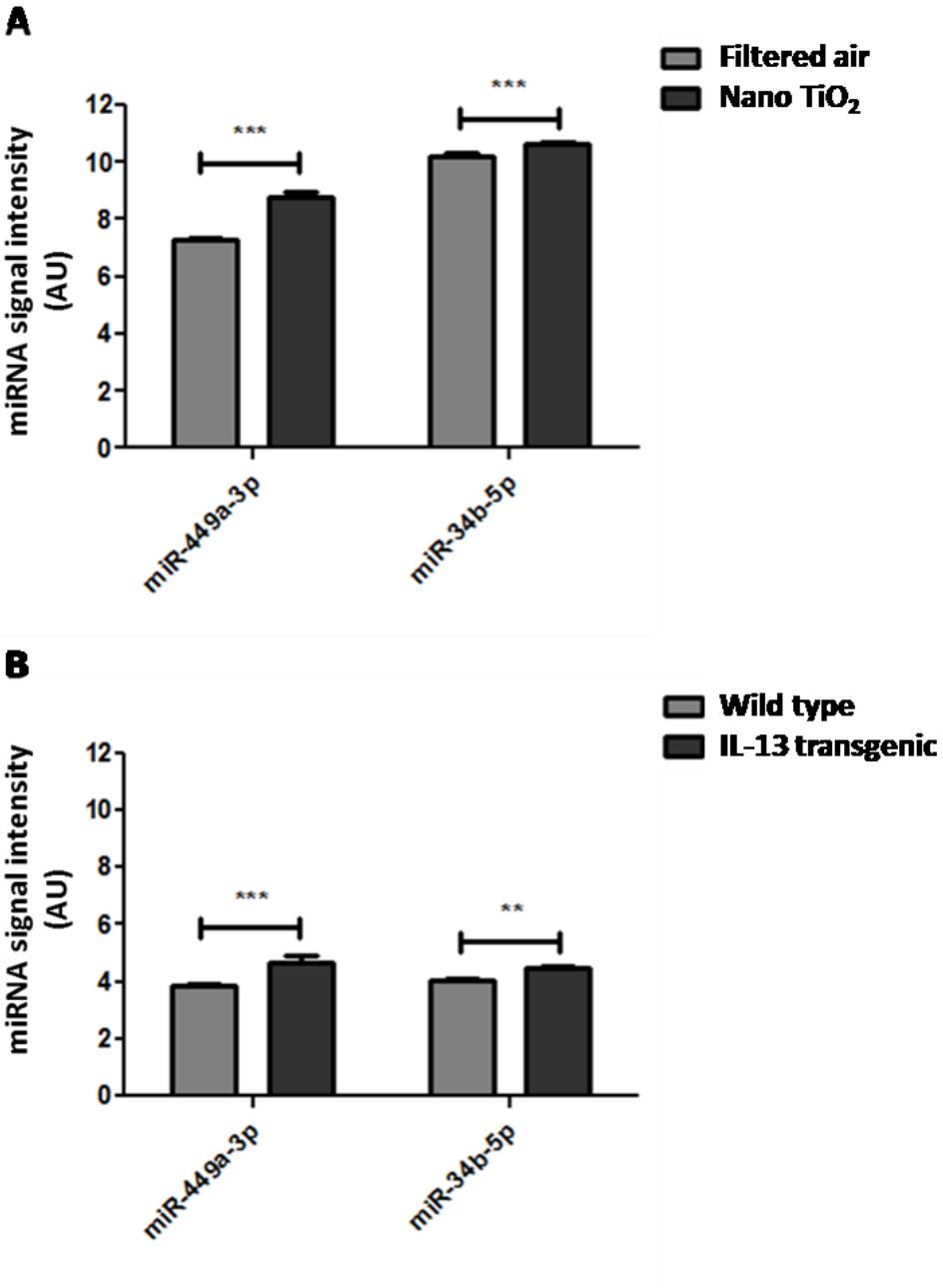


Figure 2. 7: Expression levels of miR-449a-3p and miR-34b-5p in the pulmonary tissue of mice exposed to 40mg/m3 nanoTiO2 or filtered air (A) or with constitutive or wild type IL-13 expression (B). Values were obtained from datasets and differential expression was established using the GEO2 analysis module of GEO. ** p≤ 0.01, *** p ≤ 0.001. Error bars represent standard error of the mean calculated from n=13 (A) or n= 6 (B).

2.3.7: miR-34b expression was driven independently of transcription factor activity

miR-449a/34b regulation was explored with the aim of understanding why miR-34b and 449a were differentially regulated following AZD2230 exposure despite belonging to the same miRNA family and functioning co-operatively in other models (279). The work also sought to determine why this regulatory event only occurred in the AZD2230 model but not the nanoTiO_2 or IL-13 models.

miRNA expression is strongly regulated at the transcriptional level and regulation of miR-449/34 family members by multiple transcription factors (TFs) has been validated *in vitro* within the context of carcinogenesis (280,281). Mining of the TMREC database determined that miR-34b and 449a are regulated by non-overlapping groups of transcription factors (tumour protein 53 (p53), snail family transcriptional repressor 1 (Snai1) and Zinc finger E-box-binding homeobox 1 (Zeb1) for miR-34b and cyclin dependent kinase (CDK), forkhead box protein O1 (FOXO1), retinoblastoma protein (Rb) and E2F transcription factor 1 (E2F1) for miR-449). This suggested that differential expression of p53, Snai1 or Zeb1 could have induced the differential regulation of miR-34b following AZD2230 exposure.

While no difference in Tp53 or Snai1 expression was detected, targeted analysis of the mRNA expression data showed that AZD2230 exposure induced a 48% decrease in Zeb1 expression as compared to vehicle exposure ($p < 0.05$) (**Figure 2.8A**) which correlated positively and strongly with the decreased miR-34b expression ($r = 0.90$, $p < 0.01$) (**Figure 2.8C**). This contrasted with the negative correlations that were observed between 16 and 9% decreases in Zeb1 expression ($p < 0.01$ and $p < 0.05$ respectively) following IL-13 and nanoTiO_2 exposure ($r = 0.74$ and 0.30 respectively, $p < 0.05$) (**Figure 2.8B, D and E**). As Zeb1 has been validated as a suppressor of miR-34 expression in both lung and breast adenocarcinoma cell lines (281), these results suggest that its activity contributed to up-regulation of miR-34b in the IL-13 and nanoTiO_2 models but was reduced or counteracted in the AZD2230 model specifically.

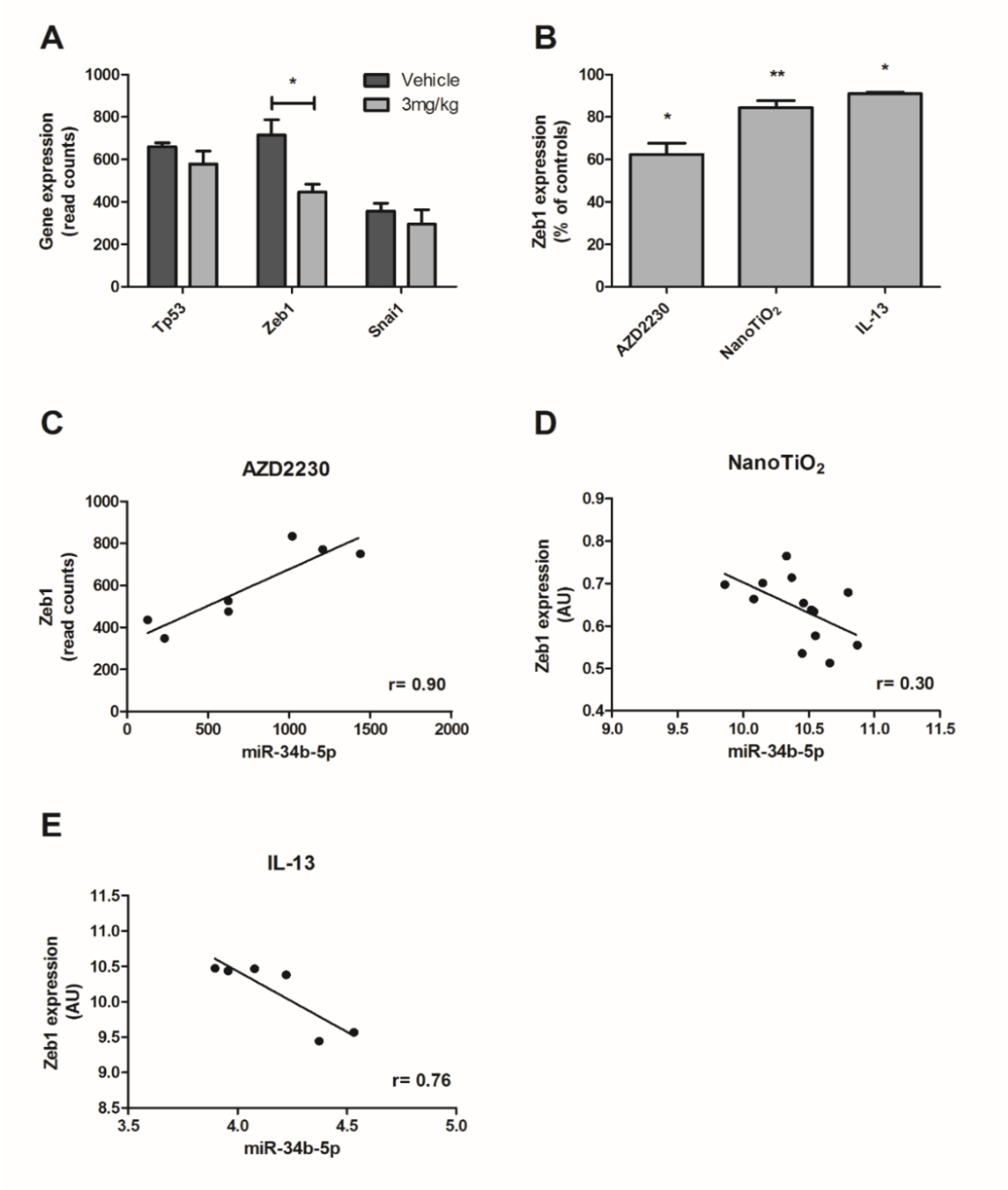


Figure 2. 8: Expression of transcription factors that target miR-34 (A and B) and their correlation with miR-34b expression in the pulmonary tissue of rats exposed to AZD2230 (C), nanoTiO$_2$ (D) or constitutive IL-13 expression (E). Gene expression values were obtained through mRNA sequencing with quantile normalisation (AZD2230 model) or by mRNA microarrays with locally weighted scatterplot smoothing normalisation (nanoTiO$_2$ and IL-13 models). Significant differences in gene expression were identified by Student's t test while correlations between transcription factor and miR-34 expression were established by Pearson's correlation analyses. Error bars represent SEM, n=6-13, * $p < 0.05$, ** $p < 0.01$.

2.4: Summary of results

- Intratracheal exposure to the pharmaceutical compound, AZD2230 induced an inflammatory phenotype (characterised by influx of immune cells) in the pulmonary tissue of rats.
- Expression of 15 miRNAs was significantly altered in association with AZD2230-induced pulmonary inflammation
- Differential expression of AZD2230-associated miRNAs was predicted to dysregulate expression of 148 inflammation-associated genes. Of these genes, 9 contribute to metabolic processes.
- Of the differentially expressed miRNAs, miR-34b and miR-449 displayed greatest specificity for pulmonary tissue when compared with 18 other tissues in healthy rats.
- Targeted analysis of microarray data from murine models of nanoTiO_2 exposure and IL-13 overexpression indicated that miR-34b and miR-449a have potential as biomarkers of pulmonary inflammation, independent of stimuli.

2.5: Discussion

Etheridge *et al.* (2011) suggest that biomarkers should possess several properties; they should be pathologically and organ specific, easily translatable between different models and non-invasively accessible (282). This body of work sought to identify alterations in miRNA expression that contribute to inflammation within the lungs and assess their suitability as biomarkers for pulmonary- specific inflammatory responses. Based upon global measurements of miRNA expression in the pulmonary tissue itself, the work was designed to direct targeted investigations into whether miRNA markers of pulmonary inflammation translate to accessible biofluids. Such markers could enable toxic responses to inhalable agents to be identified and monitored non-invasively in human cohorts, e.g. for exposomics studies or in preclinical assessments of toxicity.

The AZD2230 model of pulmonary inflammation in rats was used as a platform to identify miRNAs that regulate or are regulated by inflammatory pathways in the lungs. The model was selected because inhalation of AZD2230 induced dose-dependent infiltration of the airways by inflammatory cells which is a typical outcome of inflammatory cascades that begin within the lungs (283). Next generation sequencing produced comprehensive profiles of the miRNAs expressed within the pulmonary tissue of the rats, identifying 15 that associated significantly with the inflammatory phenotype.

Differential expression of these miRNAs was confirmed to influence the pulmonary response to AZD2230 exposure. This was established by integrating established computational target prediction algorithms with the output of complimentary mRNA sequencing data. This approach has previously furthered mechanistic understanding of conditions such as nasopharyngeal carcinoma (284) and COPD (269) and stringently bypasses the limitation that computational algorithms produce numerous false positive predictions through over-reliance on Watson-Crick pairing (265).

In this model of AZD2230 exposure, the method determined that expression of all fifteen DEmiRNAs correlated with dose-dependent changes in the expression of their predicted

mRNA targets. In particular, the miRNAs were shown to correlate with expression of genes that associate with inflammatory pathways specifically, including the TNF-α and interferon signalling pathways and AP-1 network activity. As miRNA regulatory mechanisms include degradation of mRNA molecules as well as promotion of mRNA translation (119), this suggested that the inflammatory response to AZD2230 exposure was under some post-transcriptional control by the DEmiRNAs. Furthermore, 30% of the gene targets were shown to be regulated by more than one DEmiRNA suggesting that this regulatory activity was fine-tuned and as the result of a co-operative network (119).

Many of the AZD2230-induced DEmiRNAs have been previously associated with inflammation in the lungs, indicating that their ability to represent pulmonary inflammation could apply across different *in vivo* models and human cohorts. miR-15b was shown to be over-expressed in the lungs of COPD patients (269) along with miR-34 and miR-449 (285) while miR-133b and miR-21 are up-regulated during allergic airway inflammation (286) and bleomycin-induced idiopathic pulmonary fibrosis (287). miR-365 was demonstrated to up-regulate IL-6 expression in alveolar macrophages during tuberculosis infection (279) and miR-212 has been associated with TLR signalling and modulation of NFκB expression in macrophages (288) which form the forefront of pulmonary defences.

The organ specificity of the AZD2230-associated DEmiRNAs was investigated with the aim of identifying those that were expressed characteristically by the lungs and could therefore be associated with pulmonary injury if detected in the systemic circulation. In line with previous comparisons (279,289,290), miR-34b and 449a were found to be expressed predominantly in the pulmonary tissue of healthy rats with only the testes displaying statistically similar or greater expression levels for either miRNA. As the testes are unlikely to be directly impacted by inhalable agents, the risk of this source confounding studies of pulmonary inflammation was considered to be minor. Therefore miR-34b and 449a were carried forward as candidate markers for pulmonary inflammation.

miR-34b and miR-449a possess homologous seed sequences meaning that they belong to the same functionally related family; the miR-449/34 family. This group of miRNAs is composed of six members (miR-449a, b and c which are encoded by one genomic cluster, miR-34b/c which are encoded by a second genomic cluster and miR-34a). *In vitro* pulmonary systems have shown that these miRNAs inhibit expression of cell cycle progression genes (291), which contributes to bronchial epithelial cell differentiation by inhibiting proliferative activity (292) and contributes to p53 or E2F1 mediated tumour suppression (289,291,293) alongside apoptosis (294). They also regulate multiciliogenesis in airway epithelial cells by repressing the Delta/Notch pathway (295).

For miR-34b and 449a to be considered markers of generalised pulmonary inflammation (rather than just an AZD2230 specific response), their differential expression must be applicable to multiple pulmonary inflammatory stimuli. Targeted investigations of miR-449a and 34b expression in mouse models of nanoTiO_2 exposure and constitutive IL-13 expression showed that both candidate markers were differentially expressed in additional and heterogeneous models of pulmonary inflammation. This suggested that differential expression of these miRNAs is common to pulmonary inflammation, independent of the stimulus; a result that is shared by studies of COPD and asthma cohorts (285,296) and LPS-stimulated macrophages (297).

The analysis did however, highlight an anomalous differential pattern of regulation for miR-34b in the AZD2230 model. Whilst nanoTiO_2 exposure and IL-13 activity induced significant up-regulation of both miRNAs, AZD2230 exposure only increased expression of miR-449a with miR-34b expression being significantly lower than for control samples. This is surprising because miR-449 and 34 family members are consistently shown to function redundantly and to be regulated in the same direction under experimental conditions (296,298).

It may be that the discrepancy in changes of miR-34b expression between models was contributed to by AZD2230-induced induction of DNA damage pathways. In addition to promotion of neutrophillic influx with the possibility of accompanying ROS production (which

may produce a spectrum of genotoxic effects ranging from nucleobase modification to strand breakages or crosslinks (Palmai-Pallag et al)), AZD2230 is shown to possess the molecular qualities of a non-typical DNA intercalator (namely more than two aromatic rings and a basic centre in a near-planar conformation (Borjesson et al)). In similarity to ROS induced DNA damage, DNA intercalating drugs are shown to activate p53 responses (Achanta et al, Wang and El-Deiry) which in turn regulate expression of miR-34 family members (Navarro and Leiberman). Although p53 activity is shown to enhance miR-34 expression (Navarro and Leiberman), activity of these miRNAs under DNA damaging conditions is only modestly reduced through silencing of p53 (Salzman et al) suggesting that additional regulatory molecules contribute to their response during DNA damage, potentially resulting in the decreased miR-34b expression seen in the AZD2230 model.

Indeed, pathway enrichment analysis showed that AZD2230 exposure associated with several pathways that are induced by transcription factors. As transcription factors are key regulators of miRNA expression (299) and DNA damage ((300), this lead to the hypothesis that the differential miR-34b regulation may have been caused by variation in transcription factor activity. In support, the TMREC database demonstrated that the promotors of miR-449b and 34a contain binding sites for non-overlapping sets of transcription factors.

Of the three transcription factors found to target miR-34b, only Zeb1 was differentially expressed by AZD2230 exposure, showing significant down-regulation. As Zeb1 is a validated suppressor of miR-34 (281), and its down-regulation correlated negatively with increased miR-34b expression in the nanoTiO_2 and IL-13 models, it may be that the differential miR-34b regulation was contributed to by additional regulatory events which counter-acted the activity of Zeb1.

These seemingly anomalous regulatory events could include hypermethylation of CpG islands in the miR-34 promoter which has been shown to have a silencing effect that counter-acts miR-34 induction by p53 (301) or up-regulation of miR-21 which has a suppressive effect in breast cancer cells (302). Alternatively, as p53 is a major inducer of

miR-34 expression (289) and p53 levels were not enhanced by AZD2230 exposure, this additional event could simply be an absence of agonistic activity. It must be noted however that this analysis was limited by an absence of functional protein quantification, thus excluding the impact of post-translational regulation of protein activity. Irrespective of the nature of the event, its discrepancy from the other models indicates that it is an artefact of AZD2230 exposure, potentially caused by the DNA intercalating structure of the compound. This suggests that the mechanism is unlikely to impact the use of miR-34b as a biomarker of pulmonary inflammation in new models, particularly if measured in tandem with miR-449a.

As miR-34b and 449a were not expressed exclusively within the lungs (just at higher levels than other tissues) their reliability as accessible biomarkers of pulmonary inflammation could be enhanced if they were measured as part of a wider molecular panel. In line with the over-arching aim of integrating miRNA and metabolite markers of pulmonary inflammation, eight AZD2230-associated DEmiRNAs were identified that target genes that encode metabolic pathway mediators.

Most of these gene targets are required for the synthesis or modification of pro-inflammatory lipids and were up-regulated by AZD2230 exposure, indicating that analysis of the lipid content of inflammatory samples could yield further mechanistically relevant biomarkers of pulmonary inflammation. These inflammatory lipids included prostaglandins (products of arachidonic acid metabolism that mediate allergic airway (303) and residual oil fly ash-induced inflammation (304)) and sphingolipids (inducers of IL-8 secretion by alveolar macrophages (305)).

GCLC; the gene that encodes the catalytic subunit of glutamate cysteine ligase (the rate limiting enzyme responsible for glutathione synthesis) was also dysregulated by AZD2230 exposure, showing evidence of down-regulation due to increased miR-301b activity. Glutathione (GSH) plays a critical role in protecting the lungs from oxidative stress with low levels leading to pro-inflammatory imbalances between oxidants and antioxidants (306). GCLC expression is modulated by AP-1 activity – a pathway that was dysregulated by

AZD2230 exposure- indicating that differential measurement of metabolites that belong to glutathione synthesis and activity pathways could also be a source of mechanistically relevant biomarkers of pulmonary inflammation.

2.6: Conclusion

Integration of miRNA and mRNA sequencing data confirmed a mechanistic role for miRNAs in the development of pulmonary inflammation *in vivo* and indicated that metabolic markers may also be detectable within inflamed lung tissue.

This body of work identified significant associations between the expression of miR-449a/34b and pulmonary inflammatory phenotypes with targeted measurements in healthy tissues and alternative inflammatory models indicating their candidacy as markers of stimulus-independent but pulmonary-specific inflammation. Such observations demonstrate that differential expression of miR-449a and 34b may be translatable to accessible biofluids following pulmonary insult, and could potentially be accompanied by characteristic metabolic changes.

Chapter 3: Circulating markers of pulmonary inflammation

Chapter overview

Detection of biomarkers of pulmonary inflammation in accessible sample types is an attractive proposition. The blood is a rich source of cell-derived miRNA and having identified that miR-34b and 449a are significantly differentially regulated in pulmonary tissue during inflammation, the following work sought to determine whether the same association is detectable in blood.

Targeted quantifications of extracellular miR-34b and 449a were performed in a targeted manner using a rat model of intratracheal lipopolysaccharide (LPS) exposure. These were accompanied by metabolic profiling with the aim of identifying markers of metabolic pathways that could accompany or be influenced by increased miR-34b and 449a activity.

3.1: Introduction

Following extensive exploration of their use as diagnostic and prognostic markers in the context of disease (282), extracellular miRNAs are being sought as non-invasive biomarkers for toxicological responses. Such considerations have focused primarily on adverse reactions to pharmaceuticals in the liver, kidneys, heart and retina (307–309) but evidence that exposure to ozone, ultrafine particles and metallic particles alters miRNA expression profiles in human sputum, saliva and blood (251,310,311) indicates that the approach could be applied successfully to investigations of pulmonary inflammation, particularly those relating to TRPM exposure.

Although Weber *et al.* (2010) demonstrated that extracellular miRNAs are present in 12 different biofluids (141), most biomarker searches have been performed in serum or plasma. Despite providing low yields of total RNA compared with tissue or cells, these biofluids contain approximately 350 characterised miRNA species (141) making them advantageous

for untargeted miRNA biomarker mining. Furthermore, many of the miRNAs that reside in serum and plasma localise to exosomes (312) . Exosomal miRNAs are hypothesised to contribute to intercellular communications, so changes in their concentrations are likely to provide mechanistic information regarding the cellular and molecular processes that triggered or inhibited their release.

A further advantage of using serum and plasma for miRNA biomarker studies is that these fluids are rich in metabolites (313), making them a prudent choice for inter-omics analyses. Serum in particular has been recommended for use in metabolomic analyses due to its enhanced metabolite content and stability when compared with plasma (313) and has been shown to display changes in metabolite content under conditions of pulmonary inflammation (314,315). These changes include alterations in carbohydrate and urea-arginine metabolite concentrations that correspond to changes seen in matched tissue samples (315), suggesting that the serum metabolome could be a useful source of markers for metabolic activity in inflamed lungs.

Workflows for integrating microtranscriptomic and metabolomic datasets are yet to be fully developed but integration of transcriptomic features (i.e. the product of the microtranscriptome) with metabolomic features is considered a powerful approach for enhancing mechanistic understanding of biological phenomena (316). By combining transcriptomic and metabolomic data, Cavill *et al.* (2011) demonstrated a 76% improvement in the detection rate of the pathways that underlay *in vitro* responses to chemotherapeutics as compared with the use of transcriptomics data alone (317).

To do this, the authors employed a statistical pathway-level approach that reflected the fact that genes and metabolites are linked through biochemical reactions (the building blocks of pathways) (270) rather than directly as for genes and proteins where simpler correlative integrations suffice (316). The study directed development of the webtool IMPaLA which (in addition to the gene enrichment analyses employed in **Chapter 2)** can search

simultaneously through its 3073 curated pathways, seeking those that are enriched for both genes and metabolites in an integrative manner (270).

3.1.2: Aims, hypothesis and study design

In consideration of the limited number of mechanistically relevant, circulating biomarkers that exist for pulmonary responses to inflammatory stimuli, the following study tested the hypothesis that **differential expression of the pulmonary inflammatory miRNAs (miR-34b and 449a) is present in the serum of rats during episodes of pulmonary inflammation and that accompanying metabolite markers can also be detected.**

Specifically the study sought to determine whether **serum concentrations of miR-34b and 449a are reflective of those seen in pulmonary tissue** during pulmonary inflammation and whether pulmonary inflammation is accompanied by **alterations in the serum metabolome** that may widen the panel of available biomarkers.

Modifying the approaches used by Cavill *et al.*, (2011) metabolic data (acquired globally by ^{1}H NMR spectroscopy) was integrated with the predicted gene targets of miR-34b/449a (as obtained in **Chapter 2**) to identify crossover between the pathways that were represented by the metabolite and miRNA markers. This approach aimed to add depth to the mechanistic value of individual miRNA and metabolite markers by identifying pathways that may not be detected by single-omics analyses.

Serum from the AZD2230 exposed rats was unavailable, therefore data was acquired for this study using the serum of rats that was harvested 4h after intratracheal exposure to LPS; a model that produces localised pulmonary inflammation. LPS endotoxins are a major component of the outer membrane of gram negative bacteria and as potent inducers of TLRs (**Figure 3.1**), are considered prototypical signals for activation of the innate immune system (318). As such, much of our understanding of *in vivo* pulmonary responses is attributable to models of LPS exposure (319–321) and the likelihood of circulating markers of LPS-induced pulmonary inflammation being applicable to additional models (including TRPM exposure) is strong.

With the aim of **increasing confidence in any metabolite or miRNA biomarkers found in this study**, analyses included data obtained from rats that were exposed simultaneously to LPS and the p38 MAPK inhibitor GSK258899. The rationale behind these experiments was that molecules that display altered serum concentrations in response to inflammatory stimuli will remain at control level where inflammation is inhibited, thus supporting their association with the inflammatory phenotype.

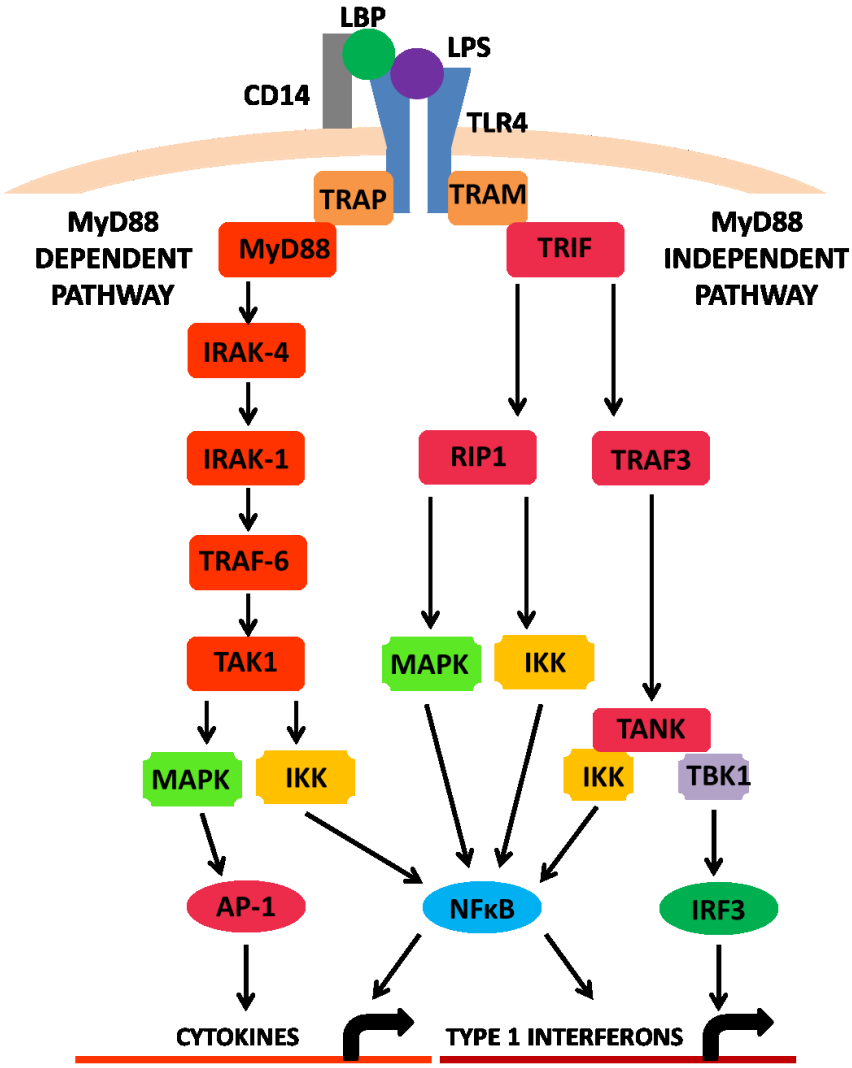


Figure 3. 1: LPS signal transduction. Upon contact with the pulmonary epithelial surface, LPS binds LBP via its lipid A group. LPB acts as a shuttle, transferring the endotoxin to cell membrane receptors such as CD14. Ligand binding at CD14 induces oligomerisation and activation of TLR4 which recruits intracellular adaptor proteins such as TIRAP and TRAM. Downstream processing may be dependent or independent of MyD88, depending on whether expression of cytokines or interferons and interferon-inducible genes is required. In the MyD88 dependent pathway, IRAK-4 phosphorylates and activates IRAK-1 which phosphorylates TRAF6 . Phosphorylated TRAF6 activates TAK1 which stimulates MAPK signalling and activates IKK regulators of NFκB signalling. These pathways enhance expression of cytokines and cytokine-inducible genes. LPS binding proteins (LBP), Toll-interleukin-1-receptor domain containing adaptor inducing interferon-β (TIRAP), Toll-interleukin-1-receptor related adaptor molecule (TRAM), Myeloid differentiation primary response gene 88 (MyD88), IL-1 receptor associated kinase-4 (IRAK-4) IL-1 receptor associated kinase-1 (IRAK-1) TNF receptor associated factor 6 (TRAF6) transforming growth factor-B-activated kinase 1 (TAK1).

3.2: Methods

3.2.1: Rat serum samples: Rat serum samples were kindly provided by Dr McKevitt's laboratory at GlaxoSmith Kline (UK). Samples were harvested from male Crl:WI(Han) rats 4h after intratracheal installation of 2 µg LPS (isolated from *E.coli* 0127:B8 and suspended in PBS), 2 µg LPS and 0.3, 3 or 30 µg/kg GSK258899 (blended with inhalation grade lactose), 30 µg/kg GSK258899 or lactose in phosphate buffered saline (PBS) as a vehicle control. To comply with ethical regulations, exsanguination was performed via the abdominal aorta under isoflurane anaesthesia and death confirmed by cervical dislocation.

3.2.2: RNA extraction: Total RNA was extracted from the plasma samples using a Trizol LS method. Plasma (200µl) was diluted 1:1 in RNase free H_2O and combined with 3.75 x volumes of Trizol LS (Life Technologies, UK) in ultra-high recovery tubes. The tubes were vortexed for 10 s, incubated for 5 mins at room temperature (RT) then spiked with 8.1 x 10^5 copies/µl of synthetic cel-miR-39 (QIAgen, Netherlands) which was used as an exogenous control. 1 x volume of chloroform was added to each sample then the tubes were vortexed again for 10 s, incubated at RT for 15 mins and centrifuged (12,000 x g, 4°C, 20 mins) to separate the solution into aqueous, precipitate and organic layers. The upper aqueous layer containing the RNA was transferred to a fresh tube, combined with 15 µg/ml GlycoBlue carrier molecule (Life technologies) and vortexed for 10 seconds with 0.75 x starting volume of 2:1 ethanol: isopropanol. Samples were incubated at RT for ten minutes then centrifuged (12,000 x g, 4°C, 20 mins) to pellet the RNA. RNA pellets were washed twice with 80% (v/v) ethanol then dried via SpeedVac (ThermoFisher Scientific, UK) using a medium heat for 4 mins before being re-suspended in 100 µl RNase free H_2O.

3.2.3: RNA purification: As plasma is highly proteinaceous, an acid: phenol clean-up procedure was performed to further purify the RNA. 100 µl RNA was combined with 100 µl 1:1 acid-phenol: chloroform and centrifuged for 15 mins (12,000 x g, 4°C). The upper aqueous phase was harvested and transferred to another tube while a further 100 µl H_2O was added to the acid-phenol: chloroform, vortexed and centrifuged (12,000 x g, 4°C) to

ensure maximal yield. The second aqueous phase was combined with the first and combined with 15 µ/ml GlycoBlue. Samples were precipitated overnight at -20°C in 1/10th volume of 3M NaOAc (pH5.2) and 2.75 x 100% ethanol then centrifuged for 10 minutes (12,000 x g, 4°C) to pellet the RNA. Once the supernatant had been discarded, RNA pellets were washed twice with 75% ethanol, dried using a SpeedVac (as above) and re-suspended in 20µl nuclease-free H_2O.

3.2.4: Total RNA and total miRNA quantifications: Total RNA was quantified using a Nanodrop 2000 UV-VIS spectrophotometer (Thermo Scientific, USA). Measurements were made in accordance with the manufacturer's instructions, measuring RNA at a wavelength of 260nm. Total miRNA was quantified using a 2100 Bioanalyzer and Small RNA Kit (Agilent) as instructed by the manufacturer.

3.2.5: cDNA synthesis: cDNA was synthesised using the TaqMan MicroRNA Reverse Transcription Kit (Applied Biosystems). For each reaction, 5 µl RNA was mixed with 10 µl mastermix containing 0.15µl of 100mM dNTP mix, 1 µl of 50U/µl multiscribe reverse transcriptase, 1.5 µl 10x RT buffer, 0.19 µl 20U/µl RNase inhibitor, 1.16 µl nuclease free H_2O and 3 µl each of reverse transcription primers for hsa-miR-449a or hsa-miR-34b and cel-miR-39. Reverse transcription was performed by incubating the samples at 16°C for 30 minutes, at 42°C for a further 30 minutes then heated to 85°C for 5 minutes to terminate the reaction. cDNA was stored at -20°c until use.

3.2.6: RTqPCR: Using a 96 well plate, 1.33 µl cDNA was combined with 18.67 µl of a mastermix containing 10 µl TaqMan 2x Universal PCR Master mix with Uracil *N*-Glycosylase (UNG), 7.67 µl nuclease-free H_2O and 1µl of 20x primers for hsa-miR-449, hsa-miR-34b or cel-miR-39. Plates were centrifuged for 5 mins at 10,000 xg and placed inside a QuantStudio 6 Flex RTqPCR System (Applied Biosystems) for data acquisition using Quantstudio 6 and 7 Flex Software. Samples were heated to 50°C for 2 minutes to activate the UNG enzyme

then to 95°C to activate taq polymerase before undergoing 40 cycles of product denaturation for 15 seconds at 95°C and product annealing and extension for 60 seconds at 60°C.

Raw data was analysed using the 2-($\Delta\Delta$ C_T) method described by Litvak and Schmittgen (2001) (322) . Briefly, changes in target expression (compared to control) were calculated using the mean cycle threshold (C_T) values of 3 technical repeats and calibrated to the accompanying change in exogenous control expression (cel-miR-39). This produced fold change values for the differences in target expression that existed between control and treated samples.

3.2.7: Functional annotation of predicted miR-34b/449a gene targets: Lists of predicted gene targets were produced for miR-34b/449a using the MiRWalk database. The molecular functions of the proteins for which these genes encode were explored using Panther Classification System with Gene Ontology version 1.2 (Paul Thomas, USA). Using manual curations and bioinformatic algorithms the database classified the genes based on gene ontology (GO) terms (323).

3.2.8: ^{1}H NMR spectroscopy: Serum samples were centrifuged for 10 minutes at 16000 *xg* to remove suspended particulate matter then combined with 10mM sodium 3-(trimethylsilyl)propionate-2,2,3,3-d4 (TSP) in D_2O and transferred to 5.00 mm NMR tubes . ^{1}H NMR spectra were acquired for the samples using a Bruker AVANCE 600 spectrometer (Bruker, Biospin, Rheinstetten, Germany) fitted with a Bruker TXI probe and an automated sample handling carousel (Bruker) at a frequency of 600.29 MHz and at a temperature of 300K. One dimensional NMR spectra were obtained using a Carr-Purcell-Meiboom-Gill (CPMG) spin-echo pulse sequence (324). Following 4 dummy scans, 32 transients were collected into 32,000 datapoints with a spectral width of 20 ppm, acquisition time of 3.07 seconds and relaxation delay of 4.00 seconds. Prior to Fourier transformation, a line broadening factor of 0.3 Hz was applied to all spectra.

3.2.9: Processing of ^{1}H NMR spectroscopic data: Spectra were imported into MATLAB R2013a (Mathworks, USA) where automatic phasing, referencing of chemical shifts to the resonance of the glucose peak (δ 5.233) and baseline correction were performed using an in-house code. Prior to peak alignment the residual water resonance (δ 4.18- 5.15 ppm) was removed and spectra exhibiting low signal: noise ratios were excluded from the analysis. The remaining data was normalised using the probabilistic quotient normalisation (PQN) method to protect against influences from non-biological variations in metabolite dilution such as pipetting error.

For multivariate analyses, full resolution spectra (29813 data points) were reduced to 45 data points (corresponding to individual peaks) by integration. To obtain the reduced resolution data, metabolite peaks were assigned using Chenomx software version 7.7 (Chenomx Inc, Canada). Assignments were confirmed by comparing the output of Statistical Total Correlation Spectroscopy (STOCSY) (which identified peaks with highly correlating concentrations ($r^2 \geq 0.9$) as belonging to a common molecule) with spectra from the Human Metabolome Database Version 3.6 (available at http://www.hmdb.ca/). These assignments directed selection of representative peaks for each metabolite from which peak areas were integrated based on manually assigned minima and maxima. Where metabolites contributed peaks at multiple resonances, the least overlapped peaks were selected for integration in order to produce the cleanest values.

3.2.10: Multivariate statistical analysis of ^{1}H NMR spectroscopic data: Feature metabolites were identified using multivariate approaches. Reduced resolution values were imported into SIMCA-P+ 14 (Umetrics, Sweden) and subjected to Pareto scaling. Principal Component Analysis (PCA) was performed to examine overall variance within the dataset and Partial Least Squares- Discriminant Analysis (PLS-DA) was implemented to model associations between metabolic profile and treatment type. PLS-DA modelling split the spectral data into a test set and a validation set and attempted to predict which classes the spectra in the validation set belonged to by comparing their metabolic content with that of

test set spectra. Modelling provided a Q^2 value that represented the goodness of prediction produced by the model, and thus, diagnosed its performance . Models that produced Q^2 values ≤ 0.5 were considered to have good predictive power and metabolites that displayed weights ≤ -0.2 or ≥ 0.2 in the PLS-DA loadings plots were treated as feature metabolites that were potentially influential to the model. The validity of PLS-DA modelling was assessed by permutations test. This cross-validation method rearranged the dataset into 1000 different permutations and compared their predictive power with that of the original dataset, providing R^2Y and Q^2Y values that indicated a valid model if below 0.40 and 0.05 respectively.

3.2.11: Integrated pathway analysis of miRNA quantification and ^{1}H NMR spectroscopic data: In order to study pathway level metabolic interactions, Pearson's correlation analyses were performed in a global manner using the reduced resolution values from the ^{1}H NMR experiment. Correlation coefficients ≥ 0.5 or ≤ -0.5 with p values ≤ 0.05 were considered to represent pathway commonality between the metabolites in question.

Cellular pathways that could have influenced the changes in feature metabolite concentration were identified using the pathway over-representation module of IMPaLA. Lists of feature and correlating metabolites and predicted gene targets for miR-34b/449a (identified using the MiRWalk database in **Chapter** 2) were input to the analysis. These were computationally compared with 3073 previously defined metabolite and gene sets (corresponding to cellular pathways) from 11 public databases (325) to identify pathways that significantly overlapped with the feature metabolite and target gene lists. Pathways were considered to be significantly over-represented in the integrated dataset if they contained ≥ 3 correlated metabolites and genes and if their joint overlap was assigned a p value ≥ 0.05 with a FDR of ≥ 20%.

3.2.12: Univariate statistical analysis of RTqPCR and ^{1}H NMR spectroscopic data: Student's T tests with FDR corrections were performed to identify statistically significant changes in the serum concentrations of feature metabolites and miR-34b/449a between

treatment groups. Correlation coefficients were compared between treatment groups using Fisher's Z tests. Any differences in concentrations or correlations with p values ≤ 0.05 and a FDR ≤ 20% were considered significant. Univariate analyses were performed using Microsoft Excel version 14.0.

3.3: Results

3.3.1 miRNAs are detectable within the serum of rats

Prior to quantifying miR-34b and 449a, the success of the RNA isolation procedure was assessed using Nanodrop 2000 and Bioanalyzer 2100 technology to measure total RNA and total miRNA concentrations within a subset of the serum samples. This check was performed because the RNA content of plasma is considerably lower than for cells and requires more steps to be isolated, posing multiple opportunities for loss of yield and the risk of obtaining poor starting material concentrations.

Samples displayed peaks at 260nm when analysed by Nanodrop 2000 UV/VIS spectrophotometer (**Figure 3.2 A**), indicating that RNA was present (with little contamination from protein that absorbs at 280nm). Across the subset total RNA yields ranged between 9.3 and 25.2 ng/ µl (**Table 3.1**), falling within the expected range of our laboratory (326) and meeting the assay requirements suggested for small RNA quantification (327). Quantification of the total miRNA content of the samples indicated that these total RNA concentrations were contributed to by miRNAs. Samples produced yields of 994.3- 21499.6 pg/ µl for RNAs falling within the expected size range for miRNA (**Table 3.1, Figure 3.2 B**).

Table 3. 1: Concentrations of total RNA and total miRNA within representative samples of rat serum. Data were acquired using Nanodrop 2000 and Bioanalyzer 2100 (with Small RNA Kit) instruments respectively. Bracketed numbers refer to two separate samples.

Sample	Total RNA (ng/ µl)	Total miRNA (pg/ µl)
Vehicle (1)	9.3	1516.1
Vehicle (2)	25.7	944.3
LPS (1)	13.3	5432.8
LPS (2)	16.7	16697.1
LPS + 0.3 µg/ kg GSK (1)	14.9	1674.1
LPS + 0.3 µg/ kg GSK (2)	7.6	1721.1
LPS + 3 µg/ kg GSK (1)	9.8	2612.0
LPS + 3 µg/ kg GSK (2)	12.7	1252.1
LPS + 30 µg/ kg GSK (1)	11.9	18504.7
LPS + 30 µg/ kg GSK (2)	25.2	21499.6
30 µg/ kg GSK (1)	19.5	18463.3
30 µg/ kg GSK (2)	14.4	16630.1

.

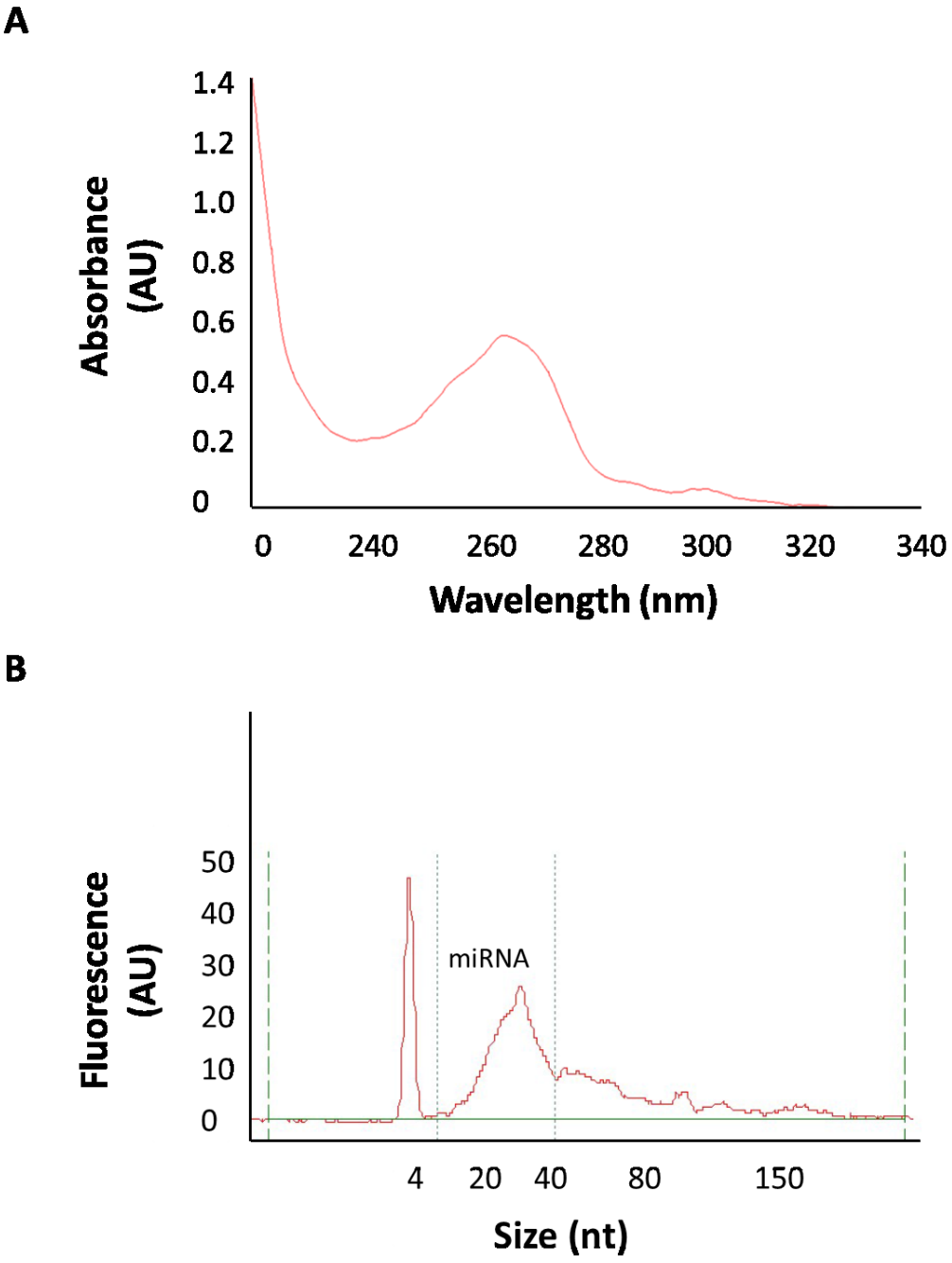


Figure 3. 2: Example spectra displaying the quantities of total RNA (A) and total miRNA (B) detectable in a representative sample of rat serum. Spectra were acquired using Nanodrop 2000 and Bioanalyzer 2100 (with Small RNA Kit) instruments respectively.

3.3.2 Serum concentrations of miR-34b and 449a are enhanced by pulmonary exposure to LPS

miR-34b and 449a were quantified within the serum of rats following 4h pulmonary exposure to LPS (2 μg) or to a non-inflammatory lactose-PBS control. These measurements aimed to determine whether the inflammation-induced changes in miR- 34 and 449 concentrations that were observed in pulmonary tissue (**Chapter 2**) are detectable in accessible blood samples.

RTqPCR measurements indicated that plasma concentrations of miR-34b and 449a were 6.09 ± 1.65 and 7.54 ± 1.84-fold greater in LPS-exposed rats compared with vehicle-exposed rats ($p \leq 0.01$) (**Figure 3.3**). These results indicate that pulmonary enhancement of miR-34b and 449a expression during inflammation translates to the serum.

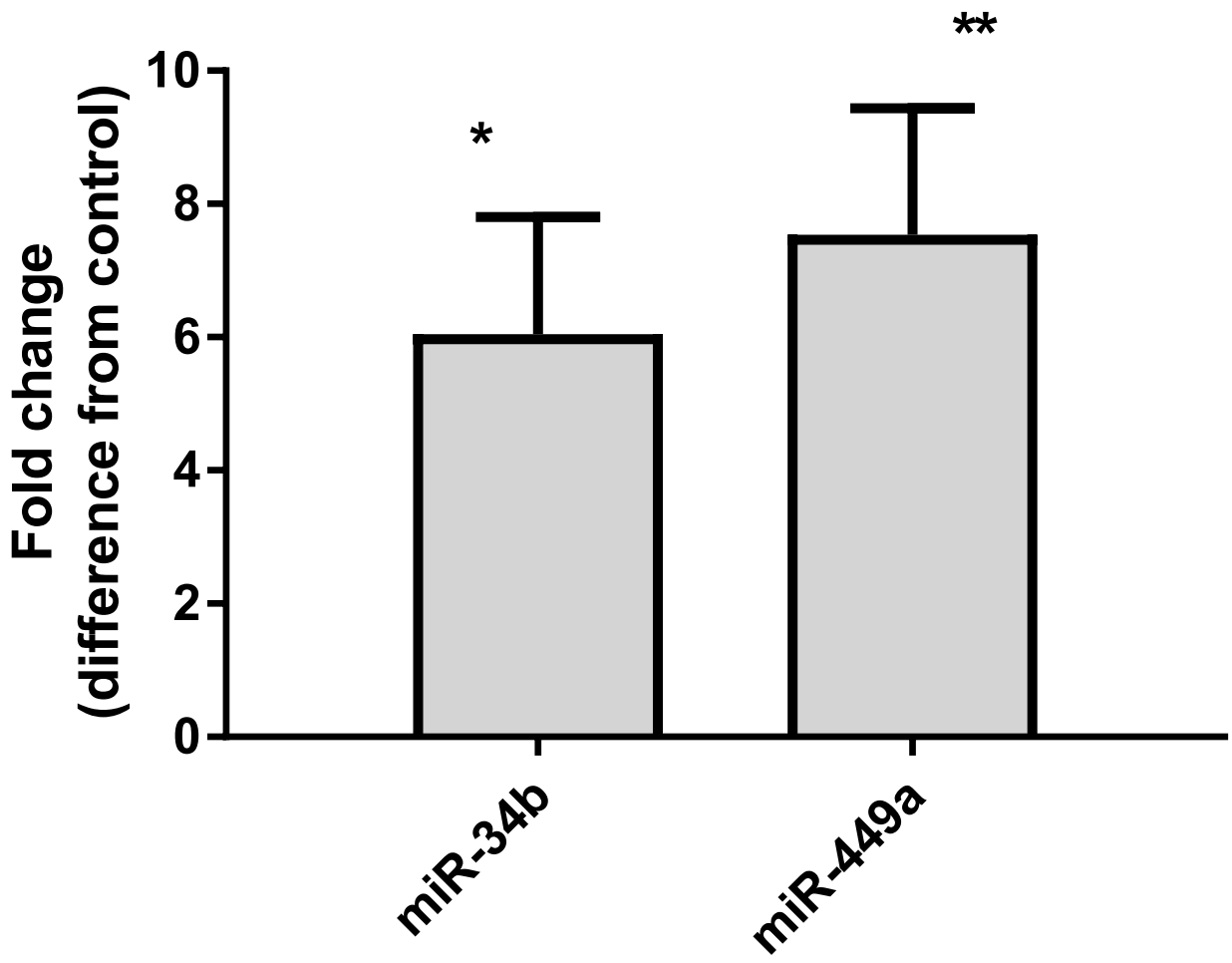


Figure 3. 3: Fold increases in miR-34b and 449a concentrations in the serum of rats following 4h pulmonary exposures to LPS (2 µg) as compared with serum from rats exposed to vehicle control. Data were acquired by RTqPCR, normalised to exogenous cel-miR-39 concentrations and analysed using the 2-(ΔΔ C_T) method. Values represent the mean ± SEM of 6-18 biological replicates, obtained from 3 technical replicates for each. Significant differences were detected between treatment groups using Student's T tests, * $p \leq 0.05$, ** $p \leq 0.01$.

3.3.3 LPS-induced increases in miR-34 and 449 expression are inhibited by p38 MAPK inhibition

To assess the association between LPS-induced pulmonary inflammation and increases in serum concentrations of miR-34b and 449a, the two miRNAs were quantified in the serum of rats that had been treated with LPS in the presence of an anti-inflammatory p38 MAPK inhibitor (GSK). The hypothesis driving this experiment was that inhibition of p38 MAPK activity (a key component of the LPS-induced inflammatory response) within the lung would prevent over-expression of miR-34b and 449a in the tissue and result in the serum concentrations remaining comparable to control.

While serum concentrations of miR-34b and 449a were elevated 0.09 and 0.25-fold by GSK exposure alone ($p = 0.09$ and 0.06, respectively), serum concentrations of both miRNAs were significantly lower in LPS exposed rats where the LPS was administered in combination with the inhibitor. When compared with samples from rats that had been exposed to LPS alone, miR-34b concentrations were 4.21, 4.12 and 4.48-fold lower in the serum of rats that were exposed to LPS in the presence of 0.3, 3.0 and 30.0 µg/ kg GSK ($p < 0.05$), becoming only 0.83, 0.91 and 0.56-fold higher than for control animals (**Figure 3.4 A**). miR-449a concentrations were also significantly decreased by GSK exposure, reducing 5.56, 5.73 and 5.99-fold in the presence of 0.3, 3.0 and 30.0 µg/ kg GSK ($p <0.01$) and becoming only 0.98, 0.81 and 0.25 fold greater than for control animals (**Figure 3.4 B**).

These results indicate that the elevations in serum concentrations of miR-34b and 449a that accompany pulmonary responses to LPS exposure are likely to be p38 MAPK dependent. Furthermore, mitigation of this response by GSK supports the association between serum concentrations of the miRNAs and inflammatory responses within the lung.

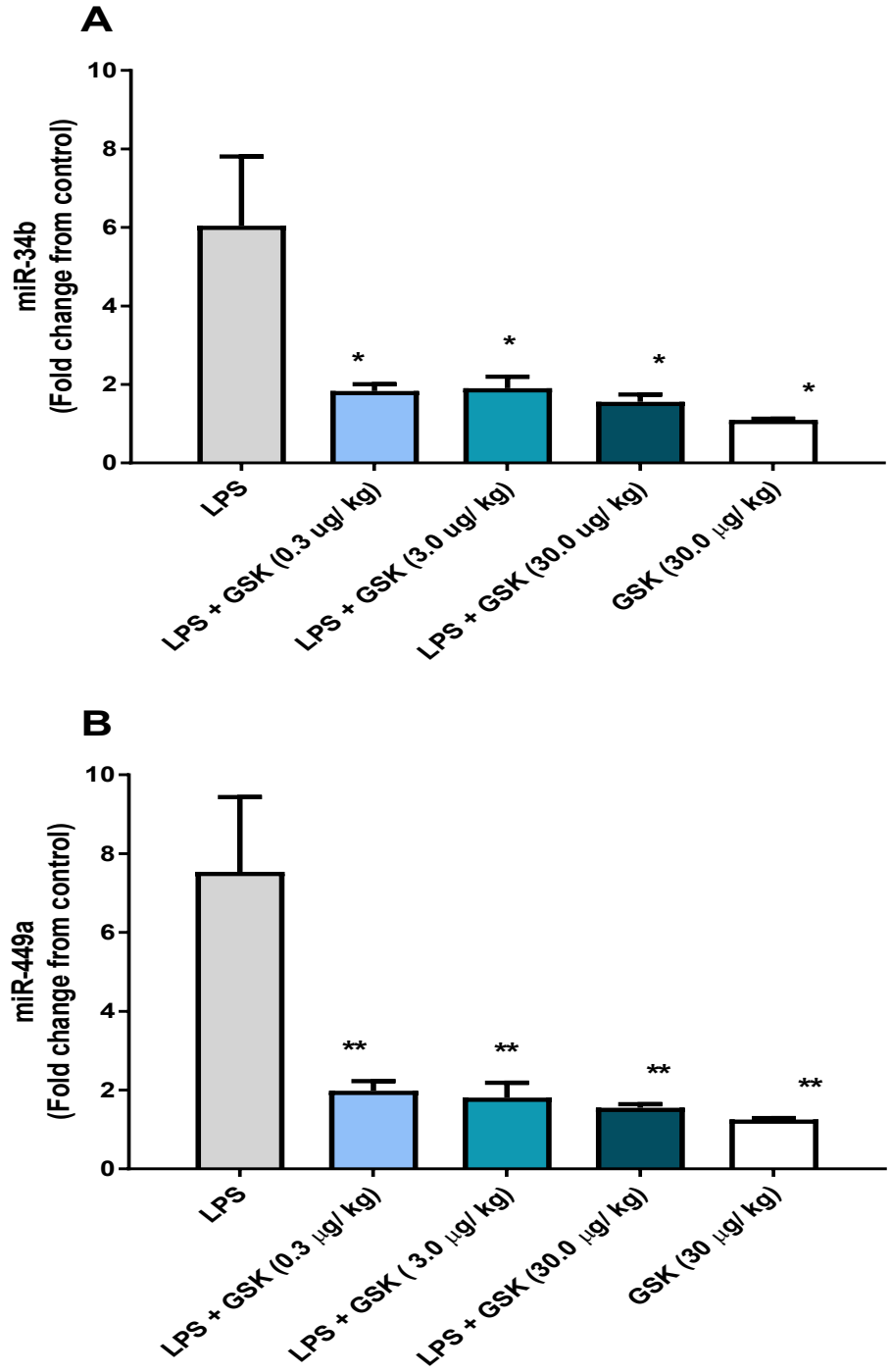


Figure 3. 4: Fold increases in miR-34b and 449a concentrations in the serum of rats following 4h pulmonary exposures to LPS in the presence of a p38/MAPK inhibitor (compared with that of rats exposed to vehicle control). Data were acquired by RTqPCR, normalised to exogenous cel-miR-39 concentrations and analysed using the 2- ($\Delta\Delta$ C_T) method. Values represent the mean ± SEM of 6-18 biological replicates, obtained from 3 technical replicates for each. Significant differences were detected between treatment groups using Student's t-tests, ** $p \leq 0.01$.

3.3.4: ^{1}H NMR spectroscopy characterised the serum metabolomes of rats following exposure to LPS in the presence or absence of a p38 MAPK inhibitor

The second aim of this study was to establish whether the LPS-induced alterations in circulating inflammatory miRNA concentrations were accompanied by changes in circulating metabolite concentrations. To meet this aim, the rat serum metabolome was characterised following inhalation of LPS and compared with that of rats that had inhaled a vehicle control or LPS with GSK.

As knowledge of pulmonary metabolic responses to inflammatory stimuli is limited, analyses were performed in an untargeted, global manner using spectra obtained by ^{1}H NMR spectroscopy and selected multivariate and univariate statistical approaches. This approach led to the detection and quantification of 45 metabolites within the samples (**Figure 3.5**) with each being present within the spectra of all treatment groups.

PCA was employed to detect and explain intrinsic variation within the dataset in an unsupervised manner. The analysis identified limited intrinsic metabolic variation within the dataset (Q^2= 0.16) that was explained using two components. 12.3% of the variation was attributed to principal component (PC) 1 which was strongly characterised by taurine and alanine content while the remainder of the variation associated with PC2 which was driven by glucose content (**Figure 3.6 A-B**).

Although most samples clustered together, independent of exposure grouping (**Figure 3.6 A**), four small sub-clusters of samples existed within the dataset. These were separated from the majority group because they contained 50-51% more taurine, 35-63% more glucose, 12-38% less alanine or 25-31% less glucose than the dataset averages (for clusters 1, 2, 3 and 4 respectively) (**Figure 3.6 A-F)**. Upon visualisation, the variation caused by increased glucose concentrations in samples LPS_4, LPS_41 and Vehicle_26 was considered an outlying phenomenon (**Figure 3.7 A**). These samples contained 83, 82 and 52% more glucose than the average for their exposure groups, compared with ranges of 25% less to

25% more and 31% less to 11% more than average for the rest of the samples in the LPS and vehicle exposure groups (respectively). As a result these spectra were removed from downstream supervised analyses to prevent them from falsely influencing the models. The remaining sample within cluster 2 showed only 8% more variation from its group average than the remaining samples so was retained within the dataset.

As the samples within clusters 1, 3 and 4 did not associate with any single exposure group but exposures were known to have been performed in four separate batches, the effect that this non-biological factor had on metabolic variation was explored. Assignment of exposure batch to the PCA plot showed that clusters 1, 3 and 4 all contained samples that were produced across the exposure batches indicating that their variability was biological in nature rather than batch dependent (**Figure 3.8)**. As this variation did not cause samples to fall outside of the 95% confidence interval (the Hotelling's T^2 ellipse) the dataset continued to be analysed as a whole.

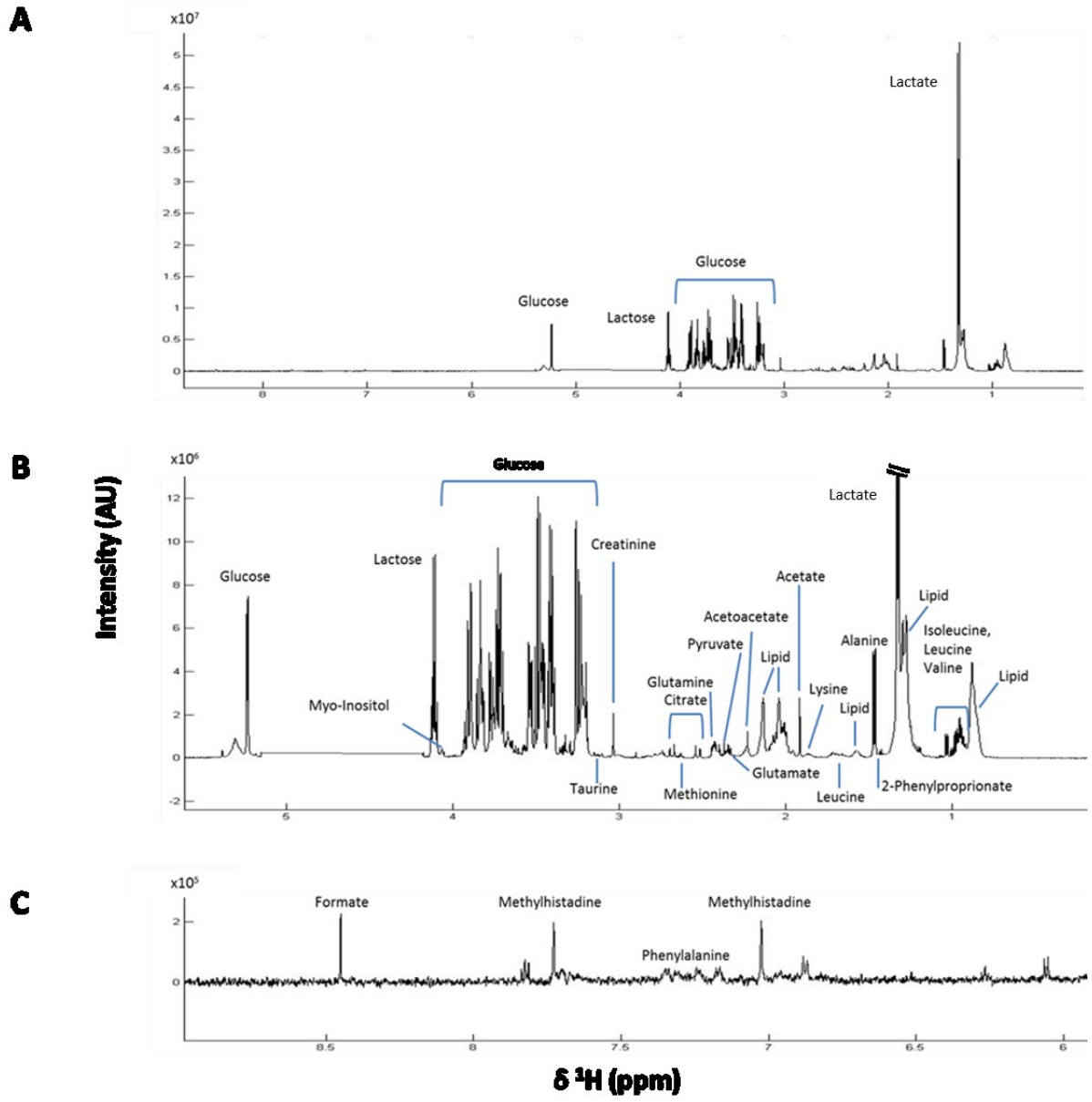


Figure 3. 5: Representative ^{1}H NMR spectra generated from the serum of male Crl:WI (Han) rats. The full spectrum is shown (A) alongside magnified views of the aliphatic (B) and aromatic (C) regions. The frequency range containing the water peak (4.18-5.15 ppm) has been removed.

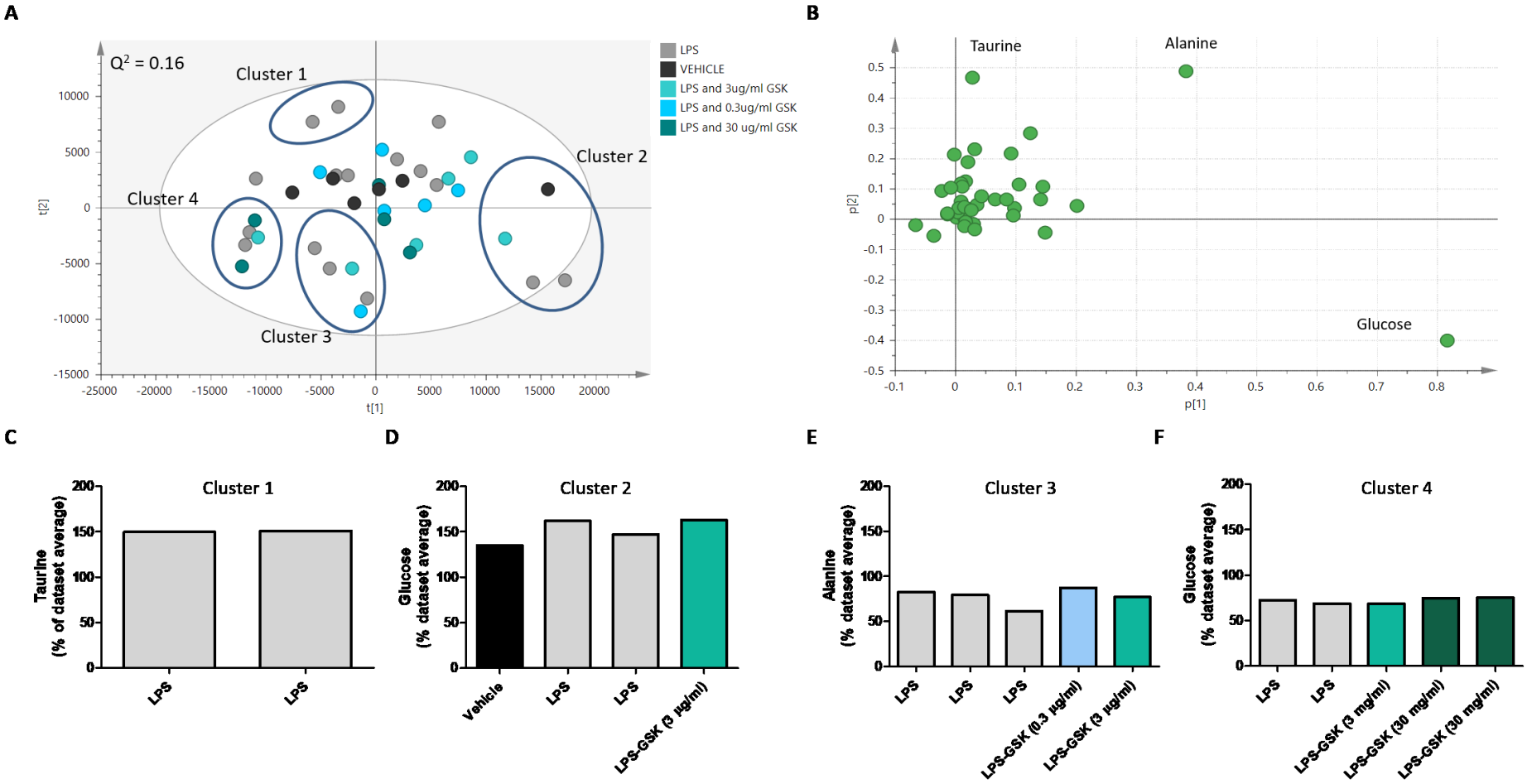


Figure 3. 6: PCA analysis of ^{1}H NMR spectra of serum samples from LPS and GSK treated rats. Scores (A) plots display intrinsic metabolic variation within the serum samples of rats (as measured by ^{1}H NMR) and loadings plots (B) highlight the metabolites that drove the variation. Concentrations of metabolites that associate with clusters 1-4 are displayed for each potentially anomalous sample as a % of the average concentrations across the dataset (C-F, respectively). All values were subjected to PQN normalisation prior to use and were Pareto scaled for multivariate analysis.

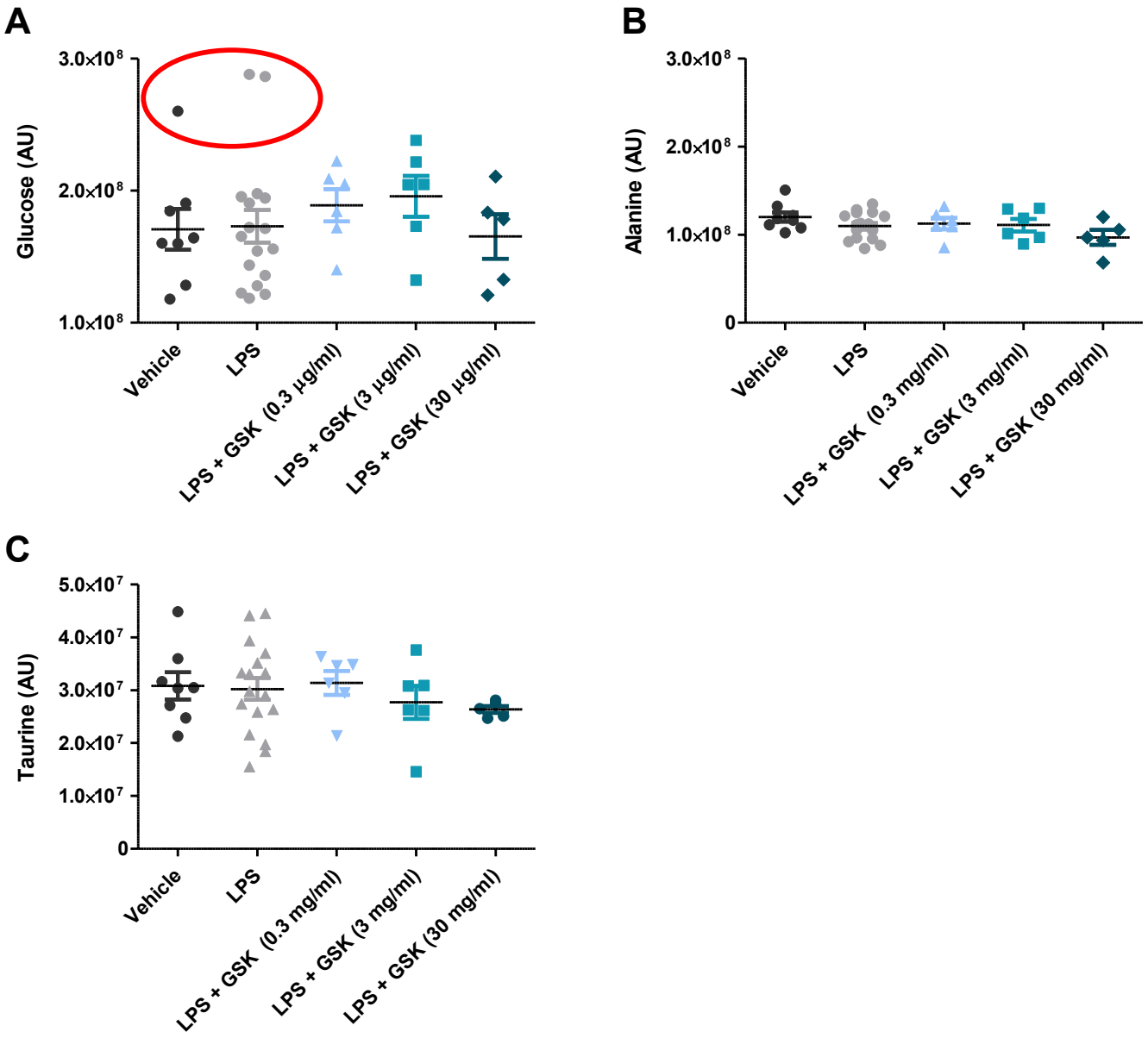


Figure 3. 7: Inter-sample variability in serum glucose, alanine and taurine concentrations. Graphs display concentrations of glucose (A), alanine (B) and taurine (C) within serum samples of rats treated with LPS, LPS and GSK (0.3-30 µg/ml) or vehicle or GSK only control substances. Outlying samples are circled in red.

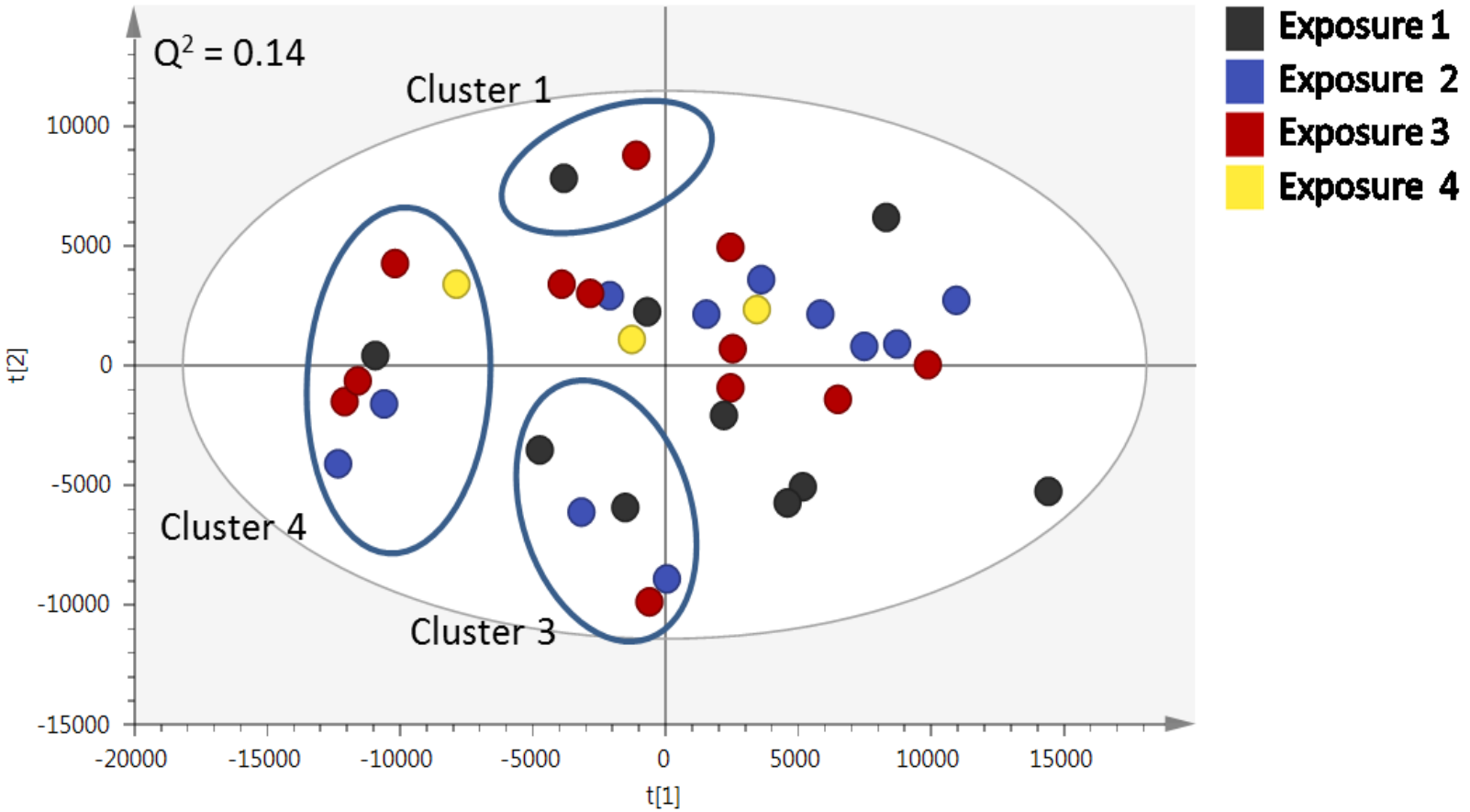


Figure 3. 8: PCA scores plot displaying intrinsic metabolic variation within the serum samples of rats with data points coloured according to session of exposure. Data was obtained using ^{1}H NMR spectroscopy, subjected to PQN normalisation and Pareto scaled prior to analysis.

3.3.5: Pulmonary exposure to LPS induces changes in the serum metabolome

PLS-DA was performed to identify metabolites that associated strongly enough with LPS exposure to distinguish the serum of LPS exposed rats from that of control animals. A cross-validated model was produced (**Figure 3.9 A**) that separated the exposure classes along one component (PC1) which explained 42% of metabolic variation between the classes (**Figure 3.9 B**). Examination of the accompanying loadings plot indicated that LPS exposure associated with greater serum concentrations of acetate and creatinine than vehicle exposure but lower serum concentrations of glutamine and alanine (**Figure 3.9 C**). The accompanying Variable Importance Plot (VIP) indicated that glutamine concentration had most bearing on sample classification when compared with the other features followed sequentially by alanine, acetate and creatinine (**Figure 3.9 D**).

The statistical significance of LPS-induced changes in feature metabolite concentration were explored using Student's t-tests with FDR corrections for multiple testing. This analysis confirmed that the serum of LPS treated rats contained 25% more acetate ($p \leq 0.05$) and 24 % less glutamine ($p \leq 0.01$). Compared with the serum of vehicle exposed rats, the serum of LPS exposed rats also contained 5% less alanine and 29% less creatinine but these changes did not reach statistical significance ($p= 0.26$ and 0.43 respectively) (**Figure 3.10**).

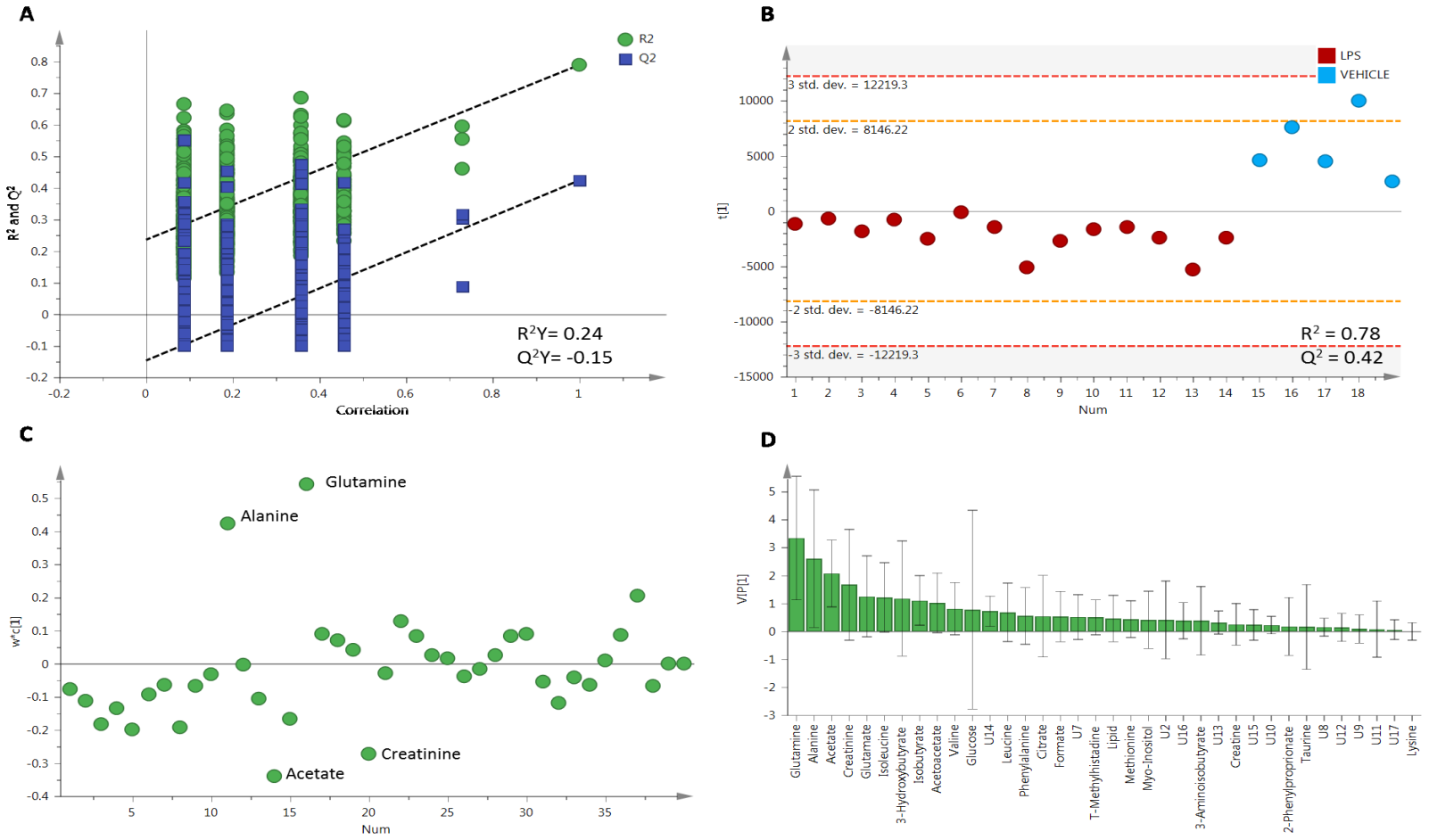


Figure 3. 9: PLS-DA analysis of the rat serum metabolome. Scores (A), loadings (B) and VIP (C) plots were used to identify metabolites that differentiate between the serum of rats treated with LPS or with a vehicle control. Data was obtained using ^{1}H NMR spectroscopy, subjected to PQN normalisation, Pareto scaled and modelled according to exposure class. Validity of the model was determined by permutations test using 999 permutations (D).

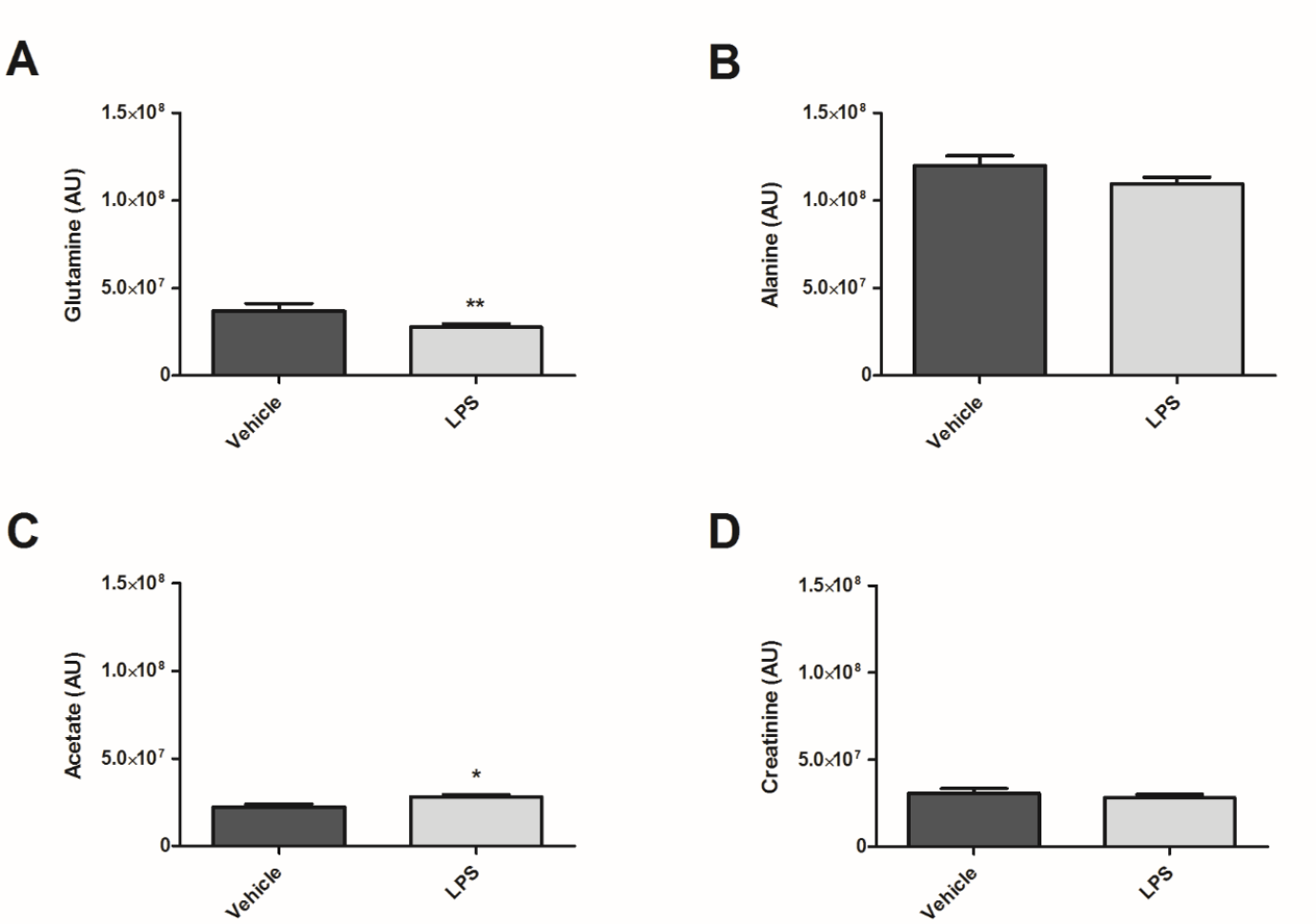


Figure 3. 10: Concentrations of feature metabolites measured within the serum of rats treated with LPS or a vehicle control. Values were obtained by ^{1}H NMR and normalised using the PQN method then significant differences were sought between exposure groups using Student's T tests with FDR correction; * $p \leq 0.05$, ** $p \leq 0.01$. Error bars represent SEM of 8 or 18 replicates (vehicle and LPs respectively).

3.3.6: LPS induced changes in the serum metabolome are p38 MAPK dependent

In order to strengthen their association with the pulmonary response to LPS exposure, the concentrations of metabolic features were compared between the sera of rats that were exposed to LPS and rats that were exposed to LPS in the presence of 0.3, 3 and 30 μg/kg GSK; an anti-inflammatory inhibitor of the p38 MAPK pathway. As with the miRNA experiment above, metabolic alterations that were induced by LPS were expected to reverse in the presence of the inhibitor, thus validating their association with the exposure.

While administration of 0.3 μg/kg GSK had no impact on LPS-induced changes in serum metabolite concentrations, the 30 μg/kg dosage inhibited LPS-induced increases in acetate concentrations by 18% ($p \leq 0.01$), retaining them at equivalent concentrations to the vehicle control (102% of control). LPS-induced decreases in glutamine concentrations were also inhibited by GSK at 30 μg/kg (29%, $p \leq 0.01$)), remaining at 98% of vehicle control level.

Treatment with 3 μg/kg GSK also inhibited LPS-induced changes in feature metabolite concentrations. In the presence of the inhibitor, glutamine concentrations were 41% higher than in LPS exposure samples ($p \leq 0.001$) and were statistically similar to the vehicle control (107% of control). LPS-induced changes in acetate concentration were also inhibited (but not significantly so) with concentrations being 8% lower than for LPS exposure samples and retained at 115% of vehicle control concentrations (**Figure 3.11**).

As exposure to GSK alone did not induce significant changes in the serum concentrations of feature metabolites, these changes were attributed to interactions between the inhibitor and pathways that had been induced by LPS recognition. Together the results validate the associations between LPS exposure and changes in serum glutamine and acetate concentrations, suggesting that they are produced as a result of p38 MAPK pathway activity.

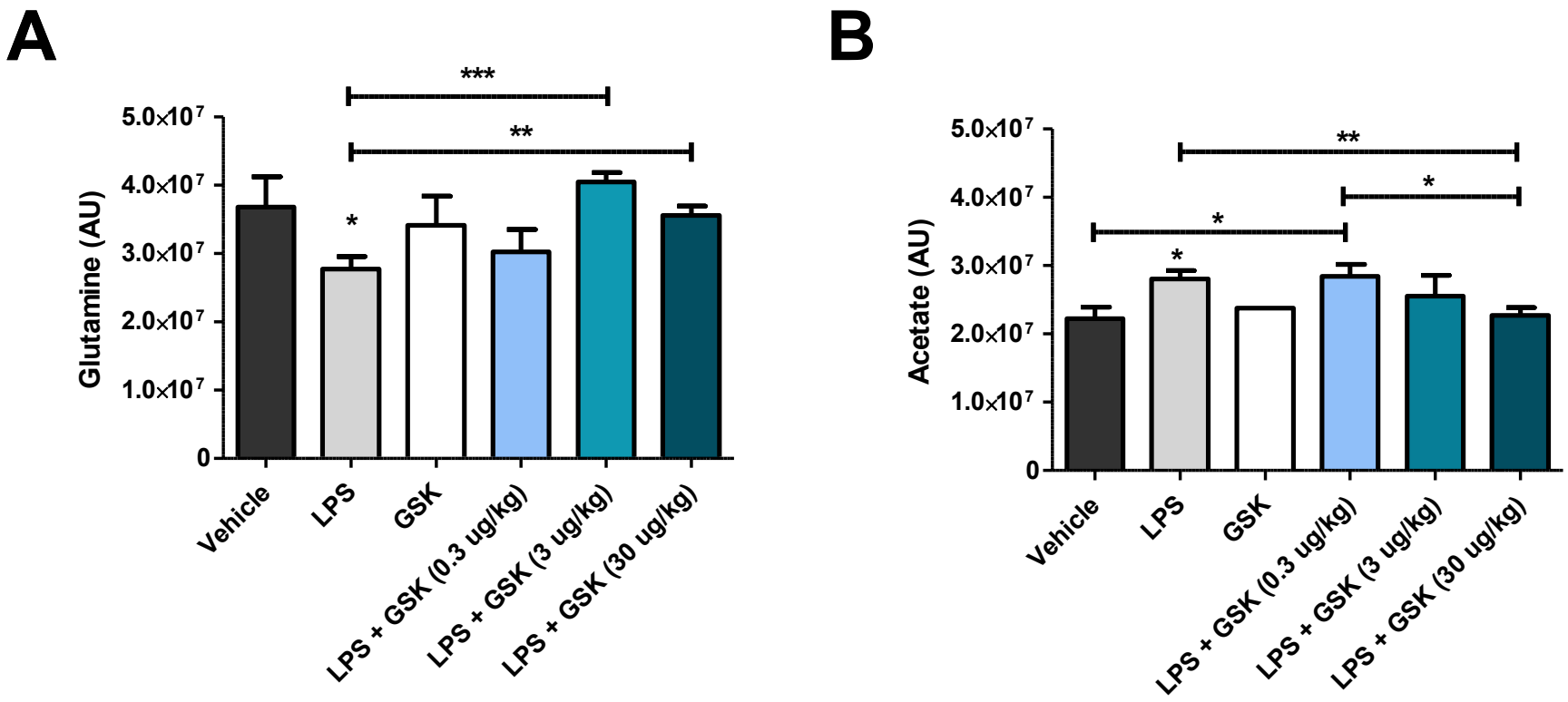


Figure 3. 11: Concentrations of feature metabolites measured within the serum of rats treated with LPS, LPS and GSK (0.3-30 µg/ml) or vehicle or GSK only controls. Values were obtained by ^{1}H NMR and normalised using the PQN method then significant differences were sought between exposure groups using Student's T tests with FDR correction; * $p \leq 0.05$, ** $p \leq 0.01$. Error bars represent SEM.

3.3.7 Intratracheal LPS exposure alters metabolic relationships within the serum of rats

Metabolites with concentrations that are strongly correlated often contribute to common metabolic pathways. Based on this rationale, correlations were measured globally between the concentrations of measured metabolites to identify which metabolic relationships had developed specifically during pulmonary inflammation and which had ceased to exist. Correlations with r values ≥ 0.5 or ≤ -0.5 were considered to be of moderate strength while those with r values ≥ 0.6 or ≤ -0.6 and ≥ 0.7 or ≤ -0.7 were considered strong and very strong (respectively). These correlations were considered to represent pathway level metabolic interactions and are displayed in **Figure 3.12**.

3.3.7.1 Intratracheal LPS exposure associates with relationships between glutamine and glucose and glutamine and glutamate in the serum metabolome

In the serum of LPS treated rats, glutamine concentrations correlated positively with glucose concentrations ($r = 0.78$, $p \leq 0.001$), positively and strongly with glutamate ($r = 0.68$, $p \leq 0.01$) and creatinine ($r = 0.65$, $p \leq 0.01$) and positively and moderately with methionine ($r = 0.54$, $p \leq 0.05$) concentrations (**Figure 3.12 A**). Further exploration of these relationships indicated that glutamine concentrations were significantly greater than those of glucose and methionine (log fold differences of 0.82 and 5.35, $p \leq 0.001$) in the LPS serum samples but significantly lower than those of glutamate or creatinine (log fold differences of -0.32 and -0.37, $p \leq 0.001$) (**Figure 3.13 A**).

Fisher's Z tests indicated that the relationships between glutamine and creatinine and glutamine and methionine that were detected in the serum of LPS exposed rats were not significantly different to those detected in the serum of vehicle treated rats ($p = 0.682$ and 0.787 respectively), suggesting that they do not associate with the inflammatory response in particular. In these control samples glutamine concentrations correlated very strongly with creatinine ($r = 0.776$, $p \leq 0.001$ and moderately with methionine ($r = 0.560$, $p \leq 0.05$) (**Figure**

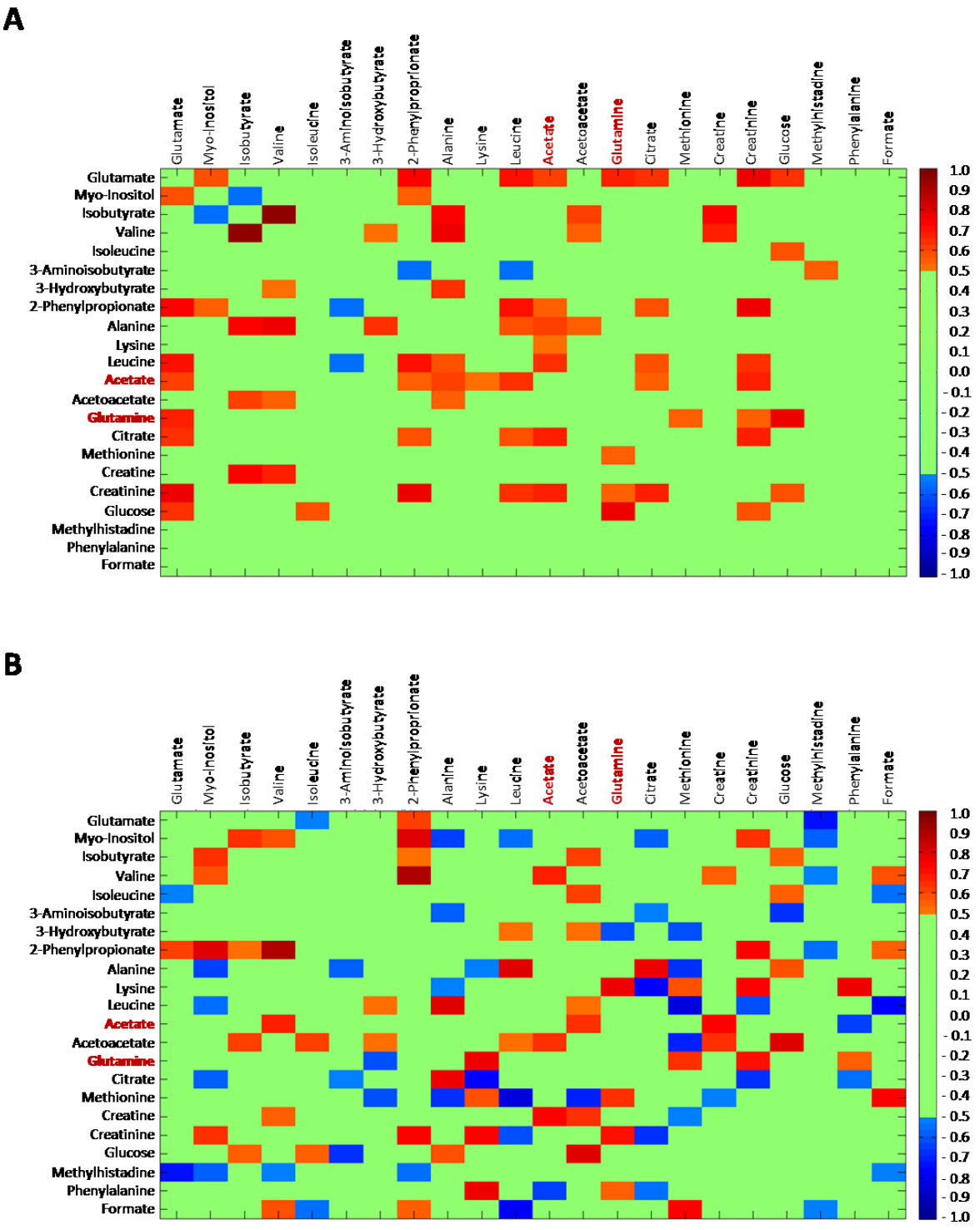


Figure 3. 12: Heat map visualisation of moderate to very strong metabolite-metabolite correlations in LPS (A) and vehicle (B) exposure serum samples. Coloured squares represent Pearson's correlation coefficients (r) calculated using PQN normalised ^{1}H NMR values obtained from 18 (A) or 8 (B) samples. Feature metabolites are labelled with bold, red text.

3.12 B) and remained significantly greater than methionine concentrations and lower than creatinine concentrations (log fold differences of 0.78 and -0.38, $p \leq 0.001$) (**Figure 3.13 B**).

In contrast, the positive correlation between glutamine and glutamate did not reach the thresholds for strength or statistical significance in vehicle samples ($r= 0.49$, $p = 0.21$) and no correlation was found between glutamine and glucose concentrations ($r= 0.06$, $p = 0.90$) (**Figure 3.12 B**) suggesting that these relationships were unique to the LPS exposed samples. In support of the use of these relationships for biomarker purposes, both glucose and glutamate concentrations were found to be significantly lower in LPS serum samples than in vehicle samples (27.31 and 14.13%, $p \leq 0.01$ 0.05) indicating that they may have contributed to the LPS-associated serum metabolome in this study (**Figure 3.14 A**).

Lysine concentrations correlated positively with glutamine concentrations in the vehicle samples ($r = 0.766$, $p \leq 0.05$) (**Figure 3.12 B**), showing significantly greater correlation than for LPS samples ($p \leq 0.05$) (for which the relationship did not exist ($r= 0.01$, $p= 0.97$)). While glutamine was more abundant than lysine in the sera of vehicle exposed rats (log fold difference of 0.51, $p \leq 0.001$) (**Figure 3.13 B**), lysine concentrations were found to increase considerably (12.86%, $p=0.06$) following exposure to LPS (**Figure 3.14**). Together these results indicate that pulmonary exposure to LPS inhibited the usual interactions that existed between glutamine and lysine and that the loss of this metabolic relationship under inflammatory conditions influenced the serum metabolome..

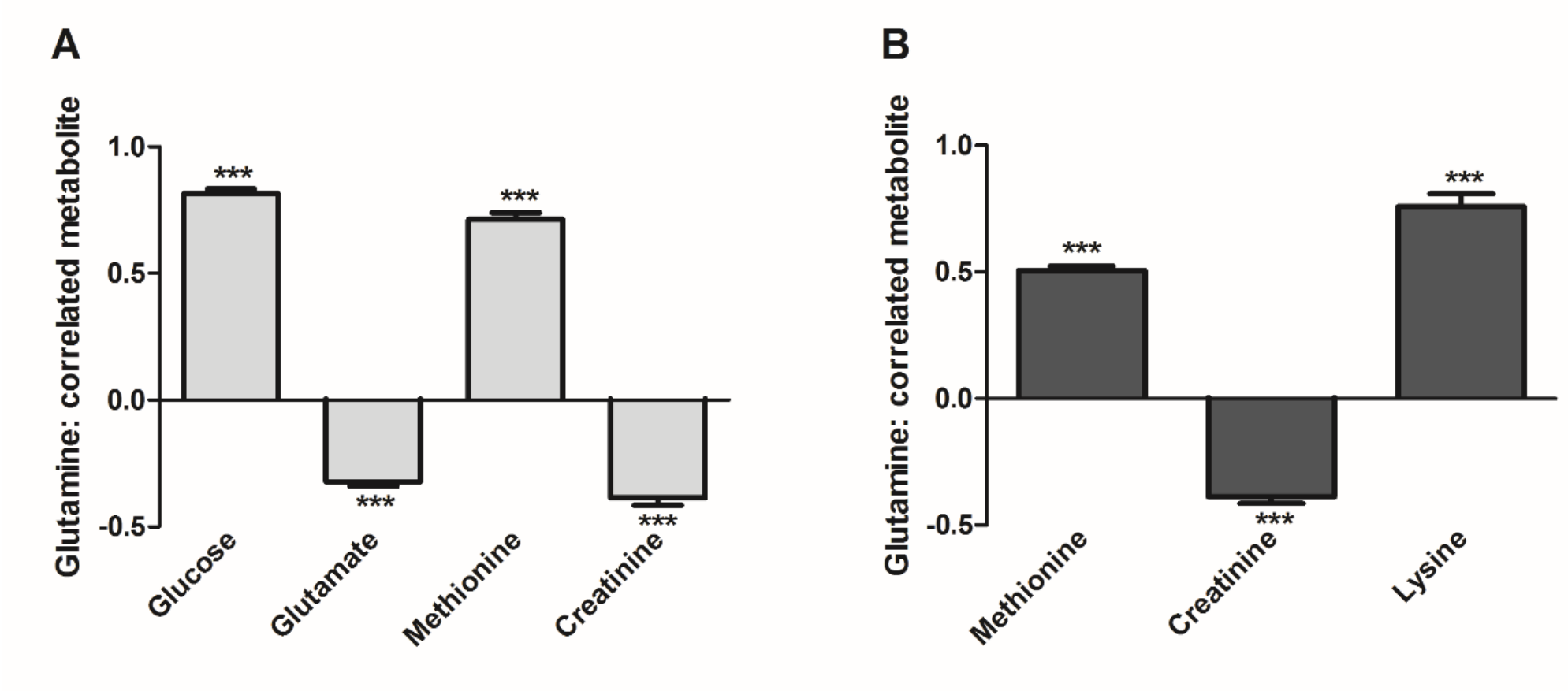


Figure 3. 13: Log fold differences in concentration between glutamine and strongly correlated metabolites in LPS (A) and vehicle (B) exposure samples. The significance of differences between glutamine and correlated metabolite concentrations was assessed by Student's t-tests, *** $p \leq 0.001$. Values display mean values obtained from 18 (LPS) or 8 (vehicle) samples with error bars representing the SEM.

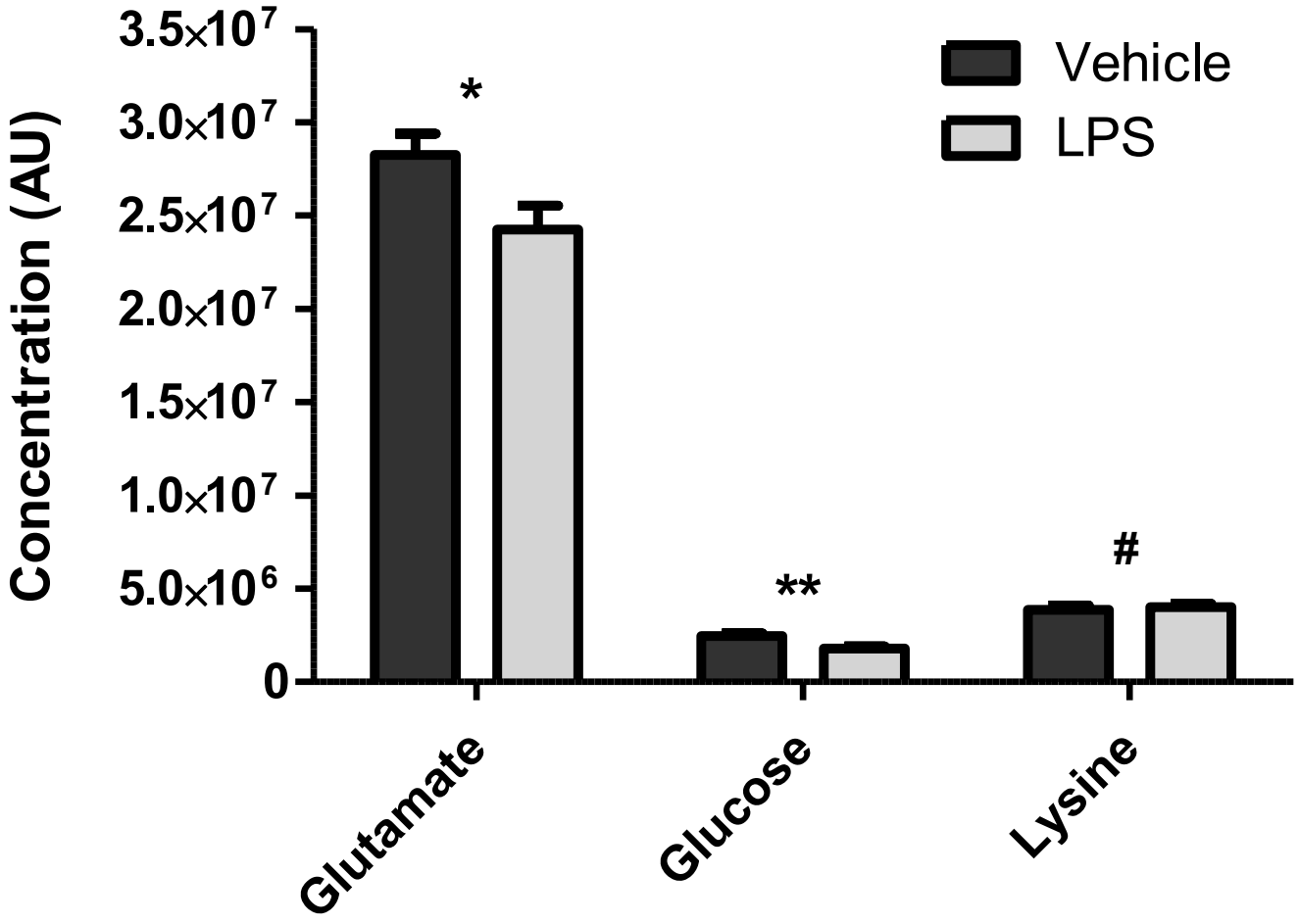


Figure 3. 14: Comparison of serum concentrations of metabolites that display correlating concentrations to glutamine in rats following exposure to LPS (A) or vehicle control (B). Data were included for metabolites that displayed significantly different correlation coefficients when compared between treatment types (as determined by Fisher's Z tests). Values were obtained by ^{1}H NMR spectroscopy and normalised using the PQN method then significant differences were sought between vehicle and LPS exposure groups using Student's t-tests with FDR correction; * $p \leq 0.05$, ** $p \leq 0.01$. Values display mean values obtained from 18 (LPS) or 8 (vehicle) samples with error bars representing the SEM.

3.3.4.2: Pulmonary LPS exposure induces relationships between acetate and glutamate and acetate and citrate but disrupts homeostatic relationships between acetate and creatine in the serum of rats.

Acetate concentrations were strongly and positively correlated with glutamate, lysine, alanine, citrate, leucine and creatinine concentrations in the serum of LPS exposed rats (r=0.61, 0.51, 0.61, 0.56, 0.64, 0.69 respectively and $p \leq 0.01$) (**Figure 3.12 A**). In these samples acetate was significantly more abundant than lysine, citrate and leucine (log fold differences of 0.82, 0.55 and 0.47, $p \leq 0.001$) and significantly less abundant than alanine (log fold difference of -0.62, $p \leq 0.001$) (**Figure 3.15 A**).

These acetate-metabolite relationships were not significant in the samples of vehicle exposed animals indicating that they developed due to pulmonary exposure to LPS. The correlations between acetate and glutamate, acetate and citrate and acetate and lysine were significantly lower in the vehicle samples than the LPS exposure samples (difference in r= 0.94, 0.69 and 0.73, $p \leq 0.05$) (**Figure 3.12 B)** indicating that these changes in metabolic interactions have potential for use as circulating markers of LPS-induced pulmonary inflammation. Such indications were supported by observations that glutamate, citrate and lysine concentrations were significantly different between LPS and vehicle exposure samples (14.13, 11.54 and 12.86%, $p \leq 0.05$ for glutamate and citrate, $p = 0.06$ for lysine) (**Figure 3.16**).

Significant exposure-related differences in correlation were also observed between creatine and acetate concentrations. No relationship was observed between these metabolites in LPS samples (r= 0.02, p= 0.93) but the correlation was positive (r= 0.731) in vehicle samples, showing a borderline significant difference to that of the LPS samples (difference in r= 0.71, p= 0.08). Compared with the vehicle control samples (where creatine concentrations were statistically similar to those of acetate (**Figure 3.15 B**)) a significant increase in serum creatine concentration was observed following LPS exposure (14.51%, $p \leq 0.05$) indicating

that LPS-induced break-down of serum acetate-creatinine relationships may have potential as a circulating biomarker.

Strong correlations between acetate and valine (r= 0.661, p = 0.07), acetate and acetoacetate (r= 0.628 p = 0.09) and acetate and phenylalanine (r= -0.644, p= 0.08) that existed in vehicle samples were also weakened to below-threshold strengths in the response to LPS exposure (**Figure 3.12**). These changes however, did not meet statistical significance using Fisher's Z tests, indicating that they do not contribute greatly to differences in metabolic pathway activity between LPS and vehicle serum samples and possess limited potential as biomarkers.

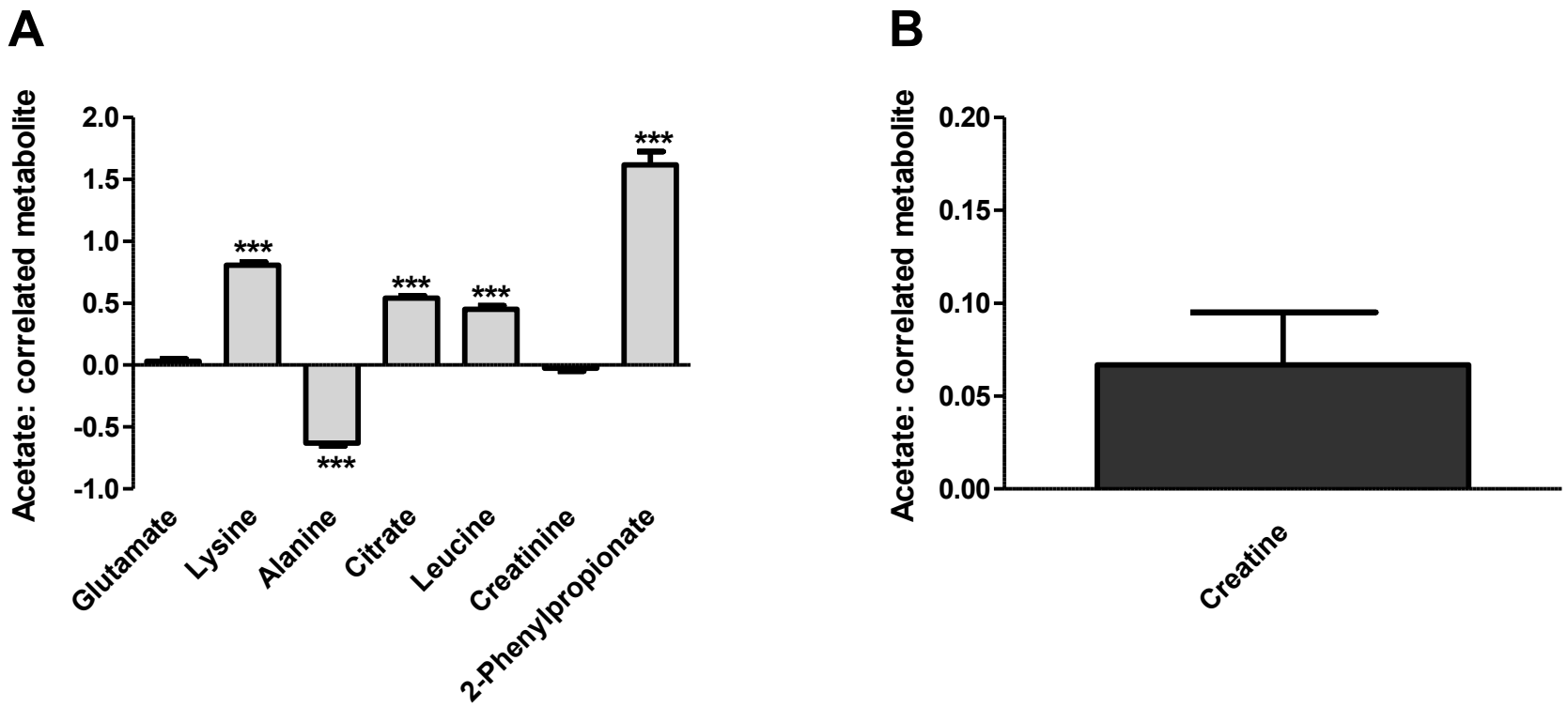


Figure 3. 15: Log fold differences in concentration between acetate and strongly correlated metabolites in LPS (A) and vehicle (B) exposure samples. The significance of differences between glutamine and correlated metabolite concentrations was assessed by Student's T tests, *** $p \leq 0.001$. Values display mean values obtained from 18 (LPS) or 8 (vehicle) samples with error bars representing the SEM.

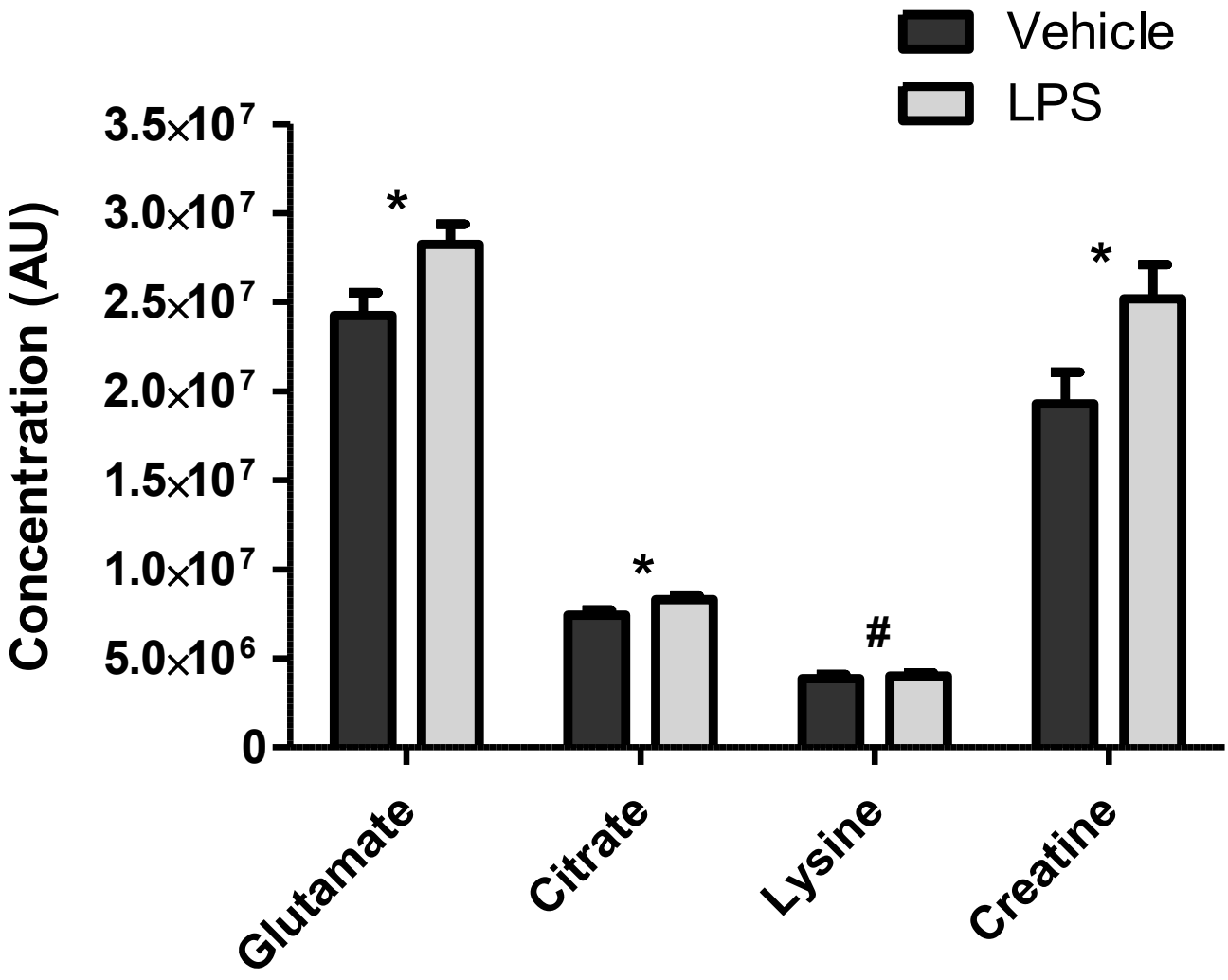


Figure 3. 16: Comparison of serum concentrations of metabolites that display correlating concentrations to acetate in rats following exposure to LPS or vehicle control. Data were included for metabolites that displayed significantly different correlation coefficients when compared between treatment types (as determined by Fisher's Z tests). Values were obtained by ^{1}H NMR spectroscopy and normalised using the PQN method then significant differences were sought between exposure groups using Student's t-tests with FDR correction; * $p \leq 0.05$, ** $p \leq 0.01$. Values display mean values obtained from 18 (LPS) or 8 (vehicle) samples with error bars representing the SEM.

3.3.5: miR-34b and 449a activity may regulate transport and metabolism of glutamine and acetate

The mechanistic strength of biomarkers can be enhanced by integrating multiple types of molecular profile. As such, cross-overs were sought between cellular pathways that may have been regulated by miR-34b/449a activity following LPS exposure and those that could have contributed to the observed concentrations of feature metabolites.

Two mechanisms by which serum metabolite concentrations can be altered during a toxicological response are changes in enzyme availability or activity and differences in cellular uptake or export of reaction substrates and products. The molecular functions of miR-34b/449a targets (identified in **Chapter 2** using miRWalk algorithms) were sought using the *Molecular Function* module of Panther Classification System. This analysis indicated that 43% of the miRNA targets possessed enzymatic or enzyme regulatory activity while a further 11% of targets were involved in transmembrane transport (**Figure 3.17 A).**

Further exploration indicated that hydrolases and helicases were the predominant enzymatic targets of the miRNAs, representing 35 and 25% of their enzymatic targets respectively (**Figure 3.17 B**) and that ion and amino acid transporters represented the majority of transporter protein targets (61 and 31% of total respectively) (**Figure 3.17 C**. Together these results indicate that miR-34b and 449a have the potential to regulate metabolic processes.

In order to determine whether over-expression of the miRNAs could have contributed to the observed changes in metabolite concentrations following pulmonary LPS exposure, pathway over-representation analyses were performed using the integrative module of IMPaLA. Lists of predicted mRNA targets for miR-34b and 449a (identified from the miRWalk database in **Chapter 2**) and the LPS-associated feature/correlated metabolites were input into the analysis and pathways that contained a minimum of 3 genes and metabolites (including the feature metabolites) were noted.

This approach indicated that the feature metabolite glutamine and its correlating metabolite glutamate contributed to a common metabolic pathway (glutamine and glutamate metabolism) and that acetate and its correlating metabolites citrate and glutamate were components of carbohydrate metabolism and transmembrane molecular transport pathways (metabolism of carbohydrates, solute carrier (SLC)-mediated transmembrane transport, transmembrane transport of small molecules and glycolysis and gluconeogenesis specifically) (**Table 3.2**).

Once again, the analysis indicated that the activity of the glutamine and glutamate pathway may be influenced by miR-34b, through its predicted ability to target glutamine dehydrogenase-1 (GLUD1) transcripts. It also suggested that glycolysis and gluconeogenesis pathways may be regulated by miR-449 through its predicted targeting of enolase 3 (ENO3) enzymes and nucleoporin 35 (NUP35).

The metabolism of carbohydrates, SLC-mediated transmembrane transport, transmembrane transport of small molecules pathways were enriched for genes that were predicted to be targeted by both miRNAs. Within the metabolism of carbohydrates pathway miR-34b was predicted to target the enzymes ketohexokinase (KHK), fructose-bisphosphate aldolase A (ALDOA) and β-hexosaminidase (HEXA) and the glycoprotein chondroitin sulphate proteoglycan 4 (CSPG4) while miR-449a was predicted to target KHK, HEXA, ALDOA, glycogenin 1 (GYG1) and ENO3 enzymes, syndecan-4 (SDC4) and biglycan (BGN) glycoproteins and NUP35.

Several members of the SLC-mediated transmembrane transport and transmembrane transport of small molecules pathways were predicted to be targeted by both miRNAs (FXYD domain containing ion transport regulator 3 (FXYD3), SLC7A8 and SLC38A5 while others were targeted by either miR-34b or miR-449a. miR-34b alone was predicted to target SLC29A1, aquaporin-4 (AQP4), SLC15A4, Sodium/potassium-transporting ATPase subunit β-transporter proteins (ATP1B3), SLC6A9, SLC02A1, SLC22A5 and SLC12A2 transporter

proteins and the enzyme adenylate cyclase (ADCY6). In contrast, miR-449a was predicted to target guanine nucleotide-binding protein subunit γ5 (GNG5), SLC7A5, SLC4A3 and NUP35 (**Table 3.2**).

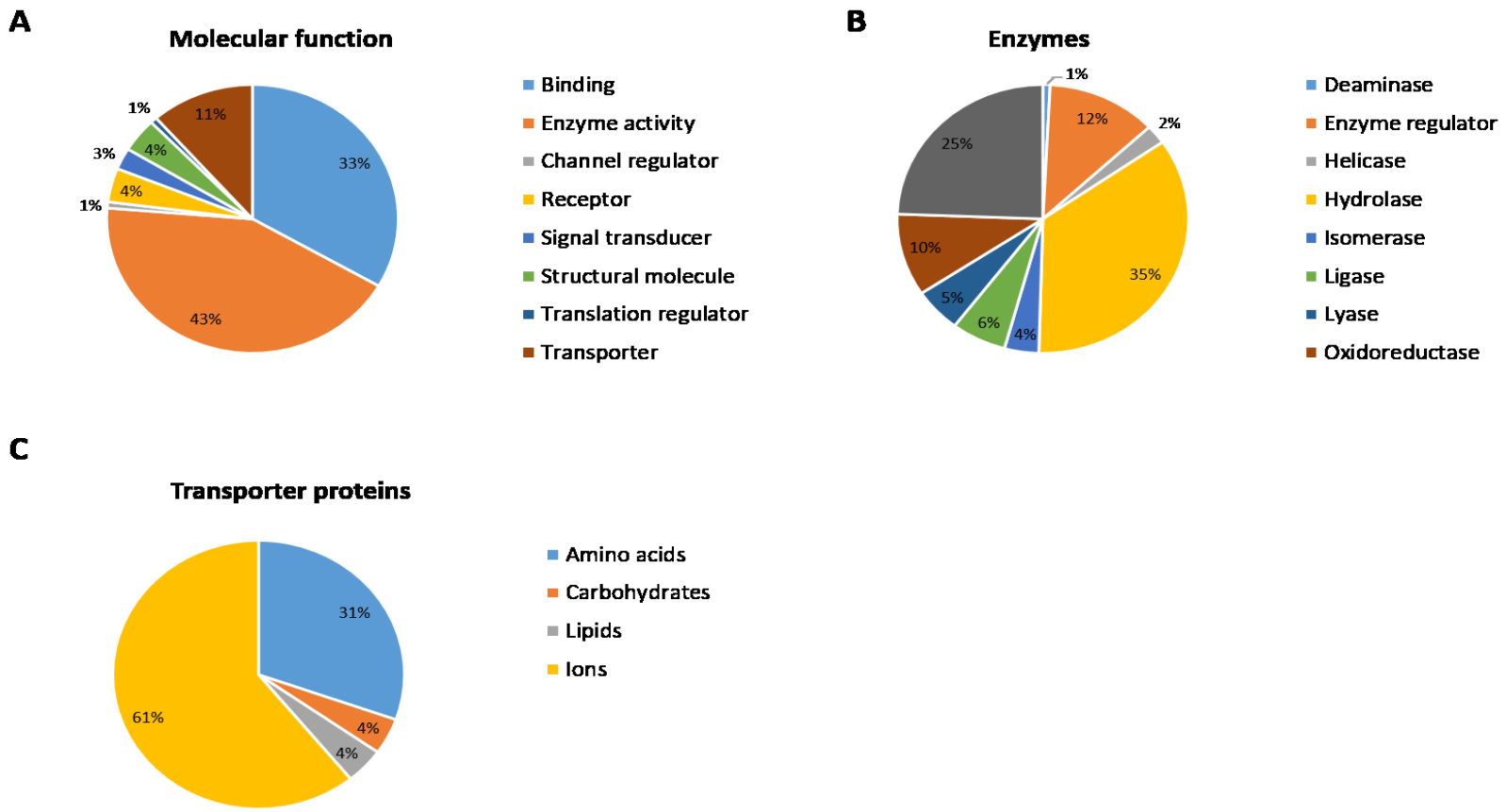


Figure 3. 17: Gene ontology classifications for the predicted mRNA targets of miR-34a/449b. Genes are classified based on their molecular function (A) with subcategories being displayed for genes belonging to the enzyme activity (B) and transporter (C) categories. Percentage values refer to the percentage of total genes that belong to each category and were determined using the functional annotation module of the Panther Classification System database. Table 3.2: Integrated pathway over-representation analysis for LPS associated metabolites and predicted miR-34b/449 gene targets. Pathway over-representation analysis was performed using the IMPaLA tool. Metabolite lists consisting of feature and correlating metabolites were input alongside lists of genes that were predicted to be targeted by miR-34b/449a by three or more modules of miRWalk (identified in Chapter 1).

Table 3. 2: Integrated pathway over-representation analysis for LPS associated metabolites and predicted miR-34b/449 gene targets. Pathway over-representation analysis was performed using the IMPaLA tool. Metabolite lists consisting of feature and correlating metabolites were input alongside lists of genes that were predicted to be targeted by miR-34b/449a by three or more modules of miRWalk (identified in Chapter 1).

Feature metabolite	Pathway name	Overlapping genes (Regulating miRNAs)	Overlapping metabolites	P value	FDR Q value
Acetate	Metabolism of carbohydrates	HEXA, ALDOA, KHK (miR-34b, 449b), AGRN, CSPG4 (miR-34b), ENO3, GYG1, SDC4, BGN, NUP35 (miR-449a)	Acetate, Citrate, Glutamate	≤ 0.001	0.012
	SLC-mediated transmembrane transport	SLC7A8, SLC38A5 (miR-34b, 449b), SLC6A9, SLC29A1, SLCO2A1, SLC22A5, SLC15A4, SLC12A2 (miR-34b), SLC7A5, SLC4A3, NUP35 (miR-449a)	Acetate, Citrate, Glutamate	≤ 0.001	0.013
	Transmembrane transport of small molecules	FXYD3, SLC7A8, SLC38A5 (miR-34b and 449a), ATP1B3, ADCY6, AQP4, SLC6A9, SLC29A1, SLCO2A1, SLC22A5, SLC15A4, SLC12A2 (miR-34b), SLC7A5, GNG5, NUP35, SLC4A3 (miR-449a)	Acetate, Citrate, Glutamate	≤ 0.001	0.046
	Glycolysis and Gluconeogenesis	NUP35, ENO3 (miR-449)	Citrate, Acetate	≤ 0.001	0.098
Glutamine	Glutaminolysis	GLUD1 (34b)	Glutamine, Glutamate	≤ 0.001	0.007

3.4: Summary of results

- Serum concentrations of miR-34b and 449a were enhanced following intratracheal exposure to LPS.
- Changes in serum concentrations of miR-34b and 449a are p38 MAPK dependent
- Intratracheal exposure to LPS induces significant changes in serum concentrations of glutamine and acetate
- LPS-induced changes to the serum metabolome are also p38 MAPK dependent
- Gene targets of miR-34b and 449a associate with some serum metabolic pathways that are dysregulated during LPS-induced pulmonary inflammation.

3.5: Discussion

In the context of pulmonary inflammation, the requirement for non-invasively accessible biomarkers is strong. Collection of pulmonary tissue samples by biopsy is uncomfortable meaning that participation rates are low for human studies and raise ethical concerns where samples from healthy subjects are required. For *in vivo* modelling, collection of pulmonary tissue requires the animals to be euthanased, restricting analyses to a single time point; a major drawback considering that inflammation includes multiple stages of development and resolution.

With this in mind, the current work aimed to determine whether the elevations in miR-34b/449a expression that were observed in rat pulmonary tissue under inflammatory conditions (**Chapter 2**) translate to circulating fluids where they can be sampled in a non-invasive manner. It also sought to determine whether pulmonary inflammatory responses lead to alterations in the serum metabolome that could be used as accompanying biomarkers for inflammatory pathways within the lungs.

Analyses were performed using a model of intra-tracheal LPS exposure, chosen because much of our understanding of pulmonary inflammatory responses has been gained from equivalent studies (319–321). Furthermore, time-courses of pulmonary inflammatory cell recruitment and cytokine release after LPS exposure have been characterised previously in the rat (328) and suggest that the 4h time point used in this study is suitable for identifying biomarkers for pro-inflammatory response pathways.

This assumption was supported by flow cytometric analysis of BALF which was taken from the rats immediately prior to blood harvest (performed and analysed by Graham Paul at Cardiff University (329)). The analysis showed that the BALF of LPS exposed animals contained approximately 300 and 1300% more white blood cells (WBC) and neutrophils than that of the control animals (**Supplementary Figure 3.1**) (329), indicating that the endotoxin induced airway infiltration by inflammatory cells. Airway infiltration is a hallmark of pulmonary

inflammation that is propagated by alterations in the activity of many cellular processes (discussed in **Chapter 1**), thus supporting the use of these animals for the current purpose.

Alongside elevations in the cellular content of BALF, serum concentrations of miR-34b and 449a were significantly elevated in animals that were exposed to LPS (as opposed to control) but remained comparable to control in the presence of the p38/MAPK inhibitor. As flow cytometric analysis confirmed that the inhibitor impaired development of airway inflammation in exposed animals (329), these observations provide evidence that miR-34b/449a could be used as circulating markers of pulmonary inflammation.

Furthermore, the inhibitor study indicates that expression of these miRNAs is representative of p38/MAPK signalling in the lung. As this pathway has been associated with pulmonary inflammatory responses to LPS exposure before (328,330) and miR-449 has been shown to regulate autophagy by modulating MAPK pathways (331), this observation highlights a mechanism that may be represented by miR-34b/449a biomarkers, indicating that they meet the criteria of being mechanistically relevant as well as easily accessible.

Although members of the miR-34/449 family have been associated previously with pulmonary inflammation, their translatability to accessible fluids is novel. Providing one explanation for such translatability, export of miRNAs into circulating fluids is widely hypothesised to be a method of paracrine or endocrine regulation (332,333) . In terms of paracrine signalling, export of miR-34b/449a into the pulmonary microvascular may provide a mechanism of propagating protective activities across the lung from the initial site of inflammatory stimulation. In support of this theory, over-expression of miR-34b or 449a has been shown to dampen pro-inflammatory cytokine signalling, promote cilia formation and reduce onset of fibrotic damage in airway models (279,297,331). Support for the miRNAs targeting extra-pulmonary cells arises from the fact that the current measurements were made using systemic blood samples and that validated targets of miR-34b/449a were over-represented in a number of non-pulmonary pathways (including calcium regulation in cardiac

cells, cholesterol biosynthesis and regulation of gene expression in muscle) following AZD2230 exposure (**Chapter 2**).

Metabolic profiles were collected from the rat serum in order to identify metabolites that could accompany miR-34b/449a as biomarkers for the response to LPS exposure and to enhance our understanding of the molecular interactions that drove the response. A combination of multivariate and univariate statistical analyses indicated that the metabolome of the rat serum was altered considerably following pulmonary exposure to LPS and that the alterations could be characterised by glutamine and acetate content.

Glutamine is the most abundant amino acid, contributing 20% of the amino acid content of plasma. Being conditionally non-essential, it is synthesised from ammonia and glutamate by the enzyme glutamine synthetase and can be produced by almost all tissues including the lungs. Once synthesised, glutamine is used as a substrate for multiple cellular purposes including nucleotide formation, acid-base balance, redox homeostasis and glucose metabolism (334).

Acetate is a short chain fatty acid (SCFA) that is considered a central component of energy metabolism in mammalian cells due to its role as a precursor for acetyl-Coenzyme A (acetyl-CoA). It is produced endogenously under hypoxic conditions via protein acetylation or exogenously by the anaerobic portion of the microbiome (335) and can be metabolised in pulmonary tissue by acetyl-CoA synthetases (336).

The observed changes in serum glutamine and acetate concentrations are consistent with clinical observations for patients with inflammatory respiratory conditions, indicating the validity of their use as accessible biomarkers for pulmonary inflammatory responses. Decreased concentrations of circulating glutamine and increased expiration of acetate have been identified for patients with COPD, emphysema, asthma, pulmonary fibrosis or cystic fibrosis (337–341). In further support of this statement of validity, glutamine has been shown to augment LPS-induced NFκB signalling, neutrophilic infiltration and IL-8 release in rat

pulmonary tissue (342,343) while acetate has been used to discriminate between LPS-exposed and control lung tissue in mice (344).

Importantly, these studies also provide evidence that the changes in serum glutamine and acetate concentrations that were detected in the current model had the potential to arise from pulmonary activity. As blood contacts every tissue, it is possible that the metabolites could have entered the serum from an alternative source (199), potentially during a secondary or artefactual response to pulmonary insult.

Encouragingly, Singh *et al.* (2015*)* showed that acetate and glutamine could be used to differentiate the serum metabolome of patients who were undergoing treatment for respiratory illnesses from that of patients who were undergoing the same treatment for non-respiratory conditions (345), indicating that the markers represent pathways that are characteristic of pulmonary pathophysiology specifically. In similarity to the current analysis, Singh *et al.* identified that glutamate and lysine were also discriminatory for their model (341), supporting the suggestions that these metabolites contribute to the same pathways as acetate and glutamine and that they can be measured together as a biomarker panel. Such ability could be advantageous upon translation of the markers to human studies because despite additional pathophysiologies and exposures causing similar changes to acetate or glutamine concentrations (167,346) they do not appear to occur alongside increased glutamine and lysine concentrations elsewhere (341).

Pathway over-representation analysis indicated that the LPS-induced changes in acetate and glutamine concentrations associated with alterations in glycolysis and glutaminolysis activity. Such a result is unsurprising given that many hallmarks of the inflammatory response (including chemotaxis, phagocytosis, cytokine secretion and ROS synthesis) are highly energy dependent (347) and metabolic markers of enhanced glycolysis associate with systemic LPS exposure in mice (297).

Although the contributions that glutamine and acetate make to energy metabolism (as precursors to citrate and acetyl-CoA) are well characterised (335,348), the impacts that miR-34b/449a have on their pathways remain to be explored. Inclusion of predicted miR-34b/449a targets in the over-representation analysis indicated that LPS-induced decreases in serum glutamine concentrations (and strongly correlated increases in glutamate concentrations) may have been influenced by interactions between miR-34b and GLUD1 transcripts which encode glutamate dehydrogenase; a rate limiting enzyme of glutaminolysis that catalyses oxidative deamination of glutamate to α-ketoglutarate and ammonium (349). Similarly the analysis associated miR-449a with glycolysis, suggesting that the miRNA could have regulated activity of the pathway at two separate stages by altering expression of enolase 3 (the enzyme responsible for catalysing the penultimate step of glycolysis) and nucleoporin 35 (a regulator of glucokinase activity).

Serum metabolite concentrations are contributed to by the rates at which molecules are secreted from cells into the blood, the rates at which they are excreted from the blood into the urine and the rates at which they are taken up from the blood into cells (199). As well as targeting glutaminolysis and glycolysis directly, the over-expression analysis indicated that both miR-34b and 449a could have altered serum concentrations of energy metabolites by altering the expression of amino acid transporter molecules, particularly those from the (SLC family. Supporting this suggestion, members of the SLC transporter family have been widely associated with trans-membrane transport of glutamine previously (350,351) and retinoblastoma protein (a downstream product of miR-449 activity (291)) is shown to alter glutamine transport through E2F transcription factor 3-mediated regulation of SLC1A5 expression (352).

Whilst providing strong mechanistic context for the identified biomarkers of pulmonary inflammation, the integrative pathways analysis approach may be criticised for its exclusion of pathways that were not regulated by miR-34b/449a. Metabolic pathways are governed by a highly integrative network of signalling cascades which in turn are fine-tuned by the activity

of multiple miRNAs (not just one family) and can be co-regulated by miRNA-independent mechanisms too (353). As such, the targeted miRNA approach that was used may have masked considerable amounts of this regulatory information, limiting the benefits of using a global approach to detect the metabolite markers.

As an example of this limitation, alterations in glutamine and glutamate concentration could also have been indicative of changes in glutathione synthesis (354). Glutathione plays a key role in pulmonary responses to inflammatory stimuli (including mitochondrial respiration) and its rate of synthesis may be expected to alter in response to LPS exposure (355) but the genes that facilitate its synthesis (γ-glutamylcysteine synthetase and glutathione synthetase) are not predicted targets of miR-34b/449a activity, thus excluding the process from the analysis. With the aim of maximising the hypothesis-generating potential of omics-originated biomarkers, a less conservative approach may be to include metabolite-only and integrated analyses in future work. This would promote identification of pulmonary response pathways regardless of whether they are regulated by miR-34b/449a activity.

3.6: Conclusion

This work provided novel evidence that mechanistically relevant markers of pulmonary activity can be detected in accessible fluids during a typical inflammatory response. The study found that elevations in miR-34b and 449a expression that are detectable within pulmonary tissue during inflammatory insult translate to serum under similar conditions. This presents the miRNAs as circulating biomarkers for pulmonary inflammation, indicating their potential for use in place of biopsies in human studies and for investigating multiple time-points in animal models.

Metabolomic profiling determined that these changes in miRNA concentration were accompanied by alterations to the serum metabolome, yielding acetate and glutamine as further circulating biomarkers of pulmonary inflammatory responses and suggesting that

their specificity to pulmonary-specific pathophysiology may be enhanced through concurrent measurement of additional metabolites for which they share pathways.

Achieving the aim of seeking mechanistically relevant markers of pulmonary inflammatory responses in the serum, pathway analysis indicated that the changes in metabolic marker concentration could be attributed to alterations in energy metabolism and/or the provision of substrates for those pathways. Importantly, the analysis indicated that these pathways could have been regulated by miR-34b/449a, adding weight to the conclusions that were drawn from each analytical platform and highlighting the value of integrative analyses.

Whether these markers can be used to investigate and monitor adverse pulmonary responses to TRPM remains to be determined. However, with evidence that endotoxins contribute to the composition of ambient particles (356) and titanium particles (shown to induce miR-449 over-expression in **Chapter 2**) stimulate the same receptors as LPS (357), this work provided the rationale for further investigation.

Chapter 4: Extracellular markers of pulmonary inflammation induced by traffic-related particulates

Overview

This collection of work characterised the physiochemical properties of two major traffic related particulates; diesel exhaust particles (DEP) and brake abrasion dust (BAD) and assessed their influence on human macrophage health and function using hypothesis-driven toxicological approaches. Biomarkers for the mechanisms of toxicity that the particles induced were sought and compared using metabolomics approaches, targeted quantification of inflammatory miRNAs (miR-34b/449a) and integrated pathway enrichment analyses.

4.1: Introduction

Exposure to traffic-related PM (TRPM) is considered an important cause of pulmonary inflammation due to the ubiquitous presence of the particles in ambient air (358,359), their concentration in populated and commuted areas (360) and the breadth of sub-populations that are susceptible to their pro-inflammatory effects (361–365).

In general, circulating biomarkers for pulmonary responses to TRPM exposure have been pursued in a targeted and hypothesis-driven manner, directed by well characterised pulmonary reactions to exhaust PM exposure that have been established through *in vitro* and *in vivo* modelling. As such, increases in plasma concentrations of neutrophils and platelets, pro –inflammatory cytokines (IL- 6 and IL-1β), endothelial cell adhesion molecules (I-CAM1 and V-CAM1) and neutrophilic response proteins (matrix-metalloproteinase-9 and myeloperoxidase) have all been associated with exhaust PM exposure in human cohorts (366–370).

In contrast, the responses that non-exhaust particulates (such as brake, clutch or tyre wear particles) induce in pulmonary systems are yet to be characterised (either *in vitro* or *in vivo*) with very few studies existing that could direct hypotheses for biomarker identification in

human bio-fluids (371). BAD for example, is the most abundant non-exhaust particulate species found in urban areas (contributing up to 25% of total TRPM (28)) but no further investigations have been made into its toxic potential since the discovery that it induces ROS and cytokine secretion in A549 epithelial cells (371). This lack of research interest is surprising since non-exhaust PM contributes up to 50% of total $TRPM_{10}$ (25,28), has a respirable size range and is often rich in pro-inflammatory and oxidative stress- inducing metallic species (372).

As the toxicity of TRPM is repeatedly attributed to its metallic content (51,373,374) it is possible that non-exhaust PM induces different or additional cellular pathways to carbonaceous and PAH-rich exhaust PM. Indeed, BAD-induced ROS synthesis was shown to occur in a metal-dependent manner in A549 cells (371). This indicates that existing biomarkers of TRPM exposure that originated from exhaust PM exposure studies may not fully represent the impacts that non-exhaust particles have on pulmonary systems. Thus, easily accessible biomarkers that relate specifically to non-exhaust particle toxicity must be found before we can quantify the effects that these particles have on public health and understand the mechanisms by which they impact the lungs.

Metabolomic and high throughput miRNA quantification approaches are emerging as successful methods for detecting novel and accessible biomarkers of pulmonary responses to different TRPM components. Microarray analyses have associated metallic particle exposure with differentially expressed miRNA panels in circulating cells and microvesicles (251,375) while metabolic profiling has identified links between exhaust PM exposure and decreased ATP synthesis, increased degradation of airway structural lipids, heightened availability of pro-inflammatory lipid mediators and enhanced anti-oxidant molecule production in accessible human BALF and mouse serum samples (185,376).

While the characterised inflammatory relevance of the early, hypothesis-driven, circulating markers of exhaust particle toxicity made them epidemiologically useful, (366–370), those

found through metabolite and miRNA profiling have better enhanced our knowledge of exhaust PM-induced mechanisms of toxicity. Rather than simply demonstrating that a known pro-inflammatory molecule was produced in response to exposure, they have indicated which pathways lead to the production of that molecule, whether additional pathways intersected with the characterised inflammatory process and that novel inflammatory molecules were involved too. Such an approach may prove invaluable for furthering our understanding of whether and how non-exhaust PM impacts the lungs and for detecting or monitoring these toxicities in exposed populations.

4.1.1: Hypothesis and aims

Given the nature of non-exhaust PM toxicity is largely uncharacterised, this body of work combined hypothesis-driven assessments of cellular health and function with data-driven ^{1}H NMR based metabolic profiling to evaluate the hypothesis that **exposure to BAD induces mechanistically relevant and extracellularly detectable changes in the metabolic activity of human macrophages.** Targeted quantifications of miR-34b and 449a were performed alongside these analyses to explore the hypothesis that **these circulating markers of pulmonary inflammation are applicable to TRPM- induced responses.**

Specifically the study aimed to **characterise BAD induced toxicity in cultures of U937 monocyte-derived macrophages** (a human cell line that is commonly used to characterise inflammatory responses to ambient PM exposure (377,378)) and **identify mechanistically relevant, metabolite and miRNA biomarkers for the toxicity** in the cellular supernatants that could be measured in human biofluids during future work.

In addition, the study sought to **compare the mechanisms and biomarkers of BAD induced toxicity with those induced by exposure to SRM-2975;** a well characterised and frequently studied exhaust particle obtained from the diesel engine of a forklift truck. As DEP have already been shown to influence the key inflammatory and phagocytic functions of human macrophages (94,379–383) this aim sought to establish whether **BAD and DEP do so via similar or distinct pathways**.

4.2: Materials and methods

4.2.1: Nanoparticles: SRM-2975 DEPs, purchased from the National Institute of Standards and Technology were kindly provided by Dr Mudway (King's College, London) along with BAD that had been extracted from the filters of a ventilation duct at a brake pad test rig (SMP Svensk Maskinprovning machinery testing plant, Sweden). Each filter represented a yearly collection of abrasion dusts that were produced from the brake pads of European trucks and buses. BAD had been harvested previously by Dr Mudway through methanol extraction; 1cm^3 sections of filter were submerged in high performance liquid chromatography grade methanol, vortexed for 10 minutes and sonicated for a further 10 minutes at an amplitude of 15 microns. After decanting the methanol into a fresh tube, vortexing and sonication were repeated and the resulting extracts were dried under a stream of nitrogen gas at 37° C. Both particle types were stored at -80°C as stock solutions of 1mg/ml in phosphate buffered saline (PBS).

4.2.2: Particle size measurement using dynamic light scattering (DLS): Solutions of BAD and SRM-2975 (14 µg/ml) were made in culture medium (CM); RPMI 1640 medium containing 10% foetal bovine serum, 1% L-Glutamine and 1% Penicillin-Streptomycin. The particle solutions were incubated at 37°C in humidified 5% CO2, 95% atmospheric air (standard conditions) for 0, 4 or 24h. The hydrodynamic diameters of the particles were measured using a Malvern Zetasizer Nano ZS (Malvern Instruments, UK) with 3 runs of 6 measurements being produced per sample.

4.2.3: Measurement of particulate oxidative potential: Solutions of BAD and SRM-2975 (55.5 µg/ml in chelator treated H_2O (chH_2O)) were incubated 9:1 with an antioxidant cocktail (2mM ascorbic acid (AA) and 2mM glutathione (GSH) in chH_2O for 4h at 37°C. Particles were removed from the solution through centrifugation for 1h at 13 rpm, 4°C to avoid signal interference during detection. Samples were diluted 1:60 in phosphate buffer for GSH

measurement or diluted and acidified 1:1:8 in metaphosphoric acid and ultrapure H_2O for AA measurement. Antioxidant concentrations were determined as described by Mudway *et al.* (2001), using high performance liquid chromatography for AA and a variety of the glutathione disulphide-reductase- 5,5′-dithio-bis(2-nitrobenzoic acid) recycling assay for GSH (384).

4.2.4: U937 culture and differentiation: U937 monocytes were grown and maintained in CM under standard conditions. Cells were seeded at densities of 1 $x10^6$ and 1.25 $x10^5$ cells in 12 and 96 well plates (respectively) in CM containing 4nM phorbol 12-myristate 13-acetate (PMA) to stimulate differentiation into adherent macrophages. After 96h culture in the presence of PMA, cells were rested in CM without PMA for 24h prior to experimentation.

4.2.5: Particle exposure: BAD and SRM-2975 stocks were probe sonicated for 2 minutes at 70 Hz to disperse agglomerated particles then diluted to 4-25 µg/ml in CM. Particles were applied to cells in 1ml and 200 µl volumes for 12 and 96 well plates (respectively) and incubated for 4-48h under standard conditions. Light microscopy was used to confirm even dispersion of the particles. Where appropriate, 1 µg /ml LPS was applied to particle-free cells as a pro-inflammatory positive control or 380 µM desferroxamine added alongside the particles to characterise the impact of metal chelation.

4.2.6: Quantification of intra and extracellular metals by inductively coupled plasma mass spectroscopy (ICP-MS): Cells were exposed to 4-25µg/ml BAD or DEP as described above. After 24 hours the cellular supernatants were harvested and the cells were lysed in sterile chH_2O. Supernatants and lysates were transferred to Dr Mudway who combined the samples with a yttrium internal standard (stock solution, 1ppm, SCP Science, France) and digested them in aqua regia solution (1:3 HNO_3 (60%): HCl (30%) (Merck, UK)) for 90 minutes at 100° C. Cooled digests were transferred to the Mass Spectrometry Unit at KCL for quantification of Al (isotope 27; natural abundance 100%), As (75, 100%), Ba (135; 6.95%), Cu (63; 69.17%), Fe (56; 91.75%), Mn (55; 100%), Mo (95; 15.92%), Ni (60;

26.22%), Cr (52; 83.79%), V (51; 99.75%), Sb (121; 57.21%), Zn (66; 27.90%), Cd (111, 12.80%), Ti (47, 7.44%), Ca (44, 2.08%), W (184, 30.64%), Sn (118, 24.22%) and Y (89, 100%) by ICP-MS using a NexION 350D ICP-MS (PerkinElmer, UK). These measurements were acquired by Mr Cakebread (King's College, London). Elemental concentrations (representing the means of 5 injections and corrected for background concentrations in chH_2O) were determined by Dr Mudway with reference to a standard curve produced using an ICP multi element standard solution VI CertiPUR (Merck, Lot. No. OC529648).

4.2.7: 3-[4,5-dimethylthiazol-2-yl]-2,5 diphenyl tetrazolium bromide (MTT) assay: Mitochondrial oxidoreductase activity was measured post- particulate exposure and used as an indication of cell viability. Cells were incubated with 2.5 µg/ml MTT reagent in CM for 4 hours and the formazan crystals dissolved in a 1:1 solution of 20% sodium dodecyl sulphate and dimethylformamide. Signal was measured at a wavelength of 570 nm using a microplate reader (SpectraMax 190).

4.2.8: Cytokine enzyme linked immunosorbent assays (ELISAs): Supernatants were collected post-challenge and centrifuged at 16000 *xg* for 10 minutes to remove extracellular particles. Cytokine concentrations were measured using Human IL-10, TNF-α and IL-8 ELISA Ready-SET-Go! kits (eBioscience, San Diego, CA) in accordance with the manufacturer's instructions.

4.2.9: Maintenance of bacterial stocks: Müeller Hinton (MH) broth (g/ml in deionised H_2O) was inoculated with a Newman strain of *Staphylococcus aureus* (*S. aureus*) (K. Bruce, KCL) and incubated overnight at 37°C before being streaked onto MH agar (MH broth supplemented with 0.01g/ml agar) and incubated once more overnight at 37°C. Live cultures were stored at 4°C and fresh plates were produced every 4 weeks. For experiments, a single, isolated colony was grown overnight at 37°C in MH broth. The optical density of the overnight culture was ascertained using a Jenway 6300 Visible Range Spectrophotometer

set to a wavelength of 600 nm and working cultures were produced by diluting the overnight culture to $1x10^4$ colony forming units (CFU)/ml in MH broth.

4.2.10: Quantification of bacterial phagocytosis behaviour: Working cultures of *S. aureus* were centrifuged at 5000 *xg* for 15 minutes and re-suspended in CM without antibiotics. Particulate-challenged U937s were washed 3 times with PBS and inoculated with 1ml of the *S. aureus* solution, producing a multiplicity of infection of 0.01. Contact between the macrophages and bacteria was encouraged by centrifuging the plates at 2700 *xg* for 10 minutes prior to incubation under standard conditions for 2h. Bacteria that were not ingested by the macrophages were removed by washing the cells 3 times with PBS and incubating them with 50 µg/ml gentamicin for 10 minutes. Sterile deionised H_2O was used to lyse the U937s and release their internalised bacteria into the supernatant. The supernatants were diluted 1:10 in MH broth and grown overnight at 37° C on MH agar in duplicate. *S. aureus* colonies were counted manually. Experiments were also performed following 24h exposures to 1 µg/ml benzo[a]pyrene.

4.2.11: Bacterial growth curves: Working cultures of *S. aureus* were produced using particle-free MH broth or MH broth spiked with 25 µg/ml BAD, DEP or gentamicin (as a positive control for antibacterial activity). Cultures were incubated at 37°C with 50 µl aliquots being plated in duplicate on MH agar after 0, 1, 2 and 3 hours. Plates were incubated overnight at 37° C then *S. aureus* colonies were counted manually.

4.2.12: Bicinchoninic acid (BCA) protein quantification assay: The Bicinchoninic Acid Protein Assay Kit (Sigma) was used to quantify total cellular protein concentrations for U937s after 4 and 24h exposures to particles. Assays were performed in accordance with the manufacturer's instructions.

4.2.13: Univariate statistical analysis of toxicological data: Using Microsoft Excel, raw data was normalised using total cellular protein (obtained by BCA assay) and expressed as percentages of particle-free controls. These stages were designed to exclude the influence of cytotoxicity that may have been caused by the particles and to enhance comparability between experimental repeats. Identification of significant differences between treatment types were made using GraphPad Prism (Graphpad Software, San Diego). Statistical assessment was via 1-Way ANOVA tests for DLS, oxidative potential, ICP-MS, ELISA, cell staining and bacterial phagocytosis assays and 2-Way ANOVA tests for MTT, metal chelator and bacterial growth assays. Bonferroni corrections were performed where ANOVAs found differences between treatment types with p values ≤ 0.05. Differences between values were considered statistically significant where their p value remained ≤ 0.05 after post-hoc testing.

4.2.14: RNA extractions: U937 supernatants were exposed to 1 µg/ml LPS or 4- 14 µg/ml BAD or SRM-2975 for 24h. RNA was extracted from the supernatants which were harvested immediately following the 24h exposure period and from cells following three washed in PBS.

4.2.14.1: RNA extraction from U937 lysates: Total RNA containing miRNA was extracted from U937 cells using an RNeasy Plus Mini Kit (QIAgen). In accordance with a modified protocol that was provided by the manufacturer, the cells were lysed in RLT buffer Plus. As for the LPS treated rat plasma samples used in **Chapter 3**, 8.1x105 copies/ µl of cel-miR-39 were added to the lysates (for use as an exogenous control) then genomic DNA was removed by passing the lysate through a genomic DNA Eliminator spin column by centrifugation (≥8,000 x g, RT, 30 s). The flow through was mixed with 1.5 volumes of 100% ethanol and passed through an RNeasy Mini spin column via centrifugation (≥8,000 x g, RT, 15 s). The spin column containing captured RNA was washed twice with Buffer RPE by centrifugation (≥8,000 x g, RT, 15 s) then dried by centrifuging for a further minute (≥8,000 x g, RT) before captured RNA was eluted in 40 µl nuclease free H_2O.

4.2.14.2: RNA extraction from U937 supernatants: Total RNA was extracted from the U937 lysates using the TRIzol LS method and spiked with cel-miR-39 (an exogenous control used for target data normalisation) as described in **Chapter 3.2.2-3**.

4.2.14.3: RNA quantification: Total RNA and miRNA concentrations were determined using the nanodrop spectrophotometry and bioanalyzer small RNA kit protocols described in **Chapter 3.2.4**.

4.2.15: cDNA synthesis: cDNA was produced using primers for hsa-miR-34b, hsa-miR-449a and cel-miR-39 using the protocol described in **Chapter 3.2.5**.

4.2.16: RTqPCR data acquisition and analysis: hss-miR-34b, 449a and cel-miR-39 were quantified and the resulting data analysed using the methods described in **Chapter 3.2.6**.

4.2.17: ^{1}H NMR spectroscopy: The supernatants of cells treated with 4 or 14 µg/ml BAD or DEP were centrifuged for 10 minutes at 16000 x *g* to remove suspended particulate matter then combined with 10mM TSP in D_2O and transferred to 5 mm NMR tubes. ^{1}H NMR spectra were acquired for the samples using a Bruker AVANCE 600 spectrometer (Bruker, Biospin, Rheinstetten, Germany) fitted with a Bruker TXI probe and an automated sample handling carousel (Bruker) at a frequency of 600.29 MHz and at a temperature of 300K. One dimensional NMR spectra were obtained using a CPMG spin-echo pulse sequence. Following 4 dummy scans, 32 transient scans were collected into 30,000 data points with a spectral width of 20 ppm, acquisition time of 3.07 seconds and relaxation delay of 4.00 seconds. Prior to Fourier transformation, a line broadening factor of 0.3 Hz was applied to all spectra.

4.2.17.1: Processing of ^{1}H NMR spectroscopic data: Spectra were imported into MATLAB R2013a (Mathworks, USA) where automatic phasing, referencing of chemical shifts to the resonance of the TSP internal standard (δ 0) and baseline correction were performed using an in-house code. Prior to peak alignment the residual water resonance (δ

4.40- 5.00 ppm), ethanol resonances (δ 1.10-1.24, 3.61-3.68 ppm) and TSP resonance (δ 0.00 ppm) were removed) and spectra exhibiting low signal: noise ratios were excluded from the analysis. The remaining data was normalised to complimentary values for total cellular protein to remove the influence of differences in cell number between cell cultures.

Spectra were analysed at a reduced resolution (46 data points). To obtain the reduced resolution data, metabolite peaks were assigned using Chenomx software version 7.7 (Chenomx Inc, Canada) and the Human Metabolome Database Version 3.6. These assignments directed selection of representative peaks for each metabolite from which peak areas were integrated based on manually assigned minima and maxima. Where metabolites contributed peaks at multiple resonances, the least overlapped peaks were selected for integration to produce the cleanest values.

4.2.17.2: Feature identification from ^{1}H NMR spectroscopic data: Feature metabolites were identified using Student's t-tests with FDR corrections which looked for significant differences in metabolite concentrations between control and exposure groups. Any differences in peak area with p values ≤ 0.05 and a FDR ≤ 20% were considered to be significant.

4.2.18: Over-representation analysis of metabolite and transcriptomic datasets:

Cellular pathways that may have been represented by the feature metabolites and the potential for their regulation by miR-34b/449a were identified using the over-enrichment analysis module of IMPaLA. As described in **Chapter 3**, lists of feature metabolites and predicted gene targets of miR-34b/449a were included in the analysis and pathways were considered to be significantly over-represented if their joint overlap was assigned a p value ≤ 0.05 with a FDR of ≤ 20%.

4.3: Results

4.3.1: Physicochemical characteristics of BAD and SRM-2975 particles

The compositional and physical properties of traffic-related PM may vary between sources as a result of differences in driving behaviour, vehicle condition and environmental factors such as temperature and the presence of airborne chemicals (28). Although SRM-2975 is a well characterised, commercially available particle (385), the BAD particles that were used in this study required preliminary physicochemical characterisation prior to use.

As cells were exposed to BAD and SRM-2975 in the presence of CM, the particles were sized based on their hydrodynamic diameter (diameter when suspended in a liquid) in CM. The degree to which both particle types might agglomerate during exposure to cells was assessed by measuring the particles over a time-course equivalent to the cellular exposure experiments.

At time 0, BAD had an average hydrodynamic diameter of 0.61 ± 0.07μm and a high polydispersity index (PDI) of 0.72 ± 0.05. SRM-2975 was also highly polydisperse with a PDI of 0.76 ± 0.19 but was considerably larger than the BAD (1.21 ± 0.11μm). Neither the size nor the polydispersity (distribution of hydrodynamic diameters) of either particle altered significantly across the time-course indicating that particular agglomeration or dispersion would likely be minimal during cellular exposures **(Table 4.1).**

ICP-MS was employed to measure the concentrations of 18 metals/metalloids within the particle samples. BAD was richly metallic containing 14 of the metallic species tested. Of these, Fe, Ca, Ti and Ba were most abundant (77.03 ± 0.61, 18.34 ± 0.37, 16.65 ± 0.33 and 11.79 ± 0.06 ng/μg respectively). In contrast, SRM-2975 particles contained far fewer metallic species with only Ti (17.34 ± 0.34 ng/μg), As (5.73 ± 0.14 ng/μg), V (0.05 ± 0.00 ng/μg) and Sb (0.01 ±0.00 ng/μg) being detected in the samples. While BAD and SRM-2975 contained equivalent concentrations of Ti, As and V, Sb was significantly enriched in BAD ($p \leq 0.001$) **(Table 4.2)**.

Many of the metals detected within BAD and SRM-2975 induce oxidative stress in biological systems (59,60,386) by producing ROS through redox cycling (Fe, Cu, Cr, V, Co), depleting cellular GSH (Cd) or directly binding to thiols (As) (387). As BAD and SRM-2975 differed greatly in content of these metals, the oxidative potentials of the two particles were determined based on their ability to deplete glutathione and ascorbate from a simulated respiratory tract lining fluid. In comparison to the particle free control, and consistent with an urban dust positive control particle (SRM-1648a), both BAD and SRM-2975 significantly depleted ascorbate (44 and 55% respectively, $p \leq 0.001$) after the 4 h incubation period. Significant oxidation of glutathione occurred after incubation with BAD (12%, $p \leq 0.05$) but not with SRM-2975 **(Figure 4.1)** indicating that while both particles possessed oxidative potential, their affinity for specific antioxidants may differ.

Table 4. 1: Hydrodynamic diameter of BAD and SRM-2975 as determined by DLS. Average hydrodynamic diameters (± SEM) and PDI (± SEM) of BAD and SRM-2975 samples (14 µg/ml) ascertained using dynamic light scattering after 0, 4 or 24 h incubation in CM at 37°C. Measurements were made at 25°C and values were produced over 3 runs consisting of 6 readings each.

Particle	Dispersant	Time point (hours)	Average diameter (nm)	Average PDI
BAD	CM	0	610.32 ± 72.71	0.72 ± 0.05
		4	617.53 ± 119.01	0.69 ± 0.09
		24	616.22 ± 1.59	0.60 ± 0.09
SRM 2975	CM	0	1214.33 ± 108.59	0.76 ± 0.19
		4	1179.53 ± 269.35	0.85 ± 0.11
		24	1228.23 ± 115.79	0.90 ± 0.11

.

Table 4. 2: Metal and metalloid content of BAD and SRM-2975 as determined by ICP-MS.
Values represent the mean ± **SEM** for three biological replicates. n.d = non-detected**.**

Metal	SRM 2975 concentration (ng/µg)	BAD concentration (ng/µg)
Fe	n.d.	77.03 ± 0.61
Ca	n.d.	18.34 ± 0.37
Ti	17.34 ± 0.34	16.65 ± 0.33
Ba	n.d.	11.79 ± 0.06
Al	n.d.	5.80 ± 0.10
As	5.73 ± 0.14	4.63 ± 0.37
Zn	n.d.	2.12 ± 0.02
Mn	n.d.	0.73 ± 0.01
Cu	n.d.	0.14 ±0.01
V	0.05 ± 0.00	0.06 ± 0.00
Mo	n.d.	0.08 ± 0.00
Sb	0.01± 0.00	0.05 ± 0.00
Cd	n.d.	0.01 0.00
W	n.d.	0.02 ±0.00
Cr	n.d.	n.d.
Ni	n.d.	n.d.
Sn	n.d.	n.d.
Y	n.d.	n.d.

4.3.2: U937 macrophages ingest BAD and SRM-2975 particles

The ability of U937s to ingest BAD and SRM-2975 during a 24 h exposure period was demonstrated using light microscopy. While intracellular accumulations of PM were visible after exposure to either particle type at dosages as low as 4 µg/ml, this was more pronounced for SRM-2975 than for BAD **(Figure 4.2).**

Whilst not statistically significant using three biological replicates, cells challenged with BAD for 24 h also had enriched metal content when compared with particle-free controls. They showed dose dependent increases in Ba, Mn and Fe content across the 0-25 µg/ml exposure range (up to 1379, 200, and 265 % of particle-free control, respectively). Minor dose dependent uptake was also observed for Al and Ca across the 0- 14 µg/ml exposure range (up to 245 and 126 % of particle-free control, respectively) and for As, V, Zn, Cu and Ti across the 0-8 µg/ml exposure range (up to 155, 248, 122 and 120 % of particle-free control, respectively). Contrastingly, intracellular concentrations of Cr and Ni displayed dose-dependent decreases in concentrations following BAD exposure, reducing by up to 64 and 16% (compared with particle-free controls) over the 0-25 µg/ml exposure range (**Table 4.3**).

Despite SRM-2975 being of low metal content, an increase in intra-cellular metal concentrations was also seen following 24h exposure to this particle (also non-significant in terms of statistical testing). Dose dependent increases in intracellular vanadium concentration were observed across the 0-25 µg/ml exposure range (up to 372 % of particle-free control) while minor dose-dependent increases in intracellular As and Ti concentrations were visible across the 0-8 µg/ml exposure range (up to 144 and 128 % of particle-free control respectively) **(Table 4.3)**.

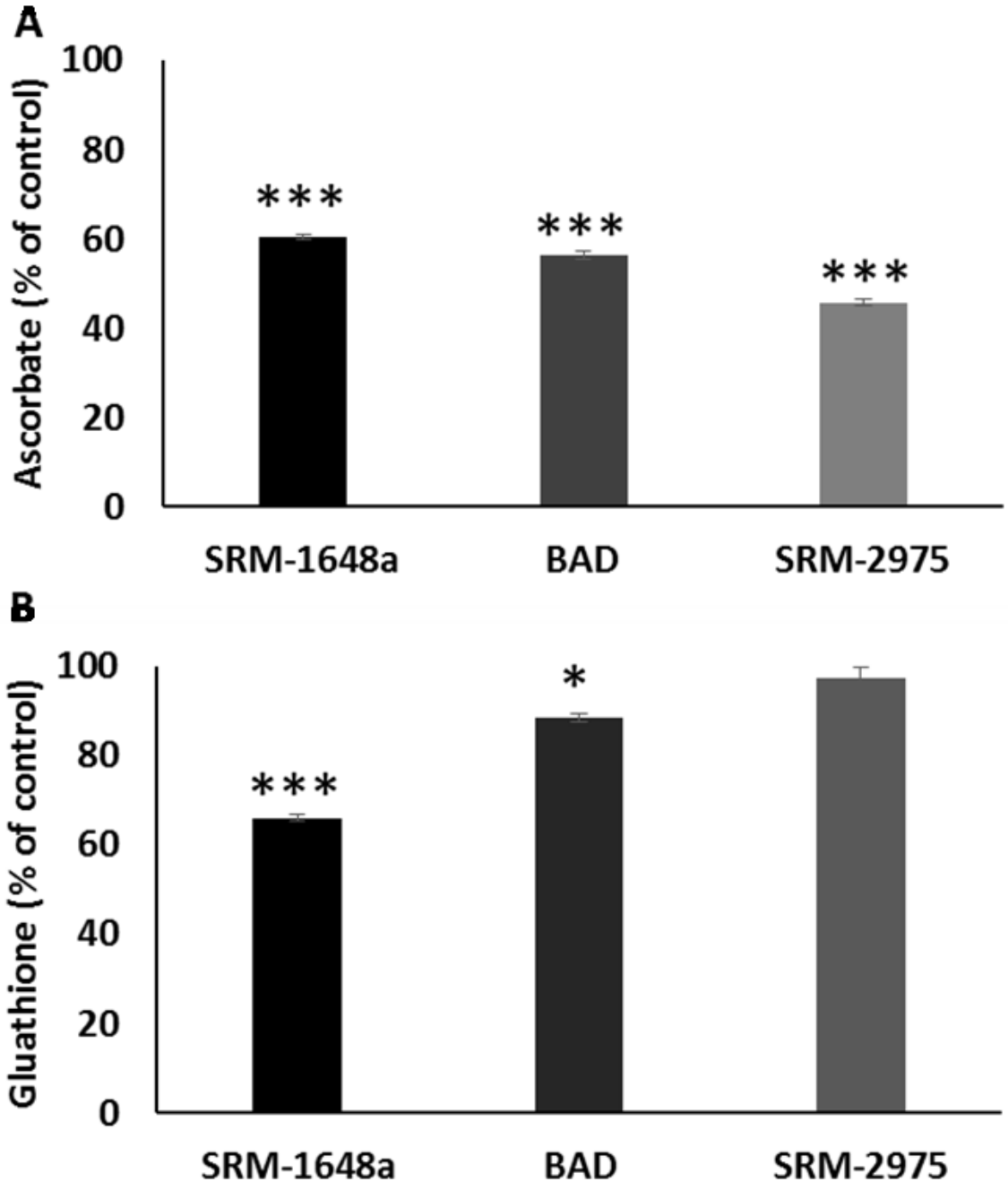


Figure 4. 1: The oxidative potential of SRM-2975 and BAD. Depletion of (A) ascorbate and (B) glutathione from an antioxidant cocktail (2mM) following 4h incubations with BAD, SRM-2975 or SRM-1648a (55.5µg in chH_20). Values are displayed as percentages of a particle-free control and represent the SEM for 3 biological replicates, each composed of 3 technical replicates.

4.3.3: BAD and SRM-2975 are not cytotoxic to U937 macrophages but cause mitochondrial dysfunction

The cytotoxic potential of the particle-cell interactions was assessed via MTT assay, using mitochondrial oxidoreductase activity as a proxy for cell viability. Over time-courses of 4-48h, neither BAD nor SRM-2975 reduced U937 viability to a statistically significant extent when dosed at 4 – 25 μg/ml **(Figure 4.3**). This indicated that the degree of cytotoxicity that was induced by ingestion of the particles did not impact strongly on the viability of the U937 cultures.

As a degree of inter-sample variability was observed in the data collected from the MTT assay (which may have contributed to acquisition of a non-statistically significant result), this result was validated by staining the nucleus and cytoplasm of the cells with fluorescent dyes. This approach sought to examine changes in nuclear or cellular area that represent necrosis or apoptosis following particulate challenge. In agreement with the MTT assay, neither particle type significantly altered the nuclear or cellular areas of the U937s (as compared with particle-free controls), even at the highest dosages (25 μg/ml), indicating that the cells had not entered into necrotic or apoptotic states **(Figure 4.4A–D)**. The cells did however display dose-dependent decreases in Mitotracker Red signal after exposure to BAD (7.2 ± 2.9 – 64.9 ± 1.0%) and SRM 2975 (30.5 ± 6.1 – 57.3 ± 1.3%). As this dye is selectively retained within healthy mitochondria, this result is indicative of mitochondrial dysfunction **(Figure 4.4 E-F)**.

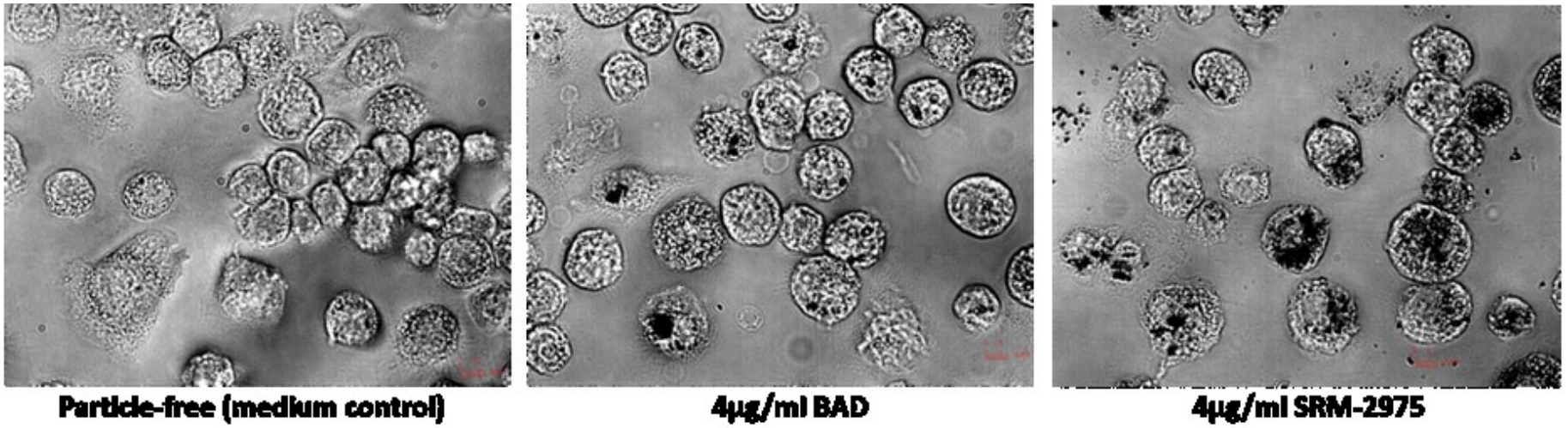


Figure 4. 2: Light micrographs of U937s following 24 h exposures to particle-free medium (A), 4 µg/ml BAD (B) or 4 µg/ml SRM- 2975 (C) at 1000 X magnification.

Table 4. 3 : Metal and metalloid content of U937 lysates following 24 h exposure to 4-25 µg/ml BAD or SRM-2975. Data were acquired by ICP-MS, normalised to total cellular protein (determined by BCA assay) and displayed as a **percentage** of a particle- free control). Values were produced using the average of three experimental replicates.

	BAD				SRM- 2975			
	4 µg/ml	**8 µg/ml**	**14 µg/ml**	**25 µg/ml**	**4 µg/ml**	**8 µg/ml**	**14 µg/ml**	**25 µg/ml**
Al	146	176	246	178	nd	Nd	nd	nd
As	114	121	120	96	136	145	143	117
Ba	599	712	935	1379	nd	Nd	nd	nd
Mn	136	140	153	200	nd	Nd	nd	nd
V	182	242	220	222	102	190	285	363
Sb	nd	nd	nd	nd	nd	Nd	nd	nd
Cd	103	72	70	121	nd	Nd	nd	nd
Cr	85	71	56	36	nd	Nd	nd	nd
Cu	114	122	103	111	nd	Nd	nd	nd
Mo	Nd	nd	nd	nd	nd	Nd	nd	nd
Ni	94	94	88	84	nd	Nd	nd	nd
Zn	117	143	144	145	nd	Nd	nd	nd
Ca	111	116	126	109	nd	Nd	nd	nd
Fe	147	160	195	266	nd	Nd	nd	nd
Y	119	122	116	119	nd	Nd	nd	nd
Ti	110	120	118	110	122	128	127	99

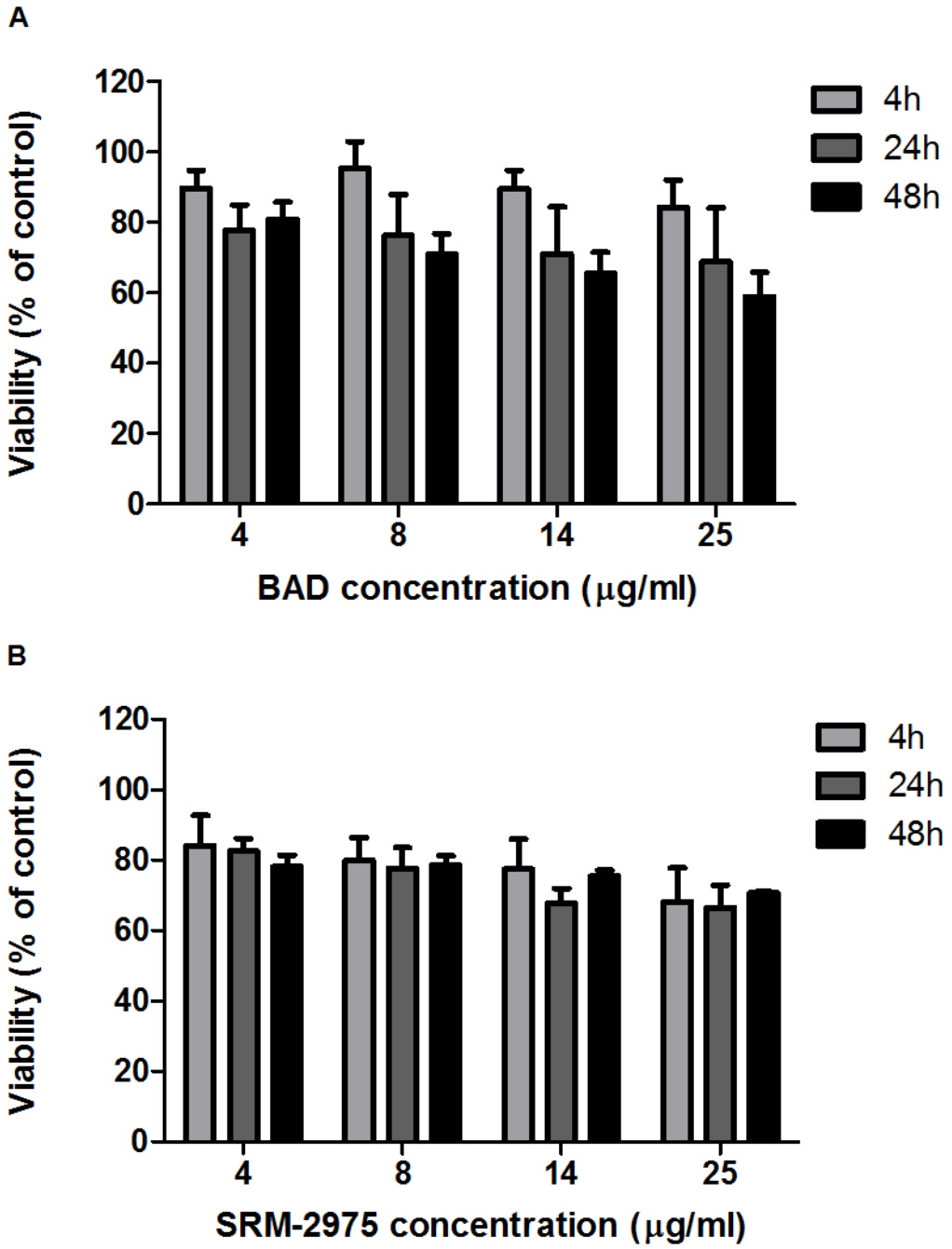


Figure 4. 3: Viability of U937s following exposure to 4-14 µg/ml BAD or SRM-2975. Measurements were made following 4-48h exposures to 4-25 µg/ml BAD (A) or SRM-2975 (B). Values are displayed as percentages of a particle-free control and represent the mean ± SEM of 6 individual measurements, each consisting of 6 technical replicates.

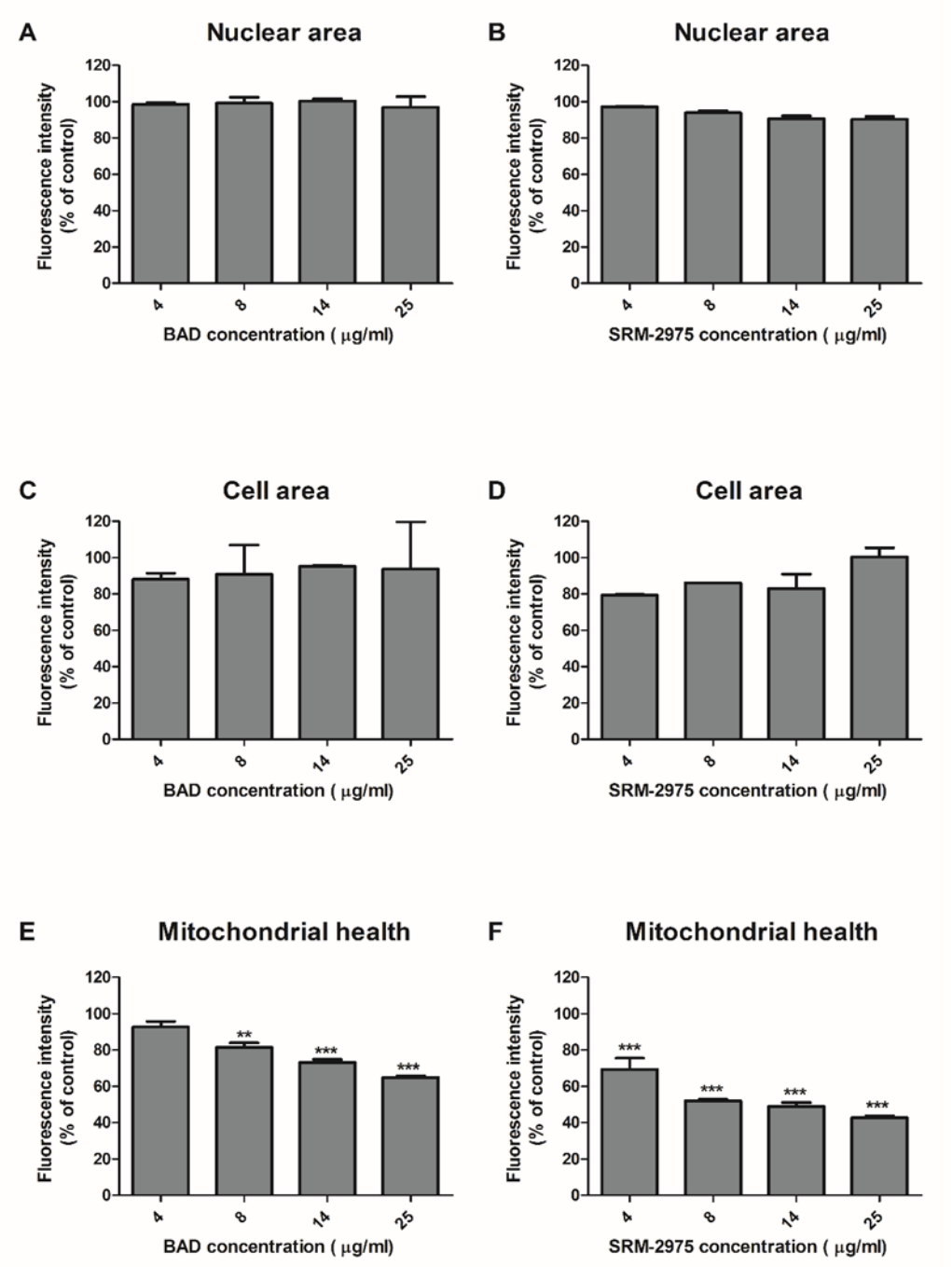


Figure 4. 4: The influence of particle exposure on metrics of cellular health. Fluorescent intensities of Hoechst nuclear stain (A and B) CellMask Deep Red cytoplasmic stain (C and D) and Mitotracker Red stain for intact mitochondrial membrane potential (E and F) in U937s after 24h exposure to 4-25 μg/ml BAD or SRM-2975. Fluorescent intensities were measured using an IN CELL analyzer 2200 and are displayed as a percentage of a particle-free control showing the mean ± SEM values produced during 2 biological replicates (composed of ~ $1x10^6$ single cell measurements). Significant differences in the fluorescence intensities of staining were identified between control and particle-treated cells using 1-way ANOVA tests with Bonferroni correction. ** $p < 0.01$, *** $p < 0.001$

4.3.4: BAD and NIST induce inflammatory responses in U937

Inhaled particles are commonly hypothesised to exert pulmonary toxicity via inflammatory mechanisms. As such, concentrations of IL-8, IL-10 and TNF-α were measured in U937 supernatants following 24h challenges with BAD or SRM-2975. In comparison to the particle-free control, BAD exposure significantly increased IL-8 secretion by 42.7-171.2% from concentrations as low as 4 μg/ml ($p \leq 0.01$- < 0.001) and IL-10 secretion by 144.8 -185.3% at concentrations ≥14 μg/ml ($p \leq 0.01$- < 0.001) (**Figure 4.5A and C**). SRM-2975 also induced significant increases in IL-8 secretion (55.2-133.7%, $p \leq 0.001$) from concentrations ≥ 4 μg/ml (**Figure 4.5B**). IL-10 secretion increased in a dose-dependent manner following SRM-2975 exposure reaching statistical significance at 25 μg/ml (216.2%, $p \leq 0.05$) (**Figure 4.5D**). Exposure to 4-25 μg/ml SRM-2975 significantly increased TNF-α secretion by 137.5, 167.5, 149.5 and 175.8% in comparison to the particle-free control ($p \leq 0.01$, 0.001, 0.001 and 0.001 respectively) (**Figure 4.5E**). In comparison, BAD exposure only induced significant increases in TNF-α secretion at the 25 μg/ml dosage (154.5%, $p \leq 0.01$) (**Figure 4.5F**). Such data indicate that both particles induce pro-inflammatory responses in U937s that are accompanied by anti-inflammatory activity at higher doses.

In order to determine whether the inflammatory responses were stimulated by the metallic portions of the particles, the cytokine measurements were repeated using the supernatants of U937s exposed to BAD or SRM-2975 (4- 25 μg/ml, 24 h) in the presence of desferroxamine (a non-specific metal ion chelator). In this system, secretion of IL-8 and TNF-α remained equivalent to the particle free control for both exposure types **(Figure 4.6 A-D)**. In contrast, IL-10 secretion was elevated in comparison to controls following exposure to BAD at doses ≥ 8 μg/ml (172.0-201.4%) or to 25 μg/ml DEP (222.4%) **(Figure 4.6 E-F)**

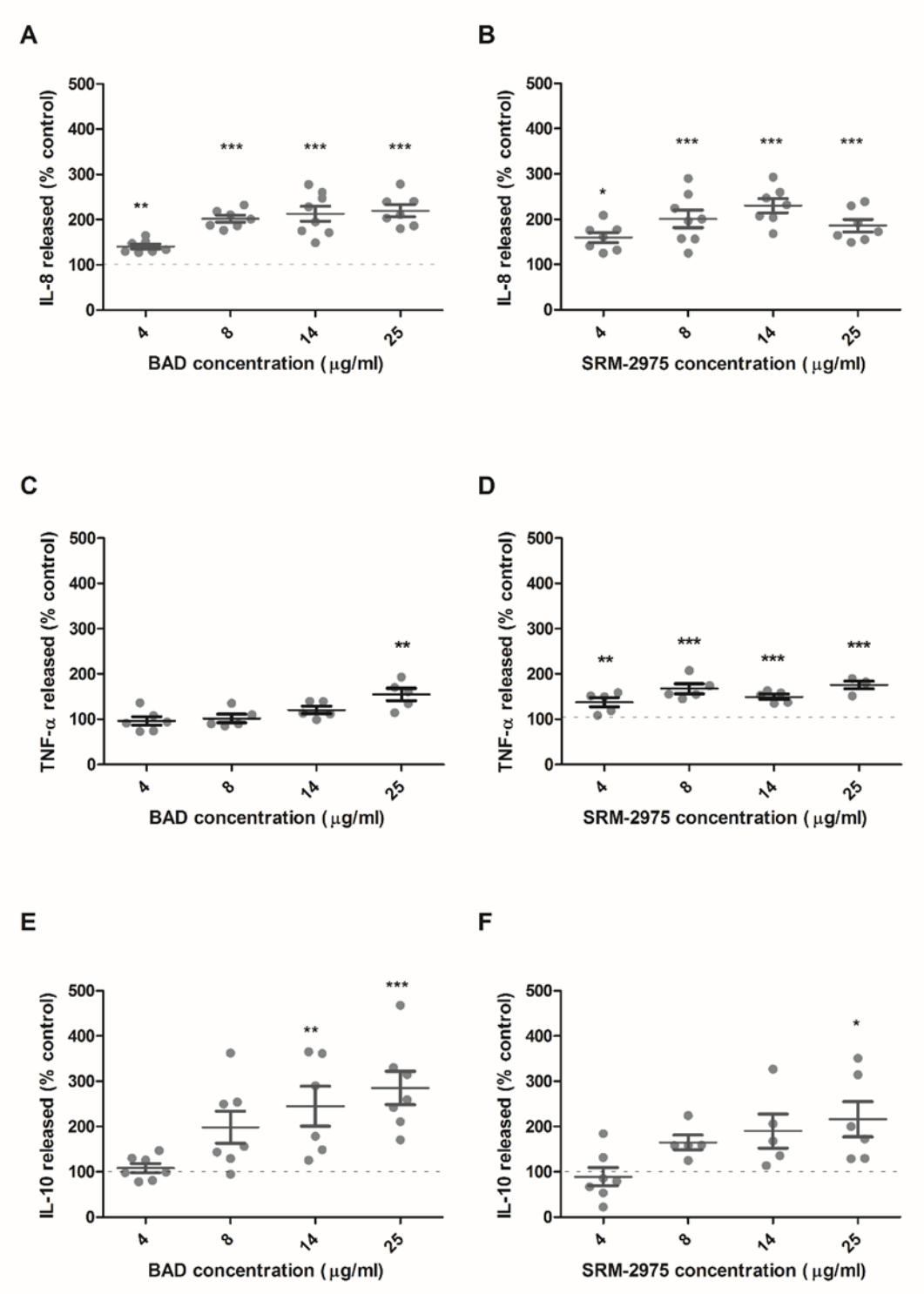


Figure 4. 5: **Particle-induced cytokine secretion.** Concentrations of IL-8 (A, B), TNF-α (C, D) and IL-10 (E, F) measured within the supernatants of U937s after 24h exposure to BAD (A, C, E) and SRM-2975 (B, D, F). Values are expressed as percentages of particle-free controls with error bars depicting the SEM generated during 5-7 replicates. Significant differences in cytokine concentration were identified between control and particle-treated cells using 1-way ANOVA tests with Bonferroni correction. * $p \leq 0.05$, ** $p \leq 0.01$, *** $p \leq 0.001$.

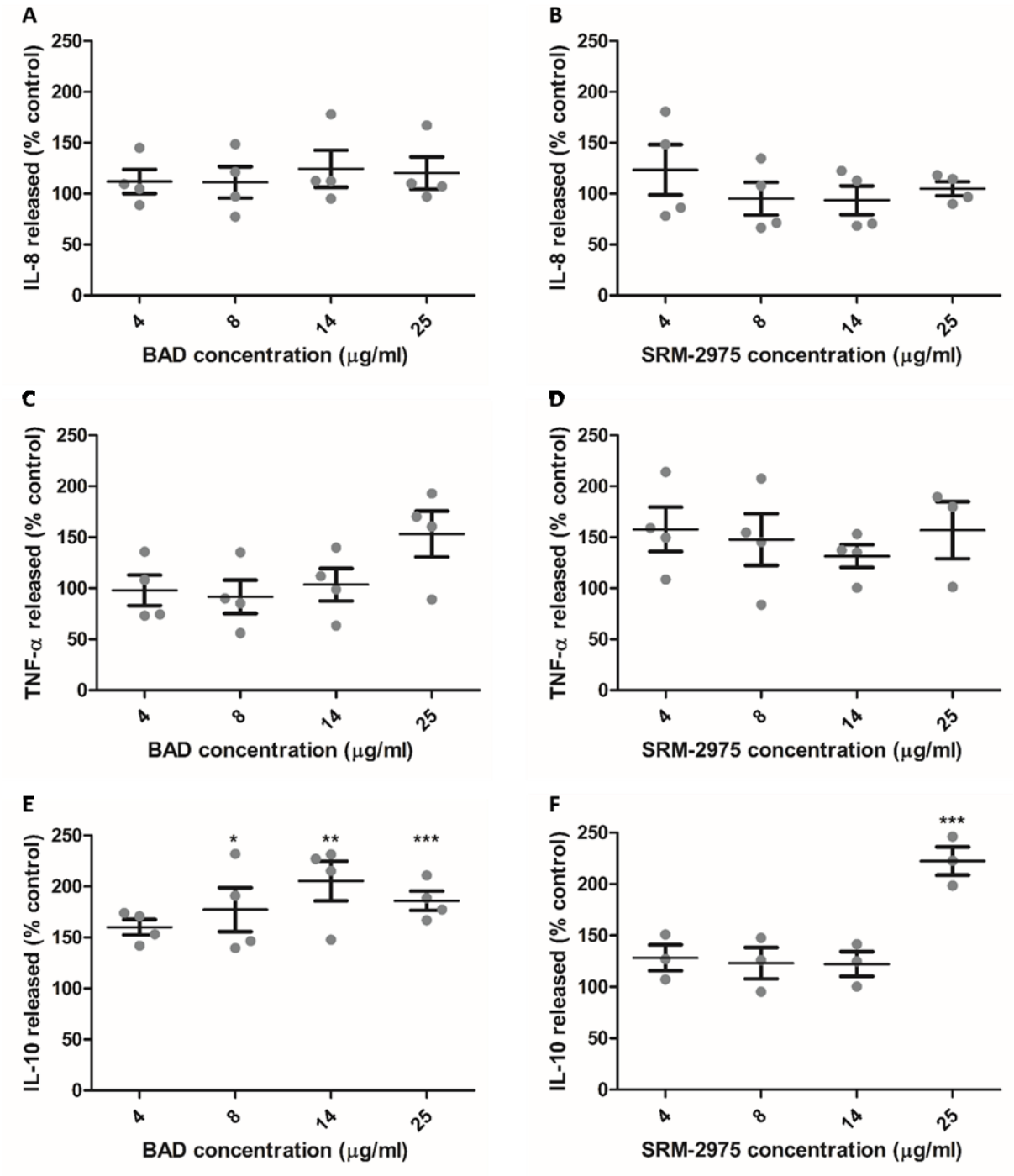


Figure 4. 6: **The influence of metals on cytokine secretion.** Concentrations of IL-8 (A, B), TNF-α (C, D) and IL-10 (E, F) measured within the supernatants of U937s after 24h exposure to BAD (A, C, E) and SRM-2975 (B, D, F) in the presence of 380 μM desferroxamine. Values are expressed as percentages of particle-free controls with error bars depicting the SEM generated during 5-7 replicates. Significant differences in cytokine concentration were identified between control and particle-treated cells using 1-way ANOVA tests with Bonferroni correction. *** $p \leq 0.001$.

4.3.5: BAD and SRM-2975 inhibit phagocytic function in U937

As IL-10 is a regulator of phagocytosis behaviour in macrophages and neutrophils (388,389), the impact that BAD and SRM-2975 exposure had on U937 phagocytic capability was assessed through measurement of the cell's capacity to ingest the respiratory pathogen S.*aureus* subsequent to particle treatment. After 24h of exposure to 4 and 8 µg/ml BAD, the number of S.*aureus* that the U937s ingested reduced by 30.0 and 29.5 % when compared with a particle-free control ($p < 0.001$ and $p < 0.01$). When BAD dosage was increased to 14 or 25 µg/ml, the number of bacteria ingested by the macrophages was further reduced to 27.9 or 26.5% of the particle-free control ($p < 0.001$) **(Figure 4.7 A)**. SRM-2975 exposure induced a similar response with the 4 µg/ml treatment reducing *S.aureus* ingestion by 43.5% ($p < 0.001$) in comparison to the particle-free control and dosages of 8, 14 and 25 µg/ml reducing bacterial ingestion by 52.0, 64.1 and 67.8%, respectively ($p < 0.001$) **(Figure 4.7 B)**. Such observations indicate that exposure to BAD or SRM-2975 can inhibit bacterial phagocytosis in U937s. *S.aureus* growth curves, produced in the presence or absence of BAD or SRM 2975, confirmed that this result was not the product of direct bactericidal or bacteriostatic interactions between the particles and bacteria **(Figure 4.8)**.

Bacterial phagocytosis behaviour was quantified in the presence of desferroxamine to identify the contribution that the metallic portions of BAD and SRM-2975 had on inhibition of U937 bacterial phagocytosis behaviour. Ingestion of *S.aureus* was increased by 41.3 and 30.8% in U937s treated with 14 and 25 µg/ml BAD in the presence of desferroxamine when compared with those treated with the particles in the absence of the chelator. *S.aureus* uptake was also increased by 31.0, 24.8 and 14.8% in U937s treated with 8, 14 and 25 µg/ml SRM-2975 in the presence of desferroxamine when compared with that of U937s treated with the particles only **(Figure 4.7 C and D)**. This observation indicates that metal ions within the particles may be key inhibitors of phagocytic behaviour.

In addition to metals, particle-bound endotoxins and PAHs contribute to particulate toxicity (60,390). As such the impact that 24 h exposures to LPS (an endotoxin) or benzo[a]pyrene (an ambient PAH) had on the phagocytic activity of U937s was investigated. At a dosage of 1 μg/ml, benzo[a]pyrene did not significantly reduce the number of *S.aureus* that the U937s ingested, suggesting that PAH were unlikely to have contributed to the anti-phagocytic behaviours of the particles. In contrast, treatment with 1 μg/ml LPS significantly reduced the number of *S.aureus* that the U937s ingested (14.4% $p \leq 0.05$) indicating that surface-bound endotoxins may have contributed to the functional toxicity of BAD and SRM-2975.

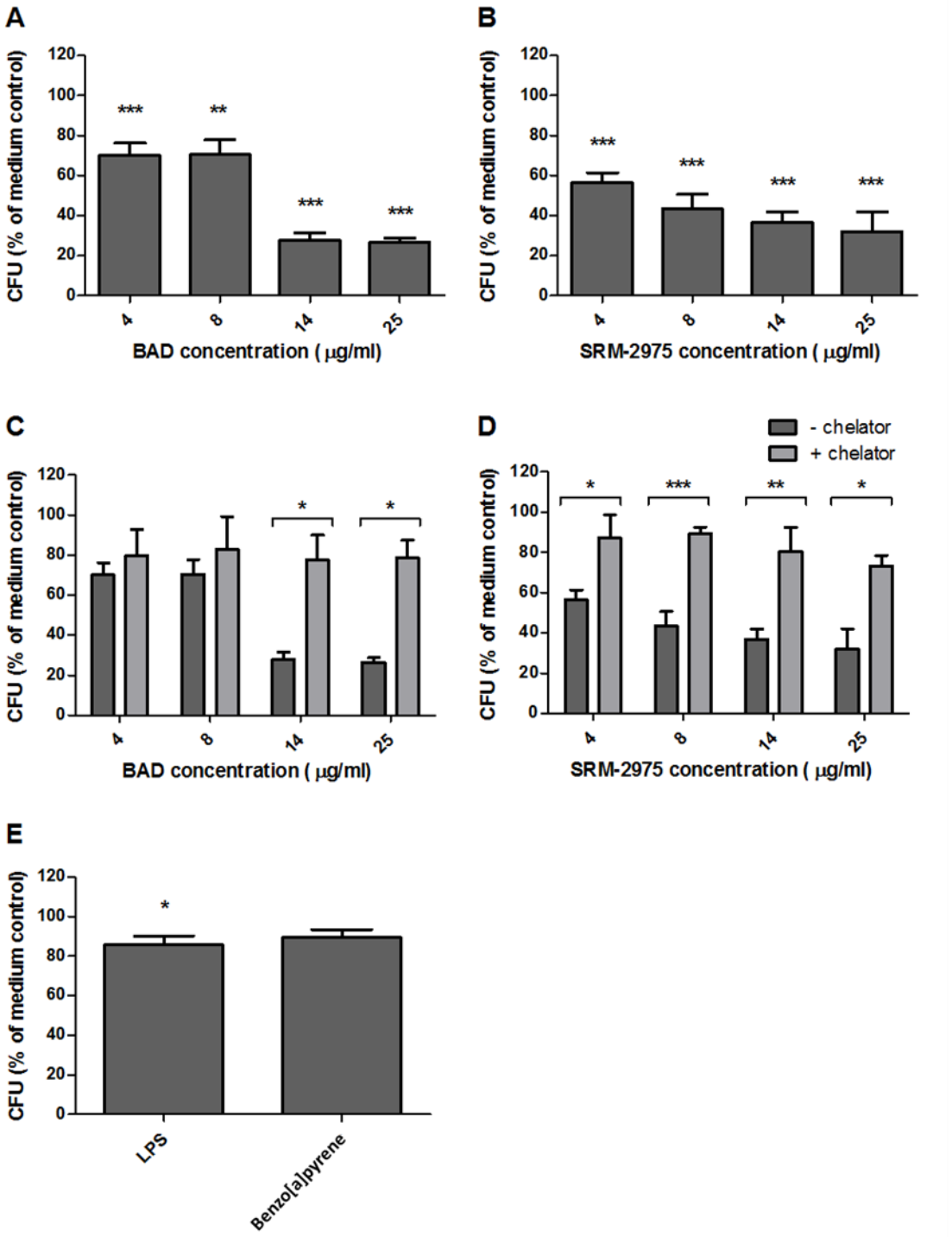


Figure 4. 7: **The influence of particles on phagocytosis behaviour.** Number of *S. aureus* ingested by U937s over a 2h period subsequent to 24h incubation with 4-25 µg/ml BAD (A) or SRM-2975 (B) ,4-25 µg/ml BAD (- chelator) or 4-25 µg/ml BAD spiked with 380 µM desferroxamine (+ chelator) (C) and 4-25 µg/ml SRM-2975 (- chelator), 4-25 µg/ml SRM-2975 spiked with 380 µM desferroxamine (+ chelator) (D) and 1 µg/ml LPS or benzo[a]pyrene (E). Values were normalised to concentrations of total cellular proteins, are presented as percentages of a particle-free control and represent the mean ± SEM of 4-6 biological repeats. Significant differences in CFU were identified between control and particle-treated cells using 1-way ANOVA tests with Bonferroni correction.

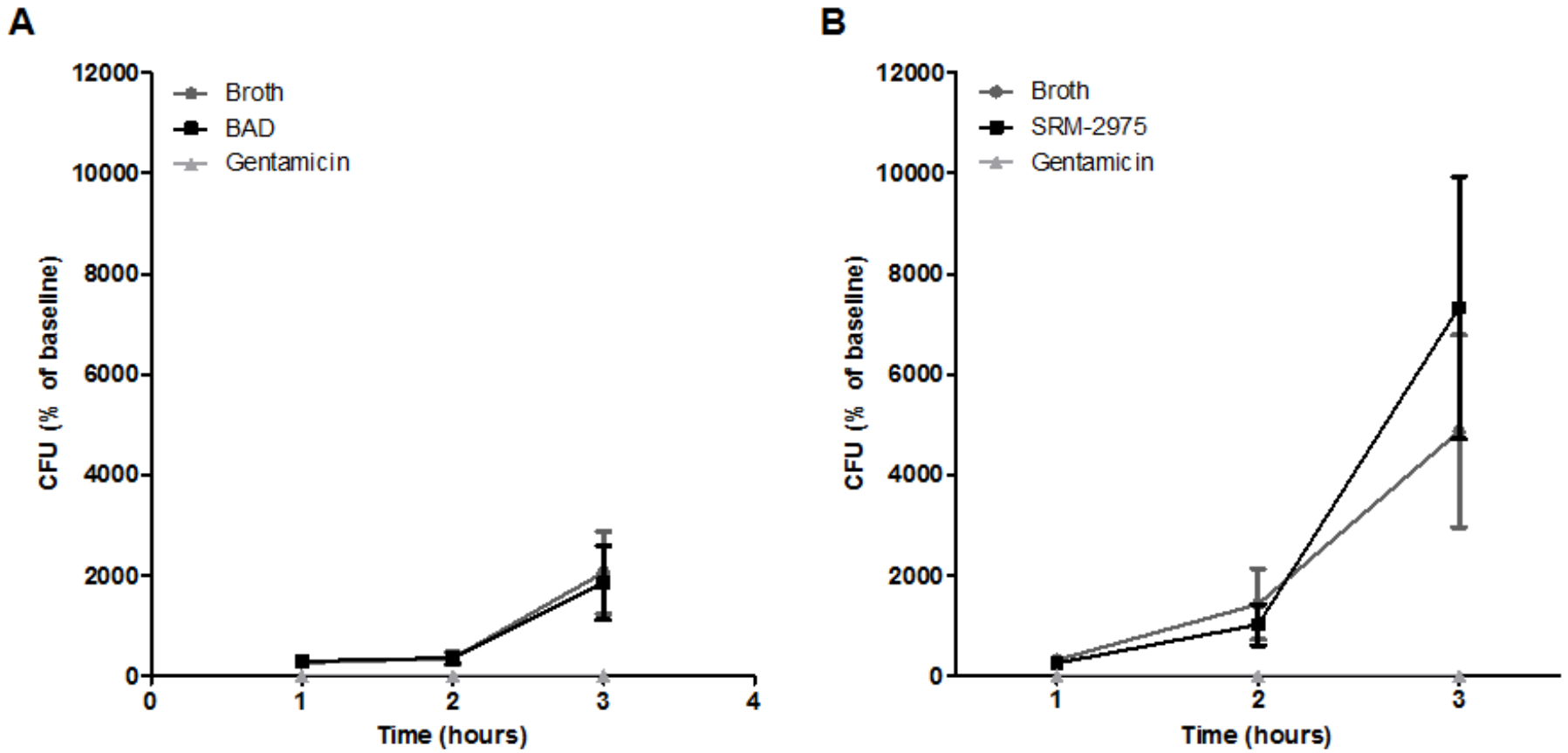


Figure 4. 8: Influence of particle exposure on bacterial growth. Number of *S.aureus* grown in the presence of 25 µg/ml BAD (A) or DEP (B) over a 3 h incubation period. Values are presented as percentages of a particle free control and represent the mean ± SEM of 4 biological repeats. Particle-induced differences in quantities of CFU were assessed at each time point using 2-way ANOVA tests with Bonferroni correction.

4.3.6: TRPM-induced up-regulation of miR-449a is detectable within U937 supernatants

Following the observations that serum concentrations of miR-34b and 449a are significantly enhanced under conditions of pulmonary inflammation (**Chapter 2**) and that BAD and DEP induce inflammatory responses in U937 macrophages (described above), it was hypothesised that the U937s would increase secretion of the miRNAs into their external environment following exposure to the particles. Following exposure to the particles (or to LPS as a positive control for inflammation), the hypothesis was tested through targeted quantification of miR-34b and 449 expression. Measurements were made firstly within macrophage lysates to establish cellular expression of the targets and secondly within the cellular supernatants to compare levels of target miRNA secretion with particle-free controls.

Prior to performance of the targeted quantifications, total RNA and miRNA concentrations were measured in the U937 lysates and supernatants using Nanodrop 2000 and Bioanalyzer 2100 technology. This aimed to clarify that the RNA isolation procedure had been successful and that miRNA exists within the supernatants of U937s. The analysis indicated that the RNA isolation procedure had been successful, with peaks visible at 260 nm on the Nanodrop spectra (representing total RNA) and between 20 and 40 nt on the Bioanalyzer spectra (representing miRNA) for both sample types (**Figure 4.9**).

The total RNA and total miRNA yields ranged between 40.4 -307.3 ng/ µl and 0.7 -5.5 ng/µl (respectively) for lysate samples (**Table 4.3**) and 8.4 -41.0 ng/µl and 1.2 -16.0 ng/µl for supernatants (**Table 4.4**). No significant differences in total RNA yield, miRNA yield or miRNA: total RNA ratios were detected between treatment groups (**Tables 4.3-4.4**), indicating that the exposures had no notable impact on RNA expression.

RTqPCR measurements detected miR-449a but not mir-34b in the lysates of U937s, suggesting that the latter is not expressed by this cell line even during an inflammatory response. In contrast, the U937 responses to BAD or DEP exposure were accompanied by

significant increases in miR-449a expression. Compared with control samples, exposure to 4 or 14 μg/ml BAD induced dose-dependent 1.4 ± 0.1 and 1.7 ± 0.3 fold increases in miR-449a expression ($p \leq 0.1$ for higher dose) while exposure to 4 or 14 μg/ml SRM-2975 induced 1.9 ± 0.1 and 2.0 ± 0.2 fold increases in expression of the miRNA ($p \leq 0.05$). These changes were statistically similar to the 1.6 ± 0.2 fold increase in miR-449a expression that was induced by the LPs positive control (**Figure 4.10 A-B**).

These patterns of expression translated into the supernatant samples with BAD exposure inducing 1.3 ± 0.2 and 2.1 ± 0.3 fold increases in extracellular miR-449a concentrations (for 4 and 14 μg/ml dosages respectively, $p \leq 0.05$) and SRM-2975 exposure increasing the concentrations from control level by 2.8 ± 0.7 and 2.7 ± 0.7 fold concentrations (for 4 and 14 μg/ml dosages respectively, $p \leq 0.05$). Once again, these increases were statistically similar to the 1.5 ± 0.2 fold increase in miR-449a expression that was induced by LPS exposure (**Figure 4.10 C-D**).

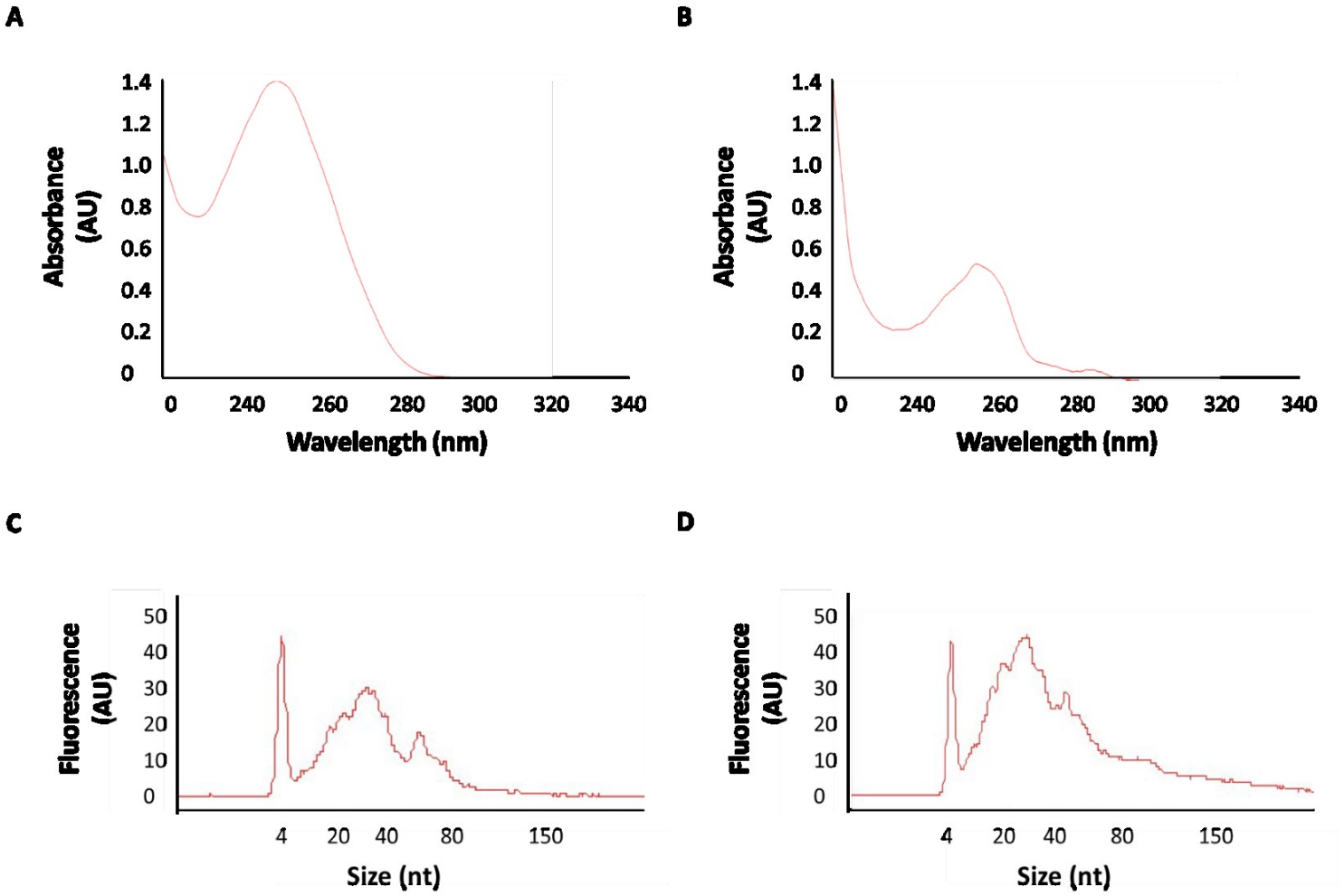


Figure 4. 9: RNA content of supernatant samples. Spectra display the quantities of total RNA (A, C) and total miRNA (B, D) detectable in representative samples of U937 lysates (A, B) and supernatants (C, D). Spectra were acquired using Nanodrop 2000 and Bioanalyzer 2100 (with Small RNA Kit) instruments respectively.

Table 4. 4: Average concentrations of total RNA and total miRNA detected in the lysates of U937s by nanodrop spectroscopy and Bioanalyzer small RNA assays. Values represent the mean ± SEM of six biological replicates.

Treatment group	Total RNA (ng/ µg)	Total miRNA (ng/ µg)	Total miRNA: Total RNA
Control	117.80 ± 34.46	2.02 ± 0.60	0.02
LPS	132.27 ± 25.22	3.66 ± 1.18	0.03
4 µg/ ml BAD	107.83 ± 56.87	2.40 ± 1.24	0.02
14 µg/ ml BAD	130.70 ± 46.85	2.47 ± 1.10	0.02
4 µg/ ml SRM-2975	180.80 ± 66.3	2.61 ± 1.36	0.01
14 µg/ ml SRM-2975	163.67 ± 41.22	3.26 ± 1.02	0.02

Table 4. 5: Concentrations of total RNA and total miRNA detected in the supernatants of U937s by Nanodrop spectroscopy and Bioanalyzer small RNA assays. Values represent the mean ± SEM of six biological replicates.

Treatment group	Total RNA (ng/ µg)	Total miRNA (ng/ µg)	Total miRNA: Total RNA
Control	15.88 ± 6.21	5.12 ± 1.65	0.33
LPS	15.95 ± 1.50	6.611 ± 2.80	0.30
4 µg/ ml BAD	16.4 ± 1.66	3.63 ± 1.12	0.22
14 µg/ ml BAD	19.97 ± 2.04	3.94 ± 0.86	0.21
4 µg/ ml SRM-2975	14.78 ± 0.62	3.21 ± 1.18	0.21
14 µg/ ml SRM-2975	15.80 ± 3.50	4.13 ± 3.23	0.26

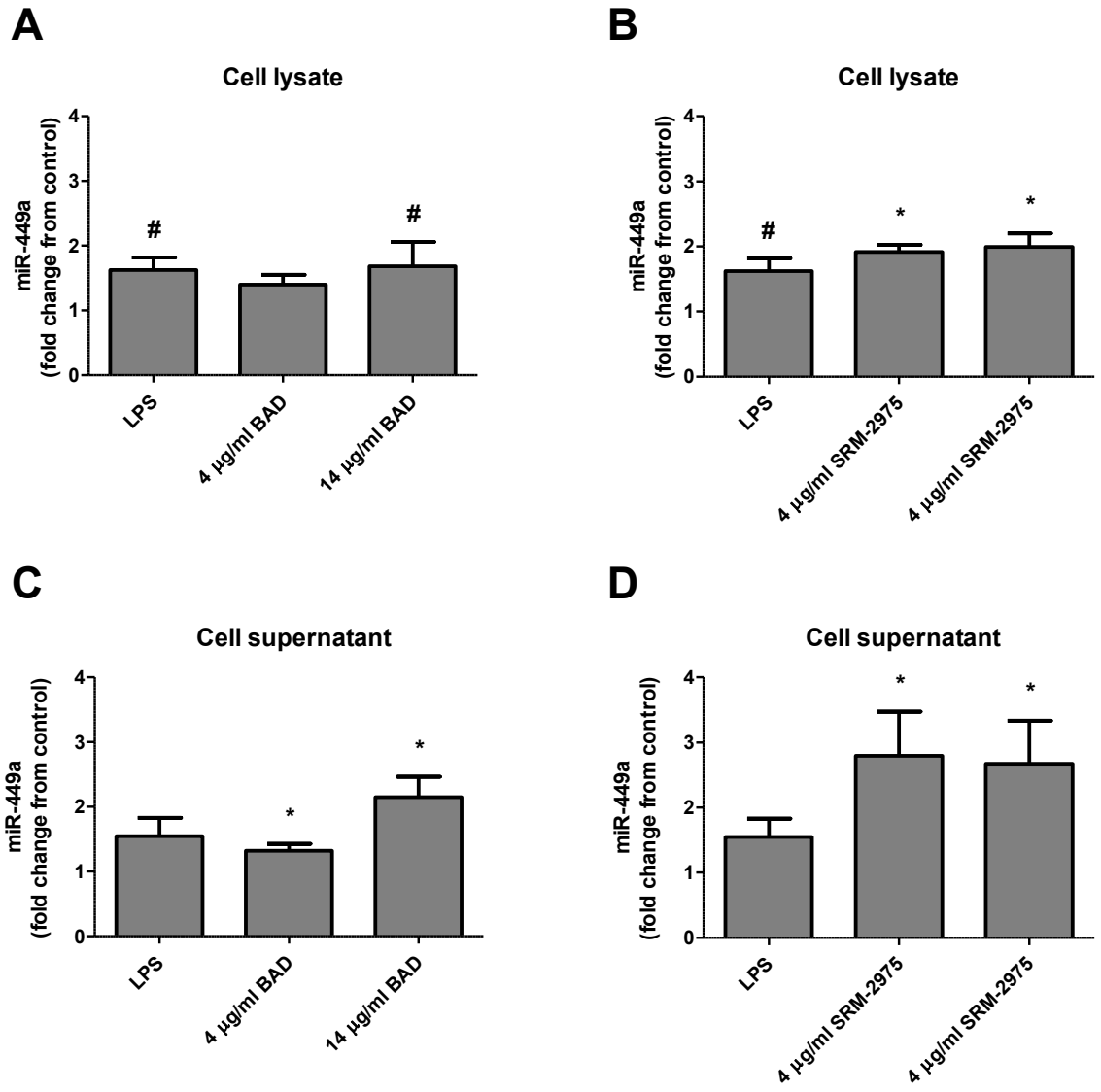


Figure 4. 10: Fold increases in miR- 449a concentrations in the cellular lysates (A,B) and supernatants of U937s following 24h exposures to 1 µg/ml LPS 04 4-14 µg/ml BAD or SRM-2975 (compared with that of cells exposed to particle free media). Data were acquired by RTqPCR, normalised to exogenous cel-miR-39 concentrations and analysed using the 2-(ΔΔ CT) method. Values represent the mean ± SEM of 3-6 biological replicates, obtained from 3 technical replicates for each. Significant differences were detected between treatment groups using Student's t- tests, # p≤ 0.1 * p ≤ 0.05.

4.3.7: U937 metabolic profiles are altered in response to pro-inflammatory stimuli

Metabolic profiling by ^{1}H NMR was performed using the supernatants of particle challenged U937s. The analysis aimed to identify metabolic pathways that were altered during BAD and SRM-2975 induced toxicity and to find metabolite markers for them. By including LPS exposures in the model, it also sought to determine whether these markers were specific to particle – induced inflammatory responses or whether they are relevant to inflammatory responses in general.

Interrogation of spectral data from CPMG experiments confirmed the presence of 29 readily annotatable metabolites in the media (**Figure 4.11**). The spectral data was compared between treatment groups to identify significant changes in metabolite concentrations. Rather than employing the multivariate techniques used in **Chapter 3**, data were interrogated using univariate statistics to minimise influence from the high intrinsic variance between values that existed within the treatment groups (potentially due to the usage of fresh bottles of media for each experimental repeat).

Following exposure to 1 μg/ml LPS, the metabolic profiles of U937 were characterised by a generalised decrease in metabolite uptake from the media (represented by concentrations that increased after treatment but remained lower than the values for cell-free media). Extracellular concentrations of *p*-aminobenzoate, succinate, valine, citrate, glucose, glutamine and isoleucine were 59, 61, 58, 58, 49, 50 and 50% greater than for control samples (respectively) ($p \leq 0.05$-0.01).

Accumulation or secretion of metabolites into the media was also influenced by LPS exposure (represented by concentrations greater than the cell-free medium baseline). Extracellular concentrations of cystine and arginine increased by 272 and 27% ($p \leq 0.05$) while extracellular pyruvate concentrations decreased by 37% when compared with controls (but remained above baseline) ($p \leq 0.01$). Finally, extracellular concentrations of leucine

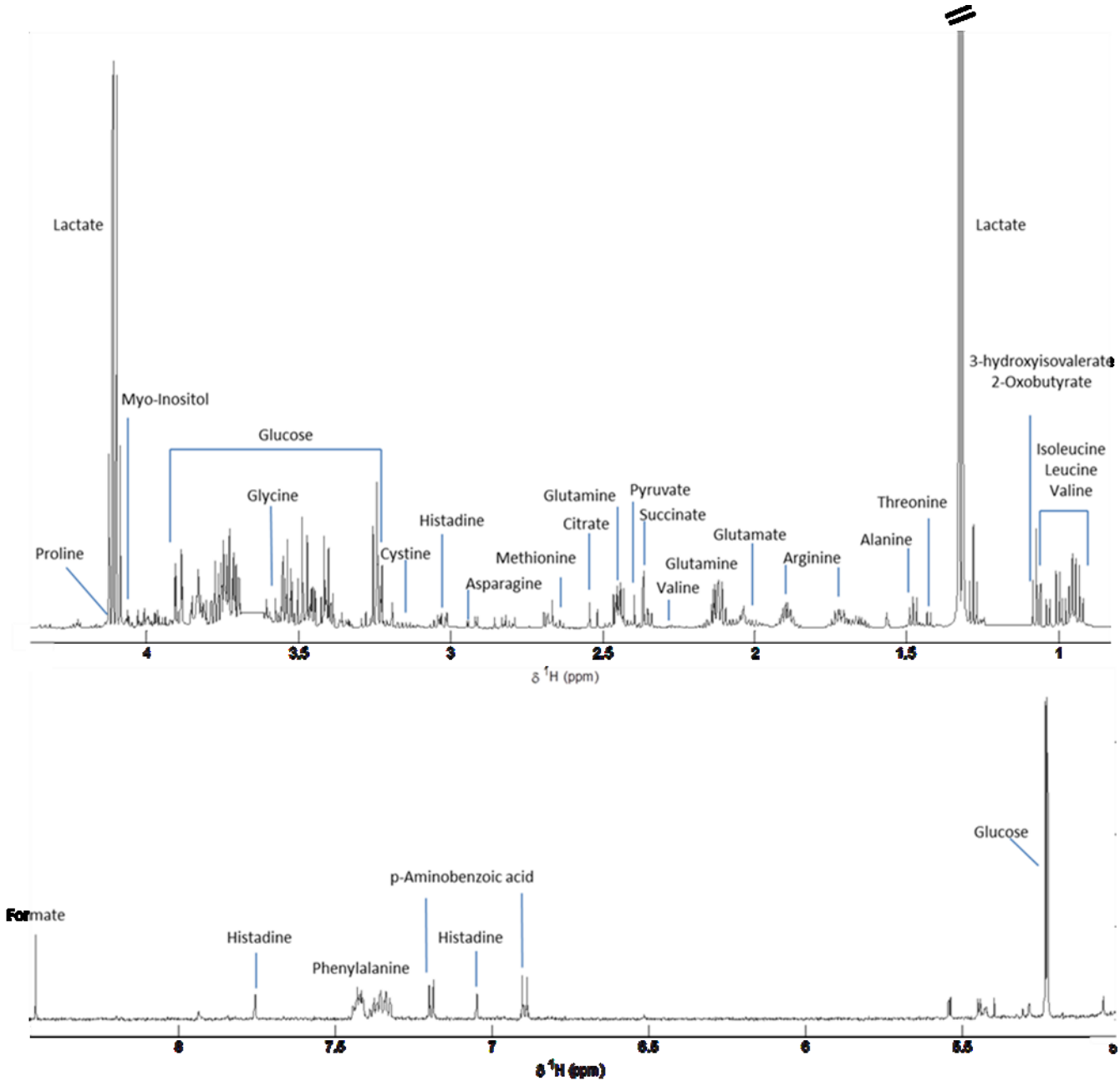


Figure 4.1 1: Exemplar ^{1}H NMR spectra generated from the supernatants of U937 macrophages cultured in RPMI 1640 medium. Chemical shift regions containing resonances of residual water (4.40-5.00 ppm) and ethanol contaminant (1.10-1.24 and 3.61-3.68 ppm) have been removed.

increased by 190% (compared with control) ($p \leq 0.05$) , increasing from values below the cell-free medium baseline to values above the baseline. This suggests that uptake of the metabolite was impaired or that net efflux occurred.

In similarity to the media of LPS treated cells, decreased uptake of *p*-aminobenzoate, valine and isoleucine, and increased accumulation or secretion of of cystine, arginine and leucine were detected in the media of cells that were exposed to BAD (in comparison to control). Differences of 44, 47, 35, 328, 52 and 58% were detected for these metabolites (respectively) following exposure to the low dose (4 µg/ml) ($p \leq 0.05$-0.01) and differences of 55, 57, 38, 321, 80 and 58 % were detected following exposure to the larger dose (14 µg/ml) ($p \leq 0.05$-0.01). A 34 % decrease in extracellular citrate uptake was also detected following exposure to 14 µg/ml BAD ($p \leq 0.05$).

In contrast to LPS treatment, exposure to BAD induced increases in the extracellular accumulation or secretion of histidine, asparagine and threonine (46, 41 and 31 % respectively for 4 µg/ml exposure and 38, 49 and 23 % for 14 µg/ml exposures) ($p \leq 0.05$-0.01), decreased uptake of lactate (38 and 48% for 4 and 14 µg/ml dosages, $p \leq 0.05$) and enhanced uptake of *myo*-inositol by 50% at the 14 µg/ml dose ($p \leq 0.05$).

DEP induced similar changes to the U937 extracellular metabolome when compared with BAD. Compared with control samples, uptake of p-aminobenzoate and citrate decreased by 70 and 79% following low DEP exposures (4 µg/ml, $p \leq 0.05$) and 51 and 68 % after higher exposure (14 µg/ml, $p \leq 0.05$). As for BAD exposure, uptake of *myo*-inositol increased by 202 and 222% following exposures to the low and higher doses (ns and $p \leq 0.05$) and accumulation or secretion of cystine, arginine, histidine, threonine, asparagine and leucine increased by 531, 207, 164, 149, 166 and 139 % for 4 µg/ml exposures ($p \leq 0.05$- 0.01) and 550, 214, 149, 155, 159 and 282% for 14 µg/ml exposures ($p \leq 0.05$- 0.01).

Unlike responses to BAD exposure but consistant with the response to LPS, glucose uptake was decreased by 66% and 68% following 4 and 14 µg/ml DEP exposures ($p \leq 0.05$).

Uptake of glutamate was also increased (by 131 and 162%) for 4 and 14 μg/ml exposures ($p \leq 0.05$, ns) but this response was specific to DEP exposure (**Figure 4.12)**.

4.3.8: Inflammatory stimuli induce alterations in common metabolic pathways in U937 macrophages

Using the features derived from the ^{1}H NMR analysis, pathways that the BAD, DEP and LPS- associated metabolic features may represent were explored by over-representation analysis using the web tool IMPaLA. Interrogation of the output (displayed in **Supplementary tables 4.1-4.3**) showed that all three inflammatory stimuli could have altered the activity of common gene expression, inflammation/immunity, oxidative stress, general metabolism and molecular transport pathways (**Table 4. 6**), indicating that they are common to inflammatory responses, independent of the stimulus .

In contrast, stimulus dependent associations were observed for amino acid, nitrogen and energy metabolism pathways and cellular signalling events. Focusing on pathways of amino acid metabolism, changes in amino acid interconversion, cysteine and methionine metabolism, *S*-methyl-5-thio-α-D-ribose 1-phosphate activity and branched chain amino acid metabolism pathway activities associated with all three stimuli but asparagine and histidine metabolism associated with DEP exposure specifically and threonine metabolism was shown to be altered by particles only.

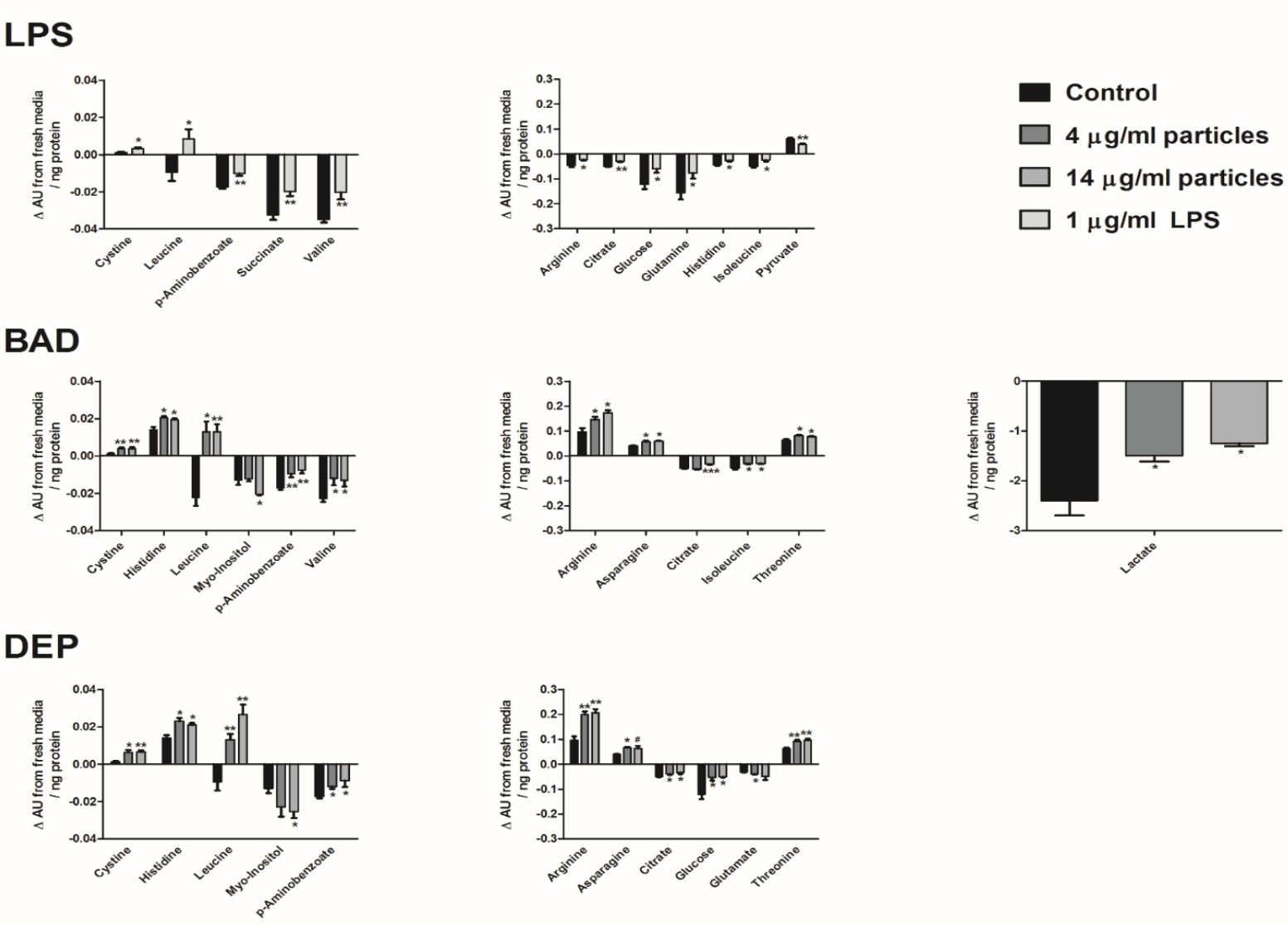


Figure 4.1 2: Quantities of feature metabolites detected within the supernatant of U937 macrophages following 24 h incubations with media control, 1 μg/ml LPS or 4- 14 μg/ml BAD or SRM-2975. Measurements were made using ^{1}H NMR spectroscopy with values normalised to total cellular protein content and presented as a percentage of a cell-free medium control. Error bars represent SEM of 4-6 biological repeats. Significant differences between treatment groups were detected using 1 Way ANOVA tests with Bonferroni correction. *p ≤ 0.05, ** p ≤ 0.01.

In the context of energy metabolism, all three stimuli associated with alterations in glutaminolysis, glycolysis and gluconeogenesis but LPS exposure alone was linked with the citric acid and Cori cycles.

In contrast, LPS exposure was excluded from associations with nitrogen metabolism pathways, with ammonia recycling associating with both BAD and DEP and biogenic amine synthesis associating with DEP only (**Table 4. 6**). Together these observations indicate that inflammatory responses may be contributed to by a combination of composition dependent and composition independent metabolic changes.

4.3.9: miR-34b/449a activity may influence inflammatory responses to particle exposure in U937 cells

Continuing with the rationale that integration of multiple molecular profiles enhances the mechanistic strength of biomarkers, integrative over-representation analyses were performed to determine whether miR-449a activity could have influenced activity of the metabolic pathways that associated with inflammatory exposures. As with the serum based analysis in **Chapter 3**, lists of predicted gene targets for miR-449a were input into IMPaLA alongside lists of feature metabolites for each exposure. The webtool searched a bank of curated pathways for those that displayed statistically significant ($p<0.05$) enrichment for both the ^{1}H NMR-derived metabolite features and gene targets of miR-34b/449a.

Comparison of the output of this integrated approach (**Supplementary tables 4.4- 4.6)** with the output of the metabolite-only analysis identified numerous common results. These included associations with molecular transport mechanisms, gene expression and amino acid metabolism for all exposures and mechanisms of nitrogen metabolism for the particle exposures. In addition, several differences were identifiable between the outputs. Of these, most notable were the inclusion of lipid metabolism pathways in responses to each stimulus

and the exclusion of oxidative stress and general metabolism pathways in the output for the integrated analysis (**Table 4.6- 4.7**).

In addition to those identified in the metabolite only analysis (5'-adenosine monophosphate-activated protein kinase (AMPK), FOXO and hypoxia-inducible factor-1 (HIF-1)), an additional five cellular signalling pathways were associated with LPS or DEP exposure following the integrated analysis. Furthermore, with the inclusion of transcriptomic information, the AMPK, FOXO and HIF-1 signalling pathways met the criteria for association with responses to all three stimuli, rather than single stimuli as previously indicated. Surprisingly, DEP exposure alone was associated with cytokine and interleukin signalling in this analysis.

In terms of energy metabolism, the addition of transcriptomic data expanded associations between exposure and the citric acid cycle, conversion of glucose to acetyl-CoA and the Cori cycle to include BAD or both particle types as stimuli. Adding to the associations that existed between all three exposures and glucose and glutamine metabolism, incorporation of the miRNA target genes indicated that the process of carbohydrate metabolism may be regulated by carbohydrate-responsive element-binding protein (ChREBP) activity (**Table 4.7**). Together these data indicate that miR-449a activity had the potential to influence the concentrations of feature metabolite usage or production in U937s following LPS or particle exposure.

Table 4. 6: Metabolic pathways enriched in the media samples of U937s following particle or endotoxin exposure. ORA was performed by entering metabolite features (detected by univariate analysis of ^{1}H NMR data) into IMPALA.

Pathway type	Pathway	LPS	BAD	DEP
Amino acid metabolism	Amino acid interconversion	✓	✓	✓
	Asparagine metabolism			✓
	Threonine metabolism		✓	✓
	Histidine metabolism			✓
	Cysteine and methionine metabolism	✓	✓	✓
	S-methyl-5-thio-α-D-ribose 1-phosphate activity	✓	✓	✓
	Valine, leucine and isoleucine biosynthesis	✓	✓	✓
	Valine, leucine and isoleucine catabolism	✓	✓	✓
Cellular signalling	AMPK signalling pathway	✓		
	FOXO signalling pathway			✓
	HIF-1 signalling pathway	✓		
Energy metabolism	Central carbon metabolism	✓	✓	✓
	Glycolysis and gluconeogenesis	✓	✓	✓
	Conversion of glucose to acetyl CoA	✓		
	Triosephosphate isomerase	✓		
	Cori Cycle	✓		
	TCA cycle and pyruvate metabolism	✓		
	Glutaminolysis	✓	✓	✓
Gene expression	Gene expression	✓	✓	✓
	tRNA aminoacylation	✓	✓	✓
Inflammation and immunity	Class I MHC mediated antigen processing & presentation	✓	✓	✓
	Leukotriene biosynthesis	✓	✓	✓
Oxidative stress	γ-glutamyl cycle	✓	✓	✓
Metabolism	Biochemical pathways part I	✓	✓	✓
	Phase II conjugation	✓	✓	✓
Molecular transport	ABC transporters	✓	✓	✓
	SLC-mediated transmembrane transport	✓	✓	✓
	Transmembrane transport of small molecules	✓	✓	✓
Nitrogen metabolism	Ammonia recycling		✓	✓
	Biogenic amine synthesis			✓

Table 4. 7: Cellular pathways that were enriched for exposure-associated feature metabolites and predicted mRNA targets of miR-449a. ORA was performed by entering metabolite features (detected by univariate analysis of ^{1}H NMR data) and predicted miR-449a targets (identified using the MirWalk database) into IMPALA.

Pathway type	Pathway	LPS	BAD	DEP
Amino acid metabolism	Amino acid interconversion	✓	✓	✓
	Alanine, aspartate and glutamate metabolism	✓	✓	✓
	Cysteine and methionine metabolism	✓	✓	✓
	Threonine metabolism			✓
	Histidine metabolism		✓	✓
	Lysine degradation	✓	✓	
	Valine, leucine and isoleucine biosynthesis	✓	✓	✓
	Valine, leucine and isoleucine degradation	✓	✓	✓
Cell signalling	AMPK signalling pathway	✓	✓	✓
	cAMP signalling pathway	✓	✓	
	FOXO signalling pathway	✓	✓	✓
	HIF-1 signalling pathway	✓	✓	✓
	IGF1R signalling cascade	✓	✓	✓
	Phospholipase D signalling pathway			✓
	SREBP signalling	✓	✓	✓
	TP53 regulates metabolic genes			✓
Energy metabolism	Central carbon metabolism	✓	✓	✓
	ChREBP regulation	✓	✓	✓
	Cori cycle	✓	✓	✓
	Glutaminolysis	✓	✓	✓
	Glycolysis and gluconeogenesis	✓	✓	✓
	Conversion of glucose to acetyl CoA	✓	✓	
	TCA cycle and pyruvate metabolism	✓	✓	
Gene expression	Gene expression	✓	✓	
	tRNA aminoacetylation	✓	✓	✓
Inflammation and immunity	Cytokine signalling in immune system			✓
	Signalling by interleukins			✓
Lipid metabolism	Fatty acid, triacylglycerol and ketone metabolism	✓	✓	✓
	Glycerophospholipid metabolism		✓	✓
	Import of palmitoyl-CoA into the mitochondrion	✓	✓	
	Metabolism of lipids and lipoproteins	✓	✓	✓
	Triosephosphate isomerase	✓	✓	✓
Molecular transport	ABC transporters	✓	✓	✓
	SLC-mediated transmembrane transport	✓	✓	✓
	Transmembrane transport of small molecules	✓	✓	✓
Nitrogen metabolism	Ammonia recycling		✓	✓
	Urea cycle	✓	✓	✓

4.4: Results summary

- Despite possessing considerable differences in metal ion content, BAD and DEP both caused significant reduction of antioxidant species in cell-free systems
- Neither particle reduced U937 viability but both induced an inflammatory response whilst reducing mitochondrial membrane integrity and phagocytic capacity
- Alterations in cytokine secretion and bacterial phagocytosis activity occurred in a metal dependent manner
- Both particles induced increases in the expression and release of miR-449a by U937s
- Stimulus independent and particle-specific changes were detectable in the extracellular metabolome following exposure to BAD, DEP or LPS but alterations to the metabolome could not be distinguished between particle species.
- Based upon *in silico* predictions of miRNA-mRNA pairings, integrated ORA indicated that miR-449a dysregulation could have contributed to alterations in molecular transport, amino acid metabolism and nitrogen metabolism.
- Compared with single-omics ORA, integrative analysis of metabolomics and transcriptomic datasets identified additional putative associations between particle exposure and dysregulation of cell signalling and energy metabolism pathways.

4.5: Discussion

With the aims of identifying mechanistically relevant biomarkers of non-exhaust PM induced pulmonary toxicity and comparing them with those produced by exhaust PM exposure, this study characterised and compared the impacts that BAD and DEP (major contributors to urban TRPM) exerted upon the health and function of U937 human macrophages. Despite the two particles being physicochemically distinct, integration of hypothesis driven toxicological approaches with hypothesis-generating metabolomics analysis and miRNA quantifications demonstrated that their toxicological signatures were strongly comparable at both functional and molecular levels. This indicates that common metabolite and miRNA markers could be used to detect macrophage responses to both types of exposure.

Targeted cytokine quantifications confirmed the appropriateness of the U937 exposure model as a source of biomarkers for TRPM-induced inflammatory mechanisms. Both particles were found to induce secretion of pro-inflammatory IL-8 (a neutrophil chemoattractant (391)) and TNF-α (an orchestrator of pro-inflammatory cascades (392)) at concentrations as low as 4 μg/ml. They also induced secretion of pro-resolving (393) IL-10 at higher doses (14 μg/ml for BAD and 25 μg/ml for DEP). Enhanced secretion of these cytokines is commonly considered representative of pulmonary inflammation (394), and the results agree with previous observations that DEP induces IL-8 and TNF-α in macrophages and epithelial cells (395,396) and that BAD enhances IL-8 secretion in A549 cell lines (371)

In agreement with these increases in typical inflammatory markers, miR-449a expression was found to be significantly enhanced by the U937s following exposures to 4 or 14 μg/ml BAD or DEP, echoing the response to LPS treatment and findings of **Chapter 2**. This outcome is novel in relation to particle toxicology but is not surprising given that both DEP and metallic PM have been shown to impact broadly on the expression of inflammation-associated miRNAs in human airway cells and monocytes (104,397).

Importantly this indicates that the associations that this project has found between miR-449 and pulmonary inflammation appear to be translatable to the context of TRPM exposure, meaning that the potential for miR-449a to be used as a biomarker of pulmonary inflammatory responses may extend to those responses induced by TRPM. More importantly, the fact that increased concentrations of miR-449 were detectable extracellularly, indicates that the marker could be used to detect the responses in accessible samples.

It may be argued that miR-449 lacks value as a biomarker because it does not distinguish between responses to exhaust and non-exhaust particles or TRPM and canonical inflammatory pathways. However, due to advances in our understanding of miRNA activity, it does offer the novel suggestion that common mechanisms underlie responses to BAD, DEP and LPS at the level of post-transcriptional regulation. Furthermore, real world exposures to TRPM refer to the inhalation of particle mixtures (including endotoxins) (6), meaning that markers that respond in the same manner to multiple components of the mixtures could give more accurate representations of the response. This may be particularly relevant given that airborne pollutants are thought to influence pulmonary health in a synergistic manner (398,399).

In contrast to the observations for miR-449a, miR-34b was not expressed by the macrophages under any experimental condition. As miR-34b was found to contribute to the circulating microtranscriptome under inflammatory conditions in the rat (**Chapter 3**) and is over-expressed in alveolar type II cells in idiopathic pulmonary fibrosis patients (400), this may suggest that alternative cell types (such as pneumocytes or neutrophils) express the miRNA *in vivo* and that the association with TRPM should be explored in these cellular systems as well . Alternatively, the phenomenon may be an artefact of the cell culture process that can be avoided upon development of *in vivo* exposure models. Such an idea is supported by observations that 33% of miRNAs (including miR-34b) were differentially

expressed between primary bronchial epithelial cells that were cultured prior to RNA harvest and those that underwent RNA isolation immediately after collection (401).

An overlying theme of this work has been to identify biomarkers that expand our current understanding of inflammatory mechanisms. As such, toxic signatures additional but complimentary to the inflammatory response were characterised in the U937s following particle exposures. High-throughput fluorescence imaging assays indicated that both particles significantly reduced mitochondrial membrane integrity in a dose-dependent manner. Such activity has previously been attributed to the ultrafine components of PM crossing the mitochondrial membrane and releasing redox cycling agents within the organelle (402).

This type of mitochondrial damage often triggers apoptotic or necrotic pathways, disrupting ATP synthesis, releasing caspases and disrupting redox potential (403). Activity of these pathways is recognised through the characteristic swelling or shrinking of cells and through condensation of their nuclei but neither BAD nor DEP induced such changes in this study. Neither did they have a significant impact on the viability of U937 cultures as determined by mitochondrial oxidoreductase activity.

While PM has been shown to induce cell death in pulmonary cells, previous studies have used unrealistically high exposure doses (404,405) meaning that their results are unlikely to reflect *in vivo* responses as accurately as the lower dose range that was used in this study. In fact, the observation that the U937s triggered protective cytokine secretion rather than cell death in the face of mitochondrial damage indicates a strong advantage of the model. TRPM is hypothesised to induce protective anti-oxidant and inflammatory responses (51) and do not cause disability in all that are exposed, suggesting that biomarkers for the responses should be sought from models that can include adapted or reparative pathways.

Loss of function is a key component of cellular toxicity and fine and ultrafine ambient PM, metallic nanoparticles and DEP have all been shown to reduce the capacity for

macrophages to phagocytose respiratory pathogens (95,379–382). Likewise, BAD and SRM-2975 significantly impaired the ability of U937s to ingest the respiratory pathogen *S. aureus*, reducing bacterial uptake by up to 73 and 68% respectively.

Following a similar observation, Zhou *et al* (2007) demonstrated that the metallic portions of their PM impaired phagocytosis by exerting oxidative damage on proteins required during internalisation of target material (381). As the BAD and DEP that were used in this study were at least partially metallic and significantly depleted AA and GSH concentrations under acellular conditions, it is possible that their effect on U937 phagocytosis could be driven by metal-induced oxidative damage. Such a notion is supported by the fact that LPS and PAHs (found in both particle types) had minimal impact on *S. aureus* uptake but metal ion chelators restored phagocytic capacity to control level.

Metabolite biomarkers represent changes in the activity of the pathways for which they are substrates, products or intermediates (168), making them a valuable tool for exploring the mechanisms that underlie the extra-inflammatory toxicity of BAD and DEP exposure. Reflecting the commonality in effect that was seen for the particles at the levels of function and health, BAD and DEP exposure induced highly similar changes in the U937 metabolome.

While this indicates that ^{1}H NMR based metabolomic approaches do not distinguish between responses to BAD and DEP, several of the changes (increased extracellular threonine, histidine, asparagine and arginine concentrations and enhanced *myo*-inositol uptake) were not induced by LPS exposure, indicating that they were specific to PM exposure. Extrapolating further, it may be that these differences were induced by the metallic components of the particles. In addition to the evidence that metal ions drove similar alterations in cytokine secretion and phagocytic function after BAD or DEP exposure here, Oeder *et al* (2015) demonstrated clear differences in the metabolic pathways that were

impacted by metallic and non-metallic shipping exhaust exposures in airway epithelial cells (100).

Preliminary inspection of the metabolic features and the pathways for which they were enriched identified several potential associations with the observed toxicity signatures of particle exposure. For example, *myo*-inositol (an isomer of glucose and constituent of the phosphatidylinositol second messenger system (406)) has been shown to enhance phagocytic function in macrophages by promoting bacterial attraction and adhesion via depolarisation of the cellular membrane (407). It also decreases intracellularly following exposure to ZnO particles in AT1 cells (408), (which are a known inhibitor of phagocytosis in monocytes (409)) but not in response to gold nanoparticle exposure (which do not inhibit bacterial uptake (410)) in the same cell line (408). In the current study, uptake of *myo*-inositol from the culture medium was enhanced in response to particle exposure, possibly representing a protective or compensatory mechanism of phagocytic function retrieval. Supporting this suggestion, Kim *et al* (2005) suggest that a sustained supply of *myo*-inositol is required for the synthesis of membrane phospholipids in mammalian cells (406); a process that increases linearly following phagocytosis of particles (411). Furthermore, the current work found that extracellular concentrations of *myo*-inositol remained comparable to that of control cells following exposure to LPS (a treatment that had minimal impact on phagocytic capacity).

Another major example is that of altered mitochondrial pathways. Over-representation analysis indicated that the majority of the particle-influenced metabolite features contribute to pathways of branched chain amino acid (BCAA), glucose and fatty acid degradation or to glutaminolysis- all of which take place within the mitochondria or provide substrates for mitochondrial metabolism. These changes in BCAA metabolism have not been reported previously in the context of PM exposure but enrichment of culture media with BCAAs has been shown to promote phagocytosis in microglial cells (412). As BAD exposure decreased

isoleucine and valine uptake and both particles caused extracellular accumulations of leucine, it may be that reductions in mitochondrial BCAA metabolism contributed to impairment of phagocytic function in this model.

In contrast, several studies have associated PM exposure with alterations in energy metabolism. Oeder *et al.* (2015), determined that DEP reduce rates of glycolysis and citric acid cycle activity in airway epithelial cells (100) while Brower *et al.* (2016) associated biodiesel PM exposure with markers of decreased ATP synthesis in mouse serum (99). These changes in energy metabolism are unsurprising given that inflammatory stimuli promote reconfigurations of metabolic activity in macrophages, enabling energy-dependent antimicrobial processes such as cytokine synthesis and secretion (as seen for both particles) to be performed (413).

Less apparent is whether particle-induced mitochondrial dysfunction was the cause of changes in metabolic activity or the result of it. Although the relationship between mitochondrial dysfunction and BCAA metabolism has been explored in microglial phagocytes, results have been inconsistent. One study found that culture in BCAA-enriched media drove mitochondrial depolarisation (412), while others reported that BCAAs had no impact on mitochondrial activity (414), suggesting that the change in BCAA metabolism that was observed in this study could be a result of mitochondrial dysfunction. Similarly, mitochondrial membrane potential is maintained in the presence of products from oxidation pathways such as the citric acid cycle and β-oxidation of fatty acids (415,416) but these themselves take place within the mitochondria and will alter in concentration during adverse responses to mitotoxic stimuli.

Upon incorporation of miR-449a gene targets, output for the over-representation analysis showed a high degree of consistency with that of the metabolite-only analysis. Supported by knowledge that miRNAs can target several hundred genes within a single cell (117), this

indicated that heightened miR-449a activity contributed to the regulation of a great number of the observed metabolic responses. In line with the aim of enhancing characterisations of PM-induced inflammatory mechanisms, the integrated analysis also formed a number of associations between the exposures and pathways or processes that had not been detected in the metabolite-only analysis.

Several of these processes (including cytokine signalling and lipid metabolism) are already known to associate with PM-induced inflammation (94) but others have the potential to enhance our current understanding of TRPM-induced toxicity. When considered in combination with results from the targeted toxicological assays they enable novel links to be explored between features of the U937 responses to PM exposure, highlighting the benefits of integrating biomarkers that are collected via multiple approaches. As an example, AMPK signalling may be a means by which mitochondrial dysfunction contributed to increases in IL-10 expression in this model. This pathway (highlighted by the integrated over-representation analysis) is activated in the absence of ATP (417) (as may be expected in macrophages following loss of mitochondrial membrane potential (418)) and is shown to drive secretion of IL-10 (419) (enhanced by BAD and DEP exposure) and promote its pro-resolving p13K/Akt and STAT3-mediated activities (417). Similarly, changes in SREBP activity may associate with particle-induced impairment of bacterial phagocytosis given that SREBP-mediated lipogenesis is enhanced during phagocytosis (to compensate for donation of membrane segments to phagosomes) (420) and lipid metabolism pathways were altered following both types of particle exposure.

4.6: Conclusion

This body of work determined that exhaust and non-exhaust markers induce common mechanisms of toxicity in macrophages at both the functional and molecular levels and that these mechanisms are represented by changes in miR-449a (a marker of pulmonary inflammation) expression and the extracellular metabolome.

Integration of metabolomic profiling with predicted targets of miR-449a identified a number of cellular pathways and processes that have not previously been associated with TRPM exposure, promoting the suggestion that multi-omics analyses are mechanistically useful and meeting the aim of identifying biomarkers that further our knowledge of how TRPM propagates inflammatory responses in pulmonary cells.

Most importantly, the study identified that TRPM- associated biomarkers (including over-expression of miR-449a) are detectable extracellularly, indicating their candidacy as biomarkers for adverse responses to pollutants in human or animal models. If translatable to human biofluids, such a tool would be of great use for monitoring responses to exposure in high risk populations.

Chapter 5: General discussion, conclusions and possible future directions

5.1: Summary of findings

This work sought to address the hypothesis that **mechanistically relevant miRNA and metabolite biomarkers are detectable during pulmonary responses to TRPM exposure.** The over-arching aims of the project were **to identify mechanistically relevant and non-invasively accessible biomarkers for pulmonary inflammation** and to **determine whether those biomarkers could be used to explore the adverse effects of TRPM exposure.**

To achieve these aims and evaluate the hypothesis, a combination of microtranscriptomic and traditional toxicological approaches identified members of the miR-34/449 gene family as tissue markers for pulmonary inflammatory activity and observed translation of their signature into serum samples. Integration of metabolomic approaches into the workflow identified complimentary changes to the serum metabolome and determined that both the miRNA and metabolite signatures were relevant to exhaust and non- exhaust PM exposure *in vitro* (**Figure 5.1**).

5.1.1: Inflammation -associated miR-34b/449a over-expression signatures translate from pulmonary tissue to serum and from macrophages to supernatants

Following observations of their differential expression in response to three physicochemically diverse stimuli (an inhaled pharmaceutical, a metallic nanoparticle and pro-inflammatory IL-13), interrogation of microtranscriptomic profiling data identified miR-34b and miR-449a as stimulus-independent, tissue biomarkers for pulmonary inflammatory responses *in vivo*. Targeted quantifications determined that over-expression of both miRNAs was detectable in rat serum following a localised inflammatory response to intratracheal LPS instillation,

indicating that both markers could be sought within an accessible fluid as a result of prototypical inflammatory activity within the lungs.

Similarly, exhaust and non-exhaust PM-induced elevations of miR-449 expression in U937 human macrophages were detectable within the cellular supernatants, indicating that production of this marker also translates extracellularly in the context of TRPM exposure. Importantly this observation provides preliminary evidence that miR-34/449 family members could be used to detect adverse responses to TRPM exposure in accessible samples (potentially including those collected from humans). It also provides evidence that elevation of extracellular miR-449a concentrations are contributed to by macrophage behaviour during inflammation.

Whilst novel in terms of the relationship between mir-34b/449a and pulmonary inflammation, it is not surprising that the extracellular miRNA signatures reflected those of their origin tissue/cells. Circulating miRNA signatures are recurrently shown to echo changes in tissue marker expression in cancers (421,422) and miR-34b itself is up-regulated in the serum of patients with Huntington's Disease, showing the same pattern of expression as neuronal cells that express mutant huntingtin proteins *in vitro* (423).

Considering that many of the predicted targets for mir-34b and miR-449a were not differentially expressed within the pulmonary tissue of rats treated with AZD2230 and that several extra-pulmonary pathways (including regulation of cholesterol synthesis calcium signalling in cardiomyocytes) were implicated as targets for AZD2230-associated miRNAs, it may be that translation of miR-34b/449a to circulating fluids fulfils an endocrine purpose during pulmonary inflammation. Such functions could include stimulation of auxiliary phagocytes, differentiation of phagocytic pre-cursors or, given the associations between pulmonary inflammation and cardiovascular disease (424); promotion of vascular remodelling- an event that miRNAs have been demonstrated to regulate (425) .

Evidence for systemic responses to pulmonary inflammatory activity has been observed under multiple conditions. As examples, hepatic C reactive protein synthesis increases during exacerbation of lung inflammation in COPD (426) and production and release of polymorphonuclear leukocytes from the bone marrow is induced by PM_{10} exposure (427). As circulating miRNAs are widely hypothesised to contribute to inter-cell communication (250), are shown to alter protein expression in target cells (145,428) and can be specifically expressed and sorted for vesicular transport (147,429), it is not unreasonable to speculate that miR-34b/449a could contribute to extra-pulmonary activities.

The value of miR-34b/449a translating to the serum is enhanced by evidence that the miRNAs are significantly enriched in lung tissue (compared with 15 other tissue types), as this suggests that the lungs (and/or inflammatory cells that have migrated into the lungs) would be the most probable source of circulating miR-34b/449a. Care must still be taken however, when interpreting serum concentrations of miR-34b/449a as similar or greater levels of the miRNAs were detected within the bone marrow and testes (respectively). While these tissues are less likely to contribute to *in vivo* responses to controlled respiratory exposures such as intratracheal instillation, it must be recognised that ultrafine particles and water-soluble metals are capable of translocating to tissues outside of the respiratory tract, (including the heart, liver, spleen and brain) (430–432), where they may induce extracellular release of miRNAs and thus contribute to the circulating pool. Kreyling *et al* (2002) did observe however, that less than 1% of inhaled $PM_{0.1}$ translocates to secondary organs following deposition in the rat lung (431), suggesting that the influence that secondary organ exposures had on serum miRNA profiles in this study was likely to be minimal in relation to that of the lungs.

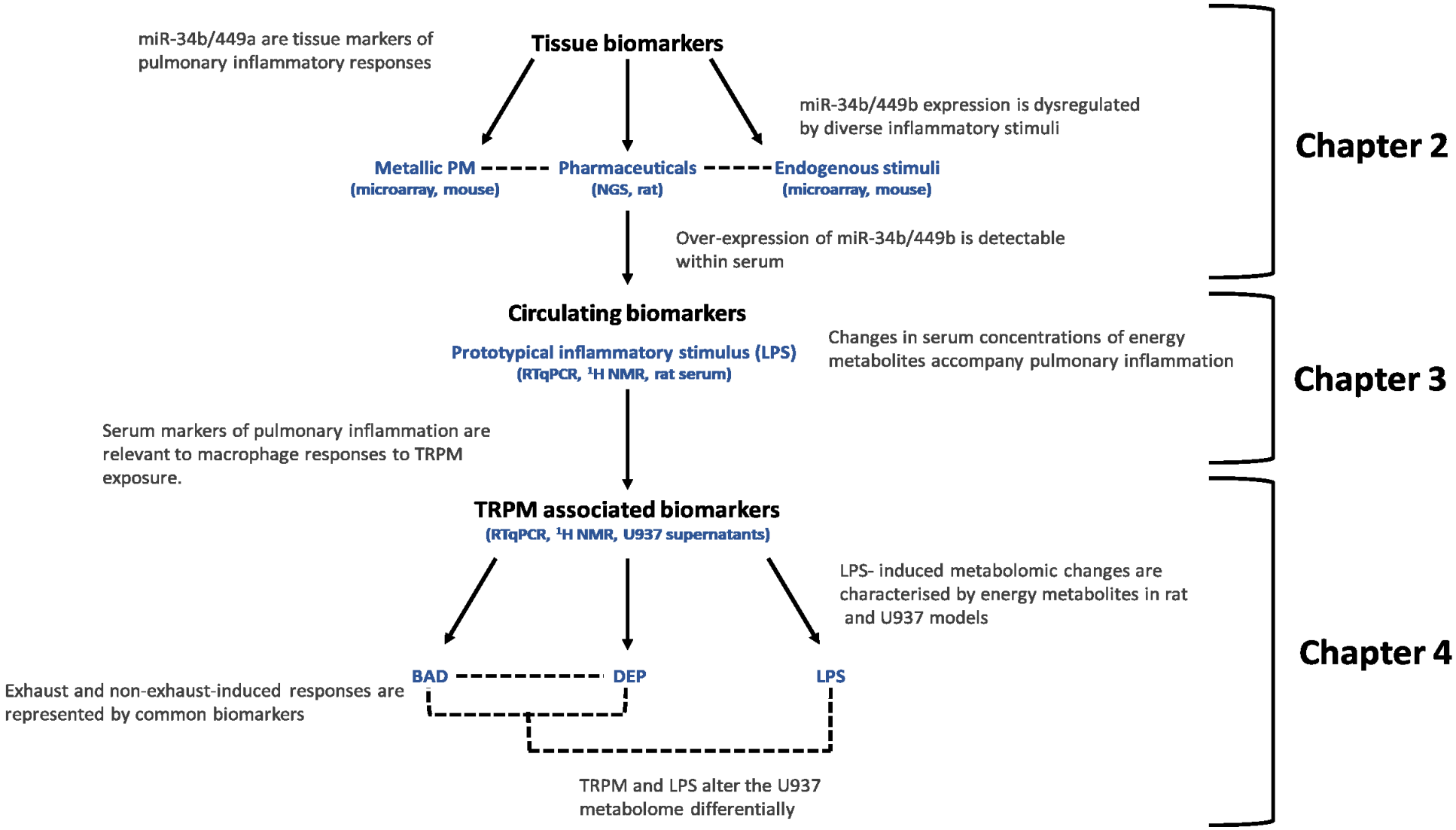


Figure 5. 1: Key observations made during the search for mechanistically relevant, accessible biomarkers of pulmonary inflammation.

5.1.2: Metabolite markers of pulmonary inflammatory responses distinguished between endotoxin and TRPM-induced responses

In contrast to the stimulus-independent nature of the miRNA markers, *in vitro* analysis indicated that endotoxin and TRPM-induced inflammatory responses could be distinguished at the metabolomic level based upon changes in extracellular concentrations of arginine, asparagine, threonine and histidine. Additional study will be required to determine whether the signature is specific to TRPM or whether other pro-inflammatory particles (such as pharmaceuticals or agricultural dusts) induce similar changes but the extracellular nature of the changes provides preliminary support for the use of this amino acid panel as a biomarker for TRPM-related pulmonary inflammation *in vivo*. If validated in serum they could provide far greater information than the use of miR-34a/449b alone; allowing TRPM-induced responses to be characterised or monitored despite the presence of heterogeneous co-exposures (as may be expected for non-intervention studies).

In this context, the distinction between endotoxin and TRPM-induced responses may be of particular use whilst investigating the role that TRPM exposure plays in bacterial exacerbations of chronic pulmonary conditions such as COPD and CF (433). Impairment of antimicrobial macrophage activities is hypothesised as a mechanism by which TRPM triggers exacerbation of these conditions, causing pathogenic accumulations in the absence of microbial clearance (434). As the U937 exposure model found that inhibition of bacterial phagocytosis is driven by TRPM but only marginally by LPS, it may be that increased extracellular concentrations of arginine, threonine, asparagine or histadine are reflective of this difference. Arginine for example, has been shown to promote phagocytosis via nitric oxide synthetase mediated changes to the cytoskeleton (435) and was differentially metabolised by LPS and TRPM-exposed macrophages, being utilised after endotoxin exposure but accumulating extracellularly during particle-induced responses.

The value of the candidate metabolite markers is enhanced by the fact that their extracellular concentrations increase following exposure. Down-regulated extracellular biomarkers can be

difficult to handle analytically; firstly because they become more difficult to measure accurately as their abundance decreases, and secondly because the measurement of response can only range between unchanged and absent (75). Here, the biomarker concentrations increase with exposure, yielding greater opportunity to assess the magnitude of responses or monitor health deterioration. While this may be advantageous considering the synergistic and heterogeneous nature of TRPM exposures (28,398), it is worth noting that the relationships between biomarker concentrations and PM exposure are not always dose-dependent. Therefore the degree to which the markers are elevated in serum may not be indicative of response severity.

Given that BAD and DEP were shown to induce the same mechanisms of toxicity in U937s, it is not surprising that the accompanying metabolic profiles could not distinguish between BAD and DEP-induced responses. Whilst promoting confidence in the mechanistic relevance of the markers, this is disappointing from a regulatory viewpoint. The contribution that non-exhaust PM (of which BAD is the major contributor (436)) makes to total TRPM emissions is forecast to increase over the coming years (28) as cleaner fuels, improved tailpipe filters and diesel-focused regulations come into play and it would be useful to monitor the effects that this has on pulmonary health. Source-specific biomarkers of pulmonary inflammation would have provided a convenient and high-throughput way to do this (particularly if they could be detected in serum) enabling decisions to be made regarding requirements for regulation of non-exhaust PM emissions.

Based on the evidence gained from this study it is difficult to predict whether the TRPM-associated metabolite signature will translate to serum (or indeed, from rat models to human cohorts). Pathway over-representation analyses indicated that LPS exposure caused the same changes in U937 energy metabolism as were seen in rat serum but also showed that many additional pathways contributed to the response *in vitro*. Such disparity between the analyses is likely to be an artefact of differences in the *in vitro* and *in vivo* environments, contributed to by differences between rat and human cellular responses to exposure,

however it may also have been contributed to by differences between the statistical approaches that were employed to analyse the two datasets.

Different strategies of analysis can be applied to metabolomics data, depending on the research question in hand and the characteristics of the dataset. Multivariate pattern recognition approaches such as PCA and PLS-DA (used here to analyse the serum data) are most commonly applied where biomarkers are sought because they consider covariance between metabolites (the source of most biochemical information), enable multiple variables to be tested simultaneously and identify those that possess the greatest discriminatory strength (437). For the U937 dataset however, intra-group variation was considered too high (relative to the number of samples per class) to perform pattern recognition techniques reliably and a simple univariate approach was employed instead that tested for exposure-associated differences in the concentrations of all identified metabolites. It may be that this univariate approach uncovered associations that contributed more subtly to LPS-induced variations in the metabolome and that application of this approach to the serum dataset would uncover *in vivo* translatability for those metabolites too. If so, this observation might provide support for the translatability of amino acid markers to the serum following TRPM exposure as well.

5.1.3: Multi-omics approaches enhanced the mechanistic value of pulmonary inflammatory biomarkers

As regulators of the proteome or components of biochemical reactions, omics-gathered miRNA and metabolite biomarkers possess huge mechanistic relevance. Coupled with pathway enrichment algorithms, panels of these markers have the power to generate novel hypotheses regarding the molecular interactions that underlie responses to experimental or environmental exposures. Here for example, microtranscriptomic sequencing provided associations between pulmonary inflammation and altered synaptic signalling while metabolomic profiling indicated that TRPM exposure appears to influence nitrogen

metabolism pathways in macrophages- a phenomenon that has yet to be reported in the literature.

Integration of omics datasets (or 'multi-omics' analysis) has been shown to unlock even greater mechanistic detail than single-omics analysis (100,105). The holistic nature of the approach considers the complex interactions that take place between different molecular networks during biological responses (438) and offers greater statistical support for pathway prediction analyses, helping to validate associations made at individual omic levels. Such validation is particularly important given that most pathway identification algorithms simply assess the proportions of pathway components that are influenced under experimental conditions, regardless of whether there is statistical evidence for their interaction within the system in question (316).

Indeed, focusing on the TRPM exposure model, considerable overlap existed between pathways that were enriched for metabolite features and pathways that were enriched for miR-34b/449a gene targets. This provided confidence in the hypothesis that these pathways contribute to pulmonary responses to TRPM exposure, thereby determining which molecular interactions were represented by the TRPM-associated miRNAs and metabolites. Several of the pathways, including those relating to lipid metabolism and cell signalling (AMPK, cyclic adenosine monophosphate (cAMP), FOXO1, HIF-1α, SREBP) were not implicated by the accompanying metabolome-only analysis but have been associated with pulmonary inflammation elsewhere (439–444), demonstrating the potential that multi-omics analyses have for creating additional and relevant mechanistic associations.

Of course, given that the techniques employed the same computational method, results of this integrative analysis may be subject to the same limitations as single omics pathway analysis, meaning that they require experimental validation to be fully corroborated. Such validation would be unsurprising since FOXO1, AMPK, SREBP and HIF-1α signalling pathways are all validated targets of p38/MAPK phosphorylation (445–448) and LPS-

induced pulmonary inflammation altered serum concentrations of miR-34b/449a and accompanying metabolite markers in a p38/MAPK dependent manner.

Close inspection determined that the glutathione synthesis pathway was excluded from the multi-omics pathway analysis in both the LPS and TRPM exposure models despite metabolite-only analysis indicating its involvement in responses to both stimuli. Considering that glutamate cysteine ligase expression was significantly up-regulated by miR-301b in pulmonary tissue following AZD2230 exposure and that glutathione is a well-characterised component of protective pulmonary responses to oxidative stimuli (449) (including DEP (450) this highlights the degree of mechanistic specificity that can be obtained for individual biomarkers. The disparity between the outputs indicates that anti-oxidant production was a component of macrophage responses to TRPM and LPS exposure but was not regulated or represented by miR-34b/449a over-expression.

5.2: Advantages and limitations of study designs

5.2.1: Use of an *in vitro* exposure system for TRPM studies

Given that the circulating markers for prototypical pulmonary inflammation were identified using rodent models of pulmonary exposure, a natural progression might have been to explore their associations with TRPM exposure in a rat or mouse model rather than the chosen *in vitro* system.

Such a model would have included the systemic features that *in vitro* models are criticised for lacking (451) and inflammatory pulmonary responses are shown to include (such as the interplay between parenchymal and non-resident airway cells (10) and the modification of PM toxicity by the respiratory tract lining fluid (452)). Furthermore, both the internalised TRPM dosage and the downstream concentrations of secreted products would have been influenced by realistic pharmacokinetic factors (such as absorption, distribution and excretion) upon secretion into a circulating matrix (451).

An advantage of omics strategies is their ability to capture a molecular snapshot of a biological system at the time of sampling (453). Unrepresentatively however, the simple cell culture techniques used in this study allowed the U937 secretion products (including miRNAs, metabolites and cytokines) to remain in close proximity to the cells for 24 hours. Upon activation by pro-inflammatory mediators, macrophages undergo rapid metabolic switches that allow them to tailor their responses accordingly to the transient stages of inflammation. As such, allowing the U937 secretion products to accumulate where they may usually be removed from the pulmonary microenvironment by other cell types, molecular reactions, epithelial lining fluids or the microcirculation could have complicated interpretation of the response.

Providing an example of this, significant elevations in both pro and anti-inflammatory cytokines were observed following 24 hour exposures to BAD and DEP. As cytokine synthesis and secretion is a highly ATP dependent process but mitochondrial function and additional energy dependent processes were impaired and energy metabolism altered, it is unclear whether the increase in cytokines represents an early response to exposure that remained visible within the supernatant until sampling or whether the cells used their low energy supplies to fuel cytokine secretion throughout the response, sacrificing other energy-dependent processes for auxiliary phagocyte recruitment.

While development of an *in vivo* model of TRPM exposure will be a future goal, *in vitro* systems such as the U937 model used here do enable toxicological responses to be characterised in a defined, controllable and reproducible manner, free from confounding by adaptive or counter-regulatory responses to co-exposures and individual biological variations (453). They also enable the specific responses of individual cell types, or controlled combinations of cell types to be established; information that may be of great importance when studying the toxicity of poorly characterised exposures such as BAD. A simple compromise would be to add additional time points to the assays to determine which stages

of the inflammatory response cause elevations of miR-34b/449a expression and to better characterise the accompanying flux of metabolism.

5.2.2: Choice of methods for data integration

A strong advantage of this study is its employment of phenotypic anchoring. Particularly apparent for the TRPM model, the approach linked omics level changes (miRNA or metabolite profiling) with conventional toxicological parameters (BALF cell counts or measures of cellular health and function), enhancing the mechanistic links between the pathway biomarkers that were discovered and the toxicological endpoints that they create. This approach has been used broadly in the field of toxicogenomics (454) but has been criticised for producing biomarkers that have less prognostic relevance than the phenotype to which they are anchored (455).

Such criticism however bears little relevance to this study due to the accessible nature of the detected biomarkers. While less well characterised than neutrophilic infiltration of airway tissues or the bronchoalveolar lumen, miR-34b/449a and the accompanying panels of LPS or TRPM-associated metabolites provide evidence of inflammatory pulmonary activity that otherwise rely on invasive procedures to be detected. If translatable to human studies, these new markers will enable inflammatory responses to be detected in more heterogeneous populations; allowing studies to be performed in exposed but ‘healthy’ populations that would not generally undertake pulmonary biopsies.

Multi-omics study designs are becoming increasingly popular due to their ability to generate more mechanistic hypotheses than single-omics approaches (105). Indeed the decision to apply the approach to the context of pulmonary inflammation and TRPM exposure has recently been supported by Oeder *et al.*’s pathway analysis study (2015) which used transcriptomic, proteomic and metabolomics data to generate novel hypotheses regarding the mechanisms by which epithelial cells respond to shipping fuel exposure (100).

Three ‘taxonomies of data integration’ have been described for use in multi-omics studies; conceptual, statistical and model-based (316). In contrast to the majority of methods that are selected for integrative omics, the pathway over-representation modules of IMPaLA (used throughout this study) employ a simple conceptual approach. Despite using hypergeometric distribution statistics to identify pathways that are enriched for input genes and metabolites, the analysis does not assess statistical relationships between the features themselves, treating them as independent entities.

Such an approach has disadvantages. Although strong correlative relationships were observed between the LPS-associated metabolite features, providing evidence of pathway commonality, these were disregarded by the over-representation algorithm. Similarly the degree to which metabolite features were differentially synthesised or catabolised in response to inflammatory stimuli and their relative concentrations were excluded from the analysis meaning that the direction of pathway regulation (or progression for reversible pathways) was not provided.

While this information may have been used to build a more informative model of metabolic flux during responses to TRPM and LPS exposure, corresponding data was not available for miR-34b/449a activity. The input of these miRNAs to pulmonary response pathways was explored using computationally predicted gene targets and so experimentally validated expression values were not available for advanced pathway analyses. The use of expression values from the AZD2230 study was considered as a proxy but the possibility that miR-34b/449a has extra-pulmonary targets indicated that novel information could be masked if the analysis was restricted to targets that were validated in pulmonary tissue. Through the performance of a simple, conceptual approach, the IMPaLA over-representation module allowed these possibilities to be explored.

Furthermore, the non-statistical approach complimented the biological relationship that exists between gene transcripts and metabolites. It is important to remember that multiple regulatory interactions and cellular processes occur downstream of gene expression before

the product contributes to a biochemical pathway and that changes in the transcriptome will not cause simultaneous changes in the metabolome (316). As such, correlations between metabolites and enzyme or regulator transcripts are not always found (456,457) or are far more variable than correlations between enzymes and substrates (458). As demonstrated with the TRPM exposure model, the hypothesis generating potential of pathway analyses that seek to integrate transcriptomics and metabolomics data is therefore enhanced by the absence of correlative statistics.

5.2.3: Choice of serum as an extracellular matrix for biomarker detection

To fulfil the aim of accessible biomarker detection, a suitable biological matrix had to be selected from which miRNA and metabolite profiling and quantifications could be performed. Circulating fluids (serum or plasma) and urine were both candidates for the study as they each contain a broad range of miRNAs and metabolites (181,199) and can be harvested using minimally invasive techniques.

Urine is a popular matrix for metabolomic assessment as it can be harvested in large quantities (allowing analysis by multiple, complimentary platforms) and is well characterised in terms of metabolite content (181). For toxicological purposes, however, the urine may be best suited to targeted detection of biomarkers of exposure (such as PAH metabolites following exhaust PM exposure (82)). This is because urine is the primary route by which hydrophilic waste products are excreted (181) and so (with the exception of kidney or bladder toxicity) is less likely to contain molecules that regulate or contribute to adaptive or reparative responses in otherwise healthy organisms than serum or plasma.

In comparison to urine, blood functions as a transportation system for regulatory and functional cellular secretion products, thus facilitating the orchestration of physiological and stress response pathways (199). Caution must still be applied when considering the origin of serum/plasma markers but those that are detected are more likely to reflect toxicological

response pathways than urinary markers given the function of their matrix. Indeed, classical inflammatory and oxidative stress markers (including cytokines and lipid peroxidation products) are often detected within the serum following inflammatory pulmonary insults (459), suggesting that this matrix is a good choice for response biomarker detection.

Importantly for this project, the serum also has a richer lipidome than urine, containing > 17,000 lipid and fatty acid species compared to the 836 that have been assigned in urine (181). Considering that the miRNA markers of AZD2230-induced pulmonary inflammation were shown to regulate expression of genes that encode lipid metabolism enzymes and circulating products of airway structural lipid catabolism associate with exhaust PM exposure in mice (99), lipidomic exploration may prove a sensible starting point for future expansion of the current biomarker panel.

5.2.4: Absence of a continuous control between studies

Although macroscopic features of tissue inflammation (BALF cell counts) were comparable between the rodent models used in this study (indicating that they shared a common phenotype following their respective exposures), confidence in the translatability of tissue markers into serum could have been enhanced by including a common control exposure in each model. This would have highlighted similarities and discrepancies between the way that the animals (exposed to in different laboratories and heterogeneous in species and strain) responded to inflammatory stimuli, allowing more robust biomarkers to be applied to the TRPM exposure model.

This limitation was unavoidable given that publicly available datasets played a key role in the analysis but conscious efforts were made to minimise its impact, including selection of an exposure model for the serum study that related physicochemically or physiologically with the stimuli of the tissue models and with TRPM. As a prototypical stimulus of pulmonary inflammation, LPS induces NFκB pathways (in similarity to IL-13 (19), activates TLR4 in the

airways (like nano-titanium and DEP (229,230)) and contributes to the composition of TRPM (356). Therefore, it is not unreasonable to predict that its activity may be reflected by biomarkers that associated with nano-titanium exposure and IL-13 activity or that TRPM exposure may induce a similar signature.

Further continuity was produced by including an LPS control in the U937 model during biomarker analyses. This showed that the metabolic changes in U937 cultures were also dominated by energy metabolism pathways, indicating that the cells were responding similarly to pulmonary tissue and that comparisons could be made with greater confidence. Interestingly, the metabolic response to LPS exposure associated with a wider range of cellular pathways in the *in vitro* supernatant than it did in serum. Furthermore, many of these pathways (including cell signalling and amino acid catabolism) were also induced by TRPM exposure.

While these differences could be an artefact of the *in vitro* system (such as metabolite accumulation or phenotypic shift of the cell line), they may also be indicative of responses that occur specifically within immune cells during pulmonary inflammation or were masked by the presence of highly variable energy metabolites in multivariate models. Therefore, inclusion of the LPS control in the U937 model provided evidence that responses to TRPM exposure shared similarities with the prototypical inflammatory response which would not have been identified through direct comparison with the serum metabolome.

5.3: Impacts of findings

5.3.1: Applications for research

The biomarkers detected by this work possess a number of qualities that would benefit the study and characterisation of pulmonary inflammatory responses. Most importantly, the markers can be detected in accessible bio-fluids that are harvested inexpensively and non-invasively. In place of painful, time-consuming and daunting tissue biopsies, they offer the

opportunity to recruit larger study cohorts and perform studies of exposure-response that have greater statistical power and population representation. Of particular relevance to the context of TRPM exposure where exposed individuals often remain 'healthy', they offer an ethical method of sampling that would rarely be provided through biopsied tissue. This could allow the impacts of specific exposures or regulatory measures to be monitored in groups that better represent the general population.

The value of the accessible markers is enhanced by their specificity for pulmonary originated responses. miR-34b/449a expression was enriched in pulmonary tissue while altered concentrations of the glutamine, glutamate, acetate and lysine metabolite panel associated with pulmonary-specific inflammation here and in previous studies (345). As such, detection of these markers in place of those that can be produced by multiple tissues or organs (e.g. cytokines or pro-inflammatory lipids) could enable pulmonary-specific responses to be measured in complex *in vivo* cohorts or models without being confounded by background inflammatory sources such as dietary components (460), stress (461), or physical trauma (462).

The fact that many of the markers appear to be stimulus-independent yet mechanistically representative of prototypical inflammatory pathways indicates their potential for use in widespread contexts. For example, given the simplicity of sample preparation for metabolomic analyses and speed at which ^{1}H NMR spectral features can be measured, the serum metabolite panel could be of use during the detection of adverse pulmonary responses during clinical trials for airway pharmaceuticals. Indeed, this characteristic proved highly beneficial for the AZD2230 study, where the stimulus induced a strong inflammatory response via an unknown mechanism that contrasted with its design as an inhibitor of NFκB signalling.

5.3.2: Applications for policy makers

Despite emerging evidence that non-exhaust particles exert adverse effects on the health and function of pulmonary cells (371), the impacts that these products have on pulmonary health have not been explored *in vivo* or for human populations. Resultantly, efforts to meet the targets set by the 2008 Ambient Air Quality Directive for airborne PM focus almost exclusively on reducing exhaust emissions (463) (for which we have much evidence of toxicity). Such measures are enforced nationally or locally and include the provision of incentives to purchase hybrid and electric vehicles, expansion of low emission zones (LEZ), surcharges for diesel car owners and advancement of exhaust filtration technologies.

Actions like these have strongly reduced exhaust emissions over past decades with exhaust contributing 80-90% of road emissions in the early 1990s but reducing to approximately 50% today (464). Given the continuing imbalance between exhaust and non-exhaust focussed regulations, it is suggested that airborne concentrations of non-exhaust PM will continue to rise relative to exhaust PM (465). This is concerning given that this study found exhaust (DEP) and non-exhaust particulates (BAD) to be equally toxic upon exposure to pulmonary cells and that the prevalence of allergic and respiratory symptoms did not improve for children in London during the three years following introduction of the exhaust-focused LEZ (466).

The discovery that pulmonary-specific markers that relate to BAD exposure can be detected in serum offers the potential to explore whether non-exhaust PM has adverse effects on respiratory health. Given that no differences were seen between BAD and DEP-associated marker signatures, characterisations of the relationship between BAD exposure and pulmonary responses would need to be made under controlled chamber study conditions, free from confounding by DEP exposure (and potentially other particles of similar composition). Chamber studies have proved instrumental during characterisations of pulmonary responses to air pollutants in humans (467,468). Combined with a panel of

biomarkers that represent augmentation of widespread cellular processes, they could provide the evidence required to determine whether regulations ought to be introduced for non-exhaust emissions too.

5.4: Considerations for future work

5.4.1: *In vivo* validation of TRPM-associated biomarkers

A major future aim for this work will be to establish whether TRPM-associated response biomarkers are detectable within serum following *in vivo* exposures. As well as being directly comparable with the current work, rat models would present the advantage of a controlled exposure system, free from confounding by heterogeneous PM exposure or uncharacterised sources of systemic inflammation. Using ^{1}H NMR spectroscopy and the optimised methods of targeted miRNA quantification that were employed during the LPS rat study, changes in extracellular concentrations of miR-34b/449a and TRPM-associated metabolites could be characterised following specific types of TRPM exposure.

If successfully translated to rat serum, the markers could be sought in healthy human serum collected from A) chamber studies to validate inter-species relevance in a controlled exposure environment or B) non-intervention studies to determine whether the markers remain detectable and dose-relevant upon a background of real-world co-exposures (e.g. wood smoke, gaseous pollutants, bio-aerosols). Indeed, it will be necessary to determine whether real-world exposure doses are sufficient to alter circulating concentrations of the markers. Real world exposure doses are usually much lower than those employed within experimental models (selected to elicit detectable responses) and are cyclical rather than continuous in nature (due to the influence of human behaviours such as commuting) (469) meaning that *in vivo* human responses may be more subtle. Indeed, complimentary experiments to those presented here indicated that TRPM-induced elevations in cytokine secretion and impairment of bacterial phagocytosis abated in U937s following the introduction of a 24h particle-free ‘rest’ period prior to experimentation (**Supplementary figures 5.1 and 5.2**). As such, method optimisations such as addition of a targeted pre-

amplification step during RTqPCR may be required for the detection of TRPM-associated biomarkers in human samples.

With regards to exploring the reversible nature of TRPM-induced toxicity, an additional qualitative analysis of cytokine measurements would be informative. What remains to be determined for both particle types, is the relationships that develop between the expressed cytokines as contributors to an inflammatory network. IL-10 for example, is shown to reduce TNF-α production in human alveolar macrophages following LPS exposure (470); a mechanism that is likely to be of relevance to the current model but was not assessable when expressing cytokine release as a percentage of the control samples. In contrast, comparisons of absolute values and their correlations with one another, could uncover further mechanistic detail regarding the inflammatory response to BAD and DEP; perhaps enabling characterisation of the interplay between pro and anti-inflammatory mediators throughout the response and resolution time-courses.

As a more distant idea, it would be interesting to compare serum concentrations of TRPM-associated biomarkers between ‘healthy’ exposed populations and exposed populations who suffer from conditions that have been causally linked with PM exposure. Onset of schizophrenia is related to traffic exposure (471) and associates with increased serum concentrations of miR-449a (472) while development of type II diabetes associates with PM exposure and impacts serum concentrations of glutamine and pyruvate metabolism when accompanied by common cardiovascular complications (415). The proposed comparative studies would help determine the level of biomarker confoundment that can be expected in individuals who have responded to PM exposure in an extra-pulmonary manner, allowing assessment of how representative the biomarkers are for the wider population.

5.4.2: Validation of pathway identifications for biomarkers

As discussed above, a key limitation of this study was its dependence on computational algorithms to identify the mechanistic relevance of the inflammatory biomarkers (particularly the miRNAs). For the miRNAs, much of this limitation can be remedied *in vitro* by simply over-expressing or repressing mir-34b/449a expression in U937s (and potentially an epithelial cell line such as transformed type 1) and studying changes in the expression of target genes and proteins using a custom microarray and protein MS.

Making use of the hypothesis-generating nature of omics approaches, the same model could be used to explore the putative association between miR-34b/449a over-expression and p38/MAPK mediated alterations in cell signalling activities. Using phospho-specific western blotting it would be possible to explore the impact that miR-34b/449a has on SREBP, AMPK, HIF-1a and FOXO1 activation in pulmonary cells. Further measurement of p38/MAPK target phosphorylation could be performed following TRPM or LPS exposure in wild-type cells to validate the association under inflammatory conditions.

Before embarking upon such studies, it would be prudent to confirm the specificity of the small molecule inhibitor (GSK) that was used to produce the association between miR-34b/449a expression and the p38 MAPK pathway using a kinome array. Using this method, Bain *et al* showed that one third of small molecule inhibitors (across a panel of 60 that are commonly employed) influenced the activity of multiple non-target kinases, and suggested that conclusions drawn from studies that used these inhibitors could no longer be considered valid (473). Given that the rat genome encodes approximately 600 kinases (500 of which are orthologous to those of humans) (474), it would be informative to establish which non-target kinases (if any) were influenced by GSK in the present study as this could confirm which kinase-mediated pathways contributed to the expression of miR-34b/449a during pulmonary inflammation.

Similarly, associations between feature metabolites and the cellular processes to which they were phenotypically anchored (cytokine secretion, bacterial phagocytosis and mitochondrial

membrane depolarisation) could be explored by monitoring flux of the metabolites in the presence of agonists and inhibitors for the processes. Latrunculin A for example, is a potent inhibitor of phagocytosis that disrupts microfilament organisation in macrophages (334) while antimycin A, carbonyl cyanide 4-(trifluoromethoxy)phenylhydrazone, oligomycin and atractyloside have all been shown to disrupt mitochondrial function via mechanisms that disrupt mitochondrial membrane potential (475).

5.4.3: Untargeted lipidomics analysis

In this study, associations between pulmonary inflammation, miRNA regulation and dysregulated lipid metabolism were alluded to during responses to AZD2230, LPS and TRPM exposure, indicating that this process is a key contributor to pulmonary inflammation (irrespective of the stimulus) and that the lipidome may prove an additional source of biomarkers for pulmonary inflammatory responses.

Supporting this suggestion and the hypothesis that SREBP signalling and cholesterol biosynthesis contributed to TRPM-induced responses, PM_{10} has been observed to enhance the phospholipid and cholesterol content of murine pulmonary tissue (476) while evidence of airway lipid catabolism has been detected in mouse serum following DEP exposure (99). Lipid products such as prostaglandins and leukotrienes are widely associated with propagation and resolution of inflammatory responses in general (477) but these observations indicate that tissue-specific lipid biomarkers may be detectable extracellularly during pulmonary inflammation.

The CPMG sequence that was used to acquire ^{1}H NMR data during the LPS and TRPM exposure studies was designed to exclude broad peaks (including lipid peaks) from the spectra as they would have masked the presence of smaller metabolite peaks and restricted their quantification (478). As such, additional lipidomic profiling using untargeted MS methods should be applied to the serum and supernatant samples that were used in the LPS

and TRPM exposure studies to determine whether the exposures can be represented by lipid metabolism products. An exceptional bonus would be the discovery of lipid products that differentiate between BAD and DEP-induced responses, as these would allow the contributions that non-exhaust particles make to TRPM-induced pulmonary responses to be characterised in observational human studies.

5.5: Conclusion

Evaluating the hypothesis that **mechanistically relevant miRNA and metabolite biomarkers are detectable during pulmonary responses to TRPM exposure and can be measured in extracellular samples**, this body of work identified two miRNAs (miR-34b/449a) that are enriched specifically in pulmonary tissues, over-expressed in response to pro-inflammatory insults, detectable in serum and relatable to exhaust and non-exhaust-PM exposures. Furthermore, it demonstrated that both particle types induce characteristic alterations in concentrations of *in vivo* relevant biomarkers of energy metabolism following pulmonary insult and that additional, particle-specific metabolite signatures could be detected in biofluids.

Further experimentation is required to translate the relevance of these biomarkers to situations of human exposure but their mechanistic relevance and specificity for the pulmonary response indicates their potential as tools for monitoring and characterising pulmonary responses to TRPM exposure *in vivo*. Such opportunity could have a significant impact on air quality policies, in particular it could provide the evidence required to encourage regulation of toxic non-exhaust PM emissions.

Given that much of the work was performed using diverse and prototypical inflammatory stimuli (pharmaceuticals, metallic nanoparticles, endogenous cytokines and LPS) and are validated as applicable *in vivo*, these biomarkers may also be used to characterise or monitor other causes of pulmonary exposure. While traffic is the major environmental source

of airborne PM, adverse respiratory effects have also been associated with those produced by agricultural and industrial activity, fire burning and waste incineration (to name but a few) (479–481).

The integrated approach used here to explore the interplay between miRNA and metabolite biomarkers provided superior mechanistic detail regarding the pathways that underlie responses to LPS and TRPM exposure. This indicates that application of miR-34b/449a and metabolic profiling approaches to these additional contexts may further our understanding of them too.

References

1. Hayes W, Kruger C. Hayes' Principles and Methods of Toxicology [Internet]. 6th ed. CRC Press; 2014. Available from: https://www.crcpress.com/Hayes-Principles-and-Methods-of-Toxicology-Sixth-Edition/Hayes-Kruger/p/book/9781842145364

2. Akella A, Deshpande S. Pulmonary surfactants and their role in pathophysiology of lung disorders. Indian J Exp Biol [Internet]. 2013;51(1):5–22. Available from: http://nopr.niscair.res.in/bitstream/123456789/15282/1/IJEB 51(1) 5-22.pdf

3. Weibel ER. Morphological Basis of Alveolar-Capillary Gas Exchange. Physiol REVIE ws [Internet]. 1973 [cited 2017 Apr 18];53(2). Available from: http://physrev.physiology.org/content/physrev/53/2/419.full.pdf

4. Gehr P, Mühlfeld C, Rothen-Rutishauser B, Blank F. Particle-Lung Interactions [Internet]. 2nd ed. CRC Press; 2009. Available from: https://www.crcpress.com/Particle-Lung-Interactions-Second-Edition/Gehr-Muhlfeld-Rothen-Rutishauser-Blank/p/book/9781420072563

5. Keane MP, Strieter RM. The importance of balanced pro-inflammatory and anti-inflammatory mechanisms in diffuse lung disease. Respir Res [Internet]. 2001;3(1):5. Available from: http://dx.doi.org/10.1186/rr177

6. Nicod LP. Lung defences: an overview. Eur Respir Rev [Internet]. 2005 Dec 12;14(95):45. Available from: http://err.ersjournals.com/content/14/95/45.abstract

7. Linder J, Sisson JH. Lung Defenses. In: Dail DH, Hammar SP, editors. Pulmonary Pathology [Internet]. New York, NY: Springer New York; 1994. p. 45–56. Available from: http://dx.doi.org/10.1007/978-1-4757-3935-0_3

8. Lambrecht B, Neyt K, Van Kessel G. Pulmonary defence mechanisms and inflammatory pathways in bronchiectasis. In: Pulmonary Defence Mechanisms and Inflammatory Pathways in Bronchiectasis [Internet]. European Respiratory Society; 2011. p. 11–21. Available from: http://www.sppneumologia.pt/uploads/files/gruposdeestudo/N%25C3%25BAcleo de Estudos de Bronquiectasias N%25C3%25A3o Fibrose Qu%25C3%25ADstica/PDF77.pdf

9. Fernández Tena A, Casan Clarà P. Deposition of Inhaled Particles in the Lungs. Arch Bronconeumol (English Ed [Internet]. Elsevier; 2012 Jul [cited 2017 Mar 3];48(7):240–6. Available from: http://linkinghub.elsevier.com/retrieve/pii/S1579212912000845

10. Moldoveanu B, Otmishi P, Jani P, Walker J, Sarmiento X, Guardiola J, et al. Inflammatory mechanisms in the lung. J Inflamm Res [Internet]. Dove Medical Press; 2009;2:1–11. Available from: http://www.ncbi.nlm.nih.gov/pmc/articles/PMC3218724/

11. Gordon S. Pattern Recognition Receptors. Cell [Internet]. 2002 Dec [cited 2017 Mar 3];111(7):927–30. Available from: http://linkinghub.elsevier.com/retrieve/pii/S0092867402012011

12. Slauch JM. How does the oxidative burst of macrophages kill bacteria? Still an open question. Mol Microbiol [Internet]. 2011 May;80(3):580–3. Available from: http://www.ncbi.nlm.nih.gov/pmc/articles/PMC3109634/

13. Parent RA. Comparative biology of the normal lung [Internet]. [cited 2017 Mar 3]. Available from: http://www.sciencedirect.com/science/book/9780124045774

14. Bhattacharya J, Westphalen K. Macrophage-epithelial interactions in pulmonary alveoli. Semin Immunopathol [Internet]. 2016;38(4):461–9. Available from: http://dx.doi.org/10.1007/s00281-016-0569-x

15. Fehrenbach H. Alveolar epithelial type II cell: defender of the alveolus revisited. Respir Res [Internet]. 2001;2(1):33. Available from: http://dx.doi.org/10.1186/rr36

16. Kato T, Kitagawa S. Regulation of Neutrophil Functions by Proinflammatory Cytokines. Int J Hematol [Internet]. 2006;84(3):205. Available from: http://dx.doi.org/10.1532/IJH97.06141

17. Wright HL, Moots RJ, Bucknall RC, Edwards SW. Neutrophil function in inflammation and inflammatory diseases. Rheumatology [Internet]. 2010 Sep 1;49(9):1618–31. Available from: http://dx.doi.org/10.1093/rheumatology/keq045

18. Smolen JE, Petersen TK, Koch C, O'Keefe SJ, Hanlon WA, Seo S, et al. L-Selectin Signaling of Neutrophil Adhesion and Degranulation Involves p38 Mitogen-activated Protein Kinase. J Biol Chem [Internet]. 2000 May 26;275(21):15876–84. Available from: http://www.jbc.org/content/275/21/15876.abstract

19. Goto Y, Hogg JC, Whalen B, Shih C-H, Ishii H, van Eeden SF. Monocyte Recruitment into the Lungs in Pneumococcal Pneumonia. Am J Respir Cell Mol Biol [Internet]. American Thoracic Society - AJRCMB; 2004 May 1;30(5):620–6. Available from: http://dx.doi.org/10.1165/rcmb.2003-0312OC

20. Levy BD, Serhan CN. Resolution of Acute Inflammation In The Lung. Annu Rev Physiol [Internet]. 2014;76:467–92. Available from:

http://www.ncbi.nlm.nih.gov/pmc/articles/PMC4295924/

21. Shi C, Pamer EG. Monocyte recruitment during infection and inflammation. Nat Rev Immunol [Internet]. Nature Publishing Group, a division of Macmillan Publishers Limited. All Rights Reserved.; 2011 Nov;11(11):762–74. Available from: http://dx.doi.org/10.1038/nri3070

22. Jones HR, Robb CT, Perretti M, Rossi AG. The role of neutrophils in inflammation resolution. Semin Immunol [Internet]. 2016 Apr [cited 2017 Jul 22];28(2):137–45. Available from: http://www.ncbi.nlm.nih.gov/pubmed/27021499

23. Schif-Zuck S, Gross N, Assi S, Rostoker R, Serhan CN, Ariel A. Satiated-efferocytosis generates pro-resolving CD11b(low) macrophages: modulation by resolvins and glucocorticoids. Eur J Immunol [Internet]. 2011 Feb;41(2):366–79. Available from: http://www.ncbi.nlm.nih.gov/pmc/articles/PMC3082320/

24. Greene CM, McElvaney NG. Proteases and antiproteases in chronic neutrophilic lung disease – relevance to drug discovery. Br J Pharmacol [Internet]. Blackwell Publishing Ltd; 2009 Oct;158(4):1048–58. Available from: http://www.ncbi.nlm.nih.gov/pmc/articles/PMC2785526/

25. Amato F, Cassee FR, Denier van der Gon HAC, Gehrig R, Gustafsson M, Hafner W, et al. Urban air quality: The challenge of traffic non-exhaust emissions. J Hazard Mater [Internet]. 2014 Jun [cited 2017 Mar 3];275:31–6. Available from: http://linkinghub.elsevier.com/retrieve/pii/S030438941400315X

26. Wichmann H-E. Diesel Exhaust Particles. Inhal Toxicol [Internet]. Taylor & Francis; 2007 Jan 1;19(sup1):241–4. Available from: http://dx.doi.org/10.1080/08958370701498075

27. Pirjola L, Karjalainen P, Heikkilä J, Saari S, Tzamkiozis T, Ntziachristos L, et al. Effects of Fresh Lubricant Oils on Particle Emissions Emitted by a Modern Gasoline Direct Injection Passenger Car. Environ Sci Technol [Internet]. American Chemical Society; 2015 Mar 17;49(6):3644–52. Available from: http://dx.doi.org/10.1021/es505109u

28. Grigoratos T, Martini G. Brake wear particle emissions: a review. Environ Sci Pollut Res Int [Internet]. Berlin/Heidelberg: Springer Berlin Heidelberg; 2015;22:2491–504. Available from: http://www.ncbi.nlm.nih.gov/pmc/articles/PMC4315878/

29. Boulter P, Waymon M, harrison R. a review of abatement measures for non-exhaust particulate matter from road vehicles [Internet]. 2006. Available from: https://uk-

air.defra.gov.uk/assets/documents/reports/cat15/0706061643_Report4_Abatement_measures.pdf

30. Bukowiecki N, Lienemann P, Hill M, Figi R, Richard A, Furger M, et al. Real-World Emission Factors for Antimony and Other Brake Wear Related Trace Elements: Size-Segregated Values for Light and Heavy Duty Vehicles. Environ Sci Technol [Internet]. American Chemical Society; 2009 Nov 1;43(21):8072–8. Available from: http://dx.doi.org/10.1021/es9006096

31. Brown DM, Wilson MR, MacNee W, Stone V, Donaldson K. Size-dependent proinflammatory effects of ultrafine polystyrene particles: a role for surface area and oxidative stress in the enhanced activity of ultrafines. Toxicol Appl Pharmacol [Internet]. 2001;175. Available from: http://dx.doi.org/10.1006/taap.2001.9240

32. Garg BD, Cadle SH, Mulawa PA, Groblicki PJ, Laroo C, Parr GA. Brake Wear Particulate Matter Emissions. Environ Sci Technol [Internet]. American Chemical Society; 2000 Nov 1;34(21):4463–9. Available from: http://dx.doi.org/10.1021/es001108h

33. Kupiainen KJ, Tervahattu H, Räisänen M, Mäkelä T, Aurela M, Hillamo R. Size and Composition of Airborne Particles from Pavement Wear, Tires, and Traction Sanding. Environ Sci Technol [Internet]. American Chemical Society; 2005 Feb 1;39(3):699–706. Available from: http://dx.doi.org/10.1021/es035419e

34. Department of Health and Human Services. Diesel Exhaust Particles [Internet]. Report on Carcinogens, 14th Edition. 2000 [cited 2017 Apr 18]. Available from: https://ntp.niehs.nih.gov/ntp/roc/content/profiles/dieselexhaustparticulates.pdf

35. Heyder J. Deposition of Inhaled Particles in the Human Respiratory Tract and Consequences for Regional Targeting in Respiratory Drug Delivery. Proc Am Thorac Soc [Internet]. 2004 Dec 1 [cited 2017 Jul 22];1(4):315–20. Available from: http://pats.atsjournals.org/cgi/doi/10.1513/pats.200409-046TA

36. Karagulian F, Belis CA, Dora CFC, Prüss-Ustün AM, Bonjour S, Adair-Rohani H, et al. Contributions to cities' ambient particulate matter (PM): A systematic review of local source contributions at global level. Atmos Environ [Internet]. 2015 Nov [cited 2017 Mar 3];120:475–83. Available from: http://linkinghub.elsevier.com/retrieve/pii/S1352231015303320

37. Passant N, Pang Y, Thistlewaite G, Venfield H, Whiting R, Walker C, et al. Annual Report for submission under the UNECE-Convention on Long-Range Transboundary

Air Pollution [Internet]. 2014. Available from: https://uk-air.defra.gov.uk/assets/documents/reports/cat19/1405130812_UK_IIR_2014_Final.pdf

38. Zuurbier M, Hoek G, Oldenwening M, Lenters V, Meliefste K, van den Hazel P, et al. Commuters' Exposure to Particulate Matter Air Pollution Is Affected by Mode of Transport, Fuel Type, and Route. Environ Health Perspect [Internet]. National Institute of Environmental Health Sciences; 2010 Jun;118(6):783–9. Available from: http://www.ncbi.nlm.nih.gov/pmc/articles/PMC2898854/

39. Iskandar A, Andersen ZJ, Bønnelykke K, Ellermann T, Andersen KK, Bisgaard H. Coarse and fine particles but not ultrafine particles in urban air trigger hospital admission for asthma in children. Thorax [Internet]. 2012 Feb 17;67(3):252. Available from: http://thorax.bmj.com/content/67/3/252.abstract

40. Ostro B, Roth L, Malig B, Marty M. The Effects of Fine Particle Components on Respiratory Hospital Admissions in Children. Environ Health Perspect. 2009;117:475–80.

41. Lanzinger S, Schneider A, Breitner S, Stafoggia M, Erzen I, Dostal M, et al. Ultrafine and Fine Particles and Hospital Admissions in Central Europe. Results from the UFIREG Study. Am J Respir Crit Care Med [Internet]. American Thoracic Society - AJRCCM; 2016 May 25;194(10):1233–41. Available from: http://dx.doi.org/10.1164/rccm.201510-2042OC

42. Vichit-Vadakan N, Ostro BD, Chestnut LG, Mills DM, Aekplakorn W, Wangwongwatana S, et al. Air pollution and respiratory symptoms: results from three panel studies in Bangkok, Thailand. Environ Health Perspect [Internet]. 2001 Jun;109(Suppl 3):381–7. Available from: http://www.ncbi.nlm.nih.gov/pmc/articles/PMC1240555/

43. Zemp E, Elsasser S, Schindler C, Künzli N, Perruchoud A, Domenighetti G, et al. Long-Term Ambient Air Pollution and Respiratory Symptoms in Adults (SAPALDIA Study). Am J Respir Crit Care Med [Internet]. American Thoracic SocietyNew York, NY; 1999 Apr 14 [cited 2017 Jul 22];159(4):1257–66. Available from: http://www.atsjournals.org/doi/abs/10.1164/ajrccm.159.4.9807052

44. Garshick E, Laden F, Hart JE, Caron A. Residence Near a Major Road and Respiratory Symptoms in U.S. Veterans. Epidemiology [Internet]. 2003 Nov;14(6):728–36. Available from: http://www.ncbi.nlm.nih.gov/pmc/articles/PMC1351073/

45. Lindgren A, Stroh E, Montnémery P, Nihlén U, Jakobsson K, Axmon A. Traffic-related air pollution associated with prevalence of asthma and COPD/chronic bronchitis. A cross-sectional study in Southern Sweden. Int J Health Geogr [Internet]. BioMed Central; 2009;8:2. Available from: http://www.ncbi.nlm.nih.gov/pmc/articles/PMC2649061/

46. Ghio A, Kim C, Devlin RB. Concentrated Ambient Air Particles Induce Mild Pulmonary Inflammation in Healthy Human Volunteers. Am J Respir Crit Care Med [Internet]. American Thoracic Society - AJRCCM; 2000 Sep 1;162(3):981–8. Available from: http://dx.doi.org/10.1164/ajrccm.162.3.9911115

47. Nightingale J, Maggs R, Cullinan P, Donnelly LE, Rogers D, Kinnersley R, et al. Airway Inflammation after Controlled Exposure to Diesel Exhaust Particulates. Am J Respir Crit Care Med [Internet]. American Thoracic Society - AJRCCM; 2000 Jul 1;162(1):161–6. Available from: http://dx.doi.org/10.1164/ajrccm.162.1.9908092

48. Autrup H. Ambient Air Pollution and Adverse Health Effects. Procedia - Soc Behav Sci [Internet]. 2010 [cited 2017 Mar 3];2(5):7333–8. Available from: http://linkinghub.elsevier.com/retrieve/pii/S1877042810012231

49. Sacks J, Stanek L, Luben T, Johns D, Buckley B, Brown J, et al. Particulate Matter–Induced Health Effects: Who Is Susceptible? Environ Heal Perspect [Internet]. 2011;119:446–54. Available from: https://ehp.niehs.nih.gov/1002255/

50. Steiner S, Bisig C, Petri-Fink A, Rothen-Rutishauser B. Diesel exhaust: current knowledge of adverse effects and underlying cellular mechanisms. Arch Toxicol [Internet]. Springer; 2016 Jul [cited 2017 Jul 22];90(7):1541–53. Available from: http://www.ncbi.nlm.nih.gov/pubmed/27165416

51. Kelly FJ. Oxidative stress: its role in air pollution and adverse health effects. Occup Environ Med [Internet]. 2003 Jul 25;60(8):612. Available from: http://oem.bmj.com/content/60/8/612.abstract

52. Reddy SP. The Antioxidant Response Element and Oxidative Stress Modifiers in Airway Diseases. Curr Mol Med [Internet]. 2008 Aug;8(5):376–83. Available from: http://www.ncbi.nlm.nih.gov/pmc/articles/PMC2828610/

53. Kelly FJ. Oxidative stress: Its role in air pollution and adverse health effects. [cited 2017 Jul 22]; Available from: http://oem.bmj.com/content/oemed/60/8/612.full.pdf

54. Roberts RA, Smith RA, Safe S, Szabo C, Tjalkens RB, Robertson FM. Toxicological and pathophysiological roles of reactive oxygen and nitrogen species. Toxicology

[Internet]. 2010 Oct [cited 2017 Aug 30];276(2):85–94. Available from: http://linkinghub.elsevier.com/retrieve/pii/S0300483X1000288X

55. DiStefano E, Eiguren-Fernandez A, Delfino RJ, Sioutas C, Froines JR, Cho AK. Determination of metal-based hydroxyl radical generating capacity of ambient and diesel exhaust particles. Inhal Toxicol [Internet]. Taylor & Francis; 2009 Aug 1;21(9):731–8. Available from: http://dx.doi.org/10.1080/08958370802491433

56. Alaghmand M, Blough N V. Source-Dependent Variation in Hydroxyl Radical Production by Airborne Particulate Matter. Environ Sci Technol [Internet]. American Chemical Society; 2007 Apr 1;41(7):2364–70. Available from: http://dx.doi.org/10.1021/es061902o

57. Zielinski H, Mudway IS, Bérubé KA, Murphy S, Richards R, Kelly FJ. Modeling the interactions of particulates with epithelial lining fluid antioxidants. Am J Physiol - Lung Cell Mol Physiol [Internet]. 1999 Oct 1;277(4):L719. Available from: http://ajplung.physiology.org/content/277/4/L719.abstract

58. Valavanidis A, Fiotakis K, Bakeas E, Vlahogianni T. Electron paramagnetic resonance study of the generation of reactive oxygen species catalysed by transition metals and quinoid redox cycling by inhalable ambient particulate matter. Redox Rep [Internet]. Taylor & Francis; 2005 Feb 1;10(1):37–51. Available from: http://dx.doi.org/10.1179/135100005X21606

59. Aykin-Burns N, Gurer-Orhan H, Ercal N. Toxic Metals and Oxidative Stress Part I: Mechanisms Involved in Me-tal induced Oxidative Damage. Curr Top Med Chem [Internet]. 2001;1(6):529–39. Available from: http://www.eurekaselect.com/81596/article

60. Ghio AJ, Carraway MS, Madden MC. Composition of Air Pollution Particles and Oxidative Stress in Cells, Tissues, and Living Systems. J Toxicol Environ Heal Part B [Internet]. Taylor & Francis; 2012 Jan 1;15(1):1–21. Available from: http://dx.doi.org/10.1080/10937404.2012.632359

61. Manke A, Wang L, Rojanasakul Y. Mechanisms of Nanoparticle-Induced Oxidative Stress and Toxicity. Biomed Res Int [Internet]. 2013;2013(942916). Available from: https://www.hindawi.com/journals/bmri/2013/942916/

62. Pourazar J, Mudway IS, Samet JM, Helleday R, Blomberg A, Wilson SJ, et al. Diesel exhaust activates redox-sensitive transcription factors and kinases in human airways. Am J Physiol - Lung Cell Mol Physiol [Internet]. 2005 Oct 7;289(5):L724. Available

from: http://ajplung.physiology.org/content/289/5/L724.abstract

63. Hashimoto S, Gon Y, Takeshita I, Matsumoto K, Jibiki I, Takizawa H, et al. Diesel Exhaust Particles Activate p38 MAP Kinase to Produce Interleukin 8 and RANTES by Human Bronchial Epithelial Cells and N-Acetylcysteine Attenuates p38 MAP Kinase Activation. Am J Respir Crit Care Med [Internet]. American Thoracic Society - AJRCCM; 2000 Jan 1;161(1):280–5. Available from: http://dx.doi.org/10.1164/ajrccm.161.1.9904110

64. Takizawa H, Ohtoshi T, Kawasaki S, Kohyama T, Desaki M, Kasama T, et al. Diesel Exhaust Particles Induce NF-κB Activation in Human Bronchial Epithelial Cells In Vitro: Importance in Cytokine Transcription. J Immunol [Internet]. 1999 Apr 15;162(8):4705. Available from: http://www.jimmunol.org/content/162/8/4705.abstract

65. Takizawa H, Abe S, Ohtoshi T, Kawasaki S, Takami K, Desaki M, et al. Diesel exhaust particles up-regulate expression of intercellular adhesion molecule-1 (ICAM-1) in human bronchial epithelial cells. Clin Exp Immunol [Internet]. 2000 May [cited 2017 Mar 6];120(2):356–62. Available from: http://doi.wiley.com/10.1046/j.1365-2249.2000.01213.x

66. Zhao Y, Usatyuk P V., Gorshkova IA, He D, Wang T, Moreno-Vinasco L, et al. Regulation of COX-2 Expression and IL-6 Release by Particulate Matter in Airway Epithelial Cells. Am J Respir Cell Mol Biol [Internet]. American Thoracic Society; 2009 Jan [cited 2017 Mar 6];40(1):19–30. Available from: http://www.atsjournals.org/doi/abs/10.1165/rcmb.2008-0105OC

67. Xiao GG, Wang M, Li N, Loo JA, Nel AE. Use of proteomics to demonstrate a hierarchical oxidative stress response to diesel exhaust particle chemicals in a macrophage cell line. J Biol Chem [Internet]. 2003;278. Available from: http://dx.doi.org/10.1074/jbc.M306423200

68. Becker S, Dailey L, Soukup JM, Silbajoris R, Devlin RB. TLR-2 is involved in airway epithelial cell response to air pollution particles. Toxicol Appl Pharmacol [Internet]. 2005 Feb 15 [cited 2017 Mar 6];203(1):45–52. Available from: http://www.ncbi.nlm.nih.gov/pubmed/15694463

69. Becker S, Mundandhara S, Devlin RB, Madden M. Regulation of cytokine production in human alveolar macrophages and airway epithelial cells in response to ambient air pollution particles: further mechanistic studies. Toxicol Appl Pharmacol [Internet]. 2005;207. Available from: http://dx.doi.org/10.1016/j.taap.2005.01.023

70. Shoenfelt J, Mitkus RJ, Zeisler R, Spatz RO, Powell J, Fenton MJ, et al. Involvement of TLR2 and TLR4 in inflammatory immune responses induced by fine and coarse ambient air particulate matter. J Leukoc Biol [Internet]. 2009 Aug 1 [cited 2017 Mar 6];86(2):303–12. Available from: http://www.ncbi.nlm.nih.gov/pubmed/19406832

71. Jung EJ, Avliyakulov NK, Boontheung P, Loo JA, Nel AE. Pro-oxidative DEP chemicals induce heat shock proteins and an unfolding protein response in a bronchial epithelial cell line as determined by DIGE analysis. Proteomics [Internet]. 2007 Nov [cited 2017 Jul 22];7(21):3906–18. Available from: http://www.ncbi.nlm.nih.gov/pubmed/17922515

72. Gualtieri M, Mantecca P, Cetta F, Camatini M. Organic compounds in tire particle induce reactive oxygen species and heat-shock proteins in the human alveolar cell line A549. Environ Int [Internet]. 2008 May [cited 2017 Jul 22];34(4):437–42. Available from: http://www.ncbi.nlm.nih.gov/pubmed/17976723

73. Mayeux R. Biomarkers: potential uses and limitations. NeuroRx [Internet]. Am. Soc. for Experimental NeuroTherapeutics; 2004 Apr [cited 2017 Mar 6];1(2):182–8. Available from: http://www.ncbi.nlm.nih.gov/pubmed/15717018

74. Timbrell JA. Biomarkers in toxicology. Toxicology [Internet]. 1998 [cited 2017 Apr 24];129(1):1–12. Available from: http://www.sciencedirect.com/science/article/pii/S0300483X98000584

75. Gant TW, Marczylo EL, Leonard MO. Discovery and Application of Novel Biomarkers. In Wiley-VCH Verlag GmbH & Co. KGaA; 2014 [cited 2017 Aug 15]. p. 129–50. Available from: http://doi.wiley.com/10.1002/9783527674183.ch07

76. WHO Task Group on Biomarkers and Risk Assessment: Concepts and Principles., Robinson A, United Nations Environment Programme., International Labour Organisation., World Health Organization., International Program on Chemical Safety. Biomarkers and risk assessment : concepts and principles. World Health Organization; 1993. 82 p.

77. Thier R, Brüning T, Roos PH, Rihs H-P, Golka K, Ko Y, et al. Markers of genetic susceptibility in human environmental hygiene and toxicology: The role of selected CYP, NAT and GST genes. Int J Hyg Environ Health [Internet]. 2003 Jan [cited 2017 May 9];206(3):149–71. Available from: http://linkinghub.elsevier.com/retrieve/pii/S1438463904702060

78. Ulvestad B, Randem BG, Andersson L, Ellingsen DG, Barregard L. Clara Cell Protein

as a Biomarker for Lung Epithelial Injury in Asphalt Workers. J Occup Environ Med [Internet]. 2007 Oct [cited 2017 May 17];49(10):1073–8. Available from: http://www.ncbi.nlm.nih.gov/pubmed/18000412

79. Van Miert E, Dumont X, Bernard A. CC16 as a marker of lung epithelial hyperpermeability in an acute model of rats exposed to mainstream cigarette smoke. Toxicol Lett [Internet]. 2005 [cited 2017 May 16];159(2):115–23. Available from: http://www.sciencedirect.com/science/article/pii/S0378427405001517

80. Arsalane K, Broeckaert F, Knoops B, Wiedig M, Toubeau G, Bernard A. Clara Cell Specific Protein (CC16) Expression after Acute Lung Inflammation Induced by Intratracheal Lipopolysaccharide Administration. Am J Respir Crit Care Med [Internet]. American Thoracic SocietyNew York, NY; 2000 May [cited 2017 May 16];161(5):1624–30. Available from: http://www.atsjournals.org/doi/abs/10.1164/ajrccm.161.5.9812157

81. Neophytou AM, Hart JE, Cavallari JM, Smith TJ, Dockery DW, Coull BA, et al. Traffic-related exposures and biomarkers of systemic inflammation, endothelial activation and oxidative stress: a panel study in the US trucking industry. Environ Heal [Internet]. 2013 Dec 7 [cited 2017 Mar 6];12(1):105. Available from: http://ehjournal.biomedcentral.com/articles/10.1186/1476-069X-12-105

82. Gong J, Zhu T, Kipen H, Rich DQ, Huang W, Lin W-T, et al. Urinary Polycyclic Aromatic Hydrocarbon Metabolites as Biomarkers of Exposure to Traffic-Emitted Pollutants. Environ Int [Internet]. 2015 Dec;85:104–10. Available from: http://www.ncbi.nlm.nih.gov/pmc/articles/PMC4765327/

83. Schenker MB, Samuels SJ, Kado NY, Hammond SK, Smith TJ, Woskie SR. Markers of exposure to diesel exhaust in railroad workers. Res Rep Health Eff Inst [Internet]. 1990 Oct [cited 2017 Apr 26];(33):1-51-64. Available from: http://www.ncbi.nlm.nih.gov/pubmed/2264934

84. Ohtsuka Y, Brunson KJ, Jedlicka AE, Mitzner W, Clarke RW, Zhang L-Y, et al. Genetic Linkage Analysis of Susceptibility to Particle Exposure in Mice. Am J Respir Cell Mol Biol [Internet]. 2000 May [cited 2017 Aug 5];22(5):574–81. Available from: http://www.ncbi.nlm.nih.gov/pubmed/10783129

85. Adonis M, Martínez V, Riquelme R, Ancic P, González G, Tapia R, Castro M, Lucas D, Berthou F GL. Susceptibility and exposure biomarkers in people exposed to PAHs from diesel exhaust. - PubMed - NCBI. Toxicol Lett [Internet]. 2003 [cited 2017 Aug 5];144(1):3–15. Available from: https://www.ncbi.nlm.nih.gov/m/pubmed/12919719/

86. Doberer D, Trejo Bittar HE, Wenzel SE. Should lung biopsies be performed in patients with severe asthma? Eur Respir Rev [Internet]. 2015 Sep [cited 2017 Mar 6];24(137):525–39. Available from: http://err.ersjournals.com/lookup/doi/10.1183/16000617.0045-2015

87. Needham LL, Calafat AM, Barr DB. Uses and issues of biomonitoring. Int J Hyg Environ Health [Internet]. 2007 May [cited 2017 Mar 6];210(3–4):229–38. Available from: http://linkinghub.elsevier.com/retrieve/pii/S1438463906001076

88. Beamer PI, Guerra S, Lothrop N, Stern DA, Lu Z, Billheimer D, et al. Childhood CC16 Levels are Associated with Diesel Exposure at Birth. In: B46 HEALTH EFFECTS OF AIR POLLUTION AND NANOPARTICLES [Internet]. American Thoracic Society; 2015. p. A3202–A3202. Available from: http://dx.doi.org/10.1164/ajrccm-conference.2015.191.1_MeetingAbstracts.A3202

89. Biagioni BJ, Tam S, Chen Y-WR, Sin DD, Carlsten C. Effect of controlled human exposure to diesel exhaust and allergen on airway surfactant protein D, myeloperoxidase and club (Clara) cell secretory protein 16. Clin Exp Allergy [Internet]. 2016 Sep [cited 2017 Mar 6];46(9):1206–13. Available from: http://www.ncbi.nlm.nih.gov/pubmed/27018153

90. Alexeeff C, Andrew Coull B, Gryparis A, Suh H, Sparrow D, Vokonas PS, et al. Medium-Term Exposure to Traffic-Related Air Pollution and Markers of Inflammation and Endothelial Function. Environ Health Perspect [Internet]. 2017 [cited 2017 Mar 7];119(4):481–6. Available from: https://dash.harvard.edu/bitstream/handle/1/8830769/3080929.pdf?sequence=1

91. Singh S, Singhal NK, Srivastava G, Singh MP. Omics in mechanistic and predictive toxicology. Toxicol Mech Methods [Internet]. Taylor & Francis; 2010 Sep 18 [cited 2017 Mar 6];20(7):355–62. Available from: http://www.tandfonline.com/doi/full/10.3109/15376510903559976

92. Ghosh D, Poisson LM. “Omics” data and levels of evidence for biomarker discovery. Genomics [Internet]. 2009 Jan [cited 2017 Mar 6];93(1):13–6. Available from: http://linkinghub.elsevier.com/retrieve/pii/S088875430800164X

93. Khatri P, Sirota M, Butte AJ, Kim S, Woo H. Ten Years of Pathway Analysis: Current Approaches and Outstanding Challenges. Ouzounis CA, editor. PLoS Comput Biol [Internet]. Public Library of Science; 2012 Feb 23 [cited 2017 Mar 6];8(2):e1002375. Available from: http://dx.plos.org/10.1371/journal.pcbi.1002375

94. Xiao GG, Wang M, Li N, Loo JA, Nel AE. Use of Proteomics to Demonstrate a Hierarchical Oxidative Stress Response to Diesel Exhaust Particle Chemicals in a Macrophage Cell Line. J Biol Chem [Internet]. 2003 Dec 12 [cited 2017 Mar 6];278(50):50781–90. Available from: http://www.ncbi.nlm.nih.gov/pubmed/14522998

95. Yin XJ, Dong CC, Ma JYC, Roberts JR, Antonini JM, Ma JKH. Suppression of Phagocytic and Bactericidal Functions of Rat Alveolar Macrophages by the Organic Component of Diesel Exhaust Particles. J Toxicol Environ Heal Part A [Internet]. 2007 Apr 11 [cited 2017 Mar 9];70(10):820–8. Available from: http://www.ncbi.nlm.nih.gov/pubmed/17454558

96. Yang HM, Antonini JM, Barger MW, Butterworth L, Roberts BR, Ma JK, et al. Diesel exhaust particles suppress macrophage function and slow the pulmonary clearance of Listeria monocytogenes in rats. Environ Health Perspect [Internet]. 2001 May;109(5):515–21. Available from: http://www.ncbi.nlm.nih.gov/pmc/articles/PMC1240312/

97. Coleman DL. Regulation of macrophage phagocytosis. Eur J Clin Microbiol [Internet]. 1986 Feb [cited 2017 Mar 6];5(1):1–5. Available from: http://www.ncbi.nlm.nih.gov/pubmed/3084238

98. Verheyen GR, Nuijten J-M, Van Hummelen P, Schoeters GR. Microarray analysis of the effect of diesel exhaust particles on in vitro cultured macrophages. Toxicol Vitr [Internet]. 2004 Jun [cited 2017 Mar 6];18(3):377–91. Available from: http://linkinghub.elsevier.com/retrieve/pii/S0887233303002170

99. Brower JB, Doyle-Eisele M, Moeller B, Stirdivant S, McDonald JD, Campen MJ. Metabolomic changes in murine serum following inhalation exposure to gasoline and diesel engine emissions. Inhal Toxicol [Internet]. Taylor & Francis; 2016 Apr 15;28(5):241–50. Available from: http://dx.doi.org/10.3109/08958378.2016.1155003

100. Oeder S, Kanashova T, Sippula O, Sapcariu SC, Streibel T, Arteaga-Salas JM, et al. Particulate Matter from Both Heavy Fuel Oil and Diesel Fuel Shipping Emissions Show Strong Biological Effects on Human Lung Cells at Realistic and Comparable In Vitro Exposure Conditions. PLoS One [Internet]. Public Library of Science; 2015 Jun 3;10(6):e0126536-. Available from: http://dx.doi.org/10.1371%252Fjournal.pone.0126536

101. Fitzpatrick M, Young SP. Metabolomics--a novel window into inflammatory disease. Swiss Med Wkly [Internet]. Europe PMC Funders; 2013 Jan 21 [cited 2017 Mar 6];143:w13743. Available from: http://www.ncbi.nlm.nih.gov/pubmed/23348753

102. Cavill R, Jennen D, Kleinjans J, Briedé JJ. Transcriptomic and metabolomic data integration. Brief Bioinform [Internet]. Oxford University Press; 2016 Sep [cited 2017 Mar 7];17(5):891–901. Available from: https://academic.oup.com/bib/article-lookup/doi/10.1093/bib/bbv090

103. Koike E, Hirano S, Shimojo N, Kobayashi T. cDNA Microarray Analysis of Gene Expression in Rat Alveolar Macrophages in Response to Organic Extract of Diesel Exhaust Particles. Toxicol Sci [Internet]. 2002 Jun 1;67(2):241–6. Available from: http://dx.doi.org/10.1093/toxsci/67.2.241

104. Jardim M, Fry R, Jaspers I, Dailey L, Diaz-Sanchez D. Disruption of MicroRNA Expression in Human Airway Cells by Diesel Exhaust Particles is Linked to Tumorigenesis-Associated Pathways. Environ Health Perspect [Internet]. 2009 Jun 18 [cited 2017 Mar 6];117(11):1745–51. Available from: http://www.ncbi.nlm.nih.gov/pubmed/20049127

105. Cavill R, Kamburov A, Ellis JK, Athersuch TJ, Blagrove MSC, Herwig R, et al. Consensus-Phenotype Integration of Transcriptomic and Metabolomic Data Implies a Role for Metabolism in the Chemosensitivity of Tumour Cells. PLOS Comput Biol [Internet]. Public Library of Science; 2011 Mar 31;7(3):e1001113-. Available from: http://dx.doi.org/10.1371%252Fjournal.pcbi.1001113

106. Anwar MA, Adesina-Georgiadis KN, Spagou K, Vorkas PA, Li J V., Shalhoub J, et al. A comprehensive characterisation of the metabolic profile of varicose veins; implications in elaborating plausible cellular pathways for disease pathogenesis. Sci Rep [Internet]. 2017 Dec 7 [cited 2017 Jul 2];7(1):2989. Available from: http://www.ncbi.nlm.nih.gov/pubmed/28592827

107. Wu Q, Li J V, Seyfried F, le Roux CW, Ashrafian H, Athanasiou T, et al. Metabolic phenotype-microRNA data fusion analysis of the systemic consequences of Roux-en-Y gastric bypass surgery. Int J Obes [Internet]. 2015 Jul 18 [cited 2017 Aug 7];39(7):1126–34. Available from: http://www.ncbi.nlm.nih.gov/pubmed/25783038

108. Rodrigues AC, Li X, Radecki L, Pan Y-Z, Winter JC, Huang M, et al. MicroRNA expression is differentially altered by xenobiotic drugs in different human cell lines. Biopharm Drug Dispos [Internet]. NIH Public Access; 2011 Sep [cited 2017 Jul 8];32(6):355–67. Available from: http://www.ncbi.nlm.nih.gov/pubmed/21796641

109. Koufaris C, Wright J, Currie RA, Gooderham NJ. Hepatic MicroRNA Profiles Offer Predictive and Mechanistic Insights After Exposure to Genotoxic and Epigenetic Hepatocarcinogens. Toxicol Sci [Internet]. 2012 Aug [cited 2017 Dec 19];128(2):532–

43. Available from: http://www.ncbi.nlm.nih.gov/pubmed/22584684

110. Dluzen DF, Lazarus P. MicroRNA regulation of the major drug-metabolizing enzymes and related transcription factors. Drug Metab Rev [Internet]. Taylor & Francis; 2015 Jul 3;47(3):320–34. Available from: http://www.tandfonline.com/doi/abs/10.3109/03602532.2015.1076438

111. Le Vee M, Jouan E, Stieger B, Lecureur V, Fardel O. Regulation of Human Hepatic Drug Transporter Activity and Expression by Diesel Exhaust Particle Extract. Rodrigues-Lima F, editor. PLoS One [Internet]. 2015 Mar 24 [cited 2017 Jul 8];10(3):e0121232. Available from: http://www.ncbi.nlm.nih.gov/pubmed/25803276

112. Wang Y, Liu J, Huang BO, Xu Y-M, Li J, Huang L-F, et al. Mechanism of alternative splicing and its regulation. Biomed reports [Internet]. Spandidos Publications; 2015 Mar [cited 2017 Aug 7];3(2):152–8. Available from: http://www.ncbi.nlm.nih.gov/pubmed/25798239

113. Cooper GM. The cell : a molecular approach. ASM Press; 2000. 689 p.

114. Licht K, Jantsch MF. Rapid and dynamic transcriptome regulation by RNA editing and RNA modifications. J Cell Biol [Internet]. 2016 [cited 2017 Aug 7];213(1). Available from: http://jcb.rupress.org/content/213/1/15

115. Vogel C, Marcotte EM. Insights into the regulation of protein abundance from proteomic and transcriptomic analyses. Nat Rev Genet [Internet]. 2012 Mar 13 [cited 2017 Aug 8];13(4):227–32. Available from: http://www.ncbi.nlm.nih.gov/pubmed/22411467

116. Fernie AR, Stitt M. On the Discordance of Metabolomics with Proteomics and Transcriptomics: Coping with Increasing Complexity in Logic, Chemistry, and Network Interactions Scientific Correspondence. Plant Physiol [Internet]. 2012 [cited 2017 Aug 7];158(3). Available from: http://www.plantphysiol.org/content/158/3/1139

117. Siddeek B, Inoubli L, Lakhdari N, Rachel PB, Fussell KC, Schneider S, et al. MicroRNAs as potential biomarkers in diseases and toxicology. Mutat Res Toxicol Environ Mutagen [Internet]. 2014 Apr [cited 2017 Mar 6];764–765:46–57. Available from: http://linkinghub.elsevier.com/retrieve/pii/S1383571814000254

118. Griffiths S. The miRBase Sequence Database: Release 21 [Internet]. 2014. Available from: http://www.mirbase.org/

119. Valinezhad Orang A, Safaralizadeh R, Kazemzadeh-Bavili M. Mechanisms of miRNA-

Mediated Gene Regulation from Common Downregulation to mRNA-Specific Upregulation. Int J Genomics [Internet]. Hindawi Publishing Corporation; 2014 [cited 2017 Mar 6];2014:970607. Available from: http://www.ncbi.nlm.nih.gov/pubmed/25180174

120. Olena AF, Patton JG. Genomic organization of microRNAs. J Cell Physiol [Internet]. NIH Public Access; 2010 Mar [cited 2017 Mar 6];222(3):540–5. Available from: http://www.ncbi.nlm.nih.gov/pubmed/20020507

121. Meijer HA, Smith EM, Bushell M. Regulation of miRNA strand selection: follow the leader? Biochem Soc Trans [Internet]. 2014 Aug 1 [cited 2017 Mar 6];42(4):1135–40. Available from: http://www.ncbi.nlm.nih.gov/pubmed/25110015

122. Humphreys DT, Westman BJ, Martin DIK, Preiss T. MicroRNAs control translation initiation by inhibiting eukaryotic initiation factor 4E/cap and poly(A) tail function. Proc Natl Acad Sci U S A [Internet]. National Academy of Sciences; 2005 Nov 22 [cited 2017 Mar 6];102(47):16961–6. Available from: http://www.ncbi.nlm.nih.gov/pubmed/16287976

123. Gu S, Kay MA. How do miRNAs mediate translational repression? Silence [Internet]. BioMed Central; 2010 May 7 [cited 2017 Mar 6];1(1):11. Available from: http://www.ncbi.nlm.nih.gov/pubmed/20459656

124. Fabian MR, Sundermeier TR, Sonenberg N. Understanding How miRNAs Post-Transcriptionally Regulate Gene Expression. In Springer Berlin Heidelberg; 2010 [cited 2017 Mar 6]. p. 1–20. Available from: http://link.springer.com/10.1007/978-3-642-03103-8_1

125. Pillai RS. Inhibition of Translational Initiation by Let-7 MicroRNA in Human Cells. Science (80-) [Internet]. 2005 Sep 2 [cited 2017 Mar 6];309(5740):1573–6. Available from: http://www.sciencemag.org/cgi/doi/10.1126/science.1115079

126. Chendrimada TP, Finn KJ, Ji X, Baillat D, Gregory RI, Liebhaber SA, et al. MicroRNA silencing through RISC recruitment of eIF6. Nature [Internet]. 2007 Jul 14 [cited 2017 Mar 6];447(7146):823–8. Available from: http://www.ncbi.nlm.nih.gov/pubmed/17507929

127. Behm-Ansmant I, Rehwinkel J, Doerks T, Stark A, Bork P, Izaurralde E. mRNA degradation by miRNAs and GW182 requires both CCR4:NOT deadenylase and DCP1:DCP2 decapping complexes. Genes Dev [Internet]. Cold Spring Harbor Laboratory Press; 2006 Jul 15 [cited 2017 Mar 6];20(14):1885–98. Available from:

http://www.ncbi.nlm.nih.gov/pubmed/16815998

128. Eulalio A, Tritschler F, Izaurralde E. The GW182 protein family in animal cells: New insights into domains required for miRNA-mediated gene silencing. RNA [Internet]. 2009 Aug 1 [cited 2017 Aug 7];15(8):1433–42. Available from: http://www.ncbi.nlm.nih.gov/pubmed/19535464

129. Chan EKL, Fritzler MJ. Ten years of progress in GW/P body research [Internet]. Springer; 2013 [cited 2017 Mar 6]. Available from: https://books.google.co.uk/books?id=9u67iz_VnasC&pg=PA258&lpg=PA258&dq=GW182+proteins+AND+mRNA+degradation&source=bl&ots=8QrpjogzxS&sig=bz2JwPfmYCVGJpK9Duu9KBsApWE&hl=en&sa=X&ved=0ahUKEwiZsuTH1sbPAhWpJsAKHXy2DgYQ6AEIWTAI#v=onepage&q=elongation&f=false

130. Chen C-YA, Shyu A-B. Deadenylation and P-bodies. Adv Exp Med Biol [Internet]. NIH Public Access; 2013 [cited 2017 Mar 6];768:183–95. Available from: http://www.ncbi.nlm.nih.gov/pubmed/23224971

131. Petersen CP, Bordeleau M-E, Pelletier J, Sharp PA. Short RNAs Repress Translation after Initiation in Mammalian Cells. Mol Cell [Internet]. 2006 Feb [cited 2017 Mar 6];21(4):533–42. Available from: http://linkinghub.elsevier.com/retrieve/pii/S1097276506000773

132. Nottrott S, Simard MJ, Richter JD. Human let-7a miRNA blocks protein production on actively translating polyribosomes. Nat Struct Mol Biol [Internet]. 2006 Dec 26 [cited 2017 Mar 6];13(12):1108–14. Available from: http://www.ncbi.nlm.nih.gov/pubmed/17128272

133. Place RF, Li L-C, Pookot D, Noonan EJ, Dahiya R. MicroRNA-373 induces expression of genes with complementary promoter sequences. Proc Natl Acad Sci [Internet]. 2008 Feb 5;105(5):1608–13. Available from: http://www.pnas.org/content/105/5/1608.abstract

134. Lin C-C, Liu L-Z, Addison JB, Wonderlin WF, Ivanov A V, Ruppert JM. A KLF4–miRNA-206 Autoregulatory Feedback Loop Can Promote or Inhibit Protein Translation Depending upon Cell Context. Mol Cell Biol [Internet]. 1752 N St., N.W., Washington, DC: American Society for Microbiology; 2011 Jun;31(12):2513–27. Available from: http://www.ncbi.nlm.nih.gov/pmc/articles/PMC3133414/

135. Iwasaki S, Tomari Y. Argonaute-mediated translational repression (and activation). Taylor Fr [Internet]. 2009;3(3):205–8. Available from:

http://www.tandfonline.com/doi/pdf/10.4161/fly.3.3.9025

136. Vasudevan S, Steitz JA. AU-rich-element-mediated upregulation of translation by FXR1 and Argonaute 2. Cell [Internet]. NIH Public Access; 2007 Mar 23 [cited 2017 Mar 6];128(6):1105–18. Available from: http://www.ncbi.nlm.nih.gov/pubmed/17382880

137. Ma F, Liu X, Li D, Wang P, Li N, Lu L, et al. MicroRNA-466l Upregulates IL-10 Expression in TLR-Triggered Macrophages by Antagonizing RNA-Binding Protein Tristetraprolin-Mediated IL-10 mRNA Degradation. J Immunol [Internet]. 2010 May 18;184(11):6053. Available from: http://www.jimmunol.org/content/184/11/6053.abstract

138. Chim SSC, Shing TKF, Hung ECW, Leung T -y., Lau T -k., Chiu RWK, et al. Detection and Characterization of Placental MicroRNAs in Maternal Plasma. Clin Chem [Internet]. 2008 Mar 1 [cited 2017 Mar 6];54(3):482–90. Available from: http://www.ncbi.nlm.nih.gov/pubmed/18218722

139. Lawrie CH, Gal S, Dunlop HM, Pushkaran B, Liggins AP, Pulford K, et al. Detection of elevated levels of tumour-associated microRNAs in serum of patients with diffuse large B-cell lymphoma. Br J Haematol [Internet]. Blackwell Publishing Ltd; 2008 Jun [cited 2017 Mar 6];141(5):672–5. Available from: http://doi.wiley.com/10.1111/j.1365-2141.2008.07077.x

140. Chen X, Ba Y, Ma L, Cai X, Yin Y, Wang K, et al. Characterization of microRNAs in serum: a novel class of biomarkers for diagnosis of cancer and other diseases. Cell Res [Internet]. Nature Publishing Group; 2008 Oct [cited 2017 Mar 6];18(10):997–1006. Available from: http://www.nature.com/doifinder/10.1038/cr.2008.282

141. Weber JA, Baxter DH, Zhang S, Huang DY, How Huang K, Jen Lee M, et al. The MicroRNA Spectrum in 12 Body Fluids. Clin Chem [Internet]. 2010 Nov 1 [cited 2017 Mar 7];56(11):1733–41. Available from: http://www.ncbi.nlm.nih.gov/pubmed/20847327

142. Valadi H, Ekström K, Bossios A, Sjöstrand M, Lee JJ, Lötvall JO. Exosome-mediated transfer of mRNAs and microRNAs is a novel mechanism of genetic exchange between cells. Nat Cell Biol [Internet]. 2007 Jun 7 [cited 2017 Mar 7];9(6):654–9. Available from: http://www.ncbi.nlm.nih.gov/pubmed/17486113

143. Turchinovich A, Weiz L, Burwinkel B. Extracellular miRNAs: the mystery of their origin and function. Trends Biochem Sci [Internet]. 2012 Nov [cited 2017 Mar 6];37(11):460–

5. Available from: http://linkinghub.elsevier.com/retrieve/pii/S0968000412001156

144. Pegtel DM, Cosmopoulos K, Thorley-Lawson DA, van Eijndhoven MAJ, Hopmans ES, Lindenberg JL, et al. Functional delivery of viral miRNAs via exosomes. Proc Natl Acad Sci [Internet]. 2010 Apr 6;107(14):6328–33. Available from: http://www.pnas.org/content/107/14/6328.abstract

145. Zhang Y, Liu D, Chen X, Li J, Li L, Bian Z, et al. Secreted monocytic miR-150 enhances targeted endothelial cell migration. Mol Cell [Internet]. Obesity, Silver Spring; 2010 Jul 9 [cited 2017 Mar 6];39(1):133–44. Available from: http://www.ncbi.nlm.nih.gov/pubmed/20603081

146. Gibbings DJ, Ciaudo C, Erhardt M, Voinnet O. Multivesicular bodies associate with components of miRNA effector complexes and modulate miRNA activity. Nat Cell Biol [Internet]. Nature Publishing Group; 2009 Sep 16 [cited 2017 Mar 6];11(9):1143–9. Available from: http://www.nature.com/doifinder/10.1038/ncb1929

147. Collino F, Deregibus MC, Bruno S, Sterpone L, Aghemo G, Viltono L, et al. Microvesicles Derived from Adult Human Bone Marrow and Tissue Specific Mesenchymal Stem Cells Shuttle Selected Pattern of miRNAs. PLoS One [Internet]. Public Library of Science; 2010 Jul 27;5(7):e11803-. Available from: http://dx.doi.org/10.1371%252Fjournal.pone.0011803

148. Zhou F, Li S, Jia W, Lv G, Song C, Kang C, et al. Molecular medicine reports. [Internet]. Molecular Medicine Reports. D.A. Spandidos; 2015 [cited 2017 Mar 6]. 2329-2335 p. Available from: https://www.spandidos-publications.com/mmr/12/2/2329

149. Bleck B, Grunig G, Chiu A, Liu M, Gordon T, Kazeros A, et al. MicroRNA-375 regulation of thymic stromal lymphopoietin by diesel exhaust particles and ambient particulate matter in human bronchial epithelial cells(). J Immunol [Internet]. 2013 Apr 1;190(7):3757–63. Available from: http://www.ncbi.nlm.nih.gov/pmc/articles/PMC3665109/

150. Bourdon JA, Saber AT, Halappanavar S, Jackson PA, Wu D, Hougaard KS, et al. Carbon black nanoparticle intratracheal installation results in large and sustained changes in the expression of miR-135b in mouse lung. Environ Mol Mutagen [Internet]. 2012 Jul [cited 2017 Feb 21];53(6):462–8. Available from: http://www.ncbi.nlm.nih.gov/pubmed/22753103

151. Rodosthenous RS, Coull BA, Lu Q, Vokonas PS, Schwartz JD, Baccarelli AA. Ambient particulate matter and microRNAs in extracellular vesicles: a pilot study of

older individuals. Part Fibre Toxicol [Internet]. 2016;13(1):13. Available from: http://dx.doi.org/10.1186/s12989-016-0121-0

152. Bollati V, Angelici L, Rizzo G, Pergoli L, Rota F, Hoxha M, et al. Microvesicle-associated microRNA expression is altered upon particulate matter exposure in healthy workers and in A549 cells. J Appl Toxicol [Internet]. Wiley-Blackwell; 2015 Jan [cited 2017 Mar 7];35(1):59–67. Available from: http://www.ncbi.nlm.nih.gov/pubmed/24515752

153. Thomou T, Mori MA, Dreyfuss JM, Konishi M, Sakaguchi M, Wolfrum C, et al. Adipose-derived circulating miRNAs regulate gene expression in other tissues. Nature [Internet]. 2017 Feb 15 [cited 2017 Aug 8];542(7642):450–5. Available from: http://www.ncbi.nlm.nih.gov/pubmed/28199304

154. Zhuang X, Li Z, Lin H, Gu L, Lin Q, Lu Z, et al. Integrated miRNA and mRNA expression profiling to identify mRNA targets of dysregulated miRNAs in non-obstructive azoospermia. Sci Rep [Internet]. Nature Publishing Group; 2015 Jan 28 [cited 2017 Mar 7];5:7922. Available from: http://www.ncbi.nlm.nih.gov/pubmed/25628250

155. Xu Z, Xu X, Zhong M, Hotchkiss IP, Lewandowski RP, Wagner JG, et al. Ambient particulate air pollution induces oxidative stress and alterations of mitochondria and gene expression in brown and white adipose tissues. Part Fibre Toxicol [Internet]. 2011;8(1):20. Available from: http://dx.doi.org/10.1186/1743-8977-8-20

156. Kim JW, Park S, Lim CW, Lee K, Kim B. The role of air pollutants in initiating liver disease. Toxicol Res [Internet]. Korean Society of Toxicology; 2014 Jun [cited 2017 Mar 6];30(2):65–70. Available from: http://www.ncbi.nlm.nih.gov/pubmed/25071914

157. Motta V, Angelici L, Nordio F, Bollati V, Fossati S, Frascati F, et al. Integrative Analysis of miRNA and Inflammatory Gene Expression After Acute Particulate Matter Exposure. Toxicol Sci [Internet]. US: Oxford University Press; 2013 Apr;132(2):307–16. Available from: http://www.ncbi.nlm.nih.gov/pmc/articles/PMC3595525/

158. Bollati V, Marinelli B, Apostoli P, Bonzini M, Nordio F, Hoxha M, et al. Exposure to Metal-Rich Particulate Matter Modifies the Expression of Candidate MicroRNAs in Peripheral Blood Leukocytes. Environ Health Perspect [Internet]. National Institute of Environmental Health Sciences; 2010 Jun;118(6):763–8. Available from: http://www.ncbi.nlm.nih.gov/pmc/articles/PMC2898851/

159. Fossati S, Baccarelli A, Zanobetti A, Hoxha M, Vokonas PS, Wright RO, et al.

Ambient particulate air pollution and microRNAs in elderly men. Epidemiology [Internet]. NIH Public Access; 2014 Jan [cited 2017 Aug 8];25(1):68–78. Available from: http://www.ncbi.nlm.nih.gov/pubmed/24257509

160. Pritchard CC, Cheng HH, Tewari M. MicroRNA profiling: approaches and considerations. Nat Rev Genet [Internet]. Nature Publishing Group, a division of Macmillan Publishers Limited. All Rights Reserved.; 2012 May;13(5):358–69. Available from: http://dx.doi.org/10.1038/nrg3198

161. Liu C-G, Calin GA, Volinia S, Croce CM. MicroRNA expression profiling using microarrays. Nat Protoc [Internet]. Nature Publishing Group; 2008 Apr 13 [cited 2017 Aug 8];3(4):563–78. Available from: http://www.nature.com/doifinder/10.1038/nprot.2008.14

162. Illumina. An Introduction to Next Generation Sequencing Technologys [Internet]. 2016. Available from: https://www.illumina.com/content/dam/illumina-marketing/documents/products/illumina_sequencing_introduction.pdf

163. Life Technologies Corporation. Ion torrent: Amplicon sequencing [Internet]. 2011. Available from: https://www3.appliedbiosystems.com/cms/groups/applied_markets_marketing/documents/generaldocuments/cms_094273.pdf

164. Liu J, Jennings SF, Tong W, Hong H. Next generation sequencing for profiling expression of miRNAs: technical progress and applications in drug development. J Biomed Sci Eng [Internet]. NIH Public Access; 2011 Oct [cited 2017 Aug 22];4(10):666–76. Available from: http://www.ncbi.nlm.nih.gov/pubmed/22457835

165. Harris ED, Biochemistry P, and B. Biochemical Facts behind the Definition and Properties of METABOLITES. [cited 2017 Jul 4]; Available from: https://www.fda.gov/ohrms/dockets/ac/03/briefing/3942b1_08_Harris Paper.pdf

166. Nicholson JK, Wilson ID. Opinion: Understanding “Global” Systems Biology: Metabonomics and the Continuum of Metabolism. Nat Rev Drug Discov [Internet]. Nature Publishing Group; 2003 Aug 1 [cited 2017 Jul 9];2(8):668–76. Available from: http://www.nature.com/doifinder/10.1038/nrd1157

167. Bullock C. The biochemistry of alcohol metabolism — A brief review. Biochem Educ [Internet]. Headington Hill Hall; 1990 Apr [cited 2017 Mar 7];18(2):62–6. Available from: http://linkinghub.elsevier.com/retrieve/pii/030744129090174M

168. Nicholson JK. Global systems biology, personalized medicine and molecular

epidemiology. Mol Syst Biol [Internet]. European Molecular Biology Organization; 2006 [cited 2017 Jul 9];2:52. Available from: http://www.ncbi.nlm.nih.gov/pubmed/17016518

169. Athersuch TJ, Keun HC. Metabolic profiling in human exposome studies. Mutagenesis [Internet]. Oxford University Press; 2015 Aug 18 [cited 2017 Jul 9];111(6):gev060. Available from: https://academic.oup.com/mutage/article-lookup/doi/10.1093/mutage/gev060

170. Athersuch T. Metabolome analyses in exposome studies: Profiling methods for a vast chemical space. Arch Biochem Biophys [Internet]. 2016 Jan [cited 2017 Jul 9];589:177–86. Available from: http://linkinghub.elsevier.com/retrieve/pii/S0003986115300825

171. Nicholson J, Lindon J, Holmes E. Metabonomics ' : understanding the metabolic responses of living systems to pathophysiological stimuli via multivariate statistical analysis of biological NMR spectroscopic data. xenobiotica [Internet]. 1999 [cited 2017 Jul 9];29(11):1181–9. Available from: http://www.tandfonline.com/doi/pdf/10.1080/004982599238047?needAccess=true

172. Griffiths WJ, Koal T, Wang Y, Kohl M, Enot DP, Deigner H-P. Targeted metabolomics for biomarker discovery. Angew Chem Int Ed Engl [Internet]. 2010 Jul 26 [cited 2017 Feb 22];49(32):5426–45. Available from: http://www.ncbi.nlm.nih.gov/pubmed/20629054

173. Vorkas PA, Isaac G, Holmgren A, Want EJ, Shockcor JP, Holmes E, et al. Perturbations in fatty acid metabolism and apoptosis are manifested in calcific coronary artery disease: An exploratory lipidomic study. Int J Cardiol [Internet]. 2015 Oct [cited 2017 Aug 9];197:192–9. Available from: http://linkinghub.elsevier.com/retrieve/pii/S0167527315013492

174. Ellis JK, Athersuch TJ, Thomas LDK, Teichert F, Pérez-Trujillo M, Svendsen C, et al. Metabolic profiling detects early effects of environmental and lifestyle exposure to cadmium in a human population. BMC Med [Internet]. BioMed Central; 2012;10:61. Available from: http://www.ncbi.nlm.nih.gov/pmc/articles/PMC3391181/

175. Coen M, Holmes E, Lindon JC, Nicholson JK. NMR-Based Metabolic Profiling and Metabonomic Approaches to Problems in Molecular Toxicology. Chem Res Toxicol [Internet]. 2008 Jan [cited 2017 Aug 9];21(1):9–27. Available from: http://pubs.acs.org/doi/abs/10.1021/tx700335d

176. Sureshchandra S, Rais M, Stull C, Grant K, Messaoudi I, Barsky A. Transcriptome Profiling Reveals Disruption of Innate Immunity in Chronic Heavy Ethanol Consuming Female Rhesus Macaques. Luo J, editor. PLoS One [Internet]. Public Library of Science; 2016 Jul 18 [cited 2017 Aug 22];11(7):e0159295. Available from: http://dx.plos.org/10.1371/journal.pone.0159295

177. Link G, Saada A, Pinson A, Konijn AM, Hershko C. Mitochondrial respiratory enzymes are a major target of iron toxicity in rat heart cells. J Lab Clin Med [Internet]. 1998 May [cited 2017 Feb 22];131(5):466–74. Available from: http://linkinghub.elsevier.com/retrieve/pii/S0022214398901482

178. Al-Belooshi T, John A, Tariq S, Al-Otaiba A, Raza H. Increased mitochondrial stress and modulation of mitochondrial respiratory enzyme activities in acetaminophen-induced toxicity in mouse macrophage cells. Food Chem Toxicol [Internet]. 2010 Oct [cited 2017 Aug 9];48(10):2624–32. Available from: http://linkinghub.elsevier.com/retrieve/pii/S0278691510004059

179. Barton RH, Nicholson JK, Elliott P, Holmes E. High-throughput 1H NMR-based metabolic analysis of human serum and urine for large-scale epidemiological studies: validation study. Int J Epidemiol [Internet]. 2008 Apr 1;37(suppl_1):i31–40. Available from: http://dx.doi.org/10.1093/ije/dym284

180. Psychogios N, Hau DD, Peng J, Guo AC, Mandal R, Bouatra S, et al. The Human Serum Metabolome. PLoS One [Internet]. Public Library of Science; 2011 Feb 16;6(2):e16957-. Available from: http://dx.doi.org/10.1371%252Fjournal.pone.0016957

181. Bouatra S, Aziat F, Mandal R, Guo AC, Wilson MR, Knox C, et al. The Human Urine Metabolome. PLoS One [Internet]. Public Library of Science; 2013 Sep 4;8(9):e73076-. Available from: http://dx.doi.org/10.1371%252Fjournal.pone.0073076

182. Ge Y, Bruno M, Haykal-Coates N, Wallace K, Andrews D, Swank A, et al. Proteomic Assessment of Biochemical Pathways That Are Critical to Nickel-Induced Toxicity Responses in Human Epithelial Cells. PLoS One [Internet]. Public Library of Science; 2016 Sep 14;11(9):e0162522-. Available from: http://dx.doi.org/10.1371%252Fjournal.pone.0162522

183. Malard V, Berenguer F, Prat O, Ruat S, Steinmetz G, Quemeneur E. Global gene expression profiling in human lung cells exposed to cobalt. BMC Genomics [Internet]. 2007;8(1):147. Available from: http://dx.doi.org/10.1186/1471-2164-8-147

184. Huang Y-CT, Li Z, Carter JD, Soukup JM, Schwartz DA, Yang I V. Fine ambient particles induce oxidative stress and metal binding genes in human alveolar macrophages. Am J Respir Cell Mol Biol [Internet]. American Thoracic Society; 2009 Nov [cited 2017 Aug 9];41(5):544–52. Available from: http://www.ncbi.nlm.nih.gov/pubmed/19251948

185. Surowiec I, Karimpour M, Gouveia-Figueira S, Wu J, Unosson J, Bosson JA, et al. Multi-platform metabolomics assays for human lung lavage fluids in an air pollution exposure study. Anal Bioanal Chem [Internet]. Springer Berlin Heidelberg; 2016 Jul 25 [cited 2017 Mar 7];408(17):4751–64. Available from: http://link.springer.com/10.1007/s00216-016-9566-0

186. Brower JB, Doyle-Eisele M, Moeller B, Stirdivant S, McDonald JD, Campen MJ. Metabolomic changes in murine serum following inhalation exposure to gasoline and diesel engine emissions. Inhal Toxicol [Internet]. 2016 Apr 15 [cited 2017 Mar 7];28(5):241–50. Available from: http://www.ncbi.nlm.nih.gov/pubmed/27017952

187. Hatzis C, Godleski JJ, González-Flecha B, Wolfson JM, Koutrakis P. Ambient Particulate Matter Exhibits Direct Inhibitory Effects on Oxidative Stress Enzymes. Environ Sci Technol [Internet]. American Chemical Society; 2006 Apr 1;40(8):2805–11. Available from: http://dx.doi.org/10.1021/es0518732

188. Wishart DS, Tzur D, Knox C, Eisner R, Guo AC, Young N, et al. HMDB: the Human Metabolome Database. Nucleic Acids Res [Internet]. Oxford University Press; 2007 Jan;35(Database issue):D521–6. Available from: http://www.ncbi.nlm.nih.gov/pmc/articles/PMC1899095/

189. Dona AC, Kyriakides M, Scott F, Shephard EA, Varshavi D, Veselkov K, et al. A guide to the identification of metabolites in NMR-based metabonomics/metabolomics experiments. Comput Struct Biotechnol J. 2016;14:135–53.

190. Barnes S, Benton HP, Casazza K, Cooper SJ, Cui X, Du X, et al. Training in metabolomics research. II. Processing and statistical analysis of metabolomics data, metabolite identification, pathway analysis, applications of metabolomics and its future. J Mass Spectrom [Internet]. 2016 Aug 1 [cited 2017 Jul 9];51(8):535–48. Available from: http://doi.wiley.com/10.1002/jms.3780

191. Wishart D. Human Metabolome Database: Database Statistics [Internet]. 2013 [cited 2017 Jun 12]. Available from: http://www.hmdb.ca/statistics#metabolite-statistics

192. Mbughuni MM, Jannetto PJ, Langman LJ. Mass Spectrometry Applications for

Toxicology. EJIFCC [Internet]. International Federation of Clinical Chemistry and Laboratory Medicine; 2016 Dec [cited 2017 Aug 25];27(4):272–87. Available from: http://www.ncbi.nlm.nih.gov/pubmed/28149262

193. Hore PJ. Nuclear magnetic resonance [Internet]. Oxford Chemistry Primers; [cited 2017 Aug 9]. 112 p. Available from: http://global.oup.com/ukhe/product/nuclear-magnetic-resonance-9780198703419?cc=gb&lang=en

194. Nagana Gowda GA, Raftery D. Biomarker Discovery and Translation in Metabolomics. Curr Metabolomics [Internet]. NIH Public Access; 2013 [cited 2017 Aug 24];1(3):227–40. Available from: http://www.ncbi.nlm.nih.gov/pubmed/27134822

195. Fede J-M, Thakur AP, Gooderham NJ, Turesky RJ. Biomonitoring of 2-Amino-1-methyl-6-phenylimidazo[4,5- *b*]pyridine (PhIP) and Its Carcinogenic Metabolites in Urine. Chem Res Toxicol [Internet]. American Chemical Society; 2009 Jun 15 [cited 2017 Aug 24];22(6):1096–105. Available from: http://pubs.acs.org/doi/abs/10.1021/tx900052c

196. Michopoulos F, Lai L, Gika H, Theodoridis G, Wilson I. UPLC-MS-Based Analysis of Human Plasma for Metabonomics Using Solvent Precipitation or Solid Phase Extraction. J Proteome Res [Internet]. American Chemical Society; 2009 Apr 3 [cited 2017 Dec 19];8(4):2114–21. Available from: http://pubs.acs.org/doi/abs/10.1021/pr801045q

197. Want EJ, Wilson ID, Gika H, Theodoridis G, Plumb RS, Shockcor J, et al. Global metabolic profiling procedures for urine using UPLC–MS. Nat Protoc [Internet]. Nature Publishing Group; 2010 Jun 6 [cited 2017 Dec 19];5(6):1005–18. Available from: http://www.nature.com/doifinder/10.1038/nprot.2010.50

198. Beckonert O, Keun HC, Ebbels TMD, Bundy J, Holmes E, Lindon JC, et al. Metabolic profiling, metabolomic and metabonomic procedures for NMR spectroscopy of urine, plasma, serum and tissue extracts. Nat Protoc [Internet]. 2007 Oct [cited 2017 Sep 12];2(11):2692–703. Available from: http://www.ncbi.nlm.nih.gov/pubmed/18007604

199. Psychogios N, Hau DD, Peng J, Guo AC, Mandal R, Bouatra S, et al. The Human Serum Metabolome. Flower D, editor. PLoS One [Internet]. Saunders; 2011 Feb 16 [cited 2017 Mar 7];6(2):e16957. Available from: http://dx.plos.org/10.1371/journal.pone.0016957

200. Cassiède M, Nair S, Dueck M, Mino J, McKay R, Mercier P, et al. Dataset of urinary metabolites measured by 1 H NMR analysis of normal human urine. Data Br

[Internet]. 2017 Feb [cited 2017 Sep 12];10:227–9. Available from: http://linkinghub.elsevier.com/retrieve/pii/S2352340916307612

201. Chen C, Kim S. LC-MS-based Metabolomics of Xenobiotic-induced Toxicities. Comput Struct Biotechnol J [Internet]. Research Network of Computational and Structural Biotechnology; 2013 [cited 2017 Aug 23];4:e201301008. Available from: http://www.ncbi.nlm.nih.gov/pubmed/24688689

202. Hao J, Yang T, Zhou Y, Gao G-Y, Xing F, Peng Y, et al. Serum Metabolomics Analysis Reveals a Distinct Metabolic Profile of Patients with Primary Biliary Cholangitis. Sci Rep [Internet]. 2017 Dec 11 [cited 2017 Aug 24];7(1):784. Available from: http://www.ncbi.nlm.nih.gov/pubmed/28400566

203. Hu JZ, Rommereim DN, Minard KR, Woodstock A, Harrer BJ, Wind RA, et al. Metabolomics in Lung Inflammation:A High-Resolution ^{1} H NMR Study of Mice Exposedto Silica Dust. Toxicol Mech Methods [Internet]. 2008 Jan 9 [cited 2017 Aug 9];18(5):385–98. Available from: http://www.ncbi.nlm.nih.gov/pubmed/20020862

204. Koulman A, Lane GA, Harrison SJ, Volmer DA. From differentiating metabolites to biomarkers. Anal Bioanal Chem [Internet]. Berlin/Heidelberg: Springer-Verlag; 2009 Jun;394(3):663–70. Available from: http://www.ncbi.nlm.nih.gov/pmc/articles/PMC2865640/

205. Bartel J, Krumsiek J, Theis FJ. Statistical methods for the analysis of high-throughput metabolomics data. Comput Struct Biotechnol J [Internet]. Research Network of Computational and Structural Biotechnology (RNCSB) Organization; 2013;4:e201301009. Available from: http://www.ncbi.nlm.nih.gov/pmc/articles/PMC3962125/

206. Smolinska A, Blanchet L, Buydens LMC, Wijmenga SS. NMR and pattern recognition methods in metabolomics: From data acquisition to biomarker discovery: A review. Anal Chim Acta. 2012;750:82–97.

207. Worley B, Powers R. Multivariate Analysis in Metabolomics. Curr Metabolomics [Internet]. 2013;1(1):92–107. Available from: http://www.ncbi.nlm.nih.gov/pmc/articles/PMC4465187/

208. Seagrave J, McDonald JD, Mauderly JL. In vitro versus in vivo exposure to combustion emissions. Exp Toxicol Pathol [Internet]. 2005 [cited 2017 May 6];57:233–8. Available from: http://www.sciencedirect.com/science/article/pii/S0940299305000515

209. Brunekreef B, Holgate ST. Air pollution and health. Lancet (London, England) [Internet]. 2002 Oct 19 [cited 2017 Aug 9];360(9341):1233–42. Available from: http://www.ncbi.nlm.nih.gov/pubmed/12401268

210. Banerjee A, Waters D, Camacho OM, Minet E. Quantification of plasma microRNAs in a group of healthy smokers, ex-smokers and non-smokers and correlation to biomarkers of tobacco exposure. Biomarkers [Internet]. Taylor & Francis; 2015 Mar [cited 2017 Jun 7];20(2):123–31. Available from: http://www.ncbi.nlm.nih.gov/pubmed/25598229

211. Croston TL, Nayak AP, Lemons AR, Goldsmith WT, Gu JK, Germolec DR, et al. Influence of *Aspergillus fumigatus* conidia viability on murine pulmonary microRNA and mRNA expression following subchronic inhalation exposure. Clin Exp Allergy [Internet]. 2016 Oct [cited 2017 Jun 11];46(10):1315–27. Available from: http://www.ncbi.nlm.nih.gov/pubmed/27473664

212. Cruickshank-Quinn CI, Mahaffey S, Justice MJ, Hughes G, Armstrong M, Bowler RP, et al. Transient and Persistent Metabolomic Changes in Plasma following Chronic Cigarette Smoke Exposure in a Mouse Model. Yildirim AÖ, editor. PLoS One [Internet]. Public Library of Science; 2014 Jul 9 [cited 2017 Aug 9];9(7):e101855. Available from: http://dx.plos.org/10.1371/journal.pone.0101855

213. Rider CF, Yamamoto M, Günther OP, Hirota JA, Singh A, Tebbutt SJ, et al. Controlled diesel exhaust and allergen coexposure modulates microRNA and gene expression in humans: Effects on inflammatory lung markers. J Allergy Clin Immunol [Internet]. 2016 Dec [cited 2017 Aug 9];138(6):1690–700. Available from: http://www.ncbi.nlm.nih.gov/pubmed/27283384

214. Adami H-O, Berry SCL, Breckenridge CB, Smith LL, Swenberg JA, Trichopoulos D, et al. Toxicology and epidemiology: improving the science with a framework for combining toxicological and epidemiological evidence to establish causal inference. Toxicol Sci [Internet]. Oxford University Press; 2011 Aug [cited 2017 Jun 11];122(2):223–34. Available from: http://www.ncbi.nlm.nih.gov/pubmed/21561883

215. Sheppard L, Burnett RT, Szpiro AA, Kim S-Y, Jerrett M, Pope CA, et al. Confounding and exposure measurement error in air pollution epidemiology. Air Qual Atmos Health [Internet]. Springer; 2012 Jun [cited 2017 Jun 17];5(2):203–16. Available from: http://www.ncbi.nlm.nih.gov/pubmed/22662023

216. Driscoll KE, Lindenschmidt RC, Maurer JK, Perkins L, Perkins M, Higgins J. Pulmonary response to inhaled silica or titanium dioxide. Toxicol Appl Pharmacol

[Internet]. 1991 Nov [cited 2017 Jun 25];111(2):201–10. Available from: http://www.ncbi.nlm.nih.gov/pubmed/1659753

217. Brain JD, Knudson DE, Sorokin SP, Davis MA. Pulmonary distribution of particles given by intratracheal instillation or by aerosol inhalation. Environ Res [Internet]. 1976 Feb [cited 2017 Jun 25];11(1):13–33. Available from: http://linkinghub.elsevier.com/retrieve/pii/0013935176901079

218. Dorries AM, Valberg PA. Heterogeneity of Phagocytosis for Inhaled versus Instilled Material. Am Rev Respir Dis [Internet]. 1992 Oct [cited 2017 Aug 9];146(4):831–7. Available from: http://www.ncbi.nlm.nih.gov/pubmed/1416406

219. Brown J, Wilson W, Grant L. Dosimetric Comparisons of Particle Deposition and Retention in Rats and Humans. Inhal Toxicol [Internet]. 2005;17(7–8):355–85. Available from: http://www.tandfonline.com/doi/full/10.1080/08958370590929475?scroll=top&needAccess=true

220. Hofmann W, Asgharian B. The Effect of Lung Structure on Mucociliary Clearance and Particle Retention in Human and Rat Lungs. doi.org [Internet]. Oxford University Press (OUP); 2003 Jun 1 [cited 2017 Aug 9];26(2):448–56. Available from: https://academic.oup.com/toxsci/article/73/2/448/1674375/The-Effect-of-Lung-Structure-on-Mucociliary

221. Schermuly R, Schmehl T, Gunther A, Grimminger F, Seeger W, Walmrath D. Ultrasonic Nebulization for Efficient Delivery of Surfactant in a Model of Acute Lung Injury. Am J Respir Crit Care Med [Internet]. 1997 Aug [cited 2017 Jun 25];156(2):445–53. Available from: http://www.ncbi.nlm.nih.gov/pubmed/9279222

222. Osier M, Baggs RB, Oberdörster G. Intratracheal instillation versus intratracheal inhalation: influence of cytokines on inflammatory response. Environ Health Perspect [Internet]. 1997 Sep [cited 2017 Aug 9];105 Suppl 5:1265–71. Available from: http://www.ncbi.nlm.nih.gov/pubmed/9400736

223. Nei M, Glazko G V. Estimation of Divergence Times for a Few Mammalian and Several Primate Species. Am Genet Assoc [Internet]. 2002 [cited 2017 Jun 28];93:157–64. Available from: http://php.scripts.psu.edu/nxm2/2002 Publications/2002-nei-glazko.pdf

224. Schroder K, Irvine KM, Taylor MS, Bokil NJ, Le Cao K-A, Masterman K-A, et al. Conservation and divergence in Toll-like receptor 4-regulated gene expression in

primary human versus mouse macrophages. Proc Natl Acad Sci U S A [Internet]. National Academy of Sciences; 2012 Apr 17 [cited 2017 Jun 25];109(16):E944-53. Available from: http://www.ncbi.nlm.nih.gov/pubmed/22451944

225. Crapo JD, Barry BE, Gehr P, Bachofen M, Weibel ER. Cell number and cell characteristics of the normal human lung. Am Rev Respir Dis [Internet]. 1982 Jun [cited 2017 Jun 26];125(6):740–5. Available from: http://www.ncbi.nlm.nih.gov/pubmed/7091881

226. Krombach F, Münzing S, Allmeling AM, Gerlach JT, Behr J, Dörger M. Cell size of alveolar macrophages: an interspecies comparison. Environ Health Perspect [Internet]. National Institute of Environmental Health Science; 1997 Sep [cited 2017 Jun 28];105 Suppl 5(Suppl 5):1261–3. Available from: http://www.ncbi.nlm.nih.gov/pubmed/9400735

227. Slade R, Crissman K, Norwood J, Hatch G. Comparison of Antioxidant Substances in Bronchoalveolar Lavage Cells and Fluid from Humans, Guinea Pigs, and Rats. Exp Lung Res [Internet]. Taylor & Francis; 1993 Jan 2 [cited 2017 Jun 26];19(4):469–84. Available from: http://www.tandfonline.com/doi/full/10.3109/01902149309064358

228. Vaure C, Liu Y. A comparative review of toll-like receptor 4 expression and functionality in different animal species. Front Immunol [Internet]. Frontiers Media SA; 2014 [cited 2017 Aug 9];5:316. Available from: http://www.ncbi.nlm.nih.gov/pubmed/25071777

229. Islam AS, Beidelschies MA, Huml A, Greenfield EM. Titanium particles activate toll-like receptor 4 independently of lipid rafts in RAW264.7 murine macrophages. J Orthop Res [Internet]. NIH Public Access; 2011 Feb [cited 2017 Mar 7];29(2):211–7. Available from: http://www.ncbi.nlm.nih.gov/pubmed/20806319

230. Inoue K, Takano H, Yanagisawa R, Hirano S, Ichinose T, Shimada A, et al. The role of toll-like receptor 4 in airway inflammation induced by diesel exhaust particles. Arch Toxicol [Internet]. 2006;80(5):275–9. Available from: http://dx.doi.org/10.1007/s00204-005-0040-6

231. Kim BG, Lee PH, Lee SH, Kim YE, Shin MY, Kang Y, et al. Long-Term Effects of Diesel Exhaust Particles on Airway Inflammation and Remodeling in a Mouse Model. Allergy Asthma Immunol Res [Internet]. Korean Academy of Asthma, Allergy and Clinical Immunology and Korean Academy of Pediatric Allergy and Respiratory Disease; 2016 May [cited 2017 Jul 1];8(3):246–56. Available from: http://www.ncbi.nlm.nih.gov/pubmed/26922935

232. Pickrell JA, Harris D V, Benjamin SA, Cuddihy RG, Pfleger RC, Mauderly JL. Pulmonary collagen metabolism after lung injury from inhaled 90Y in fused clay particles. Exp Mol Pathol [Internet]. 1976 Aug [cited 2017 Jul 1];25(1):70–81. Available from: http://linkinghub.elsevier.com/retrieve/pii/0014480076900186

233. Baroni T, Bodo M, D'Alessandro A, Conte C, Calvitti M, Muzi G, et al. Silica and Its Antagonistic Effects on Transforming Growth Factor-? in Lung Fibroblast Extracellular Matrix Production. J Investig Med [Internet]. 2001 Mar [cited 2017 Jun 29];49(2):146–56. Available from: http://www.ncbi.nlm.nih.gov/pubmed/11288755

234. Warnken M, Haag S, Matthiesen S, Juergens UR, Racké K. Species differences in expression pattern of arginase isoenzymes and differential effects of arginase inhibition on collagen synthesis in human and rat pulmonary fibroblasts. Naunyn Schmiedebergs Arch Pharmacol [Internet]. 2010 Apr 28 [cited 2017 Aug 9];381(4):297–304. Available from: http://link.springer.com/10.1007/s00210-009-0489-6

235. Koufaris C, Gooderham NJ. Are Differences in MicroRNA Regulation Implicated in Species-Dependent Response to Toxicological Exposures? Toxicol Sci [Internet]. Oxford University Press; 2013 Feb 1 [cited 2018 Jan 6];131(2):337–42. Available from: https://academic.oup.com/toxsci/article-lookup/doi/10.1093/toxsci/kfs302

236. Leclercq M, Diallo AB, Blanchette M. Prediction of human miRNA target genes using computationally reconstructed ancestral mammalian sequences. Nucleic Acids Res [Internet]. Oxford University Press; 2017 Jan 25 [cited 2017 Jul 2];45(2):556–66. Available from: http://www.ncbi.nlm.nih.gov/pubmed/27899600

237. Koufaris C, Valbuena GN, Pomyen Y, Tredwell GD, Nevedomskaya E, Lau C-H, et al. Systematic integration of molecular profiles identifies miR-22 as a regulator of lipid and folate metabolism in breast cancer cells. Oncogene [Internet]. Nature Publishing Group; 2016 May 19 [cited 2017 Jul 3];35(21):2766–76. Available from: http://www.nature.com/doifinder/10.1038/onc.2015.333

238. Linsen SE, de Wit E, de Bruijn E, Cuppen E. Small RNA expression and strain specificity in the rat. BMC Genomics [Internet]. 2010 Apr 19 [cited 2017 Aug 9];11(1):249. Available from: http://www.ncbi.nlm.nih.gov/pubmed/20403161

239. Wheeler BM, Heimberg AM, Moy VN, Sperling EA, Holstein TW, Heber S, et al. The deep evolution of metazoan microRNAs. Evol Dev [Internet]. 2009 Jan [cited 2017 Aug 9];11(1):50–68. Available from: http://www.ncbi.nlm.nih.gov/pubmed/19196333

240. Stone V, Johnston H, Schins RPF. Development of *in vitro* systems for nanotoxicology: methodological considerations. Crit Rev Toxicol [Internet]. Taylor & Francis; 2009 Aug 3 [cited 2017 Jun 20];39(7):613–26. Available from: http://www.tandfonline.com/doi/full/10.1080/10408440903120975

241. Goh J-Y, Weaver RJ, Dixon L, Platt NJ, Roberts RA. Development and use of *in vitro* alternatives to animal testing by the pharmaceutical industry 1980–2013. Toxicol Res [Internet]. Royal Society of Chemistry; 2015 Aug 18 [cited 2017 Jul 8];4(5):1297–307. Available from: http://xlink.rsc.org/?DOI=C5TX00123D

242. Franks TJ, Colby T V., Travis WD, Tuder RM, Reynolds HY, Brody AR, et al. Resident Cellular Components of the Human Lung: Current Knowledge and Goals for Research on Cell Phenotyping and Function. Proc Am Thorac Soc [Internet]. 2008 Sep 15 [cited 2017 May 24];5(7):763–6. Available from: http://pats.atsjournals.org/cgi/doi/10.1513/pats.200803-025HR

243. Fröhlich E, Salar-Behzadi S. Toxicological assessment of inhaled nanoparticles: role of in vivo, ex vivo, in vitro, and in silico studies. Int J Mol Sci [Internet]. Multidisciplinary Digital Publishing Institute (MDPI); 2014 Mar 18 [cited 2017 May 23];15(3):4795–822. Available from: http://www.ncbi.nlm.nih.gov/pubmed/24646916

244. Wittekindt OH. Cellular Models for In Vitro Lung Toxicology. In 2014 [cited 2017 May 4]. p. 103–21. Available from: http://link.springer.com/10.1007/978-1-4939-0521-8_5

245. Stacey G. Primary Cell Cultures and Immortal Cell Lines. In: Encyclopedia of Life Sciences [Internet]. Chichester, UK: John Wiley & Sons, Ltd; 2006 [cited 2017 Jun 19]. Available from: http://doi.wiley.com/10.1038/npg.els.0003960

246. Huang JX, Kaeslin G, Ranall M V., Blaskovich MA, Becker B, Butler MS, et al. Evaluation of biomarkers for in vitro prediction of drug-induced nephrotoxicity: comparison of HK-2, immortalized human proximal tubule epithelial, and primary cultures of human proximal tubular cells. Pharmacol Res Perspect [Internet]. 2015 Jun 1 [cited 2017 Jun 19];3(3):e00148. Available from: http://doi.wiley.com/10.1002/prp2.148

247. Klein SG, Hennen J, Serchi T, Blömeke B, Gutleb AC. Potential of coculture in vitro models to study inflammatory and sensitizing effects of particles on the lung. Toxicol Vitr [Internet]. 2011 [cited 2017 Apr 30];25(8):1516–34. Available from: http://www.sciencedirect.com/science/article/pii/S0887233311002487

248. Braakhuis HM, Giannakou C, Peijnenburg WJGM, Vermeulen J, van Loveren H, Park

MVDZ. Simple *in vitro* models can predict pulmonary toxicity of silver nanoparticles. Nanotoxicology [Internet]. 2016 Jul 2 [cited 2017 Aug 9];10(6):770–9. Available from: http://www.tandfonline.com/doi/full/10.3109/17435390.2015.1127443

249. Kweon M-H, Adhami VM, Lee J-S, Mukhtar H. Constitutive overexpression of Nrf2-dependent heme oxygenase-1 in A549 cells contributes to resistance to apoptosis induced by epigallocatechin 3-gallate. J Biol Chem [Internet]. American Society for Biochemistry and Molecular Biology; 2006 Nov 3 [cited 2017 Aug 10];281(44):33761–72. Available from: http://www.ncbi.nlm.nih.gov/pubmed/16950787

250. Turchinovich A, Samatov TR, Tonevitsky AG, Burwinkel B. Circulating miRNAs: cell–cell communication function? Front Genet [Internet]. Frontiers Media S.A.; 2013;4:119. Available from: http://www.ncbi.nlm.nih.gov/pmc/articles/PMC3695387/

251. Bollati V, Angelici L, Rizzo G, Pergoli L, Rota F, Hoxha M, et al. Microvesicle-associated microRNA expression is altered upon particulate matter exposure in healthy workers and in A549 cells. J Appl Toxicol [Internet]. Oxford, UK: BlackWell Publishing Ltd; 2015 Jan;35(1):59–67. Available from: http://www.ncbi.nlm.nih.gov/pmc/articles/PMC4125569/

252. Loret T, Peyret E, Dubreuil M, Aguerre-Chariol O, Bressot C, le Bihan O, et al. Air-liquid interface exposure to aerosols of poorly soluble nanomaterials induces different biological activation levels compared to exposure to suspensions. Part Fibre Toxicol [Internet]. 2016 Dec 3 [cited 2017 Aug 9];13(1):58. Available from: http://www.ncbi.nlm.nih.gov/pubmed/27919268

253. Durán N, Silveira CP, Durán M, Martinez DST. Silver nanoparticle protein corona and toxicity: a mini-review. J Nanobiotechnology [Internet]. BioMed Central; 2015 Sep 4 [cited 2017 Jun 20];13:55. Available from: http://www.ncbi.nlm.nih.gov/pubmed/26337542

254. Rothen-Rutishauser BM, Kiama SG, Gehr P. A three-dimensional cellular model of the human respiratory tract to study the interaction with particles. Am J Respir Cell Mol Biol [Internet]. 2005;32. Available from: http://dx.doi.org/10.1165/rcmb.2004-0187OC

255. Kaartinen L, Nettesheim P, Adler KB, Randell SH. Rat tracheal epithelial cell differentiation in vitro. In Vitro Cell Dev Biol Anim [Internet]. 1993 Jun [cited 2017 Jun 21];29A(6):481–92. Available from: http://www.ncbi.nlm.nih.gov/pubmed/7687243

256. Soneson C, Delorenzi M, Gosink MM, Li Y, Shoieb AM, Wood J, et al. A comparison

of methods for differential expression analysis of RNA-seq data. BMC Bioinformatics [Internet]. BioMed Central; 2013 [cited 2017 Mar 7];14(1):91. Available from: http://bmcbioinformatics.biomedcentral.com/articles/10.1186/1471-2105-14-91

257. Scholtens D, von Heydebreck A. Analysis of Differential Gene Expression Studies. In Springer New York; 2005 [cited 2017 Mar 7]. p. 229–48. Available from: http://link.springer.com/10.1007/0-387-29362-0_14

258. Hurd PJ, Nelson CJ. Advantages of next-generation sequencing versus the microarray in epigenetic research. Briefings Funct Genomics Proteomics [Internet]. Oxford University Press; 2009 May 1 [cited 2017 Mar 6];8(3):174–83. Available from: https://academic.oup.com/bfg/article-lookup/doi/10.1093/bfgp/elp013

259. Wang Z, Gerstein M, Snyder M. RNA-Seq: a revolutionary tool for transcriptomics. Nat Rev Genet [Internet]. NIH Public Access; 2009 Jan [cited 2017 Mar 6];10(1):57–63. Available from: http://www.ncbi.nlm.nih.gov/pubmed/19015660

260. Gresham D, Dunham MJ, Botstein D. Comparing whole genomes using DNA microarrays. Nat Rev Genet [Internet]. Nature Publishing Group; 2008 Apr [cited 2017 May 30];9(4):291–302. Available from: http://www.nature.com/doifinder/10.1038/nrg2335

261. Vliegenthart ADB, Shaffer JM, Clarke JI, Peeters LEJ, Caporali A, Bateman DN, et al. Comprehensive microRNA profiling in acetaminophen toxicity identifies novel circulating biomarkers for human liver and kidney injury. Sci Rep [Internet]. Nature Publishing Group; 2015 Oct 22 [cited 2017 Mar 7];5:15501. Available from: http://www.nature.com/articles/srep15501

262. Schultz NA, Dehlendorff C, Jensen B V., Bjerregaard JK, Nielsen KR, Bojesen SE, et al. MicroRNA Biomarkers in Whole Blood for Detection of Pancreatic Cancer. JAMA [Internet]. American Medical Association; 2014 Jan 22 [cited 2017 Mar 7];311(4):392. Available from: http://jama.jamanetwork.com/article.aspx?doi=10.1001/jama.2013.284664

263. Meder B, Keller A, Vogel B, Haas J, Sedaghat-Hamedani F, Kayvanpour E, et al. MicroRNA signatures in total peripheral blood as novel biomarkers for acute myocardial infarction. Basic Res Cardiol [Internet]. Springer-Verlag; 2011 Jan 1 [cited 2017 Mar 7];106(1):13–23. Available from: http://link.springer.com/10.1007/s00395-010-0123-2

264. Gori M, Arciello M, Balsano C. MicroRNAs in nonalcoholic fatty liver disease: novel

biomarkers and prognostic tools during the transition from steatosis to hepatocarcinoma. Biomed Res Int [Internet]. Hindawi Publishing Corporation; 2014 [cited 2017 Mar 7];2014:741465. Available from: http://www.ncbi.nlm.nih.gov/pubmed/24745023

265. Witkos TM, Koscianska E, Krzyzosiak WJ. Practical Aspects of microRNA Target Prediction. Curr Mol Med [Internet]. Bentham Science Publishers; 2011 Mar [cited 2017 Mar 7];11(2):93–109. Available from: http://www.ncbi.nlm.nih.gov/pubmed/21342132

266. Eduati F, di Camillo B, Karbiener M, Scheideler M, Corà D, Caselle M, et al. Dynamic Modeling of miRNA-mediated Feed-Forward Loops. J Comput Biol [Internet]. 2012 Feb [cited 2017 May 30];19(2):188–99. Available from: http://www.ncbi.nlm.nih.gov/pubmed/22300320

267. Nunez-Iglesias J, Liu C-C, Morgan TE, Finch CE, Zhou XJ. Joint Genome-Wide Profiling of miRNA and mRNA Expression in Alzheimer's Disease Cortex Reveals Altered miRNA Regulation. Maas S, editor. PLoS One [Internet]. Public Library of Science; 2010 Feb 1 [cited 2017 Mar 7];5(2):e8898. Available from: http://dx.plos.org/10.1371/journal.pone.0008898

268. Van der Goten J, Vanhove W, Lemaire K, Van Lommel L, Machiels K, Wollants W-J, et al. Integrated miRNA and mRNA Expression Profiling in Inflamed Colon of Patients with Ulcerative Colitis. Chamaillard M, editor. PLoS One [Internet]. 2014 Dec 29 [cited 2017 Mar 7];9(12):e116117. Available from: http://www.ncbi.nlm.nih.gov/pubmed/25546151

269. Ezzie ME, Crawford M, Cho J-H, Orellana R, Zhang S, Gelinas R, et al. Gene expression networks in COPD: microRNA and mRNA regulation. Thorax [Internet]. 2012 Feb [cited 2017 Mar 7];67(2):122–31. Available from: http://thorax.bmj.com/lookup/doi/10.1136/thoraxjnl-2011-200089

270. Cavill R, Kamburov A, Ellis JK, Athersuch TJ, Blagrove MSC, Herwig R, et al. Consensus-Phenotype Integration of Transcriptomic and Metabolomic Data Implies a Role for Metabolism in the Chemosensitivity of Tumour Cells. Tucker-Kellogg G, editor. PLoS Comput Biol [Internet]. 2011 Mar 31 [cited 2017 Mar 7];7(3):e1001113. Available from: http://www.ncbi.nlm.nih.gov/pubmed/21483477

271. Minami K, Uehara T, Morikawa Y, Omura K, Kanki M, Horinouchi A, et al. miRNA expression atlas in male rat. Sci data [Internet]. Nature Publishing Group; 2014 [cited 2017 Sep 16];1:140005. Available from:

http://www.ncbi.nlm.nih.gov/pubmed/25977763

272. Wang S, Li W, Lian B, Liu X, Zhang Y, Dai E, et al. TMREC: A Database of Transcription Factor and MiRNA Regulatory Cascades in Human Diseases. Abdollahi A, editor. PLoS One [Internet]. Public Library of Science; 2015 May 1 [cited 2017 Sep 16];10(5):e0125222. Available from: http://dx.plos.org/10.1371/journal.pone.0125222

273. Ooi AT, Ram S, Kuo A, Gilbert JL, Yan W, Pellegrini M, et al. Identification of an interleukin 13-induced epigenetic signature in allergic airway inflammation. Am J Transl Res [Internet]. e-Century Publishing Corporation; 2012;4(2):219–28. Available from: http://www.ncbi.nlm.nih.gov/pmc/articles/PMC3353532/

274. Halappanavar S, Jackson P, Williams A, Jensen KA, Hougaard KS, Vogel U, et al. Pulmonary response to surface-coated nanotitanium dioxide particles includes induction of acute phase response genes, inflammatory cascades, and changes in microRNAs: A toxicogenomic study. Environ Mol Mutagen [Internet]. 2011 Jul [cited 2017 Sep 16];52(6):425–39. Available from: http://www.ncbi.nlm.nih.gov/pubmed/21259345

275. Henderson RF. Use of bronchoalveolar lavage to detect lung damage. Environ Health Perspect [Internet]. National Institute of Environmental Health Science; 1984 Jun [cited 2017 Sep 16];56:115–29. Available from: http://www.ncbi.nlm.nih.gov/pubmed/6383796

276. Tu MK, Levin JB, Hamilton AM, Borodinsky LN. Calcium signaling in skeletal muscle development, maintenance and regeneration. Cell Calcium [Internet]. NIH Public Access; 2016 Mar [cited 2017 Aug 26];59(2–3):91–7. Available from: http://www.ncbi.nlm.nih.gov/pubmed/26944205

277. Berridge MJ, Bootman MD, Roderick HL. Calcium: Calcium signalling: dynamics, homeostasis and remodelling. Nat Rev Mol Cell Biol [Internet]. Nature Publishing Group; 2003 Jul 1 [cited 2017 Aug 26];4(7):517–29. Available from: http://www.nature.com/doifinder/10.1038/nrm1155

278. Brini M, Calì T, Ottolini D, Carafoli E. Neuronal calcium signaling: function and dysfunction. Cell Mol Life Sci [Internet]. Springer Basel; 2014 Aug 19 [cited 2017 Aug 26];71(15):2787–814. Available from: http://link.springer.com/10.1007/s00018-013-1550-7

279. Song R, Walentek P, Sponer N, Klimke A, Lee JS, Dixon G, et al. miR-34/449 miRNAs are required for motile ciliogenesis by repressing cp110. Nature [Internet].

Nature Research; 2014 Jun 4 [cited 2017 Mar 7];510(7503):115–20. Available from: http://www.nature.com/doifinder/10.1038/nature13413

280. Yang X, Feng M, Jiang X, Wu Z, Li Z, Aau M, et al. miR-449a and miR-449b are direct transcriptional targets of E2F1 and negatively regulate pRb-E2F1 activity through a feedback loop by targeting CDK6 and CDC25A. Genes Dev [Internet]. Cold Spring Harbor Laboratory Press; 2009 Oct 15 [cited 2017 Mar 7];23(20):2388–93. Available from: http://www.ncbi.nlm.nih.gov/pubmed/19833767

281. Ahn Y-H, Gibbons DL, Chakravarti D, Creighton CJ, Rizvi ZH, Adams HP, et al. ZEB1 drives prometastatic actin cytoskeletal remodeling by downregulating miR-34a expression. J Clin Invest [Internet]. American Society for Clinical Investigation; 2012 Sep [cited 2017 May 30];122(9):3170–83. Available from: http://www.ncbi.nlm.nih.gov/pubmed/22850877

282. Etheridge A, Lee I, Hood L, Galas D, Wang K. Extracellular microRNA: a new source of biomarkers. Mutat Res [Internet]. NIH Public Access; 2011 Dec 1 [cited 2017 Mar 7];717(1–2):85–90. Available from: http://www.ncbi.nlm.nih.gov/pubmed/21402084

283. Gorska K, Krenke R, Domagala-Kulawik J, Korczynski P, Nejman-Gryz P, Kosciuch J, et al. Comparison of cellular and biochemical markers of airway inflammation in patients with mild-to-moderate asthma and chronic obstructive pulmonary disease: an induced sputum and bronchoalveolar lavage fluid study. J Physiol Pharmacol [Internet]. 2008 [cited 2017 Mar 7];59(6):271–83. Available from: www.jpp.krakow.pl

284. Szeto CY-Y, Lin CH, Choi SC, Yip TTC, Ngan RK-C, Tsao GS-W, et al. Integrated mRNA and microRNA transcriptome sequencing characterizes sequence variants and mRNA-microRNA regulatory network in nasopharyngeal carcinoma model systems. FEBS Open Bio [Internet]. 2014 Jan 1 [cited 2017 Mar 7];4(1):128–40. Available from: http://doi.wiley.com/10.1016/j.fob.2014.01.004

285. Mizuno S, Bogaard HJ, Gomez-Arroyo J, Alhussaini A, Kraskauskas D, Cool CD, et al. MicroRNA-199a-5p Is Associated With Hypoxia-Inducible Factor-1α Expression in Lungs From Patients With COPD. Chest [Internet]. 2012 Sep [cited 2017 Mar 7];142(3):663–72. Available from: http://www.ncbi.nlm.nih.gov/pubmed/22383663

286. Kumar M, Ahmad T, Sharma A, Mabalirajan U, Kulshreshtha A, Agrawal A, et al. Let-7 microRNA–mediated regulation of IL-13 and allergic airway inflammation. J Allergy Clin Immunol [Internet]. 2011 Nov [cited 2017 Aug 10];128(5):1077–1085.e10. Available from: http://www.ncbi.nlm.nih.gov/pubmed/21616524

287. Honeyman L, Bazett M, Tomko TG, Haston CK. MicroRNA profiling implicates the insulin-like growth factor pathway in bleomycin-induced pulmonary fibrosis in mice. Fibrogenesis Tissue Repair [Internet]. 2013 [cited 2017 Aug 10];6(1):16. Available from: http://fibrogenesis.biomedcentral.com/articles/10.1186/1755-1536-6-16

288. Nahid MA, Yao B, Dominguez-Gutierrez PR, Kesavalu L, Satoh M, Chan EKL. Regulation of TLR2-mediated tolerance and cross-tolerance through IRAK4 modulation by miR-132 and miR-212. J Immunol [Internet]. NIH Public Access; 2013 Feb 1 [cited 2017 Aug 10];190(3):1250–63. Available from: http://www.ncbi.nlm.nih.gov/pubmed/23264652

289. Bommer GT, Gerin I, Feng Y, Kaczorowski AJ, Kuick R, Love RE, et al. p53-Mediated Activation of miRNA34 Candidate Tumor-Suppressor Genes. Curr Biol [Internet]. 2007 Aug [cited 2017 Mar 7];17(15):1298–307. Available from: http://linkinghub.elsevier.com/retrieve/pii/S0960982207016387

290. Lizé M, Pilarski S, Dobbelstein M. E2F1-inducible microRNA 449a/b suppresses cell proliferation and promotes apoptosis. Cell Death Differ [Internet]. Nature Publishing Group; 2010 Mar 4 [cited 2017 Mar 7];17(3):452–8. Available from: http://www.nature.com/doifinder/10.1038/cdd.2009.188

291. Yang X, Feng M, Jiang X, Wu Z, Li Z, Aau M, et al. miR-449a and miR-449b are direct transcriptional targets of E2F1 and negatively regulate pRb-E2F1 activity through a feedback loop by targeting CDK6 and CDC25A. Genes Dev [Internet]. Cold Spring Harbor Laboratory Press; 2009 Oct 15 [cited 2017 Jul 10];23(20):2388–93. Available from: http://www.ncbi.nlm.nih.gov/pubmed/19833767

292. Wang Y, Hamond S, Dang H, Wages P, Randell S. Evidence For Non-Redundant Functions Of MiR-34/449 Family Members During Human Bronchial Epithelial Cell Differentiation. In: putting the genie back in the bottle: regulating gene expression. San Diego: American Thoracic Society; 2015.

293. Shi Y, Liu C, Liu X, Tang DG, Wang J. The microRNA miR-34a Inhibits Non-Small Cell Lung Cancer (NSCLC) Growth and the CD44hi Stem-Like NSCLC Cells. Das GM, editor. PLoS One [Internet]. Public Library of Science; 2014 Mar 4 [cited 2017 Mar 7];9(3):e90022. Available from: http://dx.plos.org/10.1371/journal.pone.0090022

294. Raver-Shapira N, Marciano E, Meiri E, Spector Y, Rosenfeld N, Moskovits N, et al. Transcriptional Activation of miR-34a Contributes to p53-Mediated Apoptosis. Mol Cell [Internet]. 2007 Jun [cited 2017 Mar 7];26(5):731–43. Available from: http://linkinghub.elsevier.com/retrieve/pii/S1097276507003188

295. Marcet B, Chevalier B, Luxardi G, Coraux C, Zaragosi L-E, Cibois M, et al. Control of vertebrate multiciliogenesis by miR-449 through direct repression of the Delta/Notch pathway. Nat Cell Biol [Internet]. Nature Research; 2011 Jun 22 [cited 2017 Mar 7];13(6):694–701. Available from: http://www.nature.com/doifinder/10.1038/ncb2241

296. Solberg OD, Ostrin EJ, Love MI, Peng JC, Bhakta NR, Hou L, et al. Airway Epithelial miRNA Expression Is Altered in Asthma. Am J Respir Crit Care Med [Internet]. 2012 Nov 15 [cited 2017 Mar 7];186(10):965–74. Available from: http://www.ncbi.nlm.nih.gov/pubmed/22955319

297. Jiang P, Liu R, Zheng Y, Liu X, Chang L, Xiong S, et al. MiR-34a inhibits lipopolysaccharide-induced inflammatory response through targeting Notch1 in murine macrophages. Exp Cell Res [Internet]. 2012 Jun [cited 2017 Mar 7];318(10):1175–84. Available from: http://linkinghub.elsevier.com/retrieve/pii/S0014482712001450

298. Bao J, Li D, Wang L, Wu J, Hu Y, Wang Z, et al. MicroRNA-449 and microRNA-34b/c function redundantly in murine testes by targeting E2F transcription factor-retinoblastoma protein (E2F-pRb) pathway. J Biol Chem [Internet]. American Society for Biochemistry and Molecular Biology; 2012 Jun 22 [cited 2017 Mar 7];287(26):21686–98. Available from: http://www.ncbi.nlm.nih.gov/pubmed/22570483

299. Breving K, Esquela-Kerscher A. The complexities of microRNA regulation: mirandering around the rules. Int J Biochem Cell Biol [Internet]. 2010 Aug [cited 2017 Mar 7];42(8):1316–29. Available from: http://linkinghub.elsevier.com/retrieve/pii/S1357272509002726

300. Christmann M, Kaina B. Transcriptional regulation of human DNA repair genes following genotoxic stress: trigger mechanisms, inducible responses and genotoxic adaptation. Nucleic Acids Res [Internet]. Oxford University Press; 2013 Oct [cited 2018 Jan 7];41(18):8403–20. Available from: http://www.ncbi.nlm.nih.gov/pubmed/23892398

301. Lodygin D, Tarasov V, Epanchintsev A, Berking C, Knyazeva T, Körner H, et al. Inactivation of miR-34a by aberrant CpG methylation in multiple types of cancer. Cell Cycle [Internet]. 2008 Aug 15 [cited 2017 Mar 7];7(16):2591–600. Available from: http://www.ncbi.nlm.nih.gov/pubmed/18719384

302. Liu X, Feng J, Tang L, Liao L, Xu Q, Zhu S. The Regulation and Function of miR-21-FOXO3a-miR-34b/c Signaling in Breast Cancer. Int J Mol Sci [Internet]. 2015 Jan 30 [cited 2017 Mar 7];16(2):3148–62. Available from:

http://www.ncbi.nlm.nih.gov/pubmed/25647415

303. Moore ML, Peebles RS. Update on the role of prostaglandins in allergic lung inflammation: Separating friends from foes, harder than you might think. J Allergy Clin Immunol [Internet]. 2006 May [cited 2017 Mar 7];117(5):1036–9. Available from: http://linkinghub.elsevier.com/retrieve/pii/S009167490504039X

304. Samet J, Reed W, Ghio A, Devlin R, Carter J, Dailey L, et al. Induction of Prostaglandin H Synthase 2 in Human Airway Epithelial Cells Exposed to Residual Oil Fly Ash. Toxicol Appl Pharmacol [Internet]. 1996 Nov [cited 2017 Mar 7];141(1):159–68. Available from: http://www.ncbi.nlm.nih.gov/pubmed/8917688

305. Abe A, Hiraoka M, Wild S, Wilcoxen SE, Paine R, Shayman JA. Lysosomal phospholipase A2 is selectively expressed in alveolar macrophages. J Biol Chem [Internet]. American Society for Biochemistry and Molecular Biology; 2004 Oct 8 [cited 2017 Mar 7];279(41):42605–11. Available from: http://www.ncbi.nlm.nih.gov/pubmed/15294901

306. Rahman I, MacNee W. Oxidative stress and regulation of glutathione in lung inflammation. Eur Respir J [Internet]. 2000;16. Available from: http://dx.doi.org/10.1034/j.1399-3003.2000.016003534.x

307. Yang X, Salminen WF, Shi Q, Greenhaw J, Gill PS, Bhattacharyya S, et al. Potential of extracellular microRNAs as biomarkers of acetaminophen toxicity in children. Toxicol Appl Pharmacol [Internet]. 2015 Apr [cited 2017 Mar 7];284(2):180–7. Available from: http://linkinghub.elsevier.com/retrieve/pii/S0041008X15000642

308. Nishimura Y, Kondo C, Morikawa Y, Tonomura Y, Torii M, Yamate J, et al. Plasma miR-208 as a useful biomarker for drug-induced cardiotoxicity in rats. J Appl Toxicol [Internet]. 2015 Feb [cited 2017 Mar 7];35(2):173–80. Available from: http://www.ncbi.nlm.nih.gov/pubmed/25092230

309. Nassirpour R, Mathur S, Gosink MM, Li Y, Shoieb AM, Wood J, et al. Identification of tubular injury microRNA biomarkers in urine: comparison of next-generation sequencing and qPCR-based profiling platforms. BMC Genomics [Internet]. 2014 [cited 2017 Aug 10];15(1):485. Available from: http://bmcgenomics.biomedcentral.com/articles/10.1186/1471-2164-15-485

310. Fry RC, Rager JE, Bauer R, Sebastian E, Peden DB, Jaspers I, et al. Air toxics and epigenetic effects: ozone altered microRNAs in the sputum of human subjects. AJP Lung Cell Mol Physiol [Internet]. 2014 Jun 15 [cited 2017 Mar 7];306(12):L1129–37.

Available from: http://ajplung.physiology.org/cgi/doi/10.1152/ajplung.00348.2013

311. Vriens A, Nawrot TS, Saenen ND, Provost EB, Kicinski M, Lefebvre W, et al. Recent exposure to ultrafine particles in school children alters miR-222 expression in the extracellular fraction of saliva. Environ Heal [Internet]. 2016 Dec 26 [cited 2017 Mar 7];15(1):80. Available from: http://ehjournal.biomedcentral.com/articles/10.1186/s12940-016-0162-8

312. Leidinger P, Backes C, Meder B, Meese E, Keller A. The human miRNA repertoire of different blood compounds. BMC Genomics [Internet]. 2014 [cited 2017 Mar 7];15(1):474. Available from: http://bmcgenomics.biomedcentral.com/articles/10.1186/1471-2164-15-474

313. Liu L, Aa J, Wang G, Yan B, Zhang Y, Wang X, et al. Differences in metabolite profile between blood plasma and serum. Anal Biochem [Internet]. 2010 Nov [cited 2017 Mar 7];406(2):105–12. Available from: http://linkinghub.elsevier.com/retrieve/pii/S0003269710004616

314. Jung J, Kim S-H, Lee H-S, Choi GS, Jung Y-S, Ryu DH, et al. Serum metabolomics reveals pathways and biomarkers associated with asthma pathogenesis. Clin Exp Allergy [Internet]. 2013 Apr [cited 2017 Mar 7];43(4):425–33. Available from: http://doi.wiley.com/10.1111/cea.12089

315. Ho WE, Xu Y-J, Cheng C, Peh HY, Tannenbaum SR, Wong WSF, et al. Metabolomics Reveals Inflammatory-Linked Pulmonary Metabolic Alterations in a Murine Model of House Dust Mite-Induced Allergic Asthma. J Proteome Res [Internet]. American Chemical Society; 2014 Aug [cited 2017 Mar 7];13(8):3771–82. Available from: http://pubs.acs.org/doi/abs/10.1021/pr5003615

316. Cavill R, Jennen D, Kleinjans J, Briedé JJ. Transcriptomic and metabolomic data integration. Brief Bioinform [Internet]. 2016 Sep 1;17(5):891–901. Available from: http://dx.doi.org/10.1093/bib/bbv090

317. Kamburov A, Cavill R, Ebbels TMD, Herwig R, Keun HC. Integrated pathway-level analysis of transcriptomics and metabolomics data with IMPaLA. Bioinformatics [Internet]. 2011 Oct 15 [cited 2017 Mar 7];27(20):2917–8. Available from: http://www.ncbi.nlm.nih.gov/pubmed/21893519

318. Martin TR. Recognition of Bacterial Endotoxin in the Lungs. Am J Respir Cell Mol Biol [Internet]. 2000 Aug [cited 2017 Sep 16];23(2):128–32. Available from: http://www.ncbi.nlm.nih.gov/pubmed/10919975

319. Eutamene H, Theodorou V, Schmidlin F, Tondereau V, Garcia-Villar R, Salvador-Cartier C, et al. LPS-induced lung inflammation is linked to increased epithelial permeability: role of MLCK. Eur Respir J [Internet]. 2005 May 1 [cited 2017 Mar 7];25(5):789–96. Available from: http://www.ncbi.nlm.nih.gov/pubmed/15863634

320. Reynier F, de Vos AF, Hoogerwerf JJ, Bresser P, van der Zee JS, Paye M, et al. Gene expression profiles in alveolar macrophages induced by lipopolysaccharide in humans. Mol Med [Internet]. The Feinstein Institute for Medical Research; 2012 Dec 6 [cited 2017 Mar 7];18(1):1303–11. Available from: http://www.ncbi.nlm.nih.gov/pubmed/22952057

321. Reutershan J, Basit A, Galkina E V, Ley K. Sequential recruitment of neutrophils into lung and bronchoalveolar lavage fluid in LPS-induced acute lung injury. AJP Lung Cell Mol Physiol [Internet]. 2005 Feb 25 [cited 2017 Mar 7];289(5):L807–15. Available from: http://www.ncbi.nlm.nih.gov/pubmed/15951336

322. Livak KJ, Schmittgen TD. Analysis of Relative Gene Expression Data Using Real-Time Quantitative PCR and the 2−ΔΔCT Method. Methods [Internet]. 2001 Dec [cited 2017 Mar 7];25(4):402–8. Available from: http://linkinghub.elsevier.com/retrieve/pii/S1046202301912629

323. Thomas PD, Campbell MJ, Kejariwal A, Mi H, Karlak B, Daverman R, et al. PANTHER: a library of protein families and subfamilies indexed by function. Genome Res [Internet]. Cold Spring Harbor Laboratory Press; 2003 Sep [cited 2017 Mar 7];13(9):2129–41. Available from: http://www.ncbi.nlm.nih.gov/pubmed/12952881

324. Carr HY, Purcell EM. Effects of Diffusion on Free Precession in Nuclear Magnetic Resonance Experiments. Phys Rev [Internet]. American Physical Society; 1954 May 1;94(3):630–8. Available from: http://link.aps.org/doi/10.1103/PhysRev.94.630

325. Kamburov A, Cavill R, Ebbels TMD, Herwig R, Keun HC. Integrated pathway-level analysis of transcriptomics and metabolomics data with IMPaLA. Bioinformatics [Internet]. 2011 Oct 15;27(20):2917–8. Available from: http://dx.doi.org/10.1093/bioinformatics/btr499

326. Dudek K. The role of mRNA translational regulation in models of hepatotoxicity [Internet]. university of Leicester; 2014. Available from: file:///C:/Users/John/Downloads/2014DudekKMPhD.pdf

327. Life Technologies. TaqMan Small RNA Assays [Internet]. Life Technologies Corporation; 2011 [cited 2017 Aug 10]. p. 1–40. Available from:

https://tools.thermofisher.com/content/sfs/manuals/cms_042167.pdf

328. Haddad EB, Birrell M, McCluskie K, Ling A, Webber SE, Foster ML, et al. Role of p38 MAP kinase in LPS-induced airway inflammation in the rat. Br J Pharmacol [Internet]. Wiley-Blackwell; 2001 Apr [cited 2017 Mar 7];132(8):1715–24. Available from: http://www.ncbi.nlm.nih.gov/pubmed/11309243

329. Paul G. Defining dosimetry and implications for aerosol presentation for non-clinical development of respiratory drugs. Unpublished; 2017.

330. Nick JA, Young SK, Arndt PG, Lieber JG, Suratt BT, Poch KR, et al. Selective Suppression of Neutrophil Accumulation in Ongoing Pulmonary Inflammation by Systemic Inhibition of p38 Mitogen-Activated Protein Kinase. J Immunol [Internet]. 2002 Nov 1 [cited 2017 Mar 7];169(9):5260–9. Available from: http://www.jimmunol.org/cgi/doi/10.4049/jimmunol.169.9.5260

331. Han R, Ji X, Rong R, Li Y, Yao W, Yuan J, et al. MiR-449a regulates autophagy to inhibit silica-induced pulmonary fibrosis through targeting Bcl2. J Mol Med [Internet]. 2016 Nov 28 [cited 2017 Mar 7];94(11):1267–79. Available from: http://www.ncbi.nlm.nih.gov/pubmed/27351886

332. Chen X, Liang H, Zhang J, Zen K, Zhang C-Y. Secreted microRNAs: a new form of intercellular communication. Trends Cell Biol [Internet]. 2012 Mar [cited 2017 Mar 7];22(3):125–32. Available from: http://www.ncbi.nlm.nih.gov/pubmed/22260888

333. Valadi H, Ekström K, Bossios A, Sjöstrand M, Lee JJ, Lötvall JO. Exosome-mediated transfer of mRNAs and microRNAs is a novel mechanism of genetic exchange between cells. Nat Cell Biol [Internet]. Nature Publishing Group; 2007 Jun 7 [cited 2017 Mar 6];9(6):654–9. Available from: http://www.nature.com/doifinder/10.1038/ncb1596

334. de Oliveira CA, Mantovani B. Latrunculin A is a potent inhibitor of phagocytosis by macrophages. Life Sci [Internet]. 1988 Jan [cited 2017 Feb 19];43(22):1825–30. Available from: http://linkinghub.elsevier.com/retrieve/pii/0024320588902822

335. Shimazu T, Hirschey MD, Huang J-Y, Ho LTY, Verdin E. Acetate metabolism and aging: An emerging connection. Mech Ageing Dev [Internet]. 2010 Jul [cited 2017 Mar 7];131(7–8):511–6. Available from: http://linkinghub.elsevier.com/retrieve/pii/S0047637410000928

336. Fujino T, Kondo J, Ishikawa M, Morikawa K, Yamamoto TT. Acetyl-CoA synthetase 2, a mitochondrial matrix enzyme involved in the oxidation of acetate. J Biol Chem

[Internet]. American Society for Biochemistry and Molecular Biology; 2001 Apr 6 [cited 2017 Mar 7];276(14):11420–6. Available from: http://www.ncbi.nlm.nih.gov/pubmed/11150295

337. Morrison WL, Gibson JN, Scrimgeour C, Rennie MJ. Muscle wasting in emphysema. Clin Sci (Lond) [Internet]. 1988 Oct [cited 2017 Mar 7];75(4):415–20. Available from: http://www.ncbi.nlm.nih.gov/pubmed/3197374

338. Pouw E, Schols A, Deutz N, Wouters E. Plasma and Muscle Amino Acid Levels in Relation to Resting Energy Expenditure and Inflammation in Stable Chronic Obstructive Pulmonary Disease. Am J Respir Crit Care Med [Internet]. 1998 Sep [cited 2017 Mar 7];158(3):797–801. Available from: http://www.ncbi.nlm.nih.gov/pubmed/9731007

339. Sackesen C, Ercan H, Dizdar E, Soyer O, Gumus P, Tosun BN, et al. A comprehensive evaluation of the enzymatic and nonenzymatic antioxidant systems in childhood asthma. J Allergy Clin Immunol [Internet]. 2008 Jul [cited 2017 Mar 7];122(1):78–85. Available from: http://www.ncbi.nlm.nih.gov/pubmed/18485467

340. Kuban P, Gregus M, Foret F, Skrickova J, Kindlova D, Doubkova M, et al. Monitoring of ionic content of exhaled breath condensate in various respiratory diseases by capillary electrophoresis with contactless conductivity detection. Eur Respir J [Internet]. European Respiratory Society; 2015 Sep 30 [cited 2017 Mar 7];46(suppl 59):PA3992. Available from: http://erj.ersjournals.com/lookup/doi/10.1183/13993003.congress-2015.PA3992

341. Singh C, Rai RK, Azim A, Sinha N, Ahmed A, Singh K, et al. Metabolic profiling of human lung injury by 1H high-resolution nuclear magnetic resonance spectroscopy of blood serum. Metabolomics [Internet]. 2015;11(1):166–74. Available from: http://dx.doi.org/10.1007/s11306-014-0688-0

342. Singleton KD, Beckey VE, Wischmeyer PE. Glutamine prevents activation of NF-kappaB and stress kinase pathways, attenuates inflammatory cytokine release, and prevents acute respiratory distress syndrome (ards) following sepsis. Shock [Internet]. 2005 Dec [cited 2017 Mar 7];24(6):583–9. Available from: http://www.ncbi.nlm.nih.gov/pubmed/16317391

343. Zhang F, Wang X, Pan L, Wang W, Li N, Li J, et al. Glutamine attenuates lipopolysaccharide-induced acute lung injury. Nutrition [Internet]. Elsevier; 2009 Jun [cited 2017 Mar 7];25(6):692–8. Available from: http://www.ncbi.nlm.nih.gov/pubmed/19286350

344. Wang X, Chen W, An X, Yang D, Chen F, Bai C. A metabonomic approach to prognostic evaluation of ALI by high-resolution nuclear magnetic resonance (HR NMR) spectroscopy. Eur Respir J [Internet]. 2014 [cited 2017 Aug 10];38(Suppl 55). Available from: http://erj.ersjournals.com/content/38/Suppl_55/p2047

345. Singh C, Rai RK, Azim A, Sinha N, Ahmed A, Singh K, et al. Metabolic profiling of human lung injury by 1H high-resolution nuclear magnetic resonance spectroscopy of blood serum. Metabolomics [Internet]. Springer US; 2015 Feb 26 [cited 2017 Mar 7];11(1):166–74. Available from: http://link.springer.com/10.1007/s11306-014-0688-0

346. Adrych K, Smoczynski M, Stojek M, Sledzinski T, Slominska E, Goyke E, et al. Decreased serum essential and aromatic amino acids in patients with chronic pancreatitis. World J Gastroenterol [Internet]. Baishideng Publishing Group Inc; 2010 Sep 21 [cited 2017 Mar 7];16(35):4422–7. Available from: http://www.ncbi.nlm.nih.gov/pubmed/20845509

347. Kominsky DJ, Campbell EL, Colgan SP. Metabolic Shifts in Immunity and Inflammation. J Immunol [Internet]. 2010 Apr 15 [cited 2017 Mar 7];184(8):4062–8. Available from: http://www.jimmunol.org/cgi/doi/10.4049/jimmunol.0903002

348. Rehberg M, Wetzel M, Ritter JB, Reichl U. The regulation of glutaminolysis and citric acid cycle activity during mammalian cell cultivation. IFAC Proc Vol [Internet]. 2013 [cited 2017 Mar 7];46(31):48–53. Available from: http://linkinghub.elsevier.com/retrieve/pii/S1474667016313696

349. National Center for Biotechnology Information. GLUD1 glutamate dehydrogenase 1 [Internet]. [cited 2017 Mar 5]. Available from: https://www.ncbi.nlm.nih.gov/gene/2746

350. Nicklin P, Bergman P, Zhang B, Triantafellow E, Wang H, Nyfeler B, et al. Bidirectional Transport of Amino Acids Regulates mTOR and Autophagy. Cell [Internet]. 2009 Feb 6 [cited 2017 Mar 7];136(3):521–34. Available from: http://www.ncbi.nlm.nih.gov/pubmed/19203585

351. Pochini L, Scalise M, Galluccio M, Indiveri C. Membrane transporters for the special amino acid glutamine: structure/function relationships and relevance to human health. Front Chem [Internet]. Frontiers Media SA; 2014 [cited 2017 Mar 7];2:61. Available from: http://www.ncbi.nlm.nih.gov/pubmed/25157349

352. Reynolds MR, Lane AN, Robertson B, Kemp S, Liu Y, Hill BG, et al. Control of glutamine metabolism by the tumor suppressor Rb. Oncogene [Internet]. 2014 Jan 30 [cited 2017 Mar 7];33(5):556–66. Available from:

http://www.ncbi.nlm.nih.gov/pubmed/23353822

353. Dumortier O, Hinault C, Van Obberghen E. MicroRNAs and Metabolism Crosstalk in Energy Homeostasis. Cell Metab [Internet]. 2013 Sep [cited 2017 Mar 7];18(3):312–24. Available from: http://linkinghub.elsevier.com/retrieve/pii/S1550413113002489

354. Yelamanchi SD, Jayaram S, Thomas JK, Gundimeda S, Khan AA, Singhal A, et al. A pathway map of glutamate metabolism. J Cell Commun Signal [Internet]. Springer; 2016 Mar [cited 2017 Mar 7];10(1):69–75. Available from: http://www.ncbi.nlm.nih.gov/pubmed/26635200

355. Tomasi ML, Ryoo M, Yang H, Iglesias Ara A, Ko KS, Lu SC. Molecular mechanisms of lipopolysaccharide-mediated inhibition of glutathione synthesis in mice. Free Radic Biol Med [Internet]. NIH Public Access; 2014 Mar [cited 2017 Mar 7];68:148–58. Available from: http://www.ncbi.nlm.nih.gov/pubmed/24296246

356. Behbod B, Urch B, Speck M, Scott JA, Liu L, Poon R, et al. Endotoxin in concentrated coarse and fine ambient particles induces acute systemic inflammation in controlled human exposures. Occup Environ Med [Internet]. 2013 Nov [cited 2017 Mar 7];70(11):761–7. Available from: http://www.ncbi.nlm.nih.gov/pubmed/24143017

357. Islam AS, Beidelschies MA, Huml A, Greenfield EM. Titanium particles activate Toll-like Receptor 4 independently of lipid rafts in RAW264.7 murine macrophages. J Orthop Res [Internet]. 2011 Feb;29(2):211–7. Available from: http://www.ncbi.nlm.nih.gov/pmc/articles/PMC3010285/

358. Karagulian F, Belis CA, Dora CFC, Prüss-Ustün AM, Bonjour S, Adair-Rohani H, et al. Contributions to cities' ambient particulate matter (PM): A systematic review of local source contributions at global level. Atmos Environ [Internet]. 2015 Nov [cited 2017 Mar 7];120:475–83. Available from: http://linkinghub.elsevier.com/retrieve/pii/S1352231015303320

359. Gehrig R, Hill M, Buchmann B, Imhof D, Weingartner E, Baltensperger U. Separate determination of PM10 emission factors of road traffic for tailpipe emissions and emissions from abrasion and resuspension processes. Intern J Env Pollut [Internet]. 2004;22. Available from: http://dx.doi.org/10.1504/IJEP.2004.005549

360. Zuurbier M, Hoek G, Oldenwening M, Lenters V, Meliefste K, van den Hazel P, et al. Commuters' exposure to particulate matter air pollution is affected by mode of transport, fuel type, and route. Environ Health Perspect [Internet]. National Institute of Environmental Health Science; 2010 Jun [cited 2017 Mar 7];118(6):783–9. Available

from: http://www.ncbi.nlm.nih.gov/pubmed/20185385

361. Estévez-García JA, Rojas-Roa NY, Rodríguez-Pulido AI. Occupational exposure to air pollutants: particulate matter and respiratory symptoms affecting traffic-police in Bogotá. Rev Salud Publica (Bogota) [Internet]. [cited 2017 Mar 7];15(6):889–902. Available from: http://www.ncbi.nlm.nih.gov/pubmed/25124352

362. Clougherty JE, Rossi CA, Lawrence J, Long MS, Diaz EA, Lim RH, et al. Chronic Social Stress and Susceptibility to Concentrated Ambient Fine Particles in Rats. Environ Health Perspect [Internet]. 2010 Mar 1 [cited 2017 Mar 7];118(6):769–75. Available from: http://ehp.niehs.nih.gov/0901631

363. Autrup H. Ambient Air Pollution and Adverse Health Effects. Procedia - Soc Behav Sci [Internet]. 2010 [cited 2017 Mar 7];2(5):7333–8. Available from: http://linkinghub.elsevier.com/retrieve/pii/S1877042810012231

364. Bell ML, Zanobetti A, Dominici F. Evidence on Vulnerability and Susceptibility to Health Risks Associated With Short-Term Exposure to Particulate Matter: A Systematic Review and Meta-Analysis. Am J Epidemiol [Internet]. 2013 Sep 15 [cited 2017 Mar 7];178(6):865–76. Available from: http://www.ncbi.nlm.nih.gov/pubmed/23887042

365. Bui D, Burgess J, Matheson M, Erbas B, Perret J, Morrison S, et al. Ambient wood smoke, traffic pollution and adult asthma prevalence and severity. Respirology [Internet]. 2013 Apr [cited 2017 Mar 7];18(7):n/a-n/a. Available from: http://doi.wiley.com/10.1111/resp.12108

366. Salvi S, Blomberg A, Rudell B, Kelly F, Sandström T, Holgate S, et al. Acute Inflammatory Responses in the Airways and Peripheral Blood After Short-Term Exposure to Diesel Exhaust in Healthy Human Volunteers. Am J Respir Crit Care Med [Internet]. American Thoracic SocietyNew York, NY; 1999 Mar [cited 2017 Mar 7];159(3):702–9. Available from: http://www.atsjournals.org/doi/abs/10.1164/ajrccm.159.3.9709083

367. Krishnan RM, Sullivan JH, Carlsten C, Wilkerson H-W, Beyer RP, Bammler T, et al. A randomized cross-over study of inhalation of diesel exhaust, hematological indices, and endothelial markers in humans. Part Fibre Toxicol [Internet]. BioMed Central; 2013 Mar 26 [cited 2017 Mar 7];10:7. Available from: http://www.ncbi.nlm.nih.gov/pubmed/23531317

368. Törnqvist H, Mills NL, Gonzalez M, Miller MR, Robinson SD, Megson IL, et al.

Persistent Endothelial Dysfunction in Humans after Diesel Exhaust Inhalation. Am J Respir Crit Care Med [Internet]. American Thoracic Society; 2007 Aug 15 [cited 2017 Mar 7];176(4):395–400. Available from: http://www.atsjournals.org/doi/abs/10.1164/rccm.200606-872OC

369. Alexeeff C, Andrew Coull B, Gryparis A, Suh H, Sparrow D, Vokonas PS, et al. Medium-Term Exposure to Traffic-Related Air Pollution and Markers of Inflammation and Endothelial Function. Environ Health Perspect [Internet]. 2017 [cited 2017 Mar 6];119(4):481–6. Available from: https://dash.harvard.edu/bitstream/handle/1/8830769/3080929.pdf?sequence=1

370. Neophytou AM, Hart JE, Cavallari JM, Smith TJ, Dockery DW, Coull BA, et al. Traffic-related exposures and biomarkers of systemic inflammation, endothelial activation and oxidative stress: a panel study in the US trucking industry. Environ Heal [Internet]. 2013 Dec 7 [cited 2017 Mar 7];12(1):105. Available from: http://ehjournal.biomedcentral.com/articles/10.1186/1476-069X-12-105

371. Gasser M, Riediker M, Mueller L, Perrenoud A, Blank F, Gehr P, et al. Toxic effects of brake wear particles on epithelial lung cells in vitro. Part Fibre Toxicol [Internet]. 2009;6(1):30. Available from: http://dx.doi.org/10.1186/1743-8977-6-30

372. Thorpe A, Harrison RM. Sources and properties of non-exhaust particulate matter from road traffic: A review. Sci Total Environ [Internet]. 2008 [cited 2017 Jun 1];400(1):270–82. Available from: http://www.sciencedirect.com/science/article/pii/S004896970800658X

373. Steenhof M, Gosens I, Strak M, Godri KJ, Hoek G, Cassee FR, et al. In vitro toxicity of particulate matter (PM) collected at different sites in the Netherlands is associated with PM composition, size fraction and oxidative potential--the RAPTES project. Part Fibre Toxicol [Internet]. BioMed Central; 2011 Sep 2 [cited 2017 Aug 12];8:26. Available from: http://www.ncbi.nlm.nih.gov/pubmed/21888644

374. Guastadisegni C, Kelly FJ, Cassee FR, Gerlofs-Nijland ME, Janssen NAH, Pozzi R, et al. Determinants of the Proinflammatory Action of Ambient Particulate Matter in Immortalized Murine Macrophages. Environ Health Perspect [Internet]. 2010 Jul 27 [cited 2017 Aug 12];118(12):1728–34. Available from: http://www.ncbi.nlm.nih.gov/pubmed/20663738

375. Motta V, Angelici L, Nordio F, Bollati V, Fossati S, Frascati F, et al. Integrative Analysis of miRNA and Inflammatory Gene Expression After Acute Particulate Matter Exposure. [cited 2017 Mar 7]; Available from: http://www.gene-

quantification.de/motta-et-al-microrna-inflammation-2013.pdf

376. Brower JB, Doyle-Eisele M, Moeller B, Stirdivant S, McDonald JD, Campen MJ. Metabolomic changes in murine serum following inhalation exposure to gasoline and diesel engine emissions. Inhal Toxicol [Internet]. 2016 Apr 15 [cited 2017 Mar 6];28(5):241–50. Available from: http://www.ncbi.nlm.nih.gov/pubmed/27017952

377. Franz C, Vogel A, Sciullo E, Wong P, Kuzmicky P, Kado N, et al. Induction of Proinflammatory Cytokines and C-Reactive Protein in Human Macrophage Cell Line U937 Exposed to Air Pollution Particulates. Source Environ Heal Perspect [Internet]. 2005 [cited 2017 Mar 7];113(11):1536–41. Available from: http://www.jstor.org/stable/3436568

378. Vogel CFA, Garcia J, Wu D, Mitchell DC, Zhang Y, Kado NY, et al. Activation of inflammatory responses in human U937 macrophages by particulate matter collected from dairy farms: an in vitro expression analysis of pro-inflammatory markers. Environ Heal [Internet]. 2012 Dec 28 [cited 2017 Aug 12];11(1):17. Available from: http://ehjournal.biomedcentral.com/articles/10.1186/1476-069X-11-17

379. Lundborg M, Dahlén S-E, Johard U, Gerde P, Jarstrand C, Camner P, et al. Aggregates of ultrafine particles impair phagocytosis of microorganisms by human alveolar macrophages. Environ Res [Internet]. 2006 Feb [cited 2017 Mar 9];100(2):197–204. Available from: http://www.ncbi.nlm.nih.gov/pubmed/16171796

380. Braydich-Stolle LK, Speshock JL, Castle A, Smith M, Murdock RC, Hussain SM. Nanosized Aluminum Altered Immune Function. ACS Nano [Internet]. 2010 Jul 27 [cited 2017 Mar 9];4(7):3661–70. Available from: http://www.ncbi.nlm.nih.gov/pubmed/20593840

381. Zhou H, Kobzik L. Effect of concentrated ambient particles on macrophage phagocytosis and killing of Streptococcus pneumoniae. Am J Respir Cell Mol Biol [Internet]. American Thoracic Society; 2007 Apr [cited 2017 Mar 9];36(4):460–5. Available from: http://www.ncbi.nlm.nih.gov/pubmed/17079778

382. Kodali V, Littke MH, Tilton SC, Teeguarden JG, Shi L, Frevert CW, et al. Dysregulation of Macrophage Activation Profiles by Engineered Nanoparticles. ACS Nano [Internet]. American Chemical Society; 2013 Aug 27 [cited 2017 Mar 9];7(8):6997–7010. Available from: http://pubs.acs.org/doi/abs/10.1021/nn402145t

383. Yin XJ, Dong CC, Ma JYC, Roberts JR, Antonini JM, Ma JKH. Suppression of Phagocytic and Bactericidal Functions of Rat Alveolar Macrophages by the Organic

Component of Diesel Exhaust Particles. J Toxicol Environ Heal Part A [Internet]. Taylor & Francis Group ; 2007 Apr 11 [cited 2017 Mar 6];70(10):820–8. Available from: http://www.tandfonline.com/doi/abs/10.1080/15287390701209766

384. Mudway IS, Stenfors N, Blomberg A, Helleday R, Dunster C, Marklund S., et al. Differences in basal airway antioxidant concentrations are not predictive of individual responsiveness to ozone: a comparison of healthy and mild asthmatic subjects. Free Radic Biol Med [Internet]. 2001 Oct [cited 2017 Aug 30];31(8):962–74. Available from: http://linkinghub.elsevier.com/retrieve/pii/S0891584901006712

385. Singh P, DeMarini DM, Dick CAJ, Tabor DG, Ryan J V, Linak WP, et al. Sample characterization of automobile and forklift diesel exhaust particles and comparative pulmonary toxicity in mice. Environ Health Perspect [Internet]. 2004 Jun [cited 2017 Jul 10];112(8):820–5. Available from: http://www.ncbi.nlm.nih.gov/pubmed/15175167

386. Valko M, Morris H, Cronin MTD. Metals, toxicity and oxidative stress. Curr Med Chem [Internet]. 2005 [cited 2017 Aug 13];12(10):1161–208. Available from: http://www.ncbi.nlm.nih.gov/pubmed/15892631

387. Valko M, Morris H, Cronin MTD. Metals, toxicity and oxidative stress. Curr Med Chem. 2005;12(10):1161–208.

388. Capsoni F, Minonzio F, Ongari AM, Carbonelli V, Galli A, Zanussi C. IL-10 up-regulates human monocyte phagocytosis in the presence of IL-4 and IFN-gamma. J Leukoc Biol [Internet]. 1995 Sep [cited 2017 Jul 10];58(3):351–8. Available from: http://www.ncbi.nlm.nih.gov/pubmed/7665991

389. Laichalk LL, Danforth JM, Standiford TJ. Interleukin-10 inhibits neutrophil phagocytic and bactericidal activity. FEMS Immunol Med Microbiol [Internet]. 1996 Oct [cited 2017 Jul 10];15(4):181–7. Available from: http://www.ncbi.nlm.nih.gov/pubmed/8908479

390. Li Y, Boraschi D. Endotoxin contamination: a key element in the interpretation of nanosafety studies. Nanomedicine [Internet]. Future Medicine Ltd London, UK ; 2016 Feb 20 [cited 2017 Jul 10];11(3):269–87. Available from: http://www.futuremedicine.com/doi/10.2217/nnm.15.196

391. Reynolds HY. Lung inflammation: role of endogenous chemotactic factors in attracting polymorphonuclear granulocytes. Am Rev Respir Dis [Internet]. 1983 Feb [cited 2017 Mar 9];127(2):S16-25. Available from: http://www.ncbi.nlm.nih.gov/pubmed/6338779

392. Sibille Y, Reynolds HY. Macrophages and Polymorphonuclear Neutrophils in Lung

Defense and Injury. Am Rev Respir Dis [Internet]. American Lung Association; 1990 Feb [cited 2017 Mar 9];141(2):471–501. Available from: http://www.atsjournals.org/doi/abs/10.1164/ajrccm/141.2.471

393. Mege J-L, Meghari S, Honstettre A, Capo C, Raoult D, Fallon P. The two faces of interleukin 10 in human infectious diseases. Lancet Infect Dis [Internet]. ASM Press, Washington; 2006 Sep [cited 2017 Mar 9];6(9):557–69. Available from: http://www.ncbi.nlm.nih.gov/pubmed/16931407

394. Strieter RM, Belperio JA, Keane MP. Cytokines in innate host defense in the lung. J Clin Invest [Internet]. American Society for Clinical Investigation; 2002 Mar [cited 2017 Mar 9];109(6):699–705. Available from: http://www.ncbi.nlm.nih.gov/pubmed/11901175

395. Mazzarella G, Ferraraccio F, Prati MV, Annunziata S, Bianco A, Mezzogiorno A, et al. Effects of diesel exhaust particles on human lung epithelial cells: An in vitro study. Respir Med [Internet]. 2007 Jun [cited 2017 Mar 9];101(6):1155–62. Available from: http://linkinghub.elsevier.com/retrieve/pii/S0954611106005981

396. Kafoury RM, Madden MC. Diesel exhaust particles induce the over expression of tumor necrosis factor-alpha (TNF-alpha) gene in alveolar macrophages and failed to induce apoptosis through activation of nuclear factor-kappaB (NF-kappaB). Int J Environ Res Public Health [Internet]. Multidisciplinary Digital Publishing Institute (MDPI); 2005 Apr [cited 2017 Mar 9];2(1):107–13. Available from: http://www.ncbi.nlm.nih.gov/pubmed/16705808

397. Bollati V, Angelici L, Rizzo G, Pergoli L, Rota F, Hoxha M, et al. Microvesicle-associated microRNA expression is altered upon particulate matter exposure in healthy workers and in A549 cells. J Appl Toxicol [Internet]. 2015 Jan [cited 2017 Mar 7];35(1):59–67. Available from: http://doi.wiley.com/10.1002/jat.2987

398. Mauderly JL, Samet JM. Is There Evidence for Synergy Among Air Pollutants in Causing Health Effects? Environ Health Perspect [Internet]. 2009 Jan [cited 2017 Mar 9];117(1):1–6. Available from: http://ehp.niehs.nih.gov/11654

399. Suri R, Mushtaq N, Waite R, Grigg J. Additive effect of air pollution particulate matter and cigarette smoke on pneumococcal adhesion to lower airway cells. Eur Respir J [Internet]. ERS Journals; 2012 [cited 2017 Mar 9];40(Suppl 56):P4112. Available from: http://erj.ersjournals.com/content/40/Suppl_56/P4112

400. Disayabutr S, Kim EK, Cha S-I, Green G, Naikawadi RP, Jones KD, et al. miR-34

miRNAs Regulate Cellular Senescence in Type II Alveolar Epithelial Cells of Patients with Idiopathic Pulmonary Fibrosis. Mora A, editor. PLoS One [Internet]. Public Library of Science; 2016 Jun 30 [cited 2017 Mar 9];11(6):e0158367. Available from: http://dx.plos.org/10.1371/journal.pone.0158367

401. Chen P, Edelman JD, Gharib SA. Comparative Evaluation of miRNA Expression between in Vitro and in Vivo Airway Epithelium Demonstrates Widespread Differences. Am J Pathol [Internet]. 2013 Nov [cited 2017 Aug 13];183(5):1405–10. Available from: http://www.ncbi.nlm.nih.gov/pubmed/24001474

402. Li N, Sioutas C, Cho A, Schmitz D, Misra C, Sempf J, et al. Ultrafine particulate pollutants induce oxidative stress and mitochondrial damage. Environ Health Perspect [Internet]. National Institute of Environmental Health Science; 2003 Apr [cited 2017 Aug 13];111(4):455–60. Available from: http://www.ncbi.nlm.nih.gov/pubmed/12676598

403. Ott M, Gogvadze V, Orrenius S, Zhivotovsky B. Mitochondria, oxidative stress and cell death. Apoptosis [Internet]. 2007 May 9 [cited 2017 Aug 13];12(5):913–22. Available from: http://www.ncbi.nlm.nih.gov/pubmed/17453160

404. Dagher Z, Garçon G, Billet S, Gosset P, Ledoux F, Courcot D, et al. Activation of different pathways of apoptosis by air pollution particulate matter (PM2.5) in human epithelial lung cells (L132) in culture. Toxicology [Internet]. 2006 Aug [cited 2017 Mar 9];225(1):12–24. Available from: http://linkinghub.elsevier.com/retrieve/pii/S0300483X06002460

405. Upadhyay D, Panduri V, Ghio A, Kamp DW. Particulate Matter Induces Alveolar Epithelial Cell DNA Damage and Apoptosis Role of Free Radicals and the Mitochondria. [cited 2017 Mar 9]; Available from: http://www.atsjournals.org/doi/pdf/10.1165/rcmb.2002-0269OC

406. Kim H, McGrath BM, Silverstone PH. A review of the possible relevance of inositol and the phosphatidylinositol second messenger system (PI-cycle) to psychiatric disorders—focus on magnetic resonance spectroscopy (MRS) studies. Hum Psychopharmacol Clin Exp [Internet]. 2005 Jul [cited 2017 Sep 12];20(5):309–26. Available from: http://www.ncbi.nlm.nih.gov/pubmed/15880397

407. Chen X, Zhang B, Li H, Peng X. Myo-inositol improves the host's ability to eliminate balofloxacin-resistant Escherichia coli. Sci Rep [Internet]. 2015 Jun 1 [cited 2017 Mar 9];5:10720. Available from: http://www.nature.com/articles/srep10720

408. Wong D. Exploring the small molecule effects of gold nanoparticle and ZnO exposure in human lung epithelial cells through NMR-based metabolomics. Imperial College, London; 2016.

409. Sahu D, Kannan GM, Vijayaraghavan R. Size-Dependent Effect of Zinc Oxide on Toxicity and Inflammatory Potential of Human Monocytes. J Toxicol Environ Heal Part A [Internet]. 2014 Feb 16 [cited 2017 Aug 13];77(4):177–91. Available from: http://www.ncbi.nlm.nih.gov/pubmed/24555677

410. MacParland SA, Tsoi KM, Ouyang B, Ma X-Z, Manuel J, Fawaz A, et al. Phenotype Determines Nanoparticle Uptake by Human Macrophages from Liver and Blood. 2016 [cited 2017 Sep 12]; Available from: http://pubs.acs.org/doi/pdf/10.1021/acsnano.6b06245

411. Werb Z, Cohn ZA. Plasma membrane synthesis in the macrophage following phagocytosis of polystyrene latex particles. J Biol Chem [Internet]. 1972 Apr 25 [cited 2017 Sep 12];247(8):2439–46. Available from: http://www.ncbi.nlm.nih.gov/pubmed/5019957

412. De Simone R, Vissicchio F, Mingarelli C, De Nuccio C, Visentin S, Ajmone-Cat MA, et al. Branched-chain amino acids influence the immune properties of microglial cells and their responsiveness to pro-inflammatory signals. Biochim Biophys Acta - Mol Basis Dis [Internet]. 2013 May [cited 2017 Mar 9];1832(5):650–9. Available from: http://linkinghub.elsevier.com/retrieve/pii/S0925443913000380

413. Liu L, Lu Y, Martinez J, Bi Y, Lian G, Wang T, et al. Proinflammatory signal suppresses proliferation and shifts macrophage metabolism from Myc-dependent to HIF1α-dependent. Proc Natl Acad Sci U S A [Internet]. National Academy of Sciences; 2016 Feb 9 [cited 2017 Mar 9];113(6):1564–9. Available from: http://www.ncbi.nlm.nih.gov/pubmed/26811453

414. Ribeiro CA, Sgaravatti ÂM, Rosa RB, Schuck PF, Grando V, Schmidt AL, et al. Inhibition of Brain Energy Metabolism by the Branched-chain Amino Acids Accumulating in Maple Syrup Urine Disease. Neurochem Res [Internet]. Springer US; 2008 Jan 8 [cited 2017 Mar 9];33(1):114–24. Available from: http://link.springer.com/10.1007/s11064-007-9423-9

415. Liu X, Gao J, Chen J, Wang Z, Shi Q, Man H, et al. Identification of metabolic biomarkers in patients with type 2 diabetic coronary heart diseases based on metabolomic approach. Sci Rep [Internet]. Nature Publishing Group; 2016;6:30785. Available from: http://www.ncbi.nlm.nih.gov/pmc/articles/PMC4965763/

416. Gottlieb E, Armour SM, Harris MH, Thompson CB. Mitochondrial membrane potential regulates matrix configuration and cytochrome c release during apoptosis. Cell Death Differ [Internet]. Nature Publishing Group; 2003 Jun [cited 2017 Mar 9];10(6):709–17. Available from: http://www.nature.com/doifinder/10.1038/sj.cdd.4401231

417. Zhu YP, Brown JR, Sag D, Zhang L, Suttles J. Adenosine 5'-monophosphate-activated protein kinase regulates IL-10-mediated anti-inflammatory signaling pathways in macrophages. J Immunol [Internet]. NIH Public Access; 2015 Jan 15 [cited 2017 Mar 9];194(2):584–94. Available from: http://www.ncbi.nlm.nih.gov/pubmed/25512602

418. Monick MM, Powers LS, Barrett CW, Hinde S, Ashare A, Groskreutz DJ, et al. Constitutive ERK MAPK activity regulates macrophage ATP production and mitochondrial integrity. J Immunol [Internet]. 2008 Jun 1 [cited 2017 Mar 9];180(11):7485–96. Available from: http://www.ncbi.nlm.nih.gov/pubmed/18490749

419. Sag D, Carling D, Stout RD, Suttles J. Adenosine 5'-monophosphate-activated protein kinase promotes macrophage polarization to an anti-inflammatory functional phenotype. J Immunol [Internet]. NIH Public Access; 2008 Dec 15 [cited 2017 Aug 13];181(12):8633–41. Available from: http://www.ncbi.nlm.nih.gov/pubmed/19050283

420. Shao W, Espenshade PJ. Expanding Roles for SREBP in Metabolism. Cell Metab [Internet]. 2012 Oct [cited 2017 Mar 9];16(4):414–9. Available from: http://linkinghub.elsevier.com/retrieve/pii/S1550413112003609

421. Shen J, Liu Z, Todd NW, Zhang H, Liao J, Yu L, et al. Diagnosis of lung cancer in individuals with solitary pulmonary nodules by plasma microRNA biomarkers. BMC Cancer [Internet]. BioMed Central; 2011;11:374. Available from: http://www.ncbi.nlm.nih.gov/pmc/articles/PMC3175224/

422. Waters PS, McDermott AM, Wall D, Heneghan HM, Miller N, Newell J, et al. Relationship between Circulating and Tissue microRNAs in a Murine Model of Breast Cancer. PLoS One [Internet]. Public Library of Science; 2012 Nov 30;7(11):e50459-. Available from: http://dx.doi.org/10.1371%252Fjournal.pone.0050459

423. Gaughwin P, Ciesla M, Lahiri N, Tabrizi S, Brundin P, Björkqvist M. Hsa-miR-34b is a plasma-stable microRNA that is elevated in pre-manifest Huntington's disease. Hum Mol Genet [Internet]. 2011;20(11):2235–7. Available from: https://www.ncbi.nlm.nih.gov/pubmed/21421997

424. Van Eeden S, Leipsic J, Paul Man SF, Sin DD. The Relationship between Lung

Inflammation and Cardiovascular Disease. Am J Respir Crit Care Med [Internet]. American Thoracic Society; 2012 Jul 14 [cited 2018 Jan 10];186(1):11–6. Available from: http://www.atsjournals.org/doi/abs/10.1164/rccm.201203-0455PP

425. McDonald RA, Hata A, MacLean MR, Morrell NW, Baker AH. MicroRNA and vascular remodelling in acute vascular injury and pulmonary vascular remodelling. Cardiovasc Res [Internet]. Oxford University Press; 2012 Mar 15 [cited 2018 Jan 10];93(4):594–604. Available from: https://academic.oup.com/cardiovascres/article-lookup/doi/10.1093/cvr/cvr299

426. Sin DD, Lacy P, York E, Man SFP. Effects of Fluticasone on Systemic Markers of Inflammation in Chronic Obstructive Pulmonary Disease. Am J Respir Crit Care Med [Internet]. 2004 Oct 1 [cited 2017 Aug 13];170(7):760–5. Available from: http://www.ncbi.nlm.nih.gov/pubmed/15229100

427. Mukae H, Vincent R, Quinlan K, English D, Hards J, Hogg JC, et al. The Effect of Repeated Exposure to Particulate Air Pollution (PM_{10}) on the Bone Marrow. Am J Respir Crit Care Med [Internet]. American Thoracic SocietyNew York, NY; 2001 Jan 14 [cited 2017 Aug 13];163(1):201–9. Available from: http://www.atsjournals.org/doi/abs/10.1164/ajrccm.163.1.2002039

428. Pegtel DM, Cosmopoulos K, Thorley-Lawson DA, van Eijndhoven MAJ, Hopmans ES, Lindenberg JL, et al. Functional delivery of viral miRNAs via exosomes. Proc Natl Acad Sci U S A [Internet]. National Academy of Sciences; 2010 Apr 6 [cited 2017 Mar 6];107(14):6328–33. Available from: http://www.ncbi.nlm.nih.gov/pubmed/20304794

429. Gibbings DJ, Ciaudo C, Erhardt M, Voinnet O. Multivesicular bodies associate with components of miRNA effector complexes and modulate miRNA activity. Nat Cell Biol [Internet]. Nature Publishing Group; 2009 Sep;11(9):1143–9. Available from: http://dx.doi.org/10.1038/ncb1929

430. Oberdörster G, Sharp Z, Atudorei V, Elder A, Gelein R, Kreyling W, et al. Translocation of Inhaled Ultrafine Particles to the Brain. Inhal Toxicol [Internet]. Taylor & Francis; 2004 Jan 1;16(6–7):437–45. Available from: http://dx.doi.org/10.1080/08958370490439597

431. Kreyling WG, Semmler M, Erbe F, Mayer P, Takenaka S, Schulz H, et al. TRANSLOCATION OF ULTRAFINE INSOLUBLE IRIDIUM PARTICLES FROM LUNG EPITHELIUM TO EXTRAPULMONARY ORGANS IS SIZE DEPENDENT BUT VERY LOW. J Toxicol Environ Heal Part A [Internet]. Informa UK Ltd ; 2002 Oct 12 [cited 2018 Jan 14];65(20):1513–30. Available from:

http://www.tandfonline.com/doi/abs/10.1080/00984100290071649

432. Wallenborn JG, McGee JK, Schladweiler MC, Ledbetter AD, Kodavanti UP. Systemic Translocation of Particulate Matter-Associated Metals Following a Single Intratracheal Instillation in Rats. Toxicol Sci [Internet]. Oxford University Press; 2007 Apr 10 [cited 2018 Jan 14];98(1):231–9. Available from: https://academic.oup.com/toxsci/article-lookup/doi/10.1093/toxsci/kfm088

433. Goeminne PC, Kiciński M, Vermeulen F, Fierens F, De Boeck K, Nemery B, et al. Impact of Air Pollution on Cystic Fibrosis Pulmonary Exacerbations: A Case-Crossover Analysis. Chest. 2013;143(4):946–54.

434. Chauhan AJ, Johnston SL. Air pollution and infection in respiratory illness. Br Med Bull [Internet]. 2003 Dec 1;68(1):95–112. Available from: http://dx.doi.org/10.1093/bmb/ldg022

435. Moffat FL, Han T, Li Z-M, Peck MD, Jy W, Ahn YS, et al. Supplemental L-arginine HCl augments bacterial phagocytosis in human polymorphonuclear leukocytes. J Cell Physiol [Internet]. 1996 Jul [cited 2017 Aug 13];168(1):26–33. Available from: http://www.ncbi.nlm.nih.gov/pubmed/8647919

436. Harrison RM, Jones AM, Gietl J, Yin J, Green DC. Estimation of the Contributions of Brake Dust, Tire Wear, and Resuspension to Nonexhaust Traffic Particles Derived from Atmospheric Measurements. Environ Sci Technol [Internet]. 2012 Jun 19 [cited 2017 Jun 1];46(12):6523–9. Available from: http://www.ncbi.nlm.nih.gov/pubmed/22642836

437. Saccenti E, Hoefsloot HCJ, Smilde AK, Westerhuis JA, Hendriks MMWB. Reflections on univariate and multivariate analysis of metabolomics data. Metabolomics [Internet]. 2014;10(3):361–74. Available from: http://dx.doi.org/10.1007/s11306-013-0598-6

438. Horgan RP, Kenny LC. “Omic” technologies: genomics, transcriptomics, proteomics and metabolomics. Obstet Gynaecol [Internet]. 2011 Jul 18 [cited 2016 Nov 10];13(3):189–95. Available from: http://doi.wiley.com/10.1576/toag.13.3.189.27672

439. Lawrence T, Willoughby DA, Gilroy DW. Anti-inflammatory lipid mediators and insights into the resolution of inflammation. Nat Rev Immunol [Internet]. 2002 Oct;2(10):787–95. Available from: http://dx.doi.org/10.1038/nri915

440. Lee JS, Park SJ, Cho YS, Huh JW, Oh Y-M, Lee S-D. Role of AMP-Activated Protein Kinase (AMPK) in Smoking-Induced Lung Inflammation and Emphysema. Tuberc Respir Dis (Seoul) [Internet]. The Korean Academy of Tuberculosis and Respiratory

Diseases; 2015 Jan;78(1):8–17. Available from: http://www.ncbi.nlm.nih.gov/pmc/articles/PMC4311035/

441. Tang H-F, Chen J-Q, Xie Q-M, Zheng X-Y, Zhu Y-L, Adcock I, et al. The role of PDE4 in pulmonary inflammation and goblet cell hyperplasia in allergic rats. Biochim Biophys Acta - Mol Basis Dis. 2006;1762(5):525–32.

442. Chung S, Lee TJ, Reader BF, Kim JY, Lee YG, Park GY, et al. FoxO1 regulates allergic asthmatic inflammation through regulating polarization of the macrophage inflammatory phenotype. Oncotarget [Internet]. Impact Journals LLC; 2016 Apr 5;7(14):17532–46. Available from: http://www.ncbi.nlm.nih.gov/pmc/articles/PMC4951231/

443. Whyte MKB, Walmsley SR. The Regulation of Pulmonary Inflammation by the Hypoxia-Inducible Factor–Hydroxylase Oxygen-Sensing Pathway. Ann Am Thorac Soc [Internet]. American Thoracic Society; 2014 Dec;11(Suppl 5):S271–6. Available from: http://www.ncbi.nlm.nih.gov/pmc/articles/PMC4298968/

444. Plantier L, Besnard V, Xu Y, Ikegami M, Wert SE, Hunt AN, et al. Activation of Sterol-response Element-binding Proteins (SREBP) in Alveolar Type II Cells Enhances Lipogenesis Causing Pulmonary Lipotoxicity. J Biol Chem [Internet]. 9650 Rockville Pike, Bethesda, MD 20814, U.S.A.: American Society for Biochemistry and Molecular Biology; 2012 Mar 23;287(13):10099–114. Available from: http://www.ncbi.nlm.nih.gov/pmc/articles/PMC3323060/

445. Asada S, Daitoku H, Matsuzaki H, Saito T, Sudo T, Mukai H, et al. Mitogen-activated protein kinases, Erk and p38, phosphorylate and regulate Foxo1. Cell Signal. 2007;19(3):519–27.

446. Lanna A, Henson SM, Escors D, Akbar AN. The kinase p38 activated by the metabolic regulator AMPK and scaffold TAB1 drives the senescence of human T cells. Nat Immunol [Internet]. Nature Publishing Group, a division of Macmillan Publishers Limited. All Rights Reserved.; 2014 Oct;15(10):965–72. Available from: http://dx.doi.org/10.1038/ni.2981

447. Knebel B, Lehr S, Hartwig S, Haas J, Kaber G, Dicken H-D, et al. Phosphorylation of sterol regulatory element-binding protein (SREBP)-1c by p38 kinases, ERK and JNK influences lipid metabolism and the secretome of human liver cell line HepG2. Arch Physiol Biochem [Internet]. Taylor & Francis; 2014 Dec 1;120(5):216–27. Available from: http://dx.doi.org/10.3109/13813455.2014.973418

448. Emerling BM, Platanias LC, Black E, Nebreda AR, Davis RJ, Chandel NS. Mitochondrial Reactive Oxygen Species Activation of p38 Mitogen-Activated Protein Kinase Is Required for Hypoxia Signaling. Mol Cell Biol [Internet]. 2005 Jun 15;25(12):4853–62. Available from: http://mcb.asm.org/content/25/12/4853.abstract

449. Ghezzi P. Role of glutathione in immunity and inflammation in the lung. Int J Gen Med [Internet]. Dove Medical Press; 2011;4:105–13. Available from: http://www.ncbi.nlm.nih.gov/pmc/articles/PMC3048347/

450. Al-Humadi NH, Siegel PD, Lewis DM, Barger MW, Ma JYC, Weissman DN, et al. Alteration of intracellular cysteine and glutathione levels in alveolar macrophages and lymphocytes by diesel exhaust particle exposure. Environ Health Perspect [Internet]. 2002 Apr;110(4):349–53. Available from: http://www.ncbi.nlm.nih.gov/pmc/articles/PMC1240797/

451. Yoon M, Campbell JL, Andersen ME, Clewell HJ. Quantitative in vitro to in vivo extrapolation of cell-based toxicity assay results. Crit Rev Toxicol [Internet]. Taylor & Francis; 2012 Sep 1;42(8):633–52. Available from: http://dx.doi.org/10.3109/10408444.2012.692115

452. Chuang H-C, Cheng Y-L, Lei Y-C, Chang H-H, Cheng T-J. Protective effects of pulmonary epithelial lining fluid on oxidative stress and DNA single-strand breaks caused by ultrafine carbon black, ferrous sulphate and organic extract of diesel exhaust particles. Toxicol Appl Pharmacol. 2013;266(3):329–34.

453. Ramirez T, Daneshian M, Kamp H, Bois FY, Clench MR, Coen M, et al. Metabolomics in Toxicology and Preclinical Research. ALTEX [Internet]. 2013;30(2):209–25. Available from: http://www.ncbi.nlm.nih.gov/pmc/articles/PMC3821217/

454. Paules R. Phenotypic anchoring: linking cause and effect. Environ Health Perspect [Internet]. 2003 May;111(6):A338–9. Available from: http://www.ncbi.nlm.nih.gov/pmc/articles/PMC1241511/

455. Pfannkuch F, Suter-Dick L, Mannhold R, Kubinyi H, Folkers G. Predictive Toxicology: From Vision to Reality. John Wiley & Sons; 2014. 133-134 p.

456. ter Kuile BH, Westerhoff H V. Transcriptome meets metabolome: hierarchical and metabolic regulation of the glycolytic pathway. FEBS Lett [Internet]. 2001 Jul 6 [cited 2017 Feb 14];500(3):169–71. Available from: http://doi.wiley.com/10.1016/S0014-5793%252801%252902613-8

457. Moxley JF, Jewett MC, Antoniewicz MR, Villas-Boas SG, Alper H, Wheeler RT, et al.

Linking high-resolution metabolic flux phenotypes and transcriptional regulation in yeast modulated by the global regulator Gcn4p. Proc Natl Acad Sci U S A [Internet]. National Academy of Sciences; 2009 Apr 21;106(16):6477–82. Available from: http://www.ncbi.nlm.nih.gov/pmc/articles/PMC2672541/

458. Fendt S-M, Buescher JM, Rudroff F, Picotti P, Zamboni N, Sauer U. Tradeoff between enzyme and metabolite efficiency maintains metabolic homeostasis upon perturbations in enzyme capacity. Mol Syst Biol [Internet]. Nature Publishing Group; 2010;6:356. Available from: http://www.ncbi.nlm.nih.gov/pmc/articles/PMC2872607/

459. Elvidge T, Matthews I, Gregory C, Hoogendoorn B. Feasibility of Using Biomarkers in Blood Serum as Markers of Effect Following Exposure of the Lungs to Particulate Matter Air Pollution. J Environ Sci Heal Part C [Internet]. Taylor & Francis; 2013 Jan 1;31(1):1–44. Available from: http://dx.doi.org/10.1080/10590501.2013.763575

460. Calder PC, Ahluwalia N, Brouns F, Buetler T, Clement K, Cunningham K, et al. Dietary factors and low-grade inflammation in relation to overweight and obesity. Br J Nutr [Internet]. Cambridge, UK: Cambridge University Press; 2011;106(S3):S1–78. Available from: https://www.cambridge.org/core/article/div-class-title-dietary-factors-and-low-grade-inflammation-in-relation-to-overweight-and-obesity-div/D4F1B9B32B1DE434557332EB79972100

461. Gouin J-P, Glaser R, Malarkey WB, Beversdorf D, Kiecolt-Glaser J. Chronic stress, daily stressors, and circulating inflammatory markers. Heal Psychol [Internet]. 2012 Mar;31(2):264–8. Available from: http://www.ncbi.nlm.nih.gov/pmc/articles/PMC3253267/

462. Giannoudis P V, Hildebrand F, Pape HC. Inflammatory serum markers in patients with multiple trauma. J Bone & Jt Surgery, Br Vol [Internet]. 2004 Apr 1;86–B(3):313. Available from: http://www.bjj.boneandjoint.org.uk/content/86-B/3/313.abstract

463. The european parliament and the council of the european, union. Directive 2008/50/EC of the european parliament and of the council [Internet]. 2008. Available from: http://eur-lex.europa.eu/LexUriServ/LexUriServ.do?uri=OJ:L:2008:152:0001:0044:EN:PDF

464. Denier van der Gon HAC, Gerlofs-Nijland ME, Gehrig R, Gustafsson M, Janssen N, Harrison RM, et al. The Policy Relevance of Wear Emissions from Road Transport, Now and in the Future—An International Workshop Report and Consensus Statement. J Air Waste Manage Assoc [Internet]. Taylor & Francis; 2013 Feb

1;63(2):136–49. Available from: http://dx.doi.org/10.1080/10962247.2012.741055

465. Rexeis M, Hausberger S. Trend of vehicle emission levels until 2020 – Prognosis based on current vehicle measurements and future emission legislation. Atmos Environ. 2009;43(31):4689–98.

466. Wood HE, Marlin N, Mudway IS, Bremner SA, Cross L, Dundas I, et al. Effects of Air Pollution and the Introduction of the London Low Emission Zone on the Prevalence of Respiratory and Allergic Symptoms in Schoolchildren in East London: A Sequential Cross-Sectional Study. PLoS One [Internet]. Public Library of Science; 2015 Aug 21;10(8):e0109121-. Available from: http://dx.doi.org/10.1371%252Fjournal.pone.0109121

467. McDonnell WF. Utility of controlled human exposure studies for assessing the health effects of complex mixtures and indoor air pollutants. Environ Health Perspect [Internet]. 1993 Dec;101(Suppl 4):199–203. Available from: http://www.ncbi.nlm.nih.gov/pmc/articles/PMC1519701/

468. Xu Y, Barregard L, Nielsen J, Gudmundsson A, Wierzbicka A, Axmon A, et al. Effects of diesel exposure on lung function and inflammation biomarkers from airway and peripheral blood of healthy volunteers in a chamber study. Part Fibre Toxicol [Internet]. BioMed Central; 2013 Dec 9 [cited 2017 Aug 13];10:60. Available from: http://www.ncbi.nlm.nih.gov/pubmed/24321138

469. Dewulf B, Neutens T, Lefebvre W, Seynaeve G, Vanpoucke C, Beckx C, et al. Dynamic assessment of exposure to air pollution using mobile phone data. Int J Health Geogr [Internet]. 2016;15(1):14. Available from: http://dx.doi.org/10.1186/s12942-016-0042-z

470. Armstrong L, Jordan N, Millar A. Interleukin 10 (IL-10) regulation of tumour necrosis factor alpha (TNF-alpha) from human alveolar macrophages and peripheral blood monocytes. Thorax [Internet]. 1996 Feb [cited 2018 Jan 15];51(2):143–9. Available from: http://www.ncbi.nlm.nih.gov/pubmed/8711645

471. Pedersen CB, Raaschou-Nielsen O, Hertel O, Mortensen PB. Air pollution from traffic and schizophrenia risk. Schizophr Res [Internet]. Elsevier; 2017 Feb 19;66(1):83–5. Available from: http://dx.doi.org/10.1016/S0920-9964(03)00062-8

472. Lai C-Y, Yu S-L, Hsieh MH, Chen C-H, Chen H-Y, Wen C-C, et al. MicroRNA Expression Aberration as Potential Peripheral Blood Biomarkers for Schizophrenia. PLoS One [Internet]. Public Library of Science; 2011 Jun 29;6(6):e21635-. Available

from: http://dx.doi.org/10.1371%252Fjournal.pone.0021635

473. Bain J, Plater L, Elliott M, Shpiro N, Hastie CJ, McLauchlan H, et al. The selectivity of protein kinase inhibitors: a further update. Biochem J [Internet]. Portland Press Ltd; 2007 Dec 15 [cited 2018 Jan 14];408(3):297–315. Available from: http://www.ncbi.nlm.nih.gov/pubmed/17850214

474. Kazi JU, Kabir NN, Soh J-W. Bioinformatic prediction and analysis of eukaryotic protein kinases in the rat genome. Gene [Internet]. Elsevier; 2008 Feb 29 [cited 2018 Jan 14];410(1):147–53. Available from: http://www.sciencedirect.com/science/article/pii/S0378111907006166?via%3Dihub

475. Kalbácová M, Vrbacký M, Drahota Z, Melková Z. Comparison of the effect of mitochondrial inhibitors on mitochondrial membrane potential in two different cell lines using flow cytometry and spectrofluorometry. Cytometry A [Internet]. 2003 Apr [cited 2017 Feb 19];52(2):110–6. Available from: http://www.ncbi.nlm.nih.gov/pubmed/12655654

476. Rizzo AM, Corsetto PA, Farina F, Montorfano G, Pani G, Battaglia C, et al. Repeated Intratracheal Instillation of PM10 Induces Lipid Reshaping in Lung Parenchyma and in Extra-Pulmonary Tissues. PLoS One [Internet]. Public Library of Science; 2014 Sep 26;9(9):e106855-. Available from: http://dx.doi.org/10.1371%252Fjournal.pone.0106855

477. de Paula Rogerio A, Sorgi CA, Sadikot R, Carlo T. The role of lipids mediators in inflammation and resolution. Biomed Res Int [Internet]. Hindawi; 2015 [cited 2017 Aug 13];2015:605959. Available from: http://www.ncbi.nlm.nih.gov/pubmed/25879029

478. Dona AC, Jiménez B, Schäfer H, Humpfer E, Spraul M, Lewis MR, et al. Precision High-Throughput Proton NMR Spectroscopy of Human Urine, Serum, and Plasma for Large-Scale Metabolic Phenotyping. Anal Chem [Internet]. American Chemical Society; 2014 Oct 7 [cited 2017 Sep 12];86(19):9887–94. Available from: http://pubs.acs.org/doi/10.1021/ac5025039

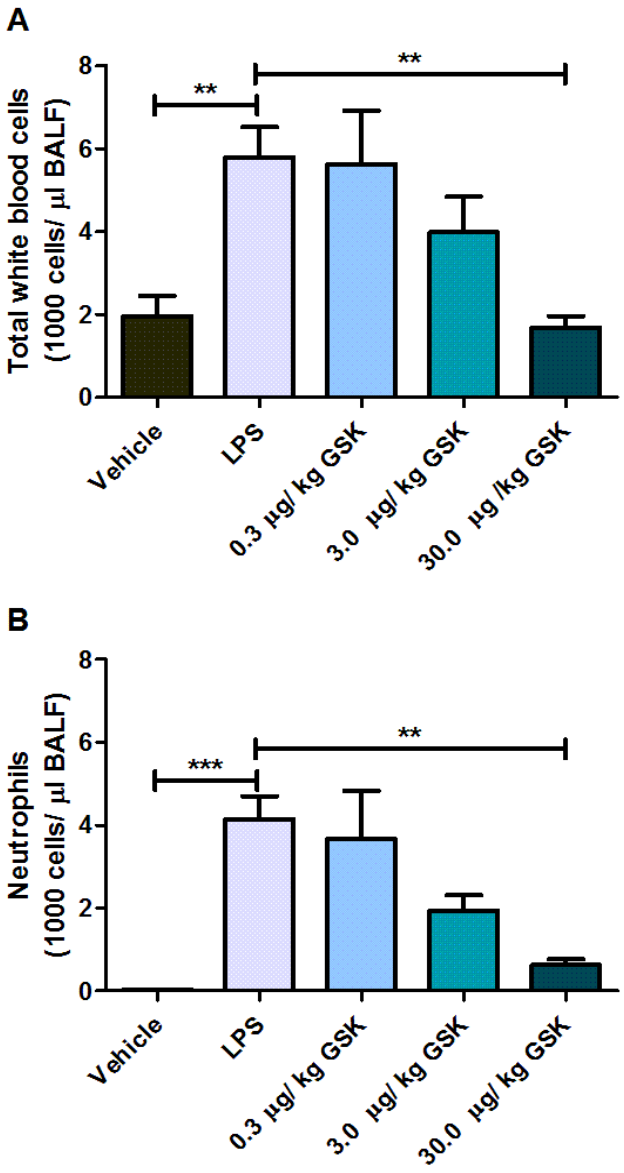
479. Riddervold IS, Bønløkke JH, Olin A-C, Grønborg TK, Schlünssen V, Skogstrand K, et al. Effects of wood smoke particles from wood-burning stoves on the respiratory health of atopic humans. Part Fibre Toxicol [Internet]. 2012;9(1):12. Available from: http://dx.doi.org/10.1186/1743-8977-9-12

480. Hu S-W, Shy CM. Health Effects of Waste Incineration: A Review of Epidemiologic Studies. J Air Waste Manage Assoc [Internet]. Taylor & Francis; 2001 Jul

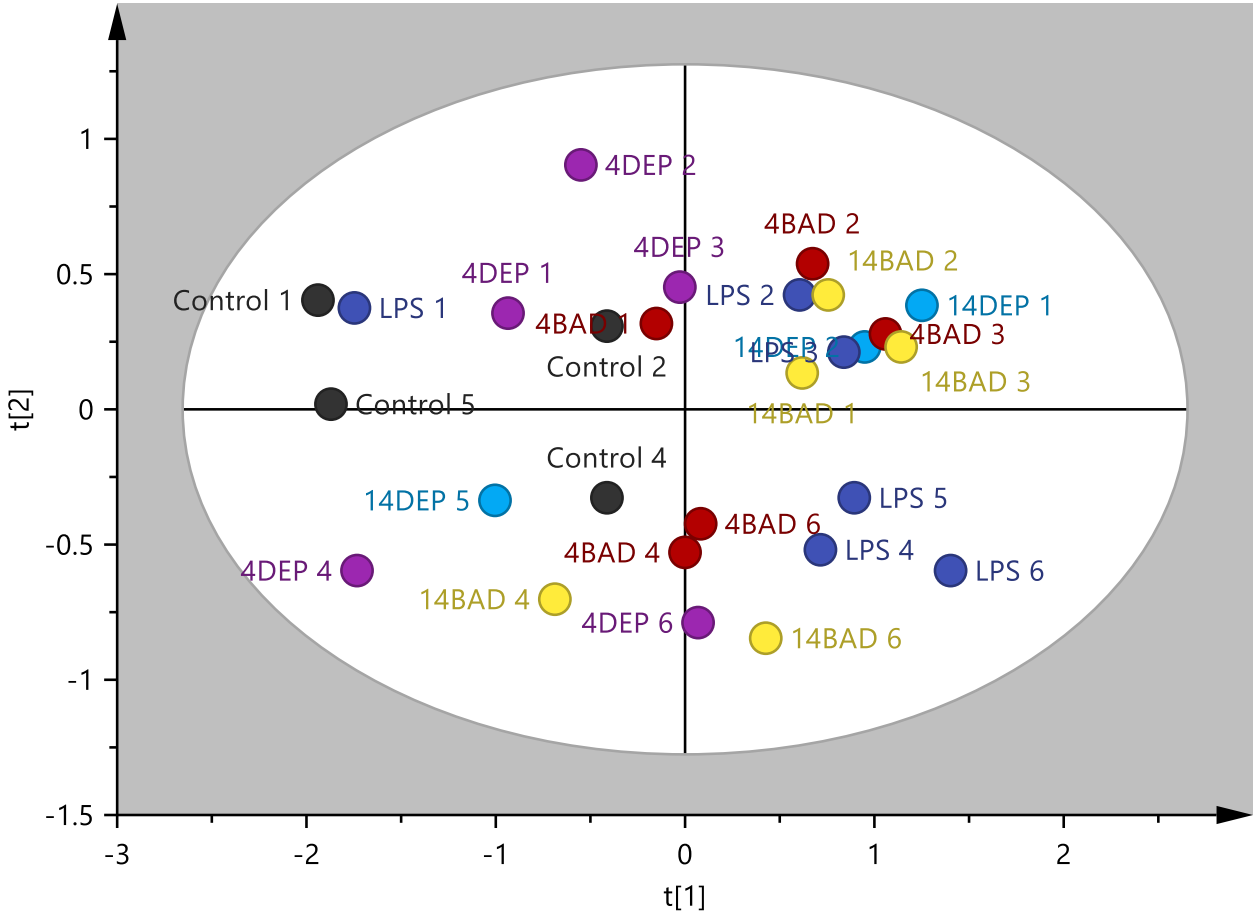
1;51(7):1100–9. Available from: http://dx.doi.org/10.1080/10473289.2001.10464324

481. May S, Romberger DJ, Poole JA. Respiratory Health Effects of Large Animal Farming Environments. J Toxicol Environ Health B Crit Rev [Internet]. 2012;15(8):524–41. Available from: http://www.ncbi.nlm.nih.gov/pmc/articles/PMC4001716/

Supplementary material



Supplementary figure 3.1: Total white blood cell (A) and neutrophil (B) counts taken from the BALF of rats following exposure to LPS, 0.3-30.0 µg/kg GSK or a vehicle control. BALF was harvested 4h after exposure and total WBC were counted using an Advia 2120 analyser. To avoid miss-gating of WBC species, 'Absolute neutrophil counts' were determined by manually counting the number of neutrophils per 100 cells and applying those percentages to the total WBC counts for each sample. Statistically significant differences in WBC and neutrophil counts were sought between exposure types using 1-Way ANOVA tests with Bonferroni corrections for multiple testing. P values ≤ 0.05 were considered indicative of a significant difference. Values represent the mean and SEM of 18 and 8 samples for LPS and vehicle treated groups and 6 samples per GSK group. All sample processing and data preparation was performed by Graham Paul (University of Cardiff) (329).



Supplementary figure 4.1: PCA scores plot displaying intrinsic variation between the metabolomes of U937 macrophages following 24h exposures to TRPM (4-14 μg/ml BAD or SRM-2975). Data was acquired using ^{1}H NMR, normalised to cellular protein content and Pareto scaled for multivariate analysis. The data display high intra-group variance, causing considerable overlap of clustering.

Supplementary table 4.1: Output from the pathway over-representation analysis module of IMPaLA using LPS- associated feature metabolites as input and excluding pathways that were assigned p values ≥ 0.05 or FDR values ≥ 20%

Pathway	Over-represented metabolites	P value	FDR
Central carbon metabolism	Citrate, glucose, valine, isoleucine, succinate, pyruvate, leucine	≤ 0.001	≤ 0.001
SLC-mediated transmembrane transport	Citrate, pyruvate, valine, isoleucine, cystine, succinate, leucine	≤ 0.001	≤ 0.001
Amino Acid interconversion	Cystine, pyruvate, valine, isoleucine, leucine	≤ 0.001	≤ 0.001
Transmembrane transport of small molecules	Citrate, pyruvate, valine, isoleucine, cystine, succinate, leucine	≤ 0.001	≤ 0.001
Valine, leucine and isoleucine biosynthesis	Pyruvate, valine, isoleucine, leucine	≤ 0.001	≤ 0.001
Biochemical Pathways Part I	Citrate, glucose, valine, isoleucine, cystine, succinate, pyruvate, leucine	≤ 0.001	≤ 0.001
S-methyl-5-thio-α-D-ribose 1-phosphate metabolism	Pyruvate, valine, isoleucine, leucine	≤ 0.001	≤ 0.001
ABC transporters	Valine, glucose, cystine, isoleucine, leucine	≤ 0.001	≤ 0.001
Alanine and aspartate metabolism	Citrate, succinate, pyruvate	≤ 0.001	≤ 0.001
Gene Expression	Succinate, pyruvate, valine, isoleucine, leucine	≤ 0.001	≤ 0.001
Transfer of Acetyl Groups into Mitochondria	Citrate, pyruvate, glucose	≤ 0.001	≤ 0.001
leukotriene biosynthesis	Valine, isoleucine, leucine	≤ 0.001	0.001
Class I MHC mediated antigen processing	Valine, isoleucine, leucine	≤ 0.001	0.002
Conversion of glucose to acetyl CoA	Succinate, citrate, pyruvate	≤ 0.001	0.002
Valine, leucine and isoleucine degradation	Valine, isoleucine, leucine	≤ 0.001	0.003
γ-glutamyl cycle	Valine, isoleucine, leucine	≤ 0.001	0.004
HIF1A and PPARG regulation of glycolysis	Glucose, pyruvate	≤ 0.001	0.006
Glyoxylate and dicarboxylate metabolism	Citrate, succinate, pyruvate	≤ 0.01	0.007
Phase II conjugation	Valine, Isoleucine, Leucine, *p*-aminobenzoate	≤ 0.01	0.008
tRNA Aminoacylation	Valine, isoleucine, leucine	≤ 0.01	0.009
Cori Cycle	Pyruvate, glucose	≤ 0.01	0.012
HIF-1 signaling pathway	Pyruvate, glucose	≤ 0.01	0.012
Glycolysis and Gluconeogenesis	Pyruvate, glucose	≤ 0.01	0.014

AMPK signaling pathway	Glucose, pyruvate	≤ 0.01	0.029
TCA cycle and pyruvate metabolism	Succinate, citrate	≤ 0.01	0.029
Pyruvate metabolism	Succinate, pyruvate	≤ 0.01	0.049
Glutaminolysis	Succinate, pyruvate	≤ 0.01	0.054
Triosephosphate isomerase	Glucose, pyruvate	≤ 0.01	0.054
Lysine degradation	Citrate, succinate	≤ 0.01	0.059
Methionine Cysteine metabolism	Pyruvate, cysteine	≤ 0.01	0.091
Glucose metabolism	Citrate, pyruvate	≤ 0.01	0.098

Supplementary table 4.2: Output from the pathway over-representation analysis module of IMPaLA using BAD- associated feature metabolites as input and excluding pathways that were assigned p values ≥ 0.05 or FDR values ≥ 20%

Pathway	**Over-represented metabolites**	**P value**	**FDR**
Amino acid interconversion	Threonine, asparagine, valine, isoleucine, cystine, leucine, histidine	≤ 0.001	≤ 0.001
tRNA aminoacetylation	Threonine, asparagine, valine, isoleucine, leucine, histidine	≤ 0.001	≤ 0.001
Leukotriene biosynthesis	Threonine, asparagine, valine, isoleucine, leucine, histidine	≤ 0.001	≤ 0.001
Class I MHC mediated antigen processing & presentation	Threonine, asparagine, valine, isoleucine, leucine, histidine	≤ 0.001	≤ 0.001
S-methyl-5-thio-α-D-ribose 1-phosphate metabolism	Threonine, asparagine, valine, isoleucine, leucine, histidine	≤ 0.001	≤ 0.001
Central carbon metabolism	Citrate, asparagine, valine, isoleucine, leucine, histidine	≤ 0.001	≤ 0.001
γ-glutamyl cycle	Threonine, asparagine, valine, isoleucine, leucine, histidine	≤ 0.001	≤ 0.001
SLC-mediated transmembrane transport	Citrate, asparagine, valine, isoleucine, cystine, *myo*-inositol, leucine, histidine	≤ 0.001	≤ 0.001
Transmembrane transport of small molecules	Citrate, asparagine, valine, isoleucine, cystine, *myo*-inositol, leucine, histidine	≤ 0.001	≤ 0.001

ABC transporters	Threonine, valine, isoleucine, cystine, *myo*-inositol, leucine, histidine	≤ 0.001	≤ 0.001
Phase II conjugation	Threonine, Asparagine, Valine, Isoleucine, *p*-minobenzoate, Leucine, Histidine	≤ 0.001	≤ 0.001
Biochemical pathways part I	Citrate, threonine, asparagine, valine, isoleucine, cystine, *myo*-inositol, leucine, histidine	≤ 0.001	≤ 0.001
Valine, leucine and isoleucine biosynthesis	Valine, isoleucine, leucine, threonine	≤ 0.001	≤ 0.001
Gene expression	Asparagine, valine, isoleucine, leucine, histidine	≤ 0.001	0.001
Glucose homeostasis	Valine, isoleucine, histidine	≤ 0.001	0.001
Valine Leucine Isoleucine degradation	Valine, isoleucine, leucine	≤ 0.001	0.005
Alanine and aspartate metabolism	Citrate, asparagine	≤ 0.001	0.031
Ammonia recycling	Asparagine, histidine	≤ 0.01	0.080
Glutaminolysis	Citrate, leucine	≤ 0.01	0.178

Table S4.3: Output from the pathway over-representation analysis module of IMPaLA using DEP- associated feature metabolites as input and excluding pathways that were assigned p values ≥ 0.05 or FDR values ≥ 20%

Pathway	**Over-represented metabolites**	**P value**	**FDR**
Central carbon metabolism	Citrate, glucose, glutamate, asparagine, leucine, histidine	≤ 0.001	0.000
Amino Acid interconversion	Threonine, asparagine, glutamate, cystine, leucine, histidine	≤ 0.001	0.000
tRNA Aminoacylation	Asparagine, histidine, glutamate, leucine, threonine	≤ 0.001	0.000
ABC transporters	Threonine, glucose, glutamate, cystine, *myo*-inositol, leucine, histidine	≤ 0.001	0.000
leukotriene biosynthesis	Asparagine, threonine, glutamate, leucine, histidine	≤ 0.001	0.000
Class I MHC mediated antigen processing	Asparagine, histidine, glutamate, leucine, threonine	≤ 0.001	0.000
S-methyl-5-thio-α-D-ribose 1-phosphate metabolism	Asparagine, threonine, glutamate, leucine, histidine	≤ 0.001	0.000
SLC-mediated transmembrane transport	Citrate, asparagine, glutamate, cystine, *myo*-inositol, leucine, histidine	≤ 0.001	0.000
Biochemical pathways part I	Citrate, threonine, asparagine, glutamate, glucose, cystine, *myo*-inositol, leucine, histidine	≤ 0.001	0.000
γ-glutamyl cycle	Asparagine, threonine, glutamate, leucine, histidine	≤ 0.001	0.000

Transmembrane transport of small molecules	Citrate, asparagine, glutamate, cystine, *myo*-inositol, leucine, histidine	≤ 0.001	0.000
Phase II conjugation	Threonine, Asparagine, Glutamate, p-Aminobenzoate, Leucine, Histidine	≤ 0.001	0.000
Alanine, aspartate and glutamate metabolism	Citrate, asparagine, glutamate	≤ 0.001	0.001
Ammonia recycling	Asparagine, glutamate, histidine	≤ 0.001	0.002
FOXO signaling pathway	Glucose, glutamate	≤ 0.001	0.002
Glutaminolysis	Citrate, glutamate, leucine	≤ 0.001	0.005
Gene expression	Asparagine, glutamate, leucine, histidine	≤ 0.001	0.010
Asparagine metabolism	Asparagine, glutamate	≤ 0.001	0.012
Methionine and cysteine metabolism	Asparagine, cystine, glutamate	≤ 0.001	0.027
Biogenic amine synthesis	Glutamate, histidine	≤ 0.001	0.028
Glycine, serine, alanine and threonine metabolism	Asparagine, glutamate, threonine	≤ 0.001	0.034
Transfer of acetyl groups into mitochondria	Citrate, glucose	≤ 0.001	0.043
Histidine catabolism	Glutamate, histidine	≤ 0.001	0.046
Valine, leucine and isoleucine biosynthesis	Leucine, threonine	≤ 0.001	0.046
Glycolysis gluconeogenesis	Glucose, glutamate	≤ 0.01	0.085

Lysine degradation	Citrate, glutamate	≤ 0.01	0.092
Valine Leucine Isoleucine degradation	Glutamate, leucine	≤ 0.01	0.109

Table S4.4: Output from the integrated pathway over-representation analysis module of IMPaLA using LPS- associated feature metabolites and predicted targets of miR-34b/449a as input and excluding pathways that were assigned p values ≥ 0.05 or FDR values ≥ 20%

Pathway	**Over-represented genes**	**Over-represented metabolites**	**P value**	**FDR**
Central carbon metabolism	MYC, LDHA, PDGFRA, PDGFRB, SLC7A5, SLC2A2, TP53, MAP2K1	Citrate, glucose, glutamate, asparagine, leucine, histidine	≤ 0.001	≤ 0.01
SLC-mediated transmembrane transport	SLC6A1, SLC7A8, SLC6A9, SLC36A1, SLC12A2, SLC18A1, SLC18A2, SLC15A4, SLCO2A1, SLC22A5, SLCO4A1, SLC38A5, SLC7A5, SLC13A5, SLC2A13, SLC30A3, SLC4A3, SLC29A1, SLC36A2, SLC2A2, SLC2A4, NUP35, SLC12A5	Citrate, asparagine, glutamate, cystine, *myo*-inositol, leucine, histidine	≤ 0.001	≤ 0.01
Transmembrane transport of small molecules	SLC6A1, SLC7A8, SLC6A9, TRPV1, SLC36A1, SLC12A2, ABCB9, SLC18A1, SLC18A2, SLC15A4, SLCO2A1, ATP4B, SLC22A5, SLCO4A1, SLC38A5, SLC7A5,	Citrate, asparagine, glutamate, cystine, *myo*-inositol, leucine, histidine	≤ 0.001	≤ 0.01

	SLC13A5, GNG5, SLC2A13, AQP8, SLC30A3, ABCD2, ATP1B3, FXYD3, AQP4, SLC4A3, ATP2B4, SLC29A1, ADCY6, SLC36A2, SLC2A2, SLC2A4, ADD1, NUP35, SLC12A5			
tRNA charging	NARS	Asparagine, threonine, glutamate, leucine, histidine	≤ 0.001	≤ 0.01
ABC transporters	ABCB9, ABCD2	Threonine, glucose, glutamate, cystine, *myo*-inositol, leucine, histidine	≤ 0.001	≤ 0.01
FOXO signaling pathway	TGFB3, MAP2K1, MAPK13, PCK1, PRKAG1, SLC2A4, SMAD3, PRKAA2, PRKAB2, GRM1	Glucose, glutamate	≤ 0.001	≤ 0.01
Glutaminolysis	SLC38A5, GLUD1, LDHA, MYC, SDHC	Citrate, glutamate, leucine	≤ 0.001	≤ 0.01
Ammonia recycling	GLUD1	Asparagine, glutamate, histidine	≤ 0.001	0.007
Alanine, aspartate and glutamate metabolism	GLUD1	Citrate, asparagine, glutamate	≤ 0.001	0.011

Amino acid synthesis and interconversion (transamination)	PSAT1, GLUD1, SERINC1, SERINC2	Asparagine, glutamate	≤ 0.001	0.025
Glycine, serine, alanine and threonine metabolism	SLC22A5, NUP35, CHDH, SLC36A1, SLC38A5	Asparagine, glutamate, threonine	≤ 0.001	0.027
Glycolysis gluconeogenesis	ALDOA, LDHA, BPGM, ENO3	Glucose, glutamate	≤ 0.001	0.038
chrebp regulation	AGT, PRKAA2, PRKAB2, PRKAG1, CXCL12	Glucose	≤ 0.01	0.059
AMP-activated protein kinase (AMPK) signaling	PRKAG1, SLC2A4, LIPE, PRKAA2, PRKAB2, TP53	Glucose	≤ 0.01	0.059
Methionine and cysteine metabolism	NUP35, SLC7A8, ACY1	Asparagine, cystine, glutamate	≤ 0.01	0.059
Triosephosphate isomerase	PCK1, SLC2A2, ALDOA, BPGM	Glucose	≤ 0.01	0.059
Glucose metabolism	GYG1, PCK1, ALDOA, ENO3, BPGM	Citrate, glutamate	≤ 0.01	0.065
HIF-1 signaling pathway	ALDOA, IFNGR1, MAP2K1, ENO3, EGLN3, LDHA, BCL2, SERPINE1	Glucose	≤ 0.01	0.068
Lactic acid cycle	SLC2A2, LDHA, SLC2A4	Glucose	≤ 0.01	0.070

Fatty acid, triacylglycerol, and ketone body metabolism	ACADL, GPD1, ACSL1, ACADVL, ACSL4, DGAT2, AGPAT1, HSD17B8, DGAT1, PPARD, PRKAA2, PRKAB2	Citrate	≤ 0.01	0.071
AMPK signaling pathway	RAB14, PRKAG1, PCK1, SLC2A4, LIPE, RAB8A, PRKAA2, CREB3L2, PRKAB2	Glucose	≤ 0.01	0.083
Sterol Regulatory Element-Binding Proteins (SREBP) signalling	SAR1A, PRKAA2, PRKAG1, PRKAB2, FDFT1	Glucose	≤ 0.01	0.091
TP53 regulates metabolic genes	PRKAG1, DDIT4, YWHAZ, CYCS, TP53, PRKAA2, PRKAB2	Glutamate	≤ 0.01	0.095
IGF1R signaling cascade	ARRB2, DAB2IP, PRKAG1, MAP2K1, CSK, PDGFRB, PEA15, PTPN11, DUSP5, IGF2, PRKAA2, DUSP9, PRKAB2, PDGFRA	Glutamate	≤ 0.01	0.095
Histidine metabolism	HNMT, CNDP1	Glutamate, histidine	≤ 0.01	0.098
Methionine cysteine metabolism	LDHA, MTR	Cystine, glutamate	≤ 0.01	0.100
Valine leucine isoleucine degradation	BCAT1, ALDH1A2	Glutamate, leucine	≤ 0.01	0.104
Glycerophospholipid metabolism	GPD1, DGAT2, PLA2G5, DGAT1, SLC38A5, SLC22A5, NUP35, AGPAT1	Cystine, threonine	≤ 0.01	0.104
Metabolism of lipids and lipoproteins	HEXA, GPD1, ACSL1, ACSL4, AP2S1, LIPE, SLC10A1, SLC10A2,	Citrate, glutamate, *myo*-inositol	≤ 0.01	0.106

	AP2A2, ACADVL, DGAT2, SC5D, FDFT1, INPP4A, DPEP3, CHDH, AGPAT1, PRKAA2, PRKAB2, DHCR7, NFYB, ACADL, PLA2G5, PPARD, CHKA, RAB14, PPP1CC, HSD17B8, DGAT1, ARF3, SACM1L, HRASLS5			
Urea cycle	SLC6A1, SLC38A5, SLC36A1, NUP35, GLUD1, SFXN3, ACY1	Asparagine, glutamate	≤ 0.01	0.106
Cytokine Signaling in Immune system	DAB2IP, IFNGR1, IL13RA1, PTPN11, ARRB2, IL22RA2, CSF1R, PDGFRA, CSK, PDGFRB, DUSP5, DUSP9, CASP3, BIRC3, NFKB2, PRKCD, LTA, IL1RL1, MAP2K1, IL1RN, PEA15, YWHAZ, PPM1B	Glutamate	≤ 0.01	0.113
Signaling by Interleukins	DAB2IP, MAP2K1, IL1RN, PDGFRB, DUSP9, PEA15, NFKB2, IL13RA1, YWHAZ, CSK, PTPN11, IL1RL1, DUSP5, CASP3, ARRB2, IL22RA2, CSF1R, PDGFRA	Glutamate	≤ 0.01	0.121
Phospholipase D signaling pathway	RRAS2, PDGFRA, PDGFRB, ADCY6, PTPN11, MAP2K1, AGPAT1, GRM1	Glutamate	≤ 0.01	0.150

Supplementary table 4.5: Output from the integrated pathway over-representation analysis module of IMPaLA using BAD- associated feature metabolites and predicted targets of miR-34b/449a as input and excluding pathways that were assigned p values ≥ 0.05 or FDR values ≥ 20%

Pathway	Over-represented genes	Over-represented metabolites	P value	FDR
Central carbon metabolism in cancer	MYC, LDHA, PDGFRA, PDGFRB, SLC7A5, SLC2A2, TP53, MAP2K1	Citrate, Glucose, Valine, Isoleucine, Succinate, Pyruvate, Leucine	≤ 0.001	≤ 0.01
SLC-mediated transmembrane transport	SLC6A1, SLC7A8, SLC6A9, SLC36A1, SLC12A2, SLC18A1, SLC18A2, SLC15A4, SLCO2A1, SLC22A5, SLCO4A1, SLC38A5, SLC7A5, SLC13A5, SLC2A13, SLC30A3, SLC4A3, SLC29A1, SLC36A2, SLC2A2, SLC2A4, NUP35, SLC12A5	Citrate, Pyruvate, Valine, Isoleucine, Cystine, Succinate, Leucine	≤ 0.001	≤ 0.01
Transmembrane transport of small molecules	SLC6A1, SLC7A8, SLC6A9, TRPV1, SLC36A1, SLC12A2, ABCB9, SLC18A1, SLC18A2, SLC15A4, SLCO2A1, ATP4B, SLC22A5, SLCO4A1, SLC38A5, SLC7A5,	Citrate, Pyruvate, Valine, Isoleucine, Cystine, Succinate, Leucine	≤ 0.001	≤ 0.01

	SLC13A5, GNG5, SLC2A13, AQP8, SLC30A3, ABCD2, ATP1B3, FXYD3, AQP4, SLC4A3, ATP2B4, SLC29A1, ADCY6, SLC36A2, SLC2A2, SLC2A4, ADD1, NUP35, SLC12A5			
Amino acid transport across the plasma membrane	SLC38A5, SLC7A8, SLC7A5, SLC36A1, SLC36A2	Valine, Cystine, Isoleucine, Leucine	≤ 0.001	≤ 0.01
Glucagon signaling pathway	LDHA, PCK1, SLC2A2, PRKAG1, PRKAA2, CREB3L2, PRKAB2	Citrate, Succinate, Glucose, Pyruvate	≤ 0.001	≤ 0.01
Glutaminolysis and cancer	SLC38A5, GLUD1, LDHA, MYC, SDHC	Citrate, Succinate, Pyruvate, Leucine	≤ 0.001	≤ 0.01
Valine, leucine and isoleucine biosynthesis	BCAT1	Pyruvate, Valine, Isoleucine, Leucine	≤ 0.001	≤ 0.01
Valine, leucine and isoleucine degradation	BCAT1, ALDH1A2	Succinate, Valine, Isoleucine, Leucine	≤ 0.001	≤ 0.01
ABC transporters	ABCB9, ABCD2	Valine, Glucose, Cystine, Isoleucine, Leucine	≤ 0.001	0.001

Glycolysis and Gluconeogenesis	ALDOA, LDHA, ENO3, PCK1, SLC2A2, SLC2A4	Pyruvate, Glucose	≤ 0.001	0.001
Conversion of glucose to acetyl CoA a	ALDOA, ENO3, BPGM, SDHC	Succinate, Citrate, Pyruvate	≤ 0.001	0.001
HIF-1 signaling pathway	ALDOA, IFNGR1, MAP2K1, ENO3, EGLN3, LDHA, BCL2, SERPINE1	Pyruvate, Glucose	≤ 0.001	0.002
Cori cycle	SLC2A2, LDHA, SLC2A4	Pyruvate, Glucose	≤ 0.001	0.002
Gene expression	MYC, CCNG1, ERCC3, DDIT4, ATP1B4, GTF2F2, POLR3D, MED4, BTG2, PUS1, NDRG1, ARID4B, EIF2B4, PRKAA2, CYCS, BUD31, TSEN34, PRKAG1, RNF34, NARS, PRKCD, PLAGL1, CNOT8, PPARD, CDC5L, SEC61A1, SMAD7, YWHAZ, PRKAB2, GATAD2B, TP53, SMAD3, NUP35, TBP, MEN1, TGFA	Succinate, Pyruvate, Valine, Isoleucine, Leucine	≤ 0.001	0.003
Gluconeogenesis	PCK1, SLC2A2, ALDOA, BPGM	Glucose, Pyruvate	≤ 0.001	0.003

Triosephosphate isomerase	PCK1, SLC2A2, ALDOA, BPGM	Glucose, Pyruvate	≤ 0.001	0.003
AMPK signaling pathway	RAB14, PRKAG1, PCK1, SLC2A4, LIPE, RAB8A, PRKAA2, CREB3L2, PRKAB2	Glucose, Pyruvate	≤ 0.001	0.003
tRNA charging	NARS	Valine, Isoleucine, Leucine	≤ 0.001	0.003
Pyruvate metabolism and citric acid (TCA) cycle	PPARD, LDHA, SDHC	Citrate, Succinate, Pyruvate	≤ 0.001	0.004
Alanine, aspartate and glutamate metabolism	GLUD1	Citrate, Succinate, Pyruvate	≤ 0.001	0.004
Fatty acid, triacylglycerol, and ketone body metabolism	ACADL, GPD1, ACSL1, ACADVL, ACSL4, DGAT2, AGPAT1, HSD17B8, DGAT1, PPARD, PRKAA2, PRKAB2	Succinate, Citrate	≤ 0.001	0.009
FOXO signaling pathway	TGFB3, MAP2K1, MAPK13, PCK1, PRKAG1, SLC2A4, SMAD3, PRKAA2, PRKAB2, GRM1	Glucose	≤ 0.001	0.011
Glycolysis / gluconeogenesis	PCK1, ALDOA, LDHA, BPGM, ENO3	Glucose, Pyruvate	≤ 0.001	0.016

The citric acid (TCA) cycle and respiratory electron transport	LDHA, SLC25A27, PPARD, CYCS, SDHC	Citrate, Succinate, Pyruvate	≤ 0.001	0.018
Import of palmitoyl-CoA into the mitochondrial matrix	PPARD, PRKAA2, PRKAB2	Citrate	≤ 0.01	0.022
cAMP signaling pathway	RRAS2, ATP1B3, MAP2K1, ADORA2A, PLCE1, ATP2B4, ATP1B4, ADCY6, NPR1, GNAI2, TSHR, LIPE, CREB3L2, PPP1CC	Succinate	≤ 0.01	0.026
Insulin signaling pathway	PRKAG1, MAP2K1, PPP1CC, FLOT2, PCK1, SLC2A4, LIPE, PRKAA2, PRKAB2	Glucose	≤ 0.01	0.028
chrebp regulation by carbohydrates and camp	AGT, PRKAA2, PRKAB2, PRKAG1, CXCL12	Glucose	≤ 0.01	0.029
AMP-activated protein kinase (AMPK) signaling	PRKAG1, SLC2A4, LIPE, PRKAA2, PRKAB2, TP53	Glucose	≤ 0.01	0.032
Sterol regulatory element-binding proteins (SREBP) signalling	SAR1A, PRKAA2, PRKAG1, PRKAB2, FDFT1	Glucose	≤ 0.01	0.064

Lactose degradation	SLC2A2, ATP1B3	Glucose	≤ 0.01	0.085
Urea cycle and metabolism of arginine, proline, glutamate, aspartate and asparagine	SLC6A1, SLC38A5, SLC36A1, NUP35, GLUD1, SFXN3, ACY1	Succinate, Pyruvate	≤ 0.01	0.089
Cysteine and methionine metabolism	BCAT1, LDHA, MTR	Pyruvate, Cystine	≤ 0.01	0.105
Amino acid interconversion	PSAT1, GLUD1, SERINC1, SERINC2	Pyruvate	≤ 0.01	0.115
Lysine degradation	ALDH1A2	Citrate, Succinate	≤ 0.01	0.121
Glutaminolysis	GLUD1	Succinate, Pyruvate	≤ 0.01	0.123
Leucine stimulation on insulin signaling	SLC7A5	Leucine	≤ 0.05	0.141
Metabolism of lipids and lipoproteins	HEXA, GPD1, ACSL1, ACSL4, AP2S1, LIPE, SLC10A1, SLC10A2, AP2A2, ACADVL, DGAT2, SC5D, FDFT1, INPP4A, DPEP3, CHDH, AGPAT1, PRKAA2, PRKAB2, DHCR7, NFYB, ACADL, PLA2G5, PPARD,	Succinate, Citrate	≤ 0.05	0.198

	CHKA, RAB14, PPP1CC, HSD17B8, DGAT1, ARF3, SACM1L, HRASLS5			

Supplementary table 4.6: Output from the integrated pathway over-representation analysis module of IMPaLA using DEP- associated feature metabolites and predicted targets of miR-34b/449a as input and excluding pathways that were assigned p values ≥ 0.05 or FDR values ≥ 20%

Pathway	**Over-represented genes**	**Over-represented metabolites**	**P value**	**FDR**
Central carbon metabolism	MYC, LDHA, PDGFRA, PDGFRB, SLC7A5, SLC2A2, TP53, MAP2K1	Citrate, Glucose, Glutamate, Asparagine, Leucine, Histidine	≤ 0.001	≤ 0.01
SLC-mediated transmembrane transport	SLC6A1, SLC7A8, SLC6A9, SLC36A1, SLC12A2, SLC18A1, SLC18A2, SLC15A4, SLCO2A1, SLC22A5, SLCO4A1, SLC38A5, SLC7A5, SLC13A5, SLC2A13, SLC30A3, SLC4A3, SLC29A1, SLC36A2, SLC2A2, SLC2A4, NUP35, SLC12A5	Citrate, Asparagine, Glutamate, Cystine, *Myo*-Inositol, Leucine, Histidine	≤ 0.001	≤ 0.01
Transmembrane transport of small molecules	SLC6A1, SLC7A8, SLC6A9, TRPV1, SLC36A1, SLC12A2, ABCB9, SLC18A1, SLC18A2, SLC15A4, SLCO2A1, ATP4B, SLC22A5, SLCO4A1, SLC38A5, SLC7A5,	Citrate, Asparagine, Glutamate, Cystine, *Myo*-Inositol, Leucine, Histidine	≤ 0.001	≤ 0.01

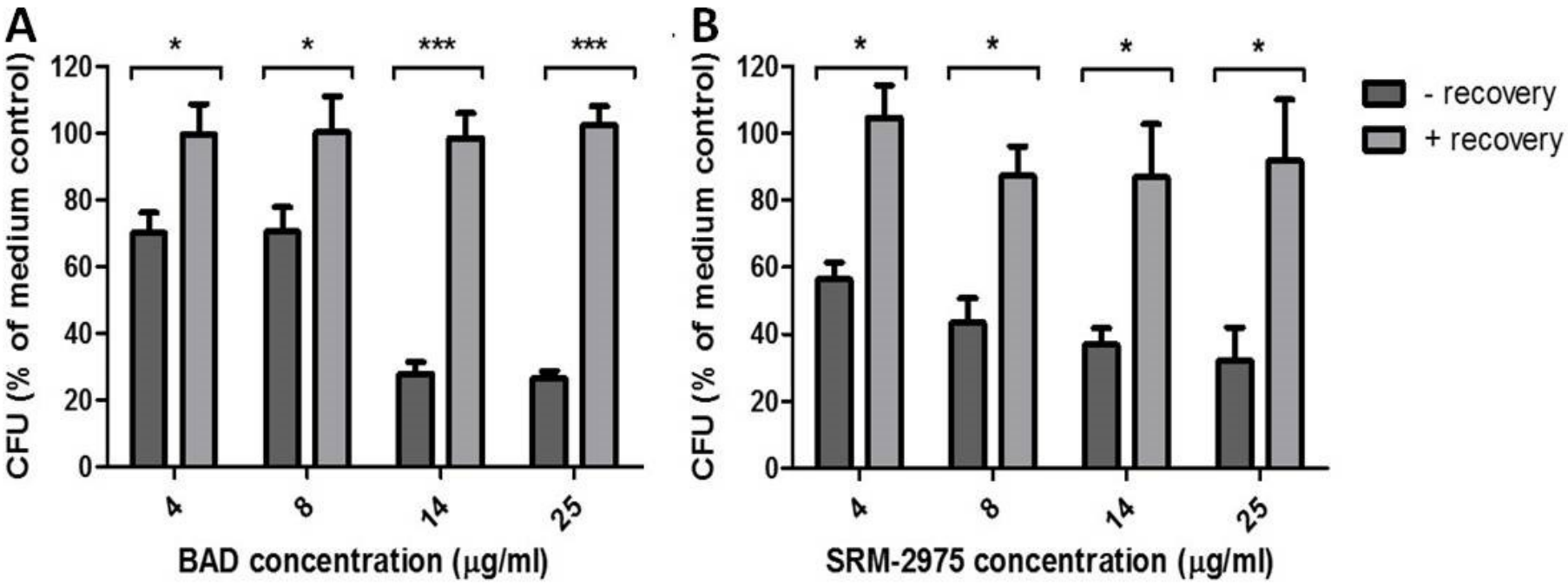
	SLC13A5, GNG5, SLC2A13, AQP8, SLC30A3, ABCD2, ATP1B3, FXYD3, AQP4, SLC4A3, ATP2B4, SLC29A1, ADCY6, SLC36A2, SLC2A2, SLC2A4, ADD1, NUP35, SLC12A5			
tRNA charging	NARS	Asparagine, Threonine, Glutamate, Leucine, Histidine	≤ 0.001	≤ 0.01
ABC transporters	ABCB9, ABCD2	Threonine, Glucose, Glutamate, Cystine, *Myo*-Inositol, Leucine, Histidine	≤ 0.001	≤ 0.01
FOXO signaling pathway	TGFB3, MAP2K1, MAPK13, PCK1, PRKAG1, SLC2A4, SMAD3, PRKAA2, PRKAB2, GRM1	Glucose, Glutamate	≤ 0.001	≤ 0.01
Glutaminolysis	SLC38A5, GLUD1, LDHA, MYC, SDHC	Citrate, Glutamate, Leucine	≤ 0.001	≤ 0.01
Ammonia recycling	GLUD1	Asparagine, Glutamate, Histidine	≤ 0.001	0.007

Alanine, aspartate and glutamate metabolism	GLUD1	Citrate, Asparagine, Glutamate	≤ 0.001	0.011
Amino acid synthesis and interconversion (transamination)	PSAT1, GLUD1, SERINC1, SERINC2	Asparagine, Glutamate	≤ 0.001	0.025
Glycine, serine, alanine and threonine metabolism	SLC22A5, NUP35, CHDH, SLC36A1, SLC38A5	Asparagine, Glutamate, Threonine	≤ 0.001	0.027
Glycolysis Gluconeogenesis	ALDOA, LDHA, BPGM, ENO3	Glucose, Glutamate	≤ 0.001	0.038
chrebp regulation	AGT, PRKAA2, PRKAB2, PRKAG1, CXCL12	Glucose	≤ 0.01	0.059
AMP-activated protein kinase (AMPK) signaling	PRKAG1, SLC2A4, LIPE, PRKAA2, PRKAB2, TP53	Glucose	≤ 0.01	0.059
Methionine and cysteine metabolism	NUP35, SLC7A8, ACY1	Asparagine, Cystine, Glutamate	≤ 0.01	0.059
Triosephosphate isomerase	PCK1, SLC2A2, ALDOA, BPGM	Glucose	≤ 0.01	0.059
Glucose metabolism	GYG1, PCK1, ALDOA, ENO3, BPGM	Citrate, Glutamate	≤ 0.01	0.065
HIF-1 signaling pathway	ALDOA, IFNGR1, MAP2K1, ENO3, EGLN3, LDHA, BCL2, SERPINE1	Glucose	≤ 0.01	0.068
Lactic acid cycle	SLC2A2, LDHA, SLC2A4	Glucose	≤ 0.01	0.070

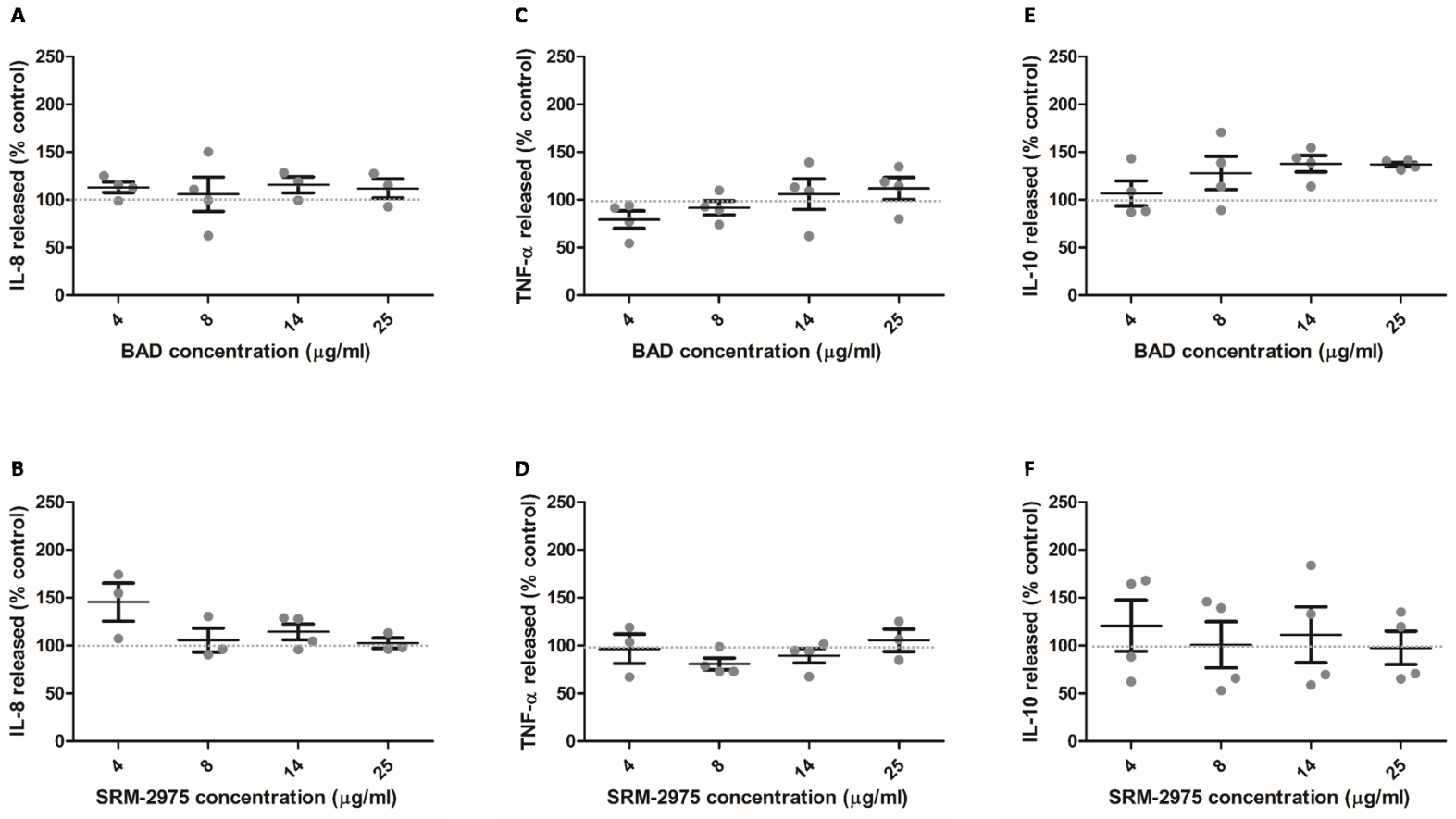
Fatty acid, triacylglycerol, and ketone body metabolism	ACADL, GPD1, ACSL1, ACADVL, ACSL4, DGAT2, AGPAT1, HSD17B8, DGAT1, PPARD, PRKAA2, PRKAB2	Citrate	≤ 0.01	0.071
AMPK signaling pathway	RAB14, PRKAG1, PCK1, SLC2A4, LIPE, RAB8A, PRKAA2, CREB3L2, PRKAB2	Glucose	≤ 0.01	0.083
Sterol regulatory element-binding proteins (SREBP) signalling	SAR1A, PRKAA2, PRKAG1, PRKAB2, FDFT1	Glucose	≤ 0.01	0.091
TP53 regulates metabolic genes	PRKAG1, DDIT4, YWHAZ, CYCS, TP53, PRKAA2, PRKAB2	Glutamate	≤ 0.01	0.095
IGF1R signaling cascade	ARRB2, DAB2IP, PRKAG1, MAP2K1, CSK, PDGFRB, PEA15, PTPN11, DUSP5, IGF2, PRKAA2, DUSP9, PRKAB2, PDGFRA	Glutamate	≤ 0.01	0.095
Histidine metabolism	HNMT, CNDP1	Glutamate, Histidine	≤ 0.01	0.098
Methionine cysteine metabolism	LDHA, MTR	Cystine, Glutamate	≤ 0.01	0.100

Valine Leucine Isoleucine degradation	BCAT1, ALDH1A2	Glutamate, Leucine	≤ 0.01	0.104
Glycerophospholipid metabolism	GPD1, DGAT2, PLA2G5, DGAT1, SLC38A5, SLC22A5, NUP35, AGPAT1	Cystine, Threonine	≤ 0.01	0.104
Metabolism of lipids and lipoproteins	HEXA, GPD1, ACSL1, ACSL4, AP2S1, LIPE, SLC10A1, SLC10A2, AP2A2, ACADVL, DGAT2, SC5D, FDFT1, INPP4A, DPEP3, CHDH, AGPAT1, PRKAA2, PRKAB2, DHCR7, NFYB, ACADL, PLA2G5, PPARD, CHKA, RAB14, PPP1CC, HSD17B8, DGAT1, ARF3, SACM1L, HRASLS5	Citrate, Glutamate, *Myo*-Inositol	≤ 0.01	0.106
Urea cycle	SLC6A1, SLC38A5, SLC36A1, NUP35, GLUD1, SFXN3, ACY1	Asparagine, Glutamate	≤ 0.01	0.106
Cytokine signaling in immune system	DAB2IP, IFNGR1, IL13RA1, PTPN11, ARRB2, IL22RA2, CSF1R, PDGFRA,	Glutamate	≤ 0.01	0.113

	CSK, PDGFRB, DUSP5, DUSP9, CASP3, BIRC3, NFKB2, PRKCD, LTA, IL1RL1, MAP2K1, IL1RN, PEA15, YWHAZ, PPM1B			
Signaling by interleukins	DAB2IP, MAP2K1, IL1RN, PDGFRB, DUSP9, PEA15, NFKB2, IL13RA1, YWHAZ, CSK, PTPN11, IL1RL1, DUSP5, CASP3, ARRB2, IL22RA2, CSF1R, PDGFRA	Glutamate	≤ 0.01	0.121
Phospholipase D signaling pathway	RRAS2, PDGFRA, PDGFRB, ADCY6, PTPN11, MAP2K1, AGPAT1, GRM1	Glutamate	≤ 0.05	0.150



Supplementary figure 5.1: Quantities of *S. aureus* ingested by U937s over a 2h period subsequent to 24h incubation with 4-25 µg/ml BAD (A) or SRM-2975 (B) then 24h incubation in particle-free media. Values were normalised to concentrations of total cellular proteins and are presented as percentages of a particle-free control and represent the mean ± SEM of 4-6 biological repeats. Significant differences in CFU were identified between particle-treated and particle rested cells using 2-way ANOVA tests with Bonferroni correction. *p ≤0.05, *** p ≤0.001



Supplementary figure 5.2: Concentrations of IL-8 (A, B), TNF-α (C, D) and IL-10 (E, F) measured within the supernatants of U937s after 24h exposure to BAD (A, C, E) and SRM-2975 (B, D, F) then 24h incubation in particle-free media. Values are expressed as percentages of particle-free controls with error bars depicting the SEM generated during 5-7 replicates. Significant differences in cytokine concentration were identified between control and particle-treated cells using 1-way ANOVA tests with Bonferroni correction. * $p \leq 0.05$, ** $p \leq 0.01$, *** $p \leq 0.001$.

Permission for inclusion of third party data: inflammatory cell counts for BALF samples used in **Chapter 3.**

Wed 23/11/2016, 10:36

Hi Liza,

My supervisors are happy for you to use the cell count data, and commented my data must not appear in your data/results section but in the discussion as a 'discussion point' or as an appendix clearly indicating it is not your work. They agreed that it would be fine as long as:

(1) Data generated during GSK Study No. R30820N, e.g. cell counts in blood and/or bronchoalveolar lavage fluid, are explicitly included as data arising from Graham Paul's thesis. These data would not be included in your results sections, but either as part of your discussion or in an appendix.
(2) It should also be clear that the animal study design and experimental conduct is Graham Paul's thesis and only the serum taken during this work was released to Imperial College London. The methods for serum analysis would then be part of your methods (but not animal study design and conduct). Methods conducted for GSK Study No. R30820N (e.g. experimental design, sampling and cell counting) may again be addressed by an appendix approach separating them from your methods.

When citing my thesis, please use the following information:

Title:	Defining dosimetry and implications for aerosol presentation for non-clinical development of respiratory drugs
Institution:	University of Cardiff, School of Pharmacy & Pharmaceutical Sciences
Author:	Graham R Paul
Year:	2017

Kind regards,

Graham Paul
I**nvestigator**
Toxicology & Biometabolism UK
Integrated Biological Platform Sciences
R&D Platform Technology & Science